TESIS DE LA UNIVERSIDAD DE ZARAGOZA

2013

118

Eva Blasco Pomar

Photoresponsive materials based on azobenzene: novel macromolecular architectures and applications

Departamento
Química Orgánica

Director/es
Oriol Langa, Luis T.
Piñol Lacambra, Milagros

http://zaguan.unizar.es/collection/Tesis

ISSN 2254-7606

Prensas de la Universidad
Universidad Zaragoza

Universidad Zaragoza
1542

Tesis Doctoral

PHOTORESPONSIVE MATERIALS BASED ON AZOBENZENE: NOVEL MACROMOLECULAR ARCHITECTURES AND APPLICATIONS

Autor

Eva Blasco Pomar

Director/es

Oriol Langa, Luis T.
Piñol Lacambra, Milagros

UNIVERSIDAD DE ZARAGOZA

Química Orgánica

Repositorio de la Universidad de Zaragoza – Zaguan http://zaguan.unizar.es

PHOTORESPONSIVE MATERIALS BASED ON AZOBENZENE: NOVEL MACROMOLECULAR ARCHITECTURES AND APPLICATIONS

Eva Blasco Pomar

Dpto. Química Orgánica

Facultad de Ciencias-ICMA

Universidad de Zaragoza-CSIC

Zaragoza, July 2013

Departamento de
Química Orgánica
Universidad Zaragoza

Los Drs. LUIS T. ORIOL LANGA, Profesor Titular del Departamento de Química Orgánica, y MILAGROS PIÑOL LACAMBRA, Profesora Titular del Departamento de Química Orgánica, pertenecientes a la Facultad de Ciencias y al Instituto de Ciencia de Materiales de Aragón de la Universidad de Zaragoza-CSIC

HACEN CONSTAR

que el trabajo original titulado "PHOTORESPONSIVE MATERIALS BASED ON AZOBENZENE: NOVEL MACROMOLECULAR ARCHITECTURES AND APPLICATIONS", ha sido realizado por Dña. EVA BLASCO POMAR bajo nuestra supervisión en el Departamento de Química Orgánica de la Facultad de Ciencias de la Universidad de Zaragoza y reúne las condiciones para su presentación como tesis doctoral.

Zaragoza, 9 a de Julio de 2013

Fdo.: Luis T. Oriol Langa Fdo.: Milagros Piñol Lacambra

Resumen

Durante estos últimos años, los materiales que responden a uno o varios estímulos externos, conocidos como materiales ‘inteligentes’, han despertado un gran interés en la comunidad científica. Una de las principales razones es la posibilidad de utilizarlos en aplicaciones en campos tan diversos como la electrónica o la medicina, entre otros. De todos los posibles, la luz es probablemente el estímulo más interesante ya que es posible controlar la respuesta del material tanto espacial como temporalmente. Existen numerosos grupos orgánicos en los que la luz puede provocar una variación reversible en sus propiedades físicas y/o químicas pero el azobenceno es sin ninguna duda el grupo fotocrómico más estudiado en la preparación de materiales que respondan a la luz. Las aplicaciones de los materiales basados en azobenceno derivan de la fotoisomerizacion reversible entre los isómeros *trans* y *cis* que experimentan.

En el grupo de investigación de Cristales Líquidos y Polímeros se han estudiado en profundidad polímeros y copolímeros con unidades azobencenos en la cadena lateral para aplicaciones ópticas, tales como el almacenamiento óptico de información. En los últimos años, el estudio se ha centrado en nuevas arquitecturas poliméricas, en concreto, copolímeros bloque dendrítico-lineales. Partiendo de los resultados previos del trabajo del grupo, en esta tesis doctoral se planteó obtener materiales con fotorrespuesta principalmente basados en azopolímeros con arquitecturas poliméricas alternativas a las convencionales basadas en estructura de cadena lateral. Los objetivos planteados para el desarrollo de esta tesis doctoral son los siguientes

- Síntesis y caracterización de copolímeros bloque dendrítico-lineales compuestos por un bloque dendrítico funcionalizado con dieciséis unidades cianoazobenceno y diferentes bloques lineales, poliestireno y poli(metacrilato de etilo) y los análogos con poli(metacrilato de metilo) (**Capítulo 2**).

- Síntesis y estudio del autoensamblaje en agua de nuevos copolímeros bloque dendrítico lineales anfífilos compuestos por un bloque lineal de

polietilenglicol y un dendron de tipo poliéster funcionalizado bien con dieciséis unidades 4-isobutiloxiazobenceno o bien codendrones con diferentes proporciones de 4-isobutiloxiazobenceno y cadenas hidrocarbonadas distribuidas aleatoriamente en la periferia. Estudio de la aplicación de estos materiales como nanotransportadores de moléculas orgánicas y liberación fotoestimulada de las mismas (**Capítulos 3 y 4**).

- Síntesis y estudio del autoensamblaje en agua de nuevos copolímeros anfífilos de tipo 'miktoarm' AB_3, así como su respuesta al irradiar con luz UV. Estos copolímeros están compuestos por un azopolímero y tres ramas idénticas de PEG o un polímero termosensible como la poli(*N*-etilacrilamida). Estudio de la respuesta a la luz, en el caso del polímero con PEG, y de la respuesta dual, luz y temperatura, en el de los polímeros con poli(*N*-etilacrilamida) de los ensamblados poliméricos (**Capítulos 5 y 6**).

- Preparación de superficies fotosensibles funcionalizadas con unidades azobenceno utilizando luz como estímulo externo tanto para la funcionalización cómo para el control de las propiedades de la superficie (**Capítulo 7**).

Acronyms List

AIBN	Azobisisobutyronitrile
ATRP	Atom Transfer Radical Polymerization
BC	Block Copolymer
bisMPA	2,2-bis(hydroxymethyl)propionic acid
CA	Contact Angle
CAC	Critical Agregation Concentration
CMC	Critical Micellar Concentration
CRP	Controlled Radical Polymerization
Cryo-TEM	Cryogenic Transmission Electron Microscopy
CuAAC	Copper-catalyzed Azide–Alkyne Cycloaddition
DCC	*N,N*-dicyclohexylcarbodiimide
DCM	Dichloromethane
D_h	Hydrodynamic Diameter
DLS	Dynamic Light Scattering
DMF	*N,N*-Dimethylformamide
DMSO	Dimethyl sulfoxide
DPTS	4-(Dimethylamino)pyridinium 4-toluenesulfonate
DSC	Differential Scanning Calorimetry
ESI	Electrospray ionization
FTIR	Fourier Transform Infrared Spectroscopy
HMTETA	*N,N,N',N'',N''*-hexamethyltriethylenetetramine
LCST	Lower Critical Solution Temperature
LDBC	Linear-Dendritic Block Copolymer
LPL	Linear Polarized Light
MEK	Methyl ethyl ketone

M_n	Number Average Molecular Weight
MS	Mass Spectrometry
NITEC	Nitrile Imine-mediated Tetrazole-Ene Cycloaddition
NMR	Nuclear Magnetic Resonance
PDEAA	Poly(*N,N*-diethylacrylamide)
PEG	Polyethylene glycol
PEMA	Poly(ethyl methacrylate)
PMDETA	*N,N,N',N'',N''*- pentamethyldiethylenetriamine
PMMA	Poly(methyl methacrylate)
PNIPAM	Poly(*N*-isopropylacrylamide)
POM	Polarized Optical Microscopy
PPI	Poly(propylene imine)
PS	Poly(styrene)
RAFT	Reversible Addition–Fragmentation Transfer
SEC	Size Exclusion Chromatography
TBAF	Tetra-*n*-butylammonium fluoride
TEM	Transmission Electron Microscopy
T_g	Glass transition Temperature
TGA	Thermogravimetric Analysis
THF	Tetrahydrofuran
TMS	Trimethylsilyl
ToF-SIMS	Time-of-Flight Secondary Ion Mass Spectrometry
TsOH	4-Toluenesulfonic Acid
UV	Ultraviolet
Vis	Visible
XPS	X-Ray Photoelectron Spectroscopy

Contents

Chapter 1. General Introduction

Chapter 2. Linear-Dendritic Block Copolymers for Optical Applications

Chapter 3. Amphiphilic Linear-Dendritic Block Copolymers: Self-assembly and Photoresponse

Chapter 4. Amphiphilic Linear-Dendritic Block Copolymers using Azobenzene-Aliphatic Codendrons: Self-assembly and Photoresponse

Chapter 5. Miktoarm Star Polymer Architecture as Alternative to Amphiphilic Block Copolymers

Chapter 6. Dual Responsive Miktoarm Star Polymers

Chapter 7. Light Responsive Surfaces

CHAPTER 1

General Introduction

1.1 Photoresponsive Materials

Stimuli responsive materials have been widely studied in the last years. These materials play an important role in a broad range of fields including biomedicine, microelectronics, optics or sensors among others.[1-4] Nevertheless, the design and synthesis of new materials with controlled and predictable properties is still a challenge. Most of the materials reported in literature are polymers due to their versatility and processability.[1-3] Photoresponsive polymers have one or more properties that can be significantly changed in a controlled fashion on receiving an external stimulus. The most widely investigated stimuli are pH, temperature, light as well as magnetic fields among others. Light is an especially attractive stimulus allowing temporal and spatial control. The light response of a material can be achieved by incorporation of photochromic moieties, which can reversibly switch between two states with different absorption spectra upon light irradiation. During this process, other properties as refractive index, dielectric constant, redox potential and molecular geometry can also be modified. Some organic molecules in which this photochromic effect has been observed are collected in **Scheme 1.1**. This effect can be due to either photoinduced reactions or isomerisation.[5]

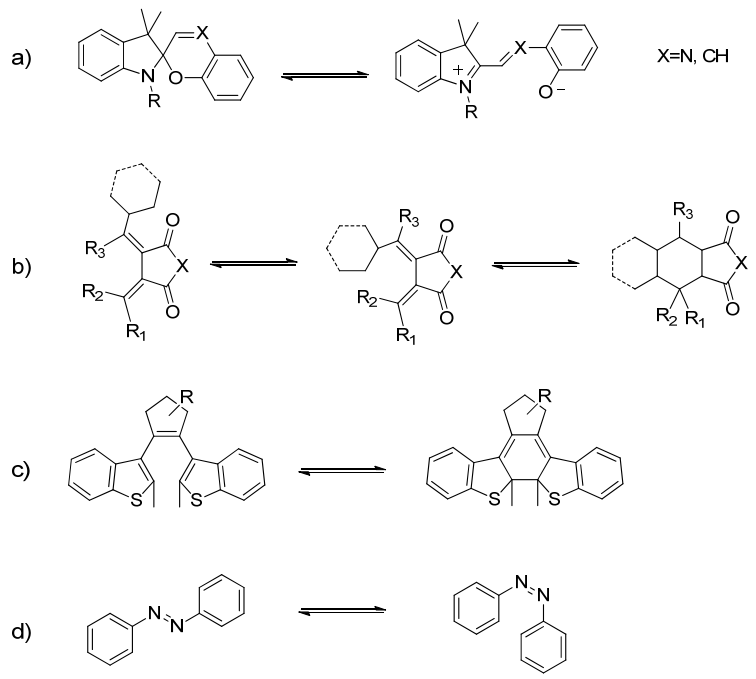

Scheme 1.1. *Photochromic moieties: a) spiropyrans and spirooxazines, b) fulgides, c) diarylethenes and d) azobenzenes*

However, the most studied photoresponsive moiety is the azobenzene.[10] Upon irradiation, azobenzene suffers a reversible *trans*-to-*cis* isomerisation (**Figure 1.1**), this photoisomerisation is accompanied by a fast change in the geometric shape and polarity of the molecule. For most azobenzene compounds, the *trans* isomer is thermodynamically more stable than the *cis* isomer. The wavelength at which azobenzene isomerisation occurs depends on the particular structure of each azo molecule.[11] Usually, azobenzene exhibits a low intensity n-π* absorption in the visible region, and a much higher intensity π-π* absorption in the UV region(see spectra in **Figure 1.1**).

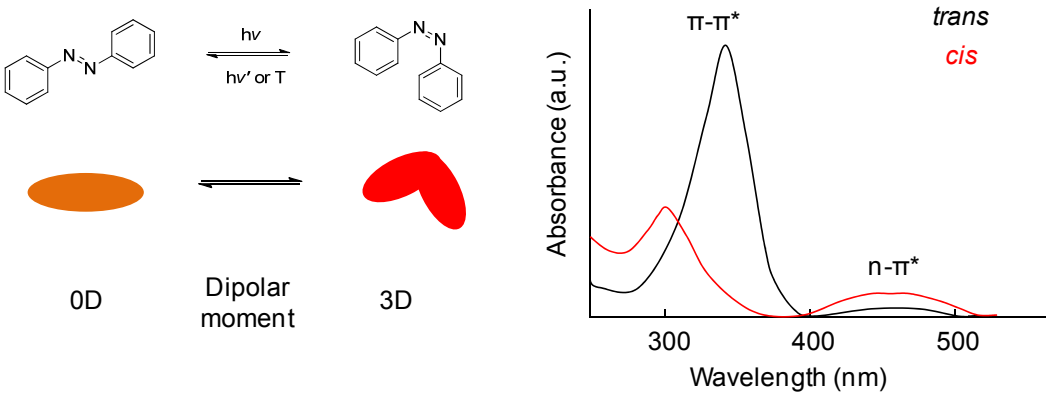

Figure 1.1 *Azobenzene isomerisation (left) and a representative UV spectra of the two isomers of an azobenzene (right)*

The incorporation of these moieties into polymers makes them promising candidates in potential application in different fields ranging from data storage to photomechanical actuators among others (see Section 1.3).

1.2 Azopolymers: Structrure & Synthesis

1.2.1 Azobenzene Homopolymers

Azopolymers are polymers containing azobenzene moieties. These moieties can be incorporated into a polymeric structure in three different ways: a) host-guest systems, b) main chain azobenzene polymers and c) side chain azobenzene polymers, as it is schematically represented in **Figure 1.2**.

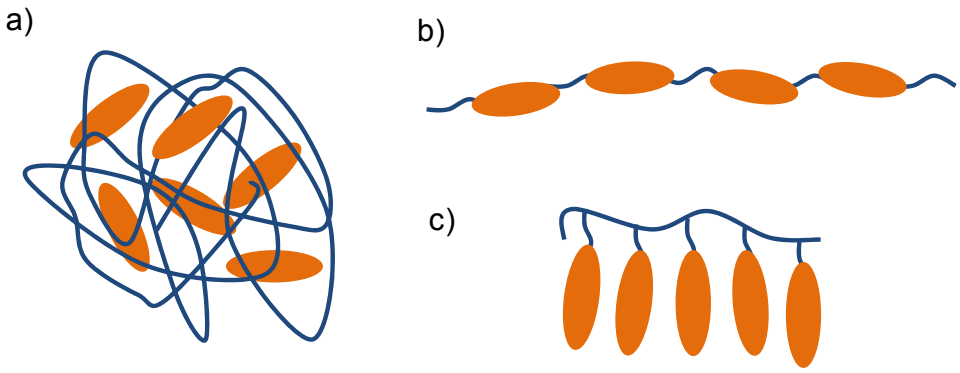

Figure 1.2 *Schematic representation of different azobenzene containing polymers: a) host-guest system, b) main chain azobenzene polymer and c) side chain azobenzene polymer*

Host-guest systems are formed by low molecular weight azobenzene molecules dispersed in a polymer matrix. This approach is the easiest strategy to prepare azobenzene based polymers (**Figure 1.2a**). It allows to keep the processability and the mechanical stability characteristics of the polymeric host material while the optical properties can be, to some extent, modulated by tuning of the composition of the mixture.[12-14] Nevertheless, macroscopic segregation of the chromophore and the matrix might occur, which is the major drawback. An alternative to circumvent this problem is the linkage of azobenzene moieties to a polymer. Azobenzene moieties can be incorporated either in the main chain (**Figure 1.2b**) or in the side chain as pendant groups (**Figure 1.2c**). Several main chain azobenzene polymers have been prepared and studied as liquid crystal actuators.[15,16] Nevertheless, azobenzene side chain polymers have been widely explored, especially poly(acrylates) and poly(methacrylates) derivatives. It is in the latter type of polymers in which we will focus this section.

1.2.1.1 Synthesis of Azobenzene Homopolymers by Direct Polymerization

There are two synthetic approaches for the preparation of azobenzene side chain homopolymers which are direct polymerization of an azomonomer and azobenzene postfunctionalization of a polymer previously synthesised. **Scheme 1.2** shows a representation of both possibilities.

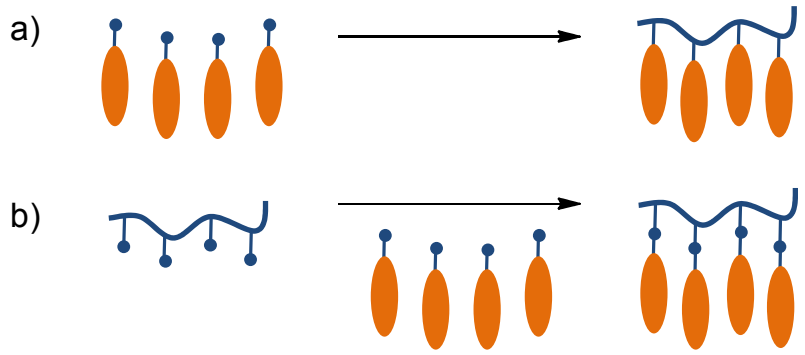

Scheme 1.2 *Different strategies for the preparation of azobenzene homopolymers: a) direct polymerization, b) azobenzene postfunctionalization*

The main advantage of the direct polymerization of a monomeric azobenzene is that the obtained polymers posses a well controlled composition having an azobenzene moiety per repeating unit. Hvilsted and coworkers have reported the synthesis of different series of liquid crystalline polyesters by step polymerization.[17-19] Nevertheless, the vast majority of the reported azopolymers are polyacrylates and polymethacrylates. Traditionally, these azobenzene acrylates and methacrylates derivatives have been polymerized by free radical polymerization in solution using conventional experimental conditions (e.g. AIBN as thermal initiator in dry organic solvents such as DMF, THF or dioxane). The main drawback of this strategy is that the polymerization process of azobenzene (meth)acrylates is limited by the radical transfer reaction promoted by the azo group that seems to be associated to the formation of hydrazyl radicals[20,21] and azopolymers can be obtained with uncontrolled and low molecular weights.

In the last decades, different controlled radical polymerization (CRP) techniques[22,23] have been employed to obtain azopolymers, including atom

transfer radical polymerization (ATRP) and reversible addition fragmentation chain transfer polymerization (RAFT) among others.

ATRP was first reported by the groups of Matyjaszewski and Sawamoto in 1995.[24-26] This polymerization process is based on the transfer of an atom (usually an halogen) from a 'dormant' initiator or polymeric chain to a transition metal complex. The transition metal is oxidised when the halogen atom is transferred and a free radical is generated. Polymerization is propagated by the addition of monomer molecules to the thus generated free radicals (**Scheme 1.3**). Since the dormant state of the polymer is preferred in this equilibrium, side reactions including undesired termination are suppressed and a well control in the molecular weight and polydispersity of the polymers is achieved. ATRP can be mediated by a variety of transition metals from which copper is the most widely employed.

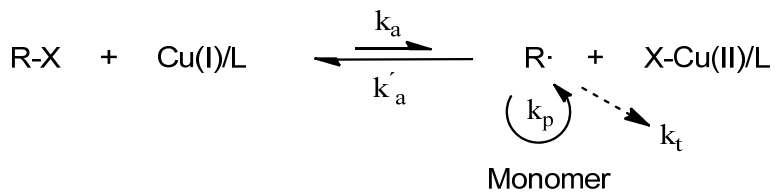

Scheme 1.3 *ATRP polymerization mechanism. X = Halide, L = Ligand*

Alkyl bromides such as 2-bromoisobutyrate derivatives (R-X) as the initiator and Cu(I) metal salts (CuBr or CuCl) in combination with nitrogen ligands such as *N,N,N',N'',N''*-hexamethyltriethylenetetramine (HMTETA), *N,N,N',N'',N''*-penta methyldiethylenetriamine PMDETA or bipyridine ligands are the most commonly catalytic systems used for the ATRP polymerization of azobenzene (meth)acrylates. Keller and coworkers obtained the first azopolymer by ATRP[27] and since then, the technique has been large described for the preparation of azopolymers for different purposes (**Scheme 1.4**).

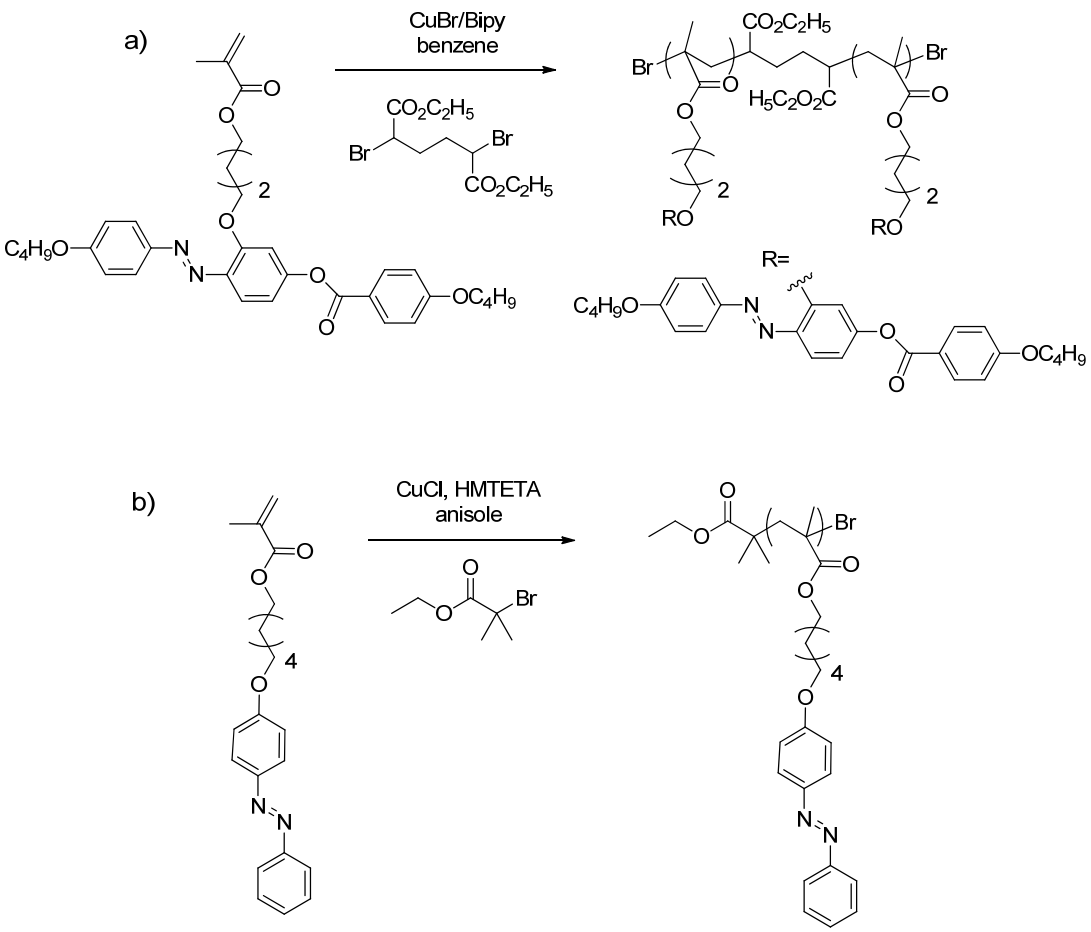

Scheme 1.4 *Examples of azopolymers obtained by ATRP*[27,28]

RAFT polymerization was discovered at Commonwealth Scientific and Industrial Research Organisation (CSIRO) in 1998.[29,30] In this polymerization, thiocarbonylthio compounds (RAFT agents), such as dithioesters, thiocarbamates, and xanthates, are employed to mediate the polymerization via a reversible chain-transfer process. The accepted mechanism of the RAFT process consists of a sequence of addition-fragmentation equilibria as it is shown in **Scheme 1.5**. Initiation is achieved by decomposition of an initiator and subsequent propagation. In the early stages of the polymerization, addition of a propagating radical to the thiocarbonylthio compound is followed by fragmentation of the intermediate radical into a polymeric thiocarbonylthio compound and a new radical (R·). Addition of R· to the monomer forms a new propagating radical (Pm·). A rapid equilibrium, i.e. main equilibrium, between the propagating radicals (Pn· and Pm·) and the dormant species results in an

equal probability for all chains to grow and enables the production of narrow dispersity polymers with a thiocarbonylthio end group.

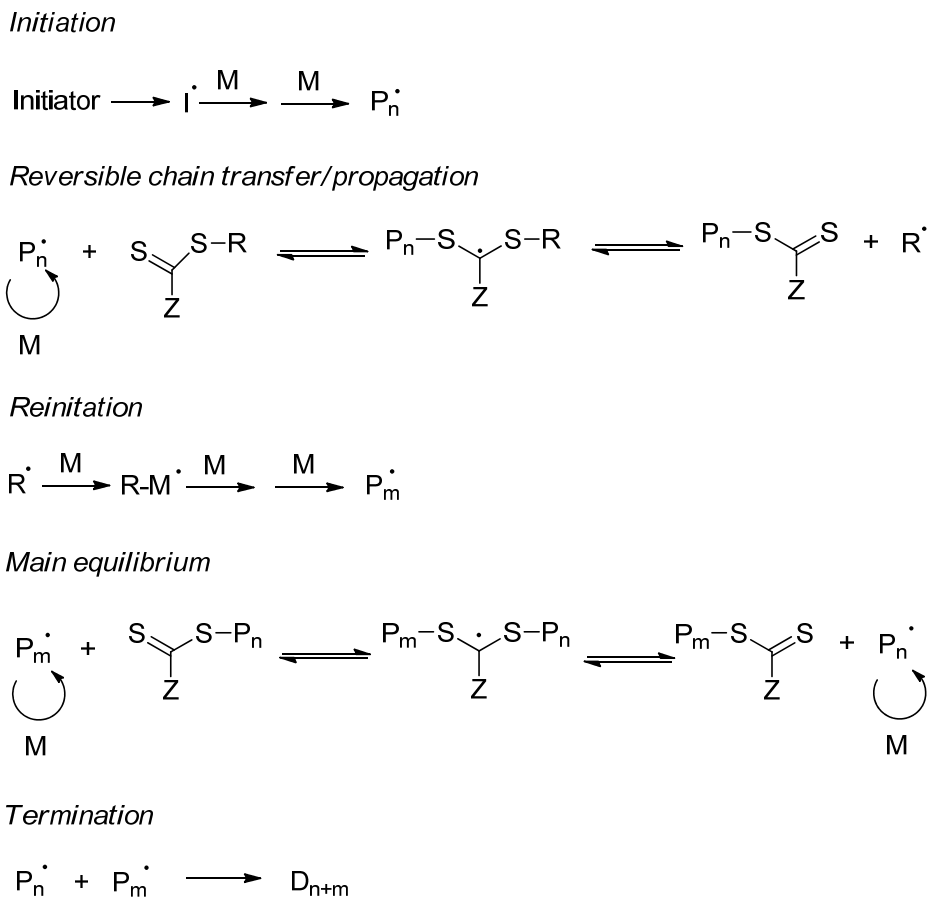

Scheme 1.5 *Accepted mechanism of the RAFT polymerization*

In order to have a good control of the polymerization for a specific monomer, the choice of a suitable RAFT agent is required. Both the R and Z groups of a RAFT agent should be carefully selected (**Table 1.1**). Generally, R· should be more stable than P_n· in order to have an efficient fragmentation and initiation of the polymerization. The structure of the Z group is equally important. Stabilising Z groups such as phenyl moieties are efficient in styrene and methacrylate polymerization, but they retard polymerization of acrylates and inhibit polymerization of vinyl esters. On the other hand, very weakly stabilizing groups, such as $–NR_2$ in dithiocarbamates or –OR in xanthates, are good for vinyl esters but inefficient for styrene.

Table 1.1 *Compatibility of common RAFT agents with different monomers*

RAFT agents	styrenes	acrylates	acrylamides	methacrylates	methacrylamides
$C_{12}H_{25}S$–C(=S)–S–CH$_2$–CN	+++	+++	+++	—	—
Ph–C(=S)–S–C(CH$_3$)$_2$–CN	++	+	—	+++	+++
Ph–C(=S)–S–C(CH$_3$)(CN)–CH$_2$–CH$_2$–C(=O)–OH	++	+	+	+++	+++
$C_{12}H_{25}S$–C(=S)–S–C(CH$_3$)$_2$–CN	+++	++	++	+++	+++
$C_{12}H_{25}S$–C(=S)–S–C(CN)(CH$_3$)–CH$_2$–CH$_2$–C(=O)–OH	+++	++	++	+++	+++
$C_{12}H_{25}S$–C(=S)–S–C(CH$_3$)$_2$–C(=O)–OH	+++	+++	+++	+	+

As an example, **Scheme 1.6** shows a well defined azobenzene homopolymer reported by Zhu and coworkers synthesised *via* RAFT polymerization in anisole and using 2-cyanoprop-2-yl 1-dithionaphthalate as the RAFT agent and AIBN as the initiator.[33]

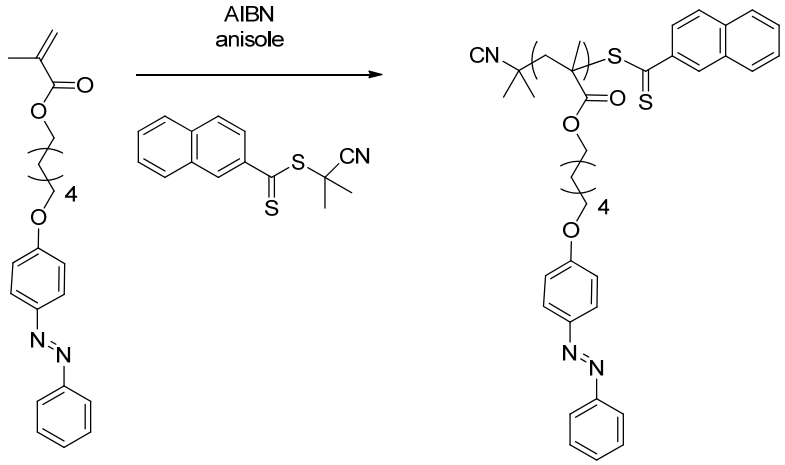

Scheme 1.6 *Examples of an azopolymer obtained by RAFT*[33]

In summary, azomonomers have been successfully polymerized either by ATRP[27,28,31,32] or more recently by RAFT[33-35] polymerizations. In some cases, these monomers not only have been used for the preparation of homopolymers but also for the preparation of copolymers as it will be described in the next section.

1.2.1.2 Synthesis of Azobenzene Homopolymers by Postfunctionalisation

The second approach to achieve azopolymers consists of azobenzene postfuncionalization of an homopolymer having reactive groups in the repeating unit. In this case, highly effective and reliable reactions are required for obtaining polymers having well defined and reproducible macromolecular structure. High yield reactions as azocoupling, esterification and the Schotten-Baumann reaction are some of the reactions employed for azopolymers by postfunctionalisation of polymeric skeletons (**Scheme 1.7**).[36-39]

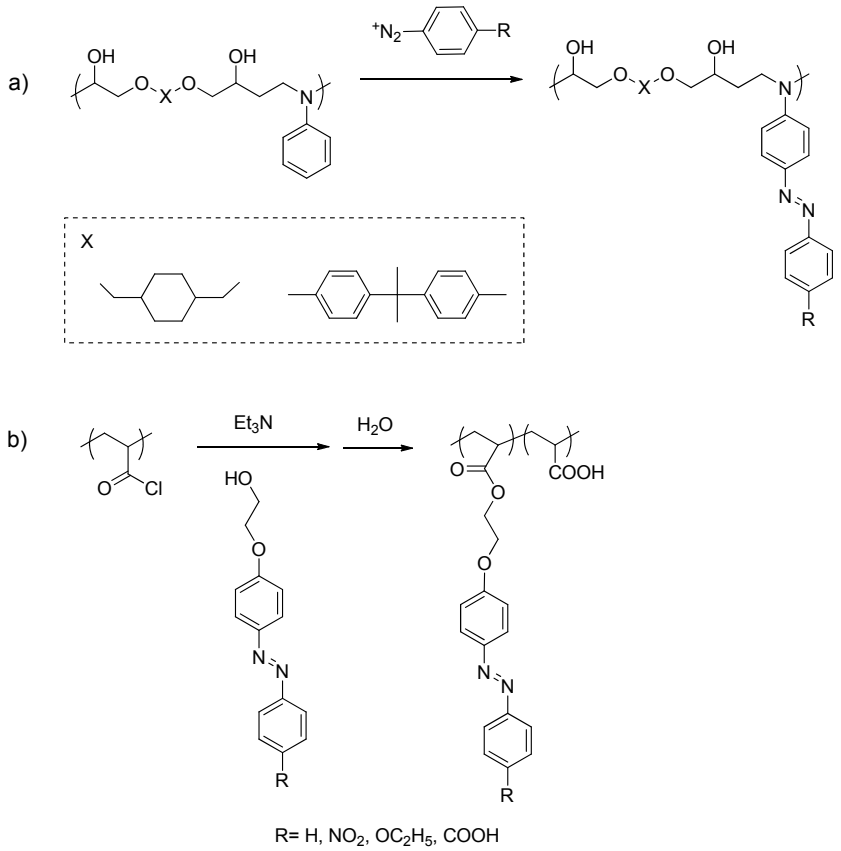

Scheme 1.7 *Examples of preparation of azopolymers by employing a) azocoupling reaction[36] or b) Schotten-Baumann reaction[39]*

Recently, 'Click chemistry' reactions have opened up new possibilities in Materials and Polymer Science. 'Click chemistry' is the term that was introduced by K. B. Sharpless in 2001 to describe reactions which are responding to several criteria.[40] These reactions must be modular, wide in scope, give very high yields and be stereospecific (but not necessarily enantioselective). Furthermore, reaction conditions should be simple and purification, if required, must be by nonchromatographic methods. There are several types of reaction which fulfill these criteria, including the copper(I) catalysed azide/alkyne cycloaddition (CuAAC) reaction,[40,41] thiol-ene,[42-44] Diels-Alder,[45] as well as selected examples of Michael additions[45] (**Scheme 1.8**). CuAAC is one of the most widely employed click reactions to date.[46-48] **Scheme 1.9** shows an example of the preparation of an azobenzene homopolymer by postunctionalization of poly(propargyl methacrylate) employing CuAAC click reaction.[38]

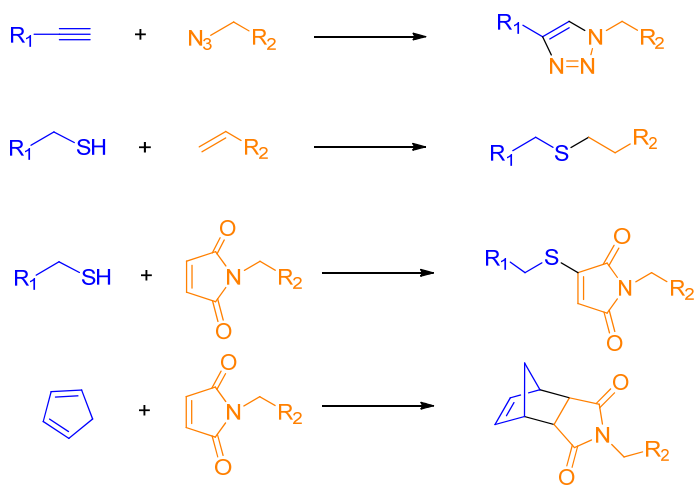

Scheme 1.8 *Examples of click reactions: a) CuAAC, b) thiol-ene, c) Michael adition, d) Diels-Alder*

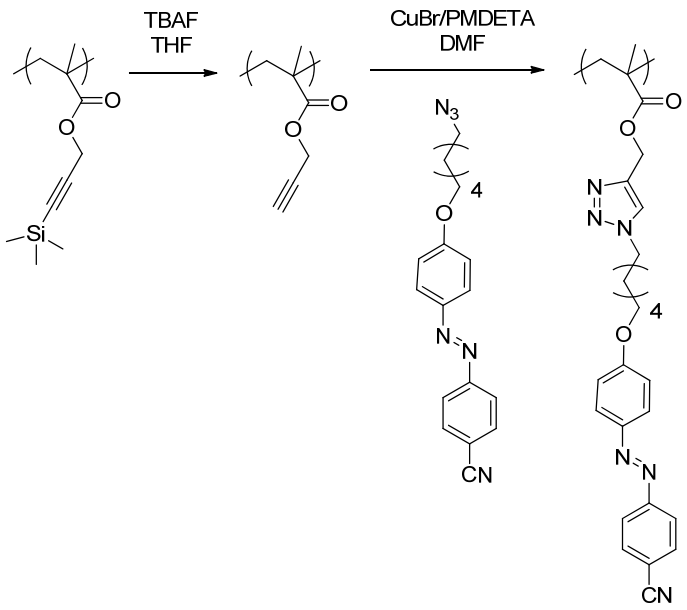

Scheme 1.9 *Example of preparation of an azopolymer by employing CuAAC*[38]

1.2.2 Azobenzene Linear Copolymers

A very simple strategy to control the properties of the final material by copolymerization where the feed molar ratio and structure of the comonomers can be adjusted. Different statistical copolymers which contain, in addition to azobenzene repeating units, monomers of different nature as well as block copolymers (refer to next section) have been prepared for different purposes (**Figure 1.3**).

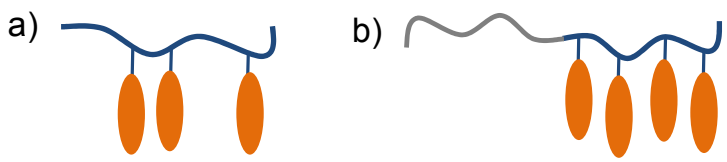

Figure 1.3 *Schematic representations of azobenzene containing a) statistical copolymers and b) block copolymers*

As a representative example, **Figure 1.4** depicts a copolymer described by Ikeda and coworkers.[49] They have successfully prepared random copolymers

with azobenzene and biphenyl or tolane mesogenic moieties, and methyl methacrylate.[49,50] The incorporation of liquid crystalline comonomers as tolane increases th birefringence values achieved by photoorientation of the azobenzene moieties.

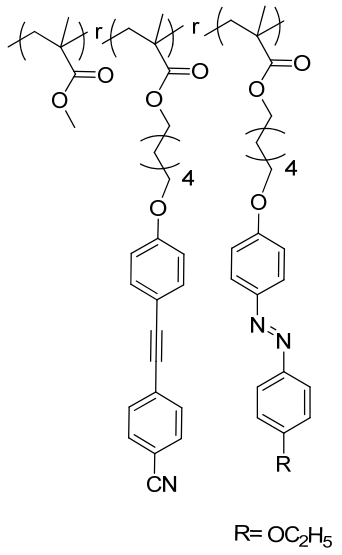

Figure 1.4 *Example of an azobenzene containing random copolymer reported by Ikeda and coworkers*[49]

Preparation of azobenzene containing statistical copolymers does not imply additional synthetic strategies since the polymerization process is conducted under the same experimental conditions than for homopolymers. In the case that the comonomers have similar reactivity, a good agreement between the feed comonomers ratio and the copolymer composition is reached.[51,52] Nevertheless, the preparation of copolymers having a block architecture usually requires a well designed polymerization sequence as it will be shown in the next section.

1.2.2.1 Azobenzene Linear-Linear Block Copolymers

It is well know that BCs are able to undergo microphase separation at the nanoscale leading to well defined morphologies is the solid state. Generally, diblock copolymers can form in the solid state spheres, cylinders, lamellaes or

continues phases. These microstructures can be tuned by adjusting the relative volume fraction of each block (f), Flory-Huggins interaction parameter (χ), and the degree of polymerization (N). **Figure 1.5** shows a typical phase diagram of a coil-coil diblock copolymer. Furthemore, amphiphilic BC are able to self-assemble in solution forming different nanostructures such as micelles, nanospheres, vesicles among others (see Section 1.3.2).[53-58]

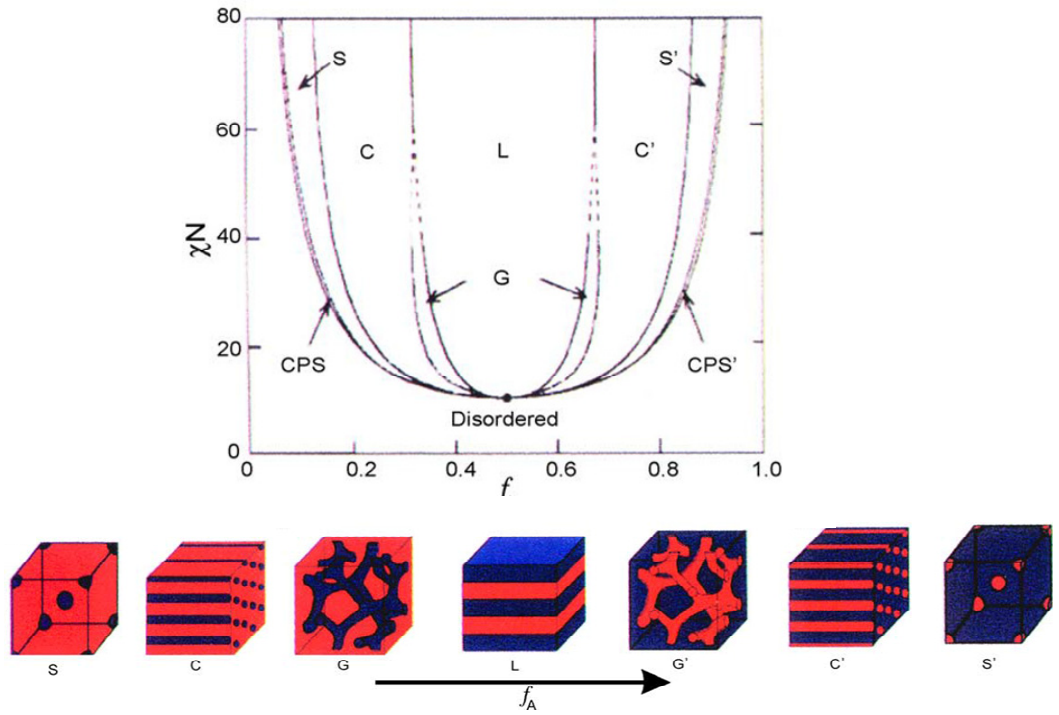

Figure 1.5 *Schematic diblock copolymer phase diagram: f= volume, χ= Flory-Huggins interaction parameter and N= degree of polymerization (top). Different nanostructures formed by BCs: S= spheres, C=cylinders, G= gyroid and L=lamellar. (Image adapted from ref.57)*

Azobenzene containing BCs can combine in the same material light responsive properties with self-assembly abilities making the resulting nanostructures of interest in nanotechnology (see Section 1.3).

Linear-linear azobenzene BCs can be approached by several general strategies as it is collected in **Scheme 1.10**. Direct polymerization of azomonomers by using a macroinitiator composed of a non azopolymer is the strategy most widely used for the preparation of these BCs (**Scheme 1.10a**). More specifically, ATRP macroinitiators based on poly(ethylene glycol) (PEG)[59,60],

poly(methyl methacrylate) (PMMA)[61-63], poly(n-butyl methacrylate) (PBA)[64] as well as polystyrene (PS)[65-67] among others, have been employed for the polymerization of azomonomers (**Figure 1.6**). Besides, the alternative strategy, i.e the use of an azopolymer as the macroinitiator for the polymerization of conventional monomers, usually lead to poor results as it was reported by our research group.[61] More recently studies have employed RAFT polymerization for the preparation of these BCs by using a macromolecular chain transfer agent composed either poly(acrylic acid)[68] or poly(*N*-isoporopylacrylamide) (PNIPAM)[69] to obtain the BCs shown in **Figure 1.7**.

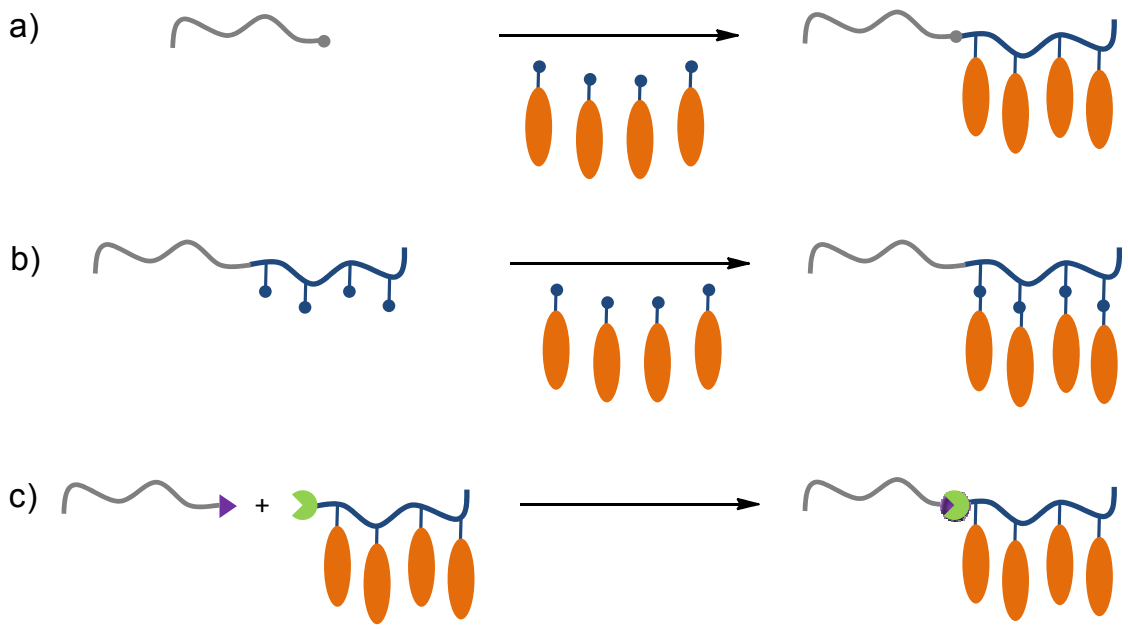

Scheme 1.10 *General synthetic approaches for the synthesis of azobenzene containing BC: a) direct polymerization by using a macroinitiator b) postfunctionalization of a conventional BC and c) coupling of preformed building blocks*

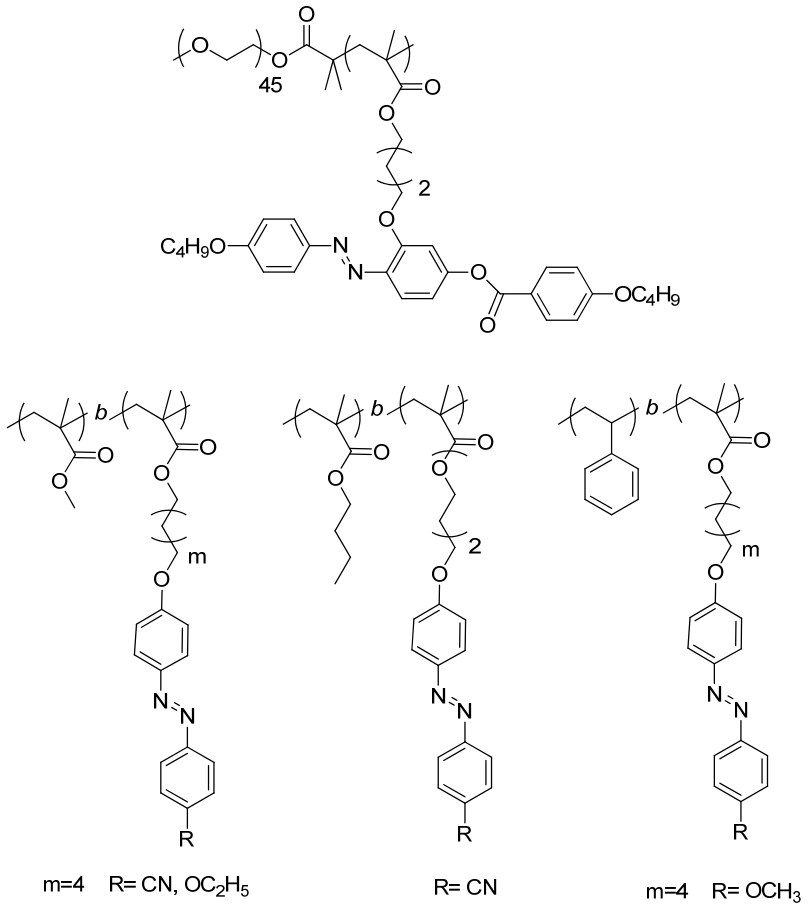

Figure 1.6 *Examples of azobenzene BCs prepared by ATRP polymerization*[42-50]

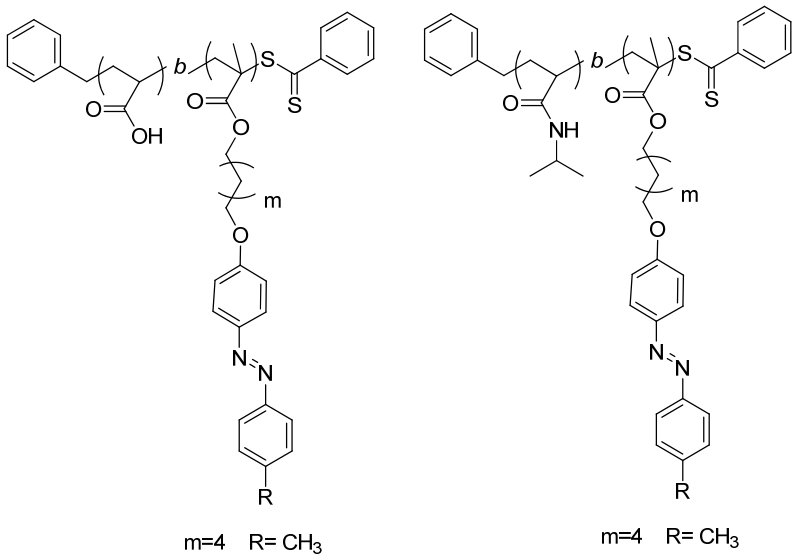

Figure 1.7 *Examples of azobenzene BCs prepared by RAFT polymerization*[68-69]

Azobenzene units can also be also introduced in a BC architecture by a postfunctionalisation reaction (**Scheme 1.10b**). For this purpose, the previously synthesised BC should contain one block with reactive groups. By this approach, Gronski et al. prepared the first liquid crystal BC.[70] Some years later, the same strategy was used by Schmidt and coworkers for the preparation of azobenzene containing block copolymers (**Scheme 1.11**).[66] Firstly, the polybutadiene block was converted in a polyalcohol by hydroboration and finally the hydroxyl groups were functionalised with azobenzene units by an esterification reaction.

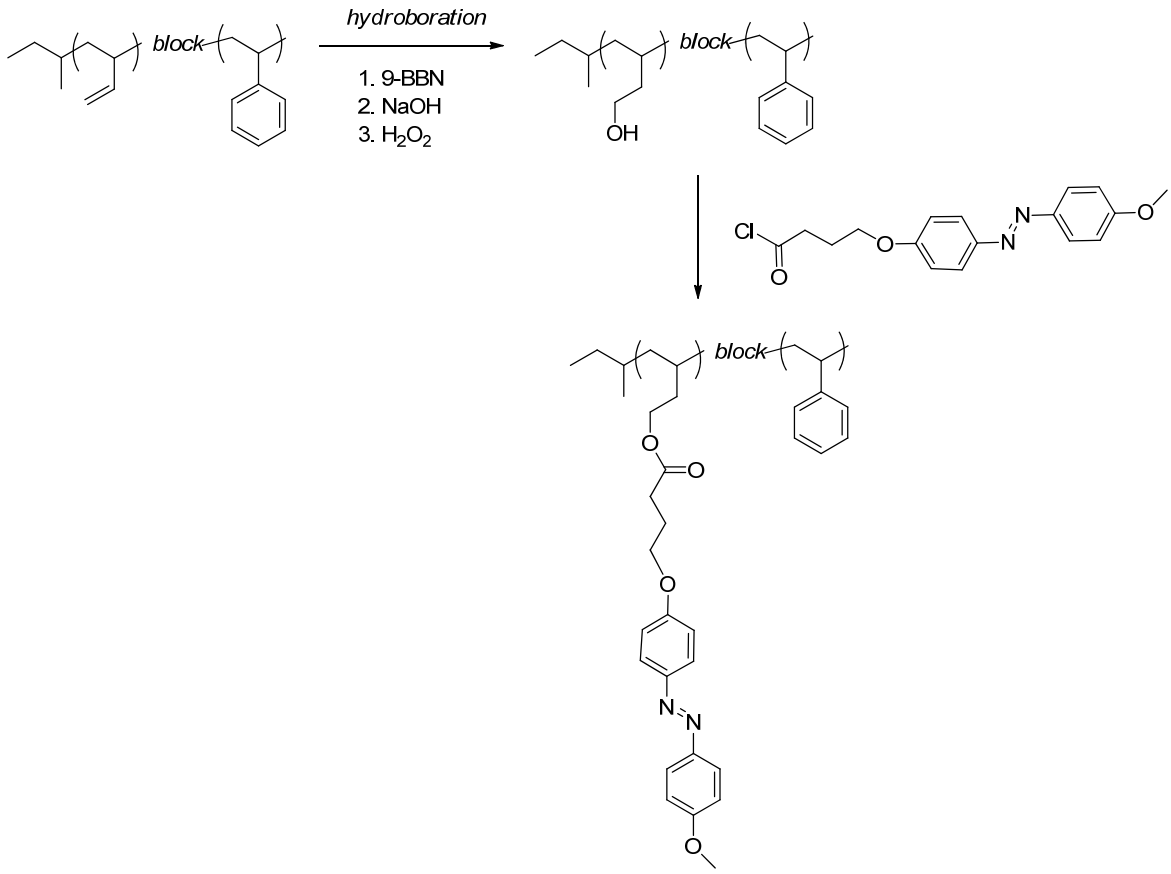

Scheme 1.11 *Synthesis of an azobenezene BC by postfunctionalization*[66]

The last possibility consists of the coupling of two blocks previously prepared (**Scheme 1.10c**). This strategy requires the synthesis of polymers containing complementary end-chain group allowing the subsequent coupling. Although this is the most versatile synthetic approach, it relies on the availability of highly

efficient and selective chemistry under mild conditions, which are the main features of the 'click chemistry' reactions. Combination of controlled radical polymerization that allows the synthesis of polymers with reactive ending groups, and 'click chemistry' is the best option for this approach as was recently demonstrated in the example collected in **Scheme 1.12**. On one hand, PMMA was synthesised by using an ATRP initiator containing an azide group, and on the other hand an azopolymer was also prepared by ATRP but using an initiator containing a complementary alkyne group. Both blocks were finally coupled by CuAAC reaction.

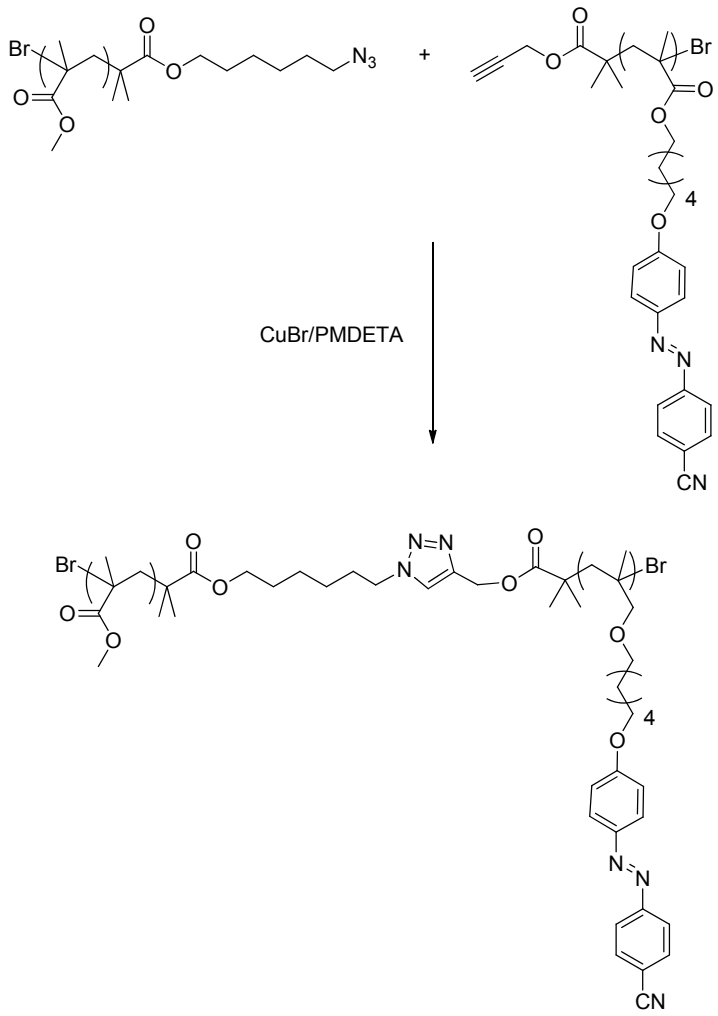

Scheme 1.12 *Synthesis of an azobenzene BC by CuAAC*[71]

1.2.3 Other Azobenzene Macromolecular Architectures

Most of the reported azopolymers possess a linear structure. Nevertheless, other azobenzene macromolecular architectures have also been studied (**Figure 1.8**). In the next sections, a general overview about dendritic structures, linear-dendritic BC (LDBC) and miktoarm star polymers will be presented since they are connected (in particular linear-dendritic BC and miktoarm) with the materials aimed in this thesis.

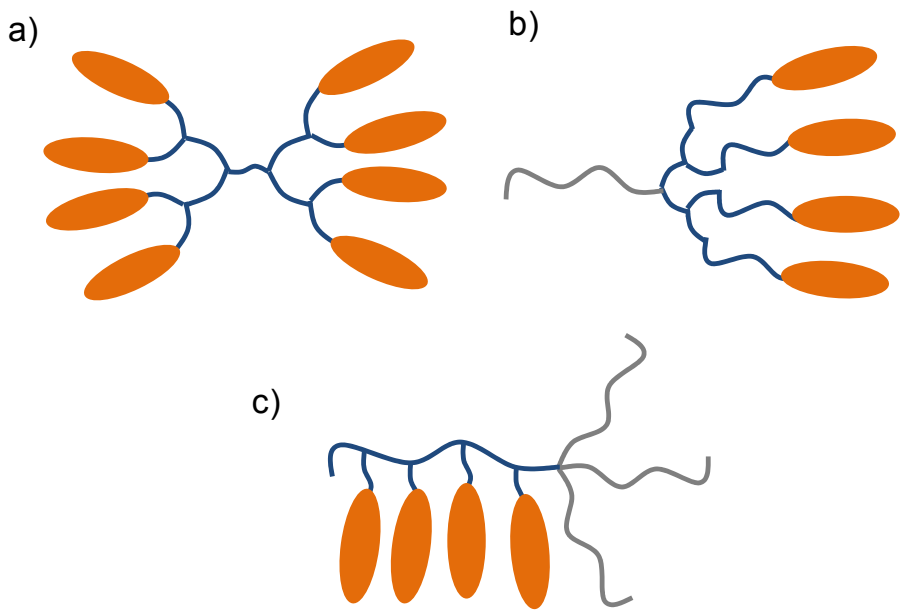

Figure 1.8 *Azobenzene containing macromolecular structures: a) dendrimer, b) linear-dendritic BC and c) miktoarm star polymer*

1.2.3.1 Dendritic Structures

Dendritic structures like dendrimers and dendrons are one of the most promising polymeric structures and have been the object of a growing number of publications. [72-75] Dendrimers are highly branched monodisperse molecules with a nanometric size. Their unique nature, shape and size make them ideal as for interesting applications in different field as catalysis, biology and materials science.[72,73] Numerous dendritic structures have been synthesised and studied, including poly(amidoamine), poly(amide), poly(phenyl ether), and carbosilanes.[74,75]

During the last years, photoresponsive dendrimers have also been studied as an alternative to conventional linear azopolymers due to their potential applications. There are several reviews focused in these materials, including azobenzene functionalised dendrimers.[76-78] The azobenzene moieties can be located in different positions of the dendritic structure. However, dendrimers having azobenzene moieties linked to periphery is the most frequent case. Poly(propilenimine) (PPI) is the most employed dendrimer for the preparation of azodendrimers (**Figure 1.9**).[79-82] Due to the presence of amino groups at the periphery of these dendrimers, azobenzene moeites can be incorporated *via* amide linkages in most of the cases. Bifunctional codendrimers containing alkyl chains as well as other functional moieties as biphenyl or naphtyl have also been prepared.[80,82]

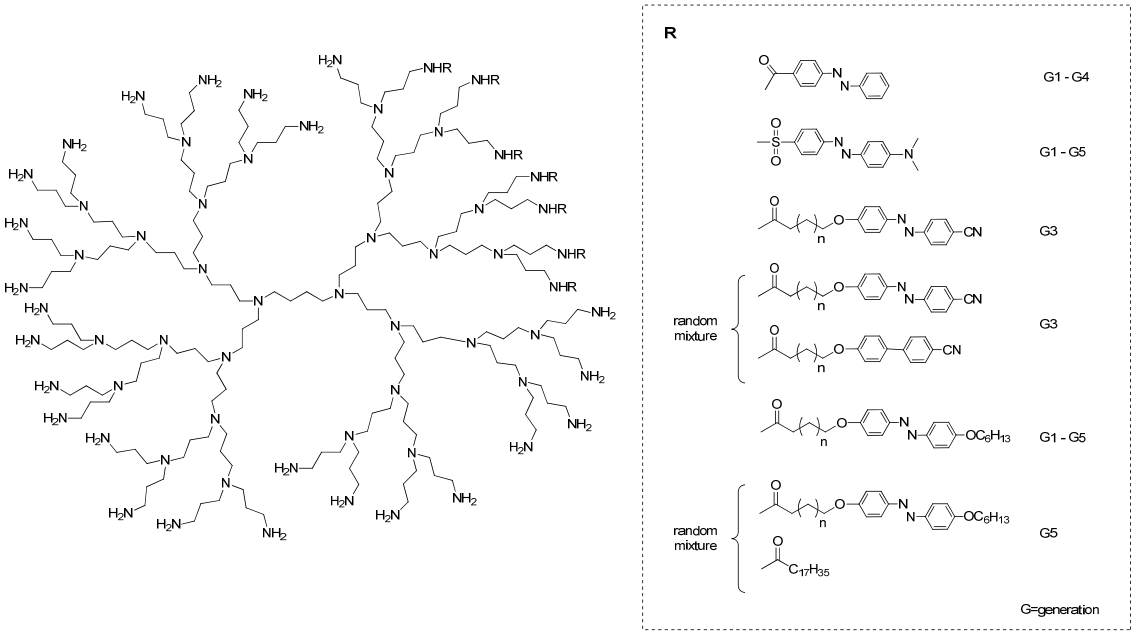

Figure 1.9 *Examples of azobenzene functionalizated PPI dendrimers*[79-82]

Other families of dendrimers such as poly(amidoamine) (PAMAM) have also been used for the preparation of azobenzene containing dendrimers.[83,84] Similarly to PPI dendrimers, azobenzene units were incorporated into the dendrons *via* amide bond formation. In some cases, the resulting azobenene containing dendrimer was not fully functionalised.[84]

In general, one of the main advantage of dendrimers is that the number of functional units introduced in the dendritic structure is better controlled than in the case of linear polymers. Dendritic and linear macromolecules can be combined in BCs containing both architectures. These new materials will be briefly reviewed below.

1.2.3.2 Linear-Dendritic Block Copolymers

Linear-dendritic BCs (LDBC) are hybrid structures composed of a linear polymer block and a dendritic block. This new architecture was first introduced by Gitsov and Fréchet[85-87] and might leads to substantial changes in some properties, such as solubility, intrinsic viscosity or microphase segregation among others, in comparison with the conventional linear-linear BC.[89]

There are three strategies used for the synthesis of these copolymers:[87] 'chain-first' route, 'dendron-first' route and the coupling of the preformed blocks, as it is collected in **Scheme 1.13**.

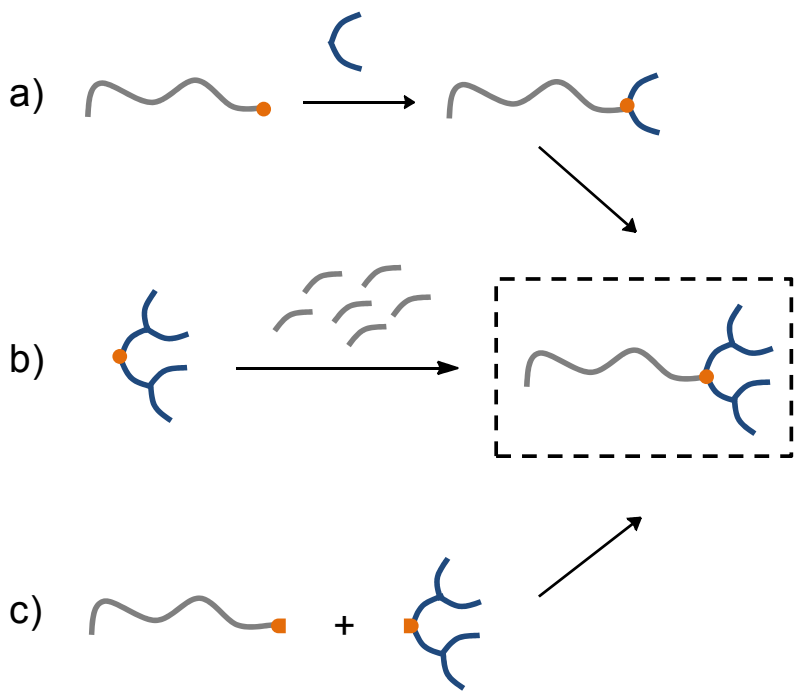

Scheme 1.13 *Synthetic approaches for the preparation of LDBC: a) 'chain-first' strategy, b) 'dendron-first' strategy and c) coupling strategy*

The **'chain-first' route** consists in the synthesis of a linear polymer having a reactive end group polymer that can be used for a divergent dendron construction (**Scheme 1.13a**). One of the first examples was reported by Meijer *et al*. by combining anionic polymerization and the divergent synthesis of PPI dendrimers.[88] Similarly, Hammond et *al*. prepared LDBC by using the amino group terminated methoxy-poly(ethyleneglycol) to grow Tomalia type dendrons on the linear chain.[89] Although the first examples were prepared following this strategy, it is not the most common strategy employed for the synthesis of these copolymers.

The **'dendron-first'** route implies that the dendron acts as the initiator for the polymerization of the linear block (**Scheme 1.13b**) and it is the most widely employed strategy so far. This concept was developed by Matyjaszewski as well as Hawker and Fréchet by using polyether dendrons as macromolecular initiators for the controlled free radical polymerization of vinyl monomers. In particular, polyether dendrons containing a benzylic 2,2,6,6-tetramethyl-1-piperidinyloxy (TEMPO) group at their focal point have been used for the nitroxide mediated polymerization of styrene (**Scheme 1.14**).[90] The ring opening polymerization (ROP) of lactones initiated by dendrons was also explored by several groups.[91,92]

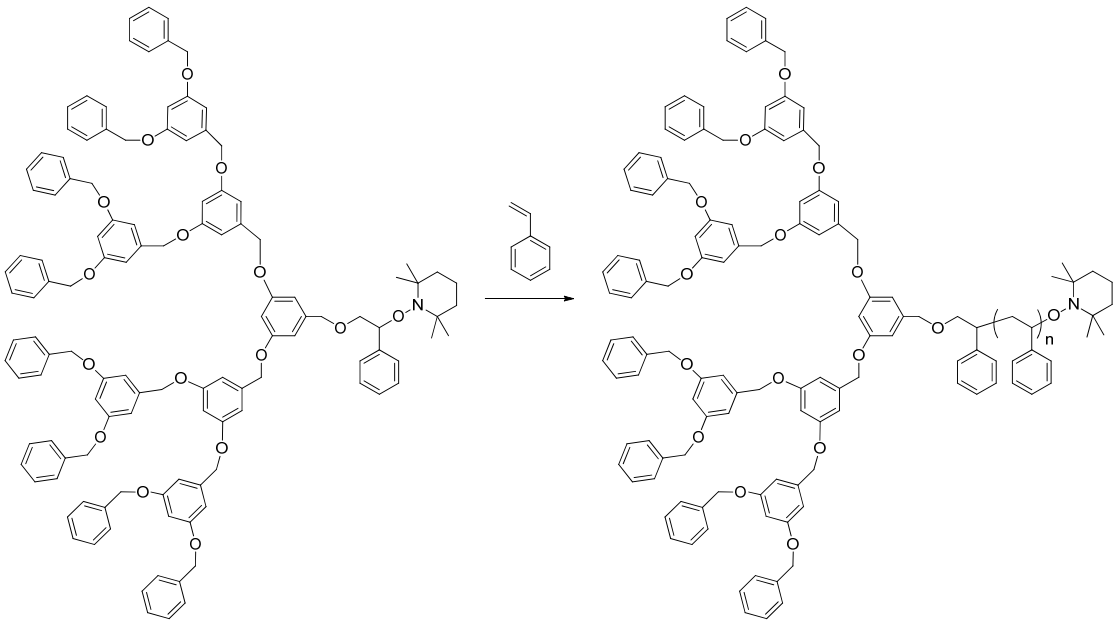

Scheme 1.14 *Example of the synthesis of a LDBC by employing the 'dendron-first' strategy*[90]

The **coupling strategy** requires the previous synthesis of the linear and dendron segments, followed by their coupling through complementary functional groups located at the end position of the linear chain and the focal point of the dendron (**Scheme 1.13c**). Although this seems to be the most versatile synthetic approach for the preparation of LDBCs, it relies on the efficiency of the coupling reaction. Initially, Williamson as well as palladium catalysed reactions were used for the coupling of different preformed blocks.[93,94] The first reported example was based on the reaction of 'living' poly(styrene) dianion with aryl ether dendrons having a benzyl bromide group at the focal point.[95] During the last years, the intense research in 'click chemistry' reactions rendered more effective coupling reactions for the preparation of these LDBCs.[96,97] **Scheme 1.15** shows an example of the synthesis of LDBC following this strategy. A dendritic block with a clickable alkyne group was first synthesised by ROP of ε-caprolactone monomer using a propargyl focal point dendrons and coupled by a click reaction with azide functionalised PEG.

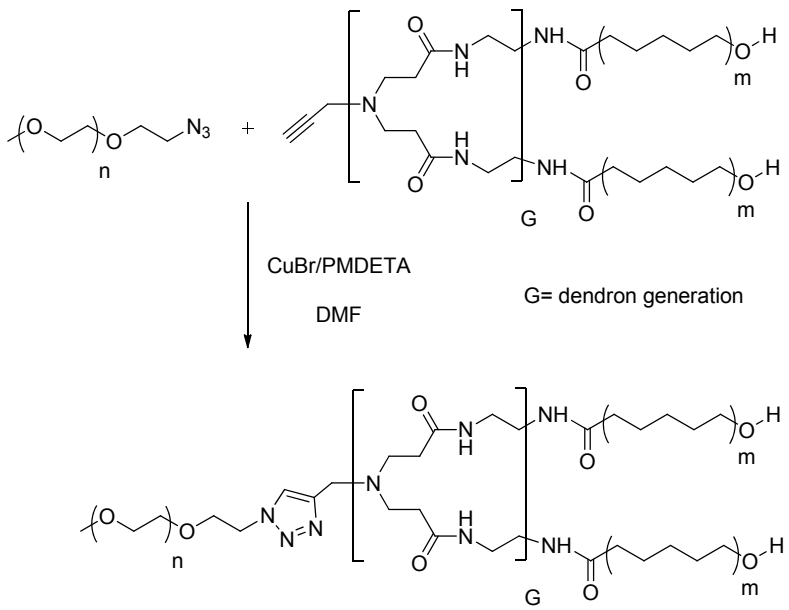

Scheme 1.15 *Example of the synthesis of a LDBC by employing the coupling strategy*[96]

As it was alrealy mentioned, one of the main advantages of the dendritic structure is the possibility of including functional moieties at the periphery. By incorporating azobenzene moieties at the periphery of a dendron, a very precise control can be exerted on the number of the photoresponsive units introduced in the macromolecule. Furthermore, using this approach the radical polymerization of azomonomers is avoided. In the last years, our research group has studied a series of photoresponsive LDBCs with azobenzene units by coupling the first four generations of dendritic aliphatic polyesters based on 2,2-di(hydroxymethyl)propionic acid (bis-MPA) functionalised at the periphery with 4-cyanoazobenzene moieties to either PEG or PMMA linear segments (**Figure 1.10**).[97-99] The LDBCs were successfully obtained by a CuAAC reaction between the azodendron bearing an azido group at the focal point and the alkyne terminated linear block. Recently, similar amphiphilic LDBCs were also reported by Shi *et al*. by combining PEG as the linear block and different generations of 4-octyloxyazobenzene functionalised PPI dendrons.[100,101]

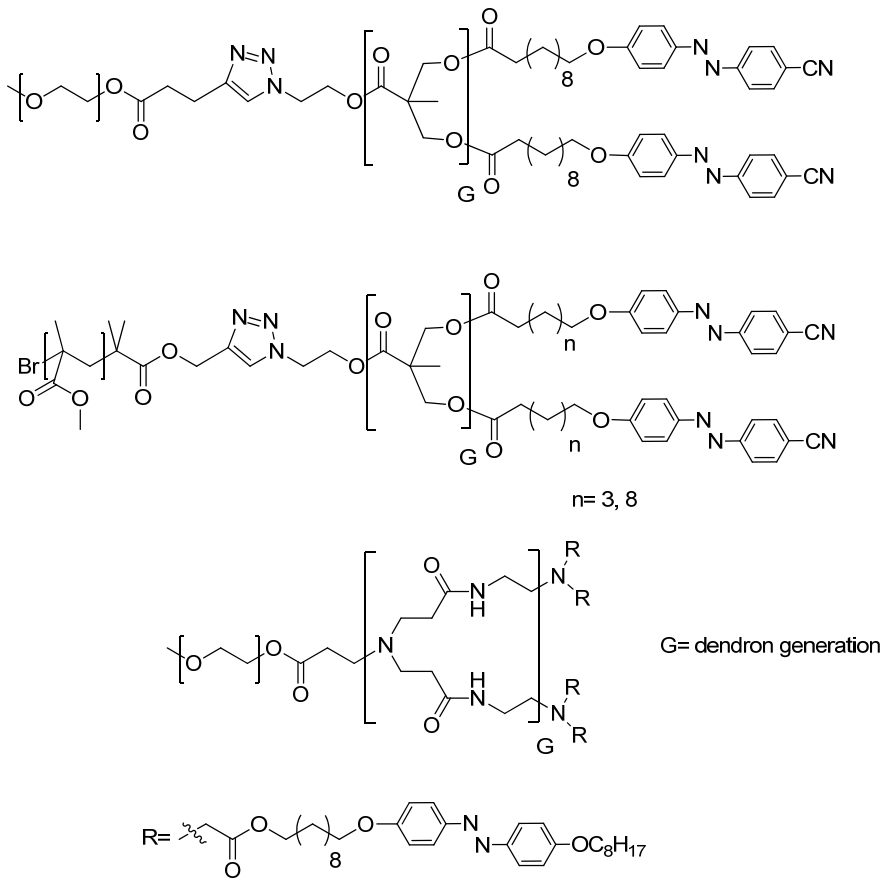

Figure 1.10 *Chemical structure of the azobenzene containing LDBCs described* [97-101] *(G represents the generation of the dendron)*

1.2.3.3 Miktoarm Star Polymers

Star branched polymers are defined as polymers having more than three polymer segments (arm segments) radiating from a core.[102] Their globular shape with multiple chain ends is responsible for their unique properties. Star polymers possess lower glass transition temperature, higher solubility and lower viscosity compared to linear analogous with the same molecular weights.[102-104] Miktoarm star polymers, also known as miktoarm polymers, have a relatively new polymeric architecture containing two or more arm species with different chemical compositions and/or molecular weights. Similar to BC, miktoarm star polymers are expected to self-assemble due to their immiscible different arm segments making them promising candidates for different applications.

There are several approaches that can be employed for the synthesis of star polymers such as 'arm-first', 'core-first' and coupling strategy. In the case of miktoarm star polymer, the preparation of the polymer is strongly dependent of the number of arms of the polymer as well as the number of different polymers of which is composed. In **Scheme 1.16** two general methods for the preparation of AB_2 miktoarm star polymers are shown as an example.

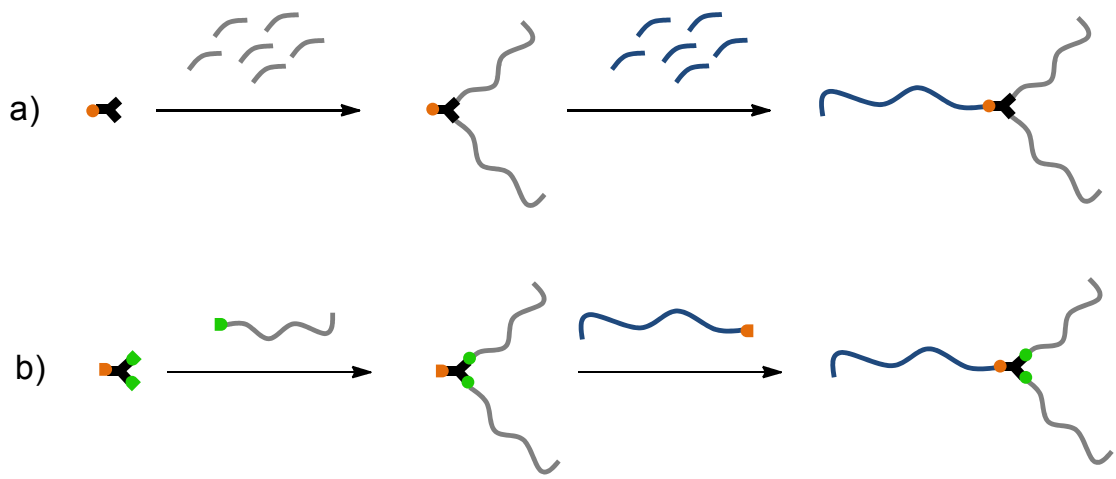

Scheme 1.16 *Synthetic approaches for the preparation of AB_2 miktoarm star polymers: a) 'core-first' strategy and b) coupling strategy*

The **"core first"** strategy consist of the synthesis of a multifunctional initiator which will act as the core (**Scheme 1.16a**). The arms can be grown by a combination of different polymerization techniques, such as living anionic polymerization, CRP or ROP. In this method, orthogonality plays an important role in the design of the multifunctional initiator. By using this strategy, several AB_2 miktoarm star polymers combining ROP and ATRP have been synthesised.[105]

The **coupling method** (**Scheme 1.16b**) consists of the coupling of a polymeric arms containing a functional end group to a multifunctional core by using highly efficient reactions. Orthogonality also plays an important role in this strategy. Many different click reactions, such as CuAAC, thiol-ene and Diels-Alder reactions, has been used.[106,107]

Only a few examples of azobenzene containing photoresponsive miktoarm polymers have been reported so far (**Figure 1.11**). He *et al.* described novel liquid crystalline miktoarm polymers composed of PEG, PS and azobenzene side chain poly(methacrylate) of various lengths [MPEG-*b*-PS-$(PMMAZO)_2$].[108,109] Firstly, a PEG macroinitiator was used for the synthesis of MPEG-*b*-PS by ATRP. Then, the bromo end groups of the resulting BCs (a consequence of the ATRP technique) were substituted in order to introduce two ATRP initiating points. In the final step, the azobenzene containing monomer was polymerized to form the target miktoarm polymers. Recently, the same authors have also reported similar photoresponsive ABC miktoarm terpolymers (MPEG)(PS)(PMMAZO).[110]

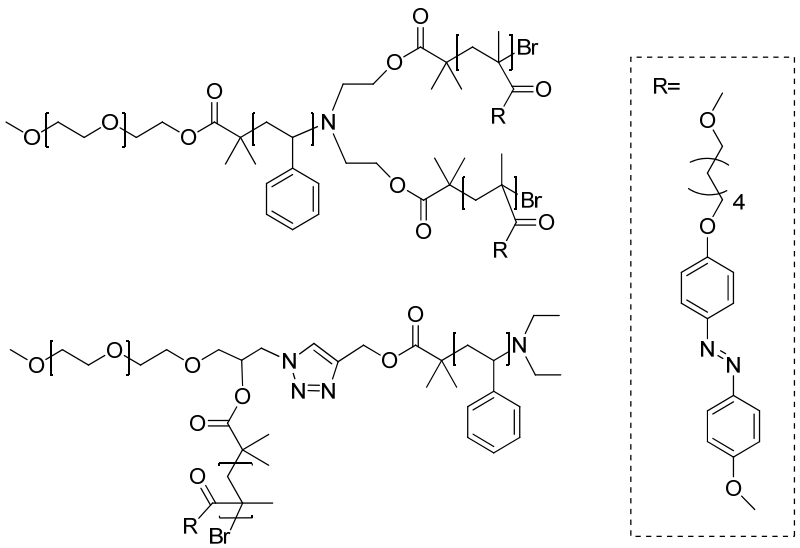

Figure 1.11 *Examples of azobenzene containing miktoarm polymers*[108-110]

1.3 Azopolymers: Photoresponsive Properties & Applications

1.3.1 Photoresponsive Properties in Bulk

Photoinduced isomerisation of azobenzenes can lead to a molecular reorientation by using linearly polarised light (LPL). In this situation, the probability of isomerisation is proportional to $\cos^2\alpha$, being α the angle between the light polarisation vector and the transition moment, which is parallel to the long axis of the azobenzene molecule. Consequetly, only azobenzene units having a parallel component to the polarisation direction of the excitation light will be excited by the incident light and the probability of isomerisation of azobenzene units that are perpendicular to the polarisation direction will be null. Since *trans*-to-*cis* back isomerisation is equal in all directions, after several cycles of *trans-cis-trans* isomerisation, azobenzene units are preferably oriented in a perpendicular plane to the polarisation direction of the excitation light producing optical anisotropy. This effect is known as *Weigert effect* and it is in the origin of the photoinduced dichroism and birefringence of azomaterials (**Figure 1.12**).

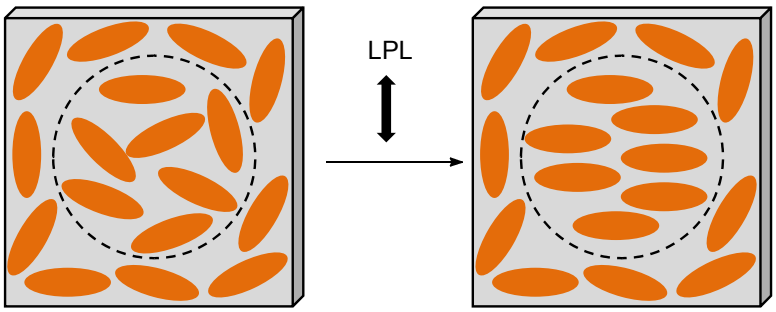

Figure 1.12 *Schematic representation of azobenzene alignment by Weigert effect*

When azobenzene is incorporated into a polymer, the photoisomerisation can provoke an increase in the orientation of the photoresponsive moieties.[10] This property leads to several applications such as optical storage or photochemical actuators among others as it will be briefly presented in the next sections.

1.3.1.1 Optical Storage

Over the last decades, development in digital technologies has required the use and storage of large amounts of data. Different technologies are being used for data storage, although optical data storage has had a great impact on our daily life. Compact disc (CD), digital versatile disc (DVD) and Blue-ray disc (BD) are broadly extended. A promising way to increase storage capacity is holographic storage.[111-116] With this method is possible to record information in a photosensitive media by recording an optical interference pattern. Several polymeric materials such as photopolymers or photorefractive polymers[117,118] have been proposed for these application although photochromic polymers and in particular, azopolymers have been widely investigated.[114,115]

A variety of homopolymers with azobenzene units has been prepared and good values of photoinduced birefringence were achieved. Nevertheless, an essential requirement of materials for optical holographic storage is the preparation of thick films having hundreds of microns. Due to the high absorption of the chromophore, films with a high content of azobenzene have a large absorption and the recording light cannot penetrate more than few micrometers through the film making these materials not suitable for volume holography. To circumvent this problem, dilution of the azobenzene content has been done by different strategies such as the random copolymerization with monomers (**Figure 1.13a)**, either non mesogenic or mesogenic ones, that do not absorb the recording light or the preparation of block copolymers (**Figure 1.13b**) with a photoresponsive block and a non absorbing one.

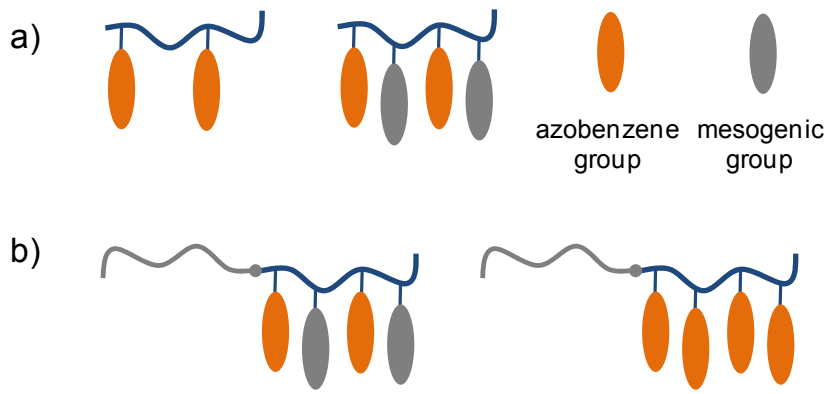

Figure 1.13 *a) Statistical copolymers containing azobenzene and a non absorbing monomer or mesogenic group and b) block copolymers*

Statistical polymers composed of azobenzene and non absorbing monomers like methyl methacrylate have been prepared.[62,121] However, the main drawback of this approach is the lack of stability of the photoinduced birefringence, due to the lack of cooperative interactions between the azobenzene units. An alternative strategy, also based in statistical copolymerization, is the use of non absorbing mesogenic comonomers (**Figure 1.13a**). Bieringer and coworkers prepared a series statistical copolymers from azobenzene and mesogenic phenyl ester monomers (**Figure 1.14**).[122] Other examples using different mesogenic moieties like tolane (**Figure 1.4**) and biphenyl (**Figure 1.14**) have been also employed for the exploration of this approach.[49,50] The presence of these mesogenic groups does not contribute to the absorption at the same wavelength as azobenzene, but they can be oriented because of cooperative motions helping to increase the stability of photoresponse. Thick films with low absorption and good optical response have been prepared although the liquid crystalline character of the materials can give problems associated to light scattering.

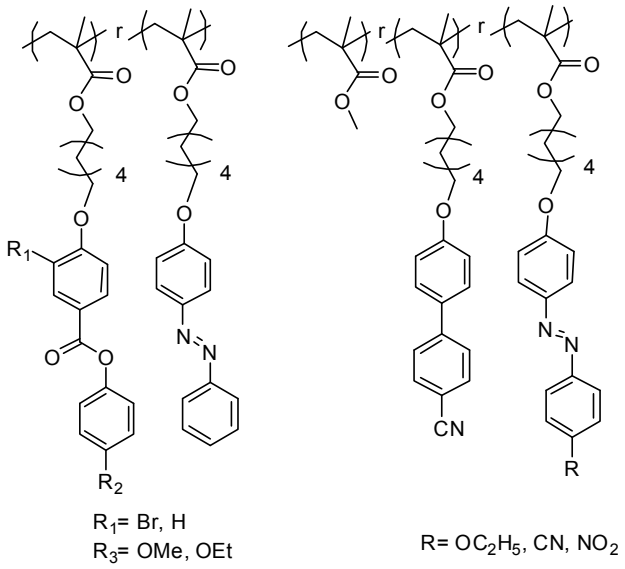

Figure 1.14 *Examples of random copolymers containing azobenzene units for optical data storage*[50,122]

A promising strategy is the use of BCs, in which one of the the block contains azobenzene units while the other one contains units that do not absorb at the recording/writing wavelength (**Figure 1.13b**). As it was noted above, BCs are able to undergo phase segregation. The advantage of this segregation is that azobenzene moieties are confined in nanometric regions preserving cooperative interactions between chromophore units. These domains are smaller than the recording wavelength and light scattering can be avoided. The expected behaviour of the chromophores in the BCs should be similar to the photoresponse of the corresponding homopolymers as it was demonstrated by our research group.[61] Most of the reported azobenzene BCs are copolymers where the non absorbing block is either PMMA[61,63] or PS (**Figure 1.15**).[66,67] The photoresponsive block can be composed of an azobenzene hompolymer or a random copolymer containing azobenzene unit and non absorbing groups.[61,63,66,123] The influence of the morphology of the microdomains as well as the length of the block in the photoinduced response has been investigated in these materials as optical storage media.[114,115] Volume holograms with high efficiency and good stability have been recorded in this materials or blends from these BCs in an attempt to achieve photoresponsive materials with very low contents of photochromic units.[66,71]

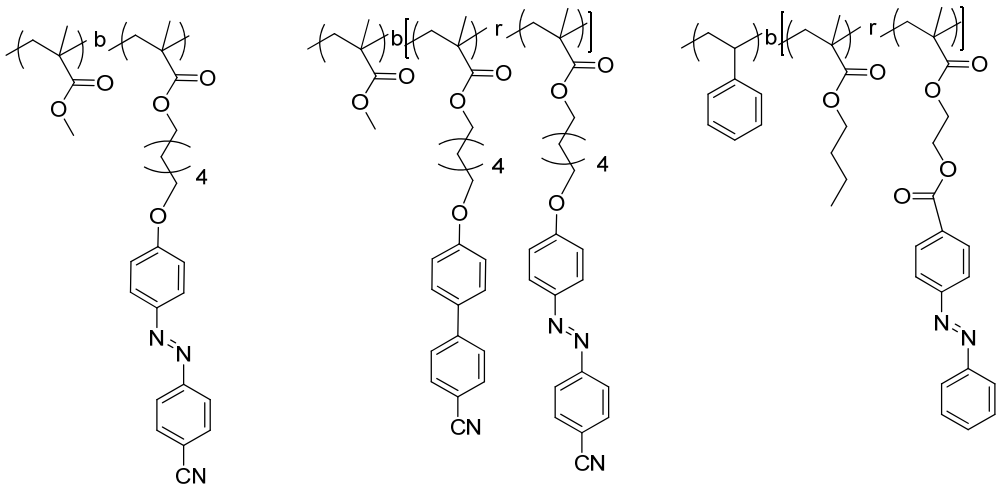

Figure 1.15 *Examples of linear-linear BC with azobenzene and mesogenic monomers* [61,63,66]

Recently, our research group explored a novel architecture, i.e. LDBCs allowing to combine the segregation ability of BCs and an exact control of the number of azobenzene units introduced per macromolecule. Several photoresponsive LDBCs have been prepared composed of dendritic aliphatic polyesters based on bis-MPA functionalised at the periphery with 4-cyanoazobenzene moieties and PEG or PMMA (**Figure 1.10**).[97,98]

1.3.1.2 Photomechanical Actuators

Another application of interest in azopolymers is the preparation of phomechanical actuators. It is well known that nematic elastomers are able to change their shape due to the nematic to isotropic transition in the material. By incorporating azobenzene moieties into an elastomer, photoinduced contractions/expansions have been observed.[124] Upon UV irradiation, azobenzene nematic elastomers suffer a reduction in alignment order as a result of the *trans*-to-*cis* isomerisation. While the rodlike *trans*-azobenzene moieties stabilise the liquid crystalline alignment, the bent *cis* forms can provoke a nematic to isotropic transition being the motor of the macroscopic contraction (**Scheme 1.17**). This deformation is reversible upon *cis*-to-*trans* back isomerisation.

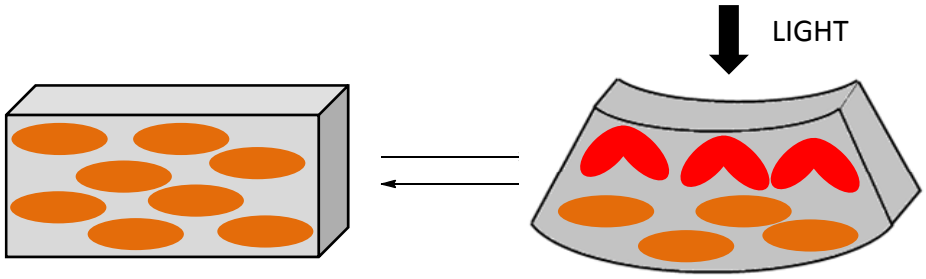

Scheme 1.17 *Schematic representation of a photoinduced deformation in an azobenzene elastomeric film*

Pioonering studies of Finkelmann and coworkers demonstrated experimentally and theoretically that large shape changes in azobenzene containing polysiloxanes based elastomers can be generated by UV irradiation.[125] Keller and coworkers first reported the synthesis of nematic azobenzene side chains elastomers by photopolymerization.[126] The polymeric films showed a fast (less than 1 min) photoinduced contraction up to 18% by irradiation with UV light (**Figure 1.16**).

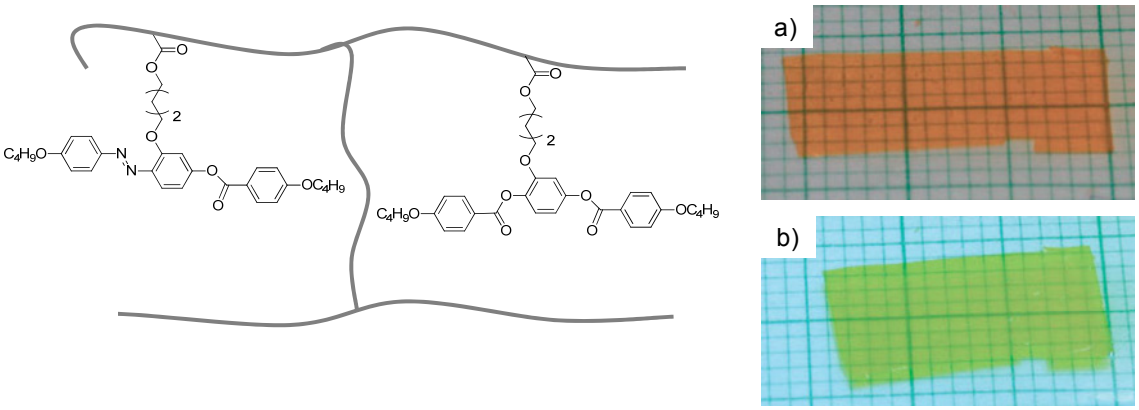

Figure 1.16 *Schematic representation of the elastomer prepared from a mixture of an azobenzene monomer, a liquid crystal monomer and 1,6-hexanediol diacrylate as crosslinker (left). Photographic frames (right) of the film (25%azo) a) before UV irradiation b) under UV irradiation (130s)*[126]

Ikeda and coworkers have also been intensively working in this field.[124,127,128] As an example, in a pioneering work they reported the preparation of films by

thermal polymerization of a liquid crystalline monomer and a diacrylate crosslinker both of which possessed azobenzene moieties.[129] Upon UV irradiation (366 nm), the film bent towards the direction of light with the bending occurring parallel to the direction of light polarisation. When the bent film were exposed to visible light (540 nm), the film was able to recovered its initial flat state (**Figure 1.17**).

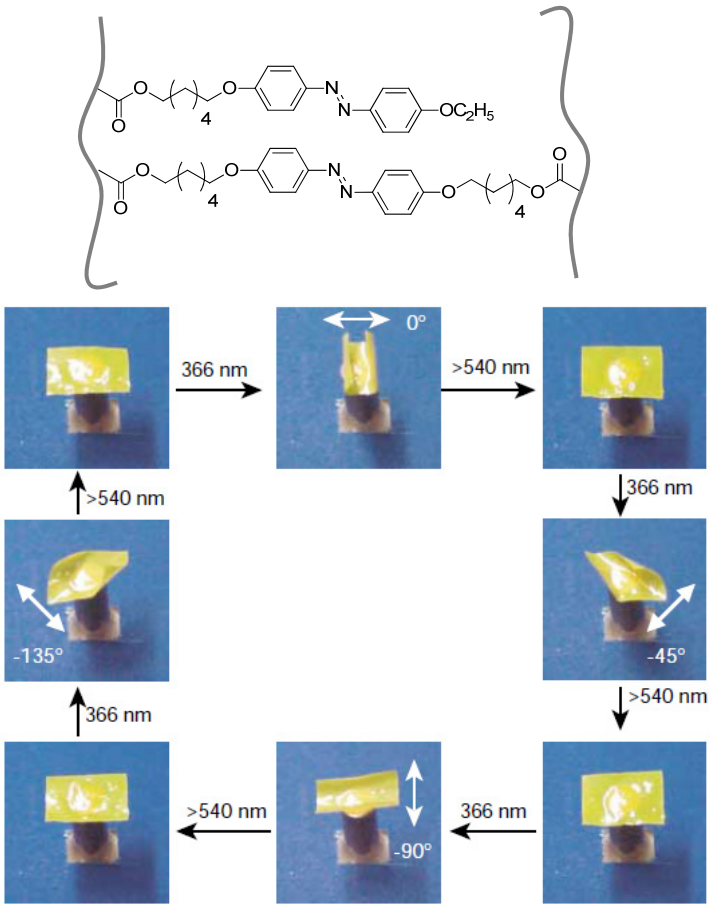

Figure 1.17 *Schematic representation of the azobenzene containing elastomer employed for preparation of the film (top) and photographic frames of the film bending in different directions (down) in response to irradiation by LPL of different angles of polarisation (white arrows) at 366 nm, and being flattened again by visible light at 540 nm*[128]

1.3.1.3 Photopatterning of Nanostructures in Block Copolymers

As mentioned above, one of the most important properties of BCs is their ability to segregate and give rise to different nanostructures (see section 1.2.2). By incorporation of azobenzene moieties in one of the blocks, photoalignment of the microdomains has been achieved.[129]

Ikeda and coworkers demonstrated this phenomenon by using a liquid crystalline BC composed of PEG and an azobenzene containing block, which is able to self-assemble in a nanostructure composed of PEG cylinders into an azobenzene containing matrix.[130] BC films of about 100 nm thickness were prepared on a glass substrate and were irradiated with LPL and annealed at 140ºC, temperature at which the BC posses a liquid crystalline behaviour. The PEG cylinders were perfectly aligned orthogonal to the polarisation of the light by the supramolecular cooperative motions of the ordered azobenzene block (**Figure 1.18**).

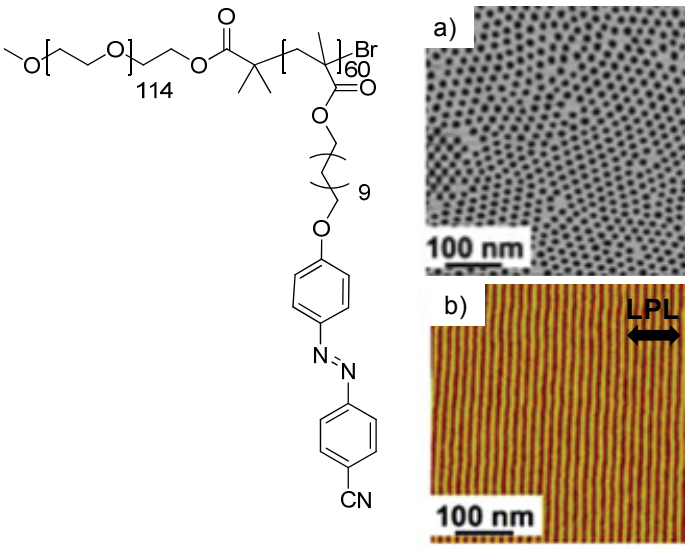

Figure 1.18 *Chemical structure of the azobenzene BC employed by Ikeda and coworkers (left). AFM images of the photooriented nanostructures (right): a) before irradiation, PEO cylinders are perpendicular to the substrate and b) after irradiation with LPL, the cylinders are aligned perpendicularly to the polarization direction of light (Image adapted from ref.130)*

Similarly, Seki and coworkers studied the photoaligment of a BC composed of PS and azopolymer which self-assembly into a PS nanocylinder structure.[131] Again, films with a thickness of about 100 nm were prepared on a glass substrate and were irradiated with LPL with different angles. Annealed non irradiated films provided PS cylinders in the upright orientation after annealing, while after irradiation with LPL cylinders were perfectly oriented in the orthogonal direction to the light. The initial situation was recovered by irradiation with non polarised light (**Figure 1.19**).

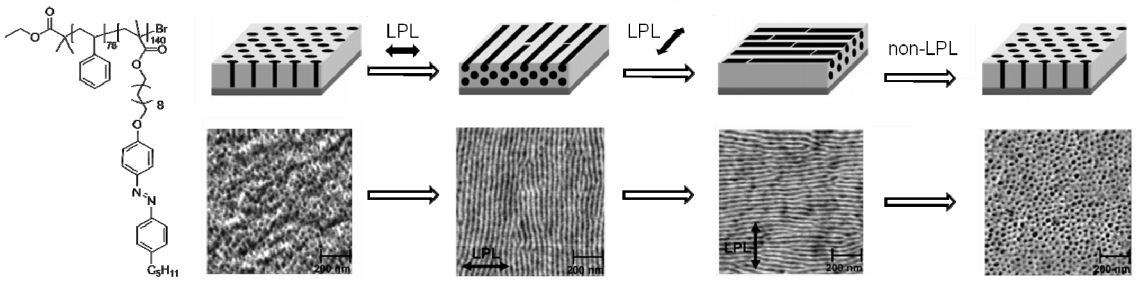

Figure 1.19 *Chemical structure of the BC employed by Seki and coworkers and AFM images of the photooriented nanostructures after irradiation with LPL (436 nm) with different angles followed by annealing (Image adapted from ref.131)*

1.3.2 Photoresponsive Properties in Solution

Photoinduced isomerisation of azobenzenes can also be used to promote changes in macromolecular self-assemblies dispersed in a liquid media, such as micelle dissociation or vesicle deformation. These photoresponsive properties are promising for applications in different areas as it will be discuss below.

1.3.2.1 Amphiphilic Block Copolymers: Self-assembly and their Applications as Controlled Delivery Systems

One of the most interesting properties of amphiphilic BCs is their ability to form in water different nanostructures like micelles and vesicles among others. In the

last years, amphiphilic BCs have received considerable attention due to the variety of applications in different fields ranging from biomedicine to catalysis.[53-58] Morphology and size of the self-assemblies can be modulated by controlling the hydrophilic/hydrophobic balance, which can be tuned by adjusting the length of the blocks and their chemical nature. On increasing volume fraction of the hydrophobic blocks, it has been observed a general evolution from spherical micelles to vesicles according to **Figure 1.20**.

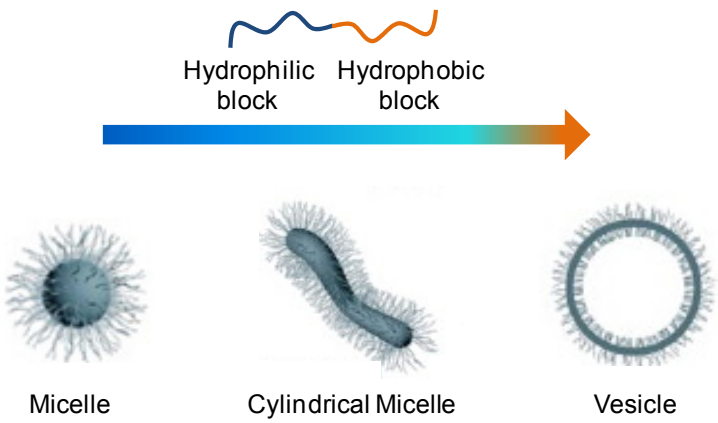

Figure 1.20 *Different morphologies found for amphiphilic BCs in aqueous media*

Polymeric micelles consist of a core formed by the hydrophobic blocks and a corona or shell formed by the hydrophilic blocks.[56] These micelles can be used as nanocarriers since hydrophobic drugs can be encapsulated in the core and transported at concentrations that can exceed their intrinsic water solubility. On the other hand, polymeric vesicles, also known as polymersomes, contains an inner volume enclosed by a thin membrane composed of a polymeric bilayer.[58] Vesicles are of particular interest as drug nanocontainers because of their internal hydrophilic cavities and robust hydrophobic membranes which can encapsulate both hydrophobic and hydrophilic molecules.

The incorporation of stimuli responsive moieties in amphiphilic BC makes them potentially useful as controlled delivery systems.[132-135] The majority of the reported stimuli responsive materials are sensitive to a few common triggers, including pH, temperature and light.[1-4] As mentioned before, the advantage of using light as external stimulus is the possibility to apply a temporal and spatial

control in the material response. Light responsiveness can be introduced in amphiphilic BCs in different ways. The most common strategy for the preparation of photocontrolled delivery systems is the incorporation of photochromic moieties in the one of the blocks of the BC (**Scheme 1.18a**). Upon UV irradiation, an alteration of the hydrophobic/hydrophobic balance due to the photoinduced reaction takes place leading to a deformation or even disruption of the self-assemblies and subsequent release of encapsulated substances. Several photochromic systems including azobenzene,[68,69,99,101,136-143] spiropyran,[144-147] dithienylethene and diazonaphthoquinone[148,149] have been study for this purpose. As an example, Mezzenga and coworkers reported the first spiropyrane functionalised amphiphilic BCs (**Figure 1.21)** which were able to form micellar aggregates in a mixture of water and ethanol. They demonstrated that the self-assemblies were able to undergo a reversible aggregation-dissolution-aggregation process in water in response to irradiation with a suitable wavelength. In the next section, several examples of amphiphilic azobenzene containing BCs will be detailed.

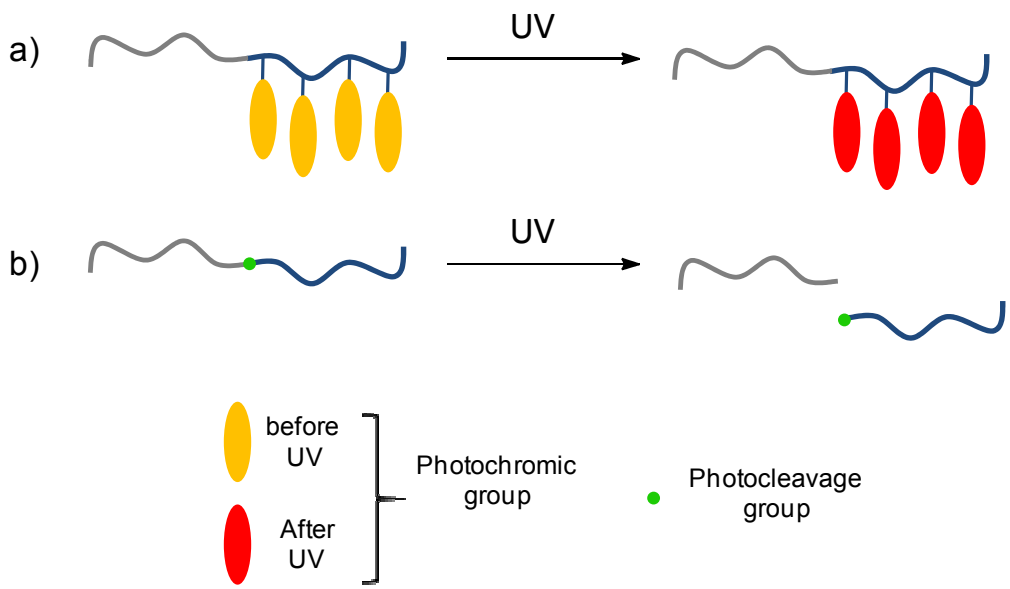

Scheme 1.18 *Schematic representation of photoresponsive BCs: a) photochromic containing BCs and b) photodegradable BCs*

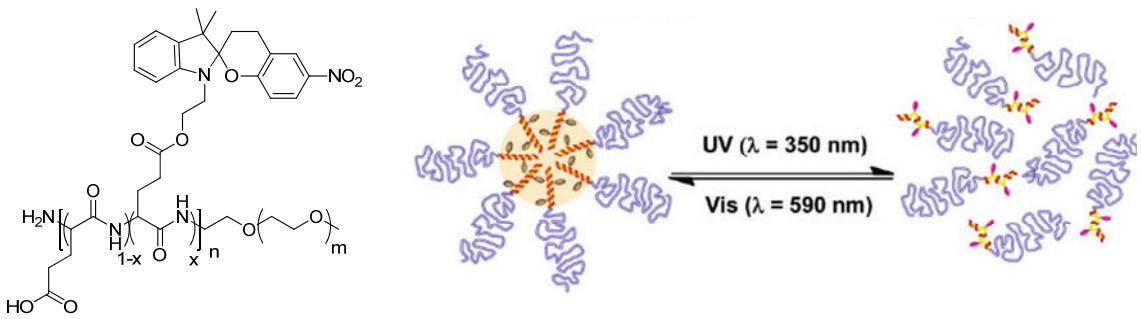

Figure 1.21 *Chemical structure of the spyropyrane functionalised amphiphilic BCs studied (left). Schematic representation of the photoresponsive micellization/dissolution process of the BCs upon irradiation (right) (Image adapted from ref.147)*

On the other hand, incorporation of photocleavage groups into the BC is also an interesting strategy to prepare controlled delivery systems (**Scheme 1.18b**). The most popular photocleavable moieties are o-nitrobenzyl-based derivatives. Burdick and coworkers prepared a BC composed of PEG and poly(caprolactone) and the photolabile 2-nitrophenylalanine as the linker of the two blocks (**Figure 1.22**).[150] This BC self-assembled into vesicles in water. Upon irradiation, a gradual collapse of the vesicles membrane took place due to the photoinduced cleavage of the linker. In comparison with photochromic containing systems, irreversibility of this light induced process is one of the disadvantages

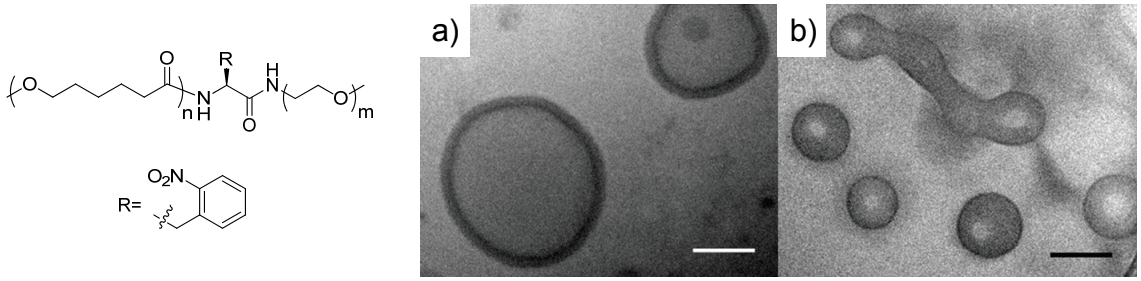

Figure 1.22 *Chemical structure of a BC composed of PEG and poly(caprolactone) and the photolabile 2-nitrophenylalanine as the linker of the two blocks (left) and Cryo-TEM images (right) of the vesicles before a) and after b) irradiation*[150]

1.3.2.2 Amphiphilic Azobenzene Block Copolymers

It is well known that UV irradiation provokes *trans*-to-*cis* isomerisation in azobenzenes and consequently, an increase of polarity accompanied by a morphological change of the chromophores. The changes occurred during UV irradiation might lead to deformation or even disruption of self-assemblies in amphiphilic BC containing this type of chromophores. Due to the promising properties of these systems as photocontrolled delivery systems, azobenzene containing amphiphilic BCs have been recently investigated.[143]

Wang et *al*. described a series of amphiphilic BCs based on azobenzene with conjugated amino (electron donor) and cyano (electron withdrawing) groups in one of the blocks.[151] The BCs consisted of a PEG block and an azobenzene containing PMMA block of different polymerization degrees giving rise to different hydrophobic/hydrophilic ratios. A 'multimorphological' aggregation behaviour in water was found depending on the hydrophobic/hydrophilic ratio (**Figure 1.23**). The BC with the higher hydrophilic/hydrophobic ratio -31/69- formed spherical micelles in water consisting of a PEG corona and an azobenzene core. Nevertheless, when the length of the azobenzene block was increased, more complicated morphologies were observed. For the BCs with a hydrophilic/hydrophobic ratio of 20/80 rod like aggregates were found, while the BC with a ratio 11/89 presented hollow nanotubes accompanied by other complicated nanostructures. On the other hand, the BC with the higher hydrophilic/hydrophobic ratio –6/94- self-assembled in water into colloidal spheres bigger in size than the spherical micelles. A similar transition from spherical micelles to rodlike aggregates and hollow nanotubes to colloidal sphere on increasing the hydrophobic ratio was also observed for amphiphilic BCs composed of PS and poly(acrylic acid).[152]

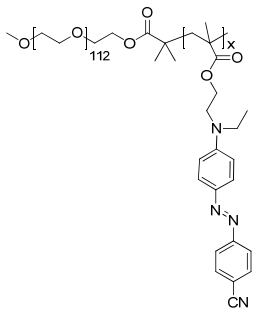

x	Phobic/Philic Ratio (wt%)
24	39/61
62	20/80
129	11/89
224	6/94

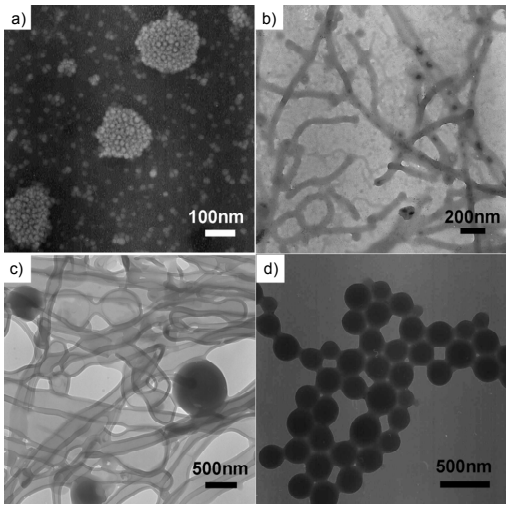

Figure 1.23 *Chemical structure of amphiphilic azobenzene BCs (left) and TEM images of the different self-assemblies in water (right): a) spherical micelles, b) rod-like aggregates, c) hollow nanotubes, d) colloidal spheres*[134]

Spherical micelles are the most common morphology obtained from azobenzene amphiphilic BCs. In most of the cases, the azopolymer is the hydrophobic block forming the core of the micelles, while the other hydrophilic block formes the corona or shell, being PEG the most commonly employed hydrophilic polymer. As an example, Yu and coworkers reported an amphiphilic BC consisting of PEG and a copolymer of azobenzene containing methacrylate and *N*-isopropylacrylamide (**Figure 1.24**).[140] This novel BC was able to self-assemble into spherical micelles in water. Although, the obtained micelles were not disrupted by the irradiation with light, it was found that the size of the micelles is dependent on the temperature.

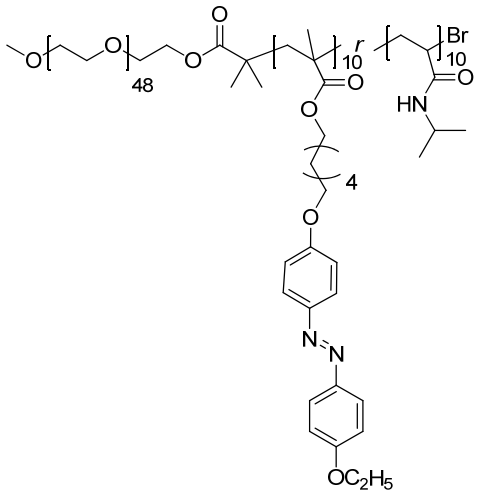

Figure 1.24 *Chemical structure of the amphiphilic azobenzene BC reported by Yu and coworkers*[140]

There are also several examples of azobenzene BCs wich are able to self-assemble into vesicles. Zhang and coworkers described an amphiphilic BC composed of poly(acrylic acid) as the hydrophilic block and an azobenzene poly(acrylate) as the hydrophobic block, which self-assembled into giant vesicles (micrometric scale) in a mixture of water and THF.[68] The photoresponsive behaviour of the vesicles was studied by irradiation with light at 365 nm in order to provoke *trans*-to-*cis* isomerisation of the azobenzene moieties. During this process, a photoinduced deformation of the vesicles was found, changing from a spherical shape to an ear-like shape (**Figure 1.25**) The same authors also reported an study with an amphiphilic composed of poly(*N*-isopropylacrylamide) (PNIPAM), a thermoresponsive block and the same azobenzene containing block as before.[69] The BC was also able to self-assembled into giant vesicles in a mixture of water and THF and upon irradiation with light of 365 nm, fusion of the vesicles was observed (**Figure 1.26**)

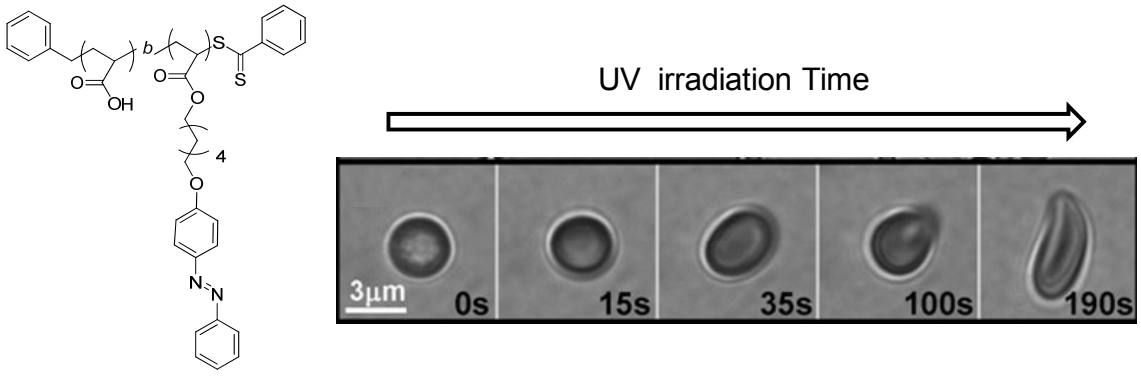

Figure 1.25 *Chemical structure an amphiphilic BC composed of poly(acrylic acid) and an azobenzene poly(acrylate) (left) and photomicrographs of the self-assemblies in a 80:20 H_2O:THF mixture under UV irradiation for different times (right)*[68]

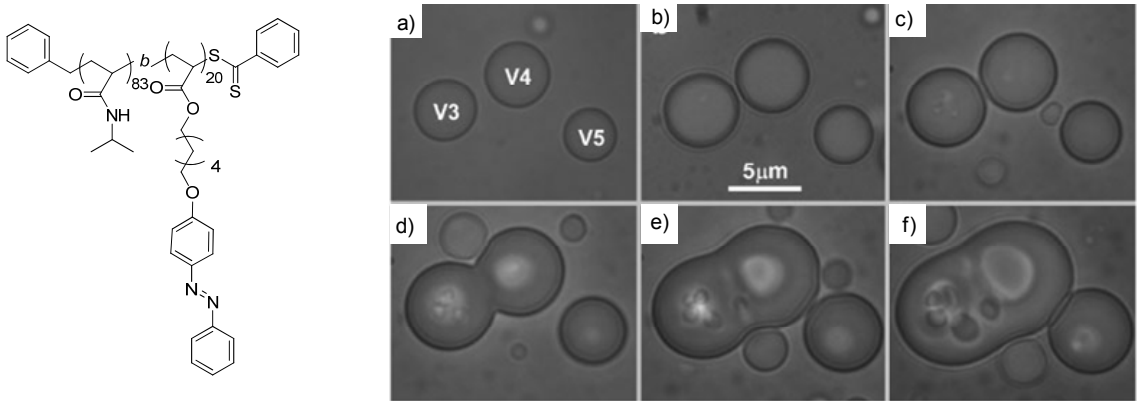

Figure 1.26 *Chemical structure an amphiphilic BC composed of PNIPAM and an azobenzene poly(acrylate) (left) and photomicrographs of the self-assemblies in a 50:50 H_2O:THF mixture under UV irradiation for different times (right): a) 0s, b) 16s, c) 33s, d) 42s, e) 58s and f) 80s*[69]

Yu and coworkers described photoresponsive vesicles from an amphiphilic BC composed of PEG and an azopyridine poly(methacrylate) in a mixture of water and THF.[138] During the irradiation process with UV light, these vesicles suffered a photoinduced process involving fusion, disruption, disintegration and rearrangement (**Figure 1.27**). The authors proposed that the changes produced during the irradiation are expected to increase the permeability of the membrane being good candidates as controlled delivery systems.

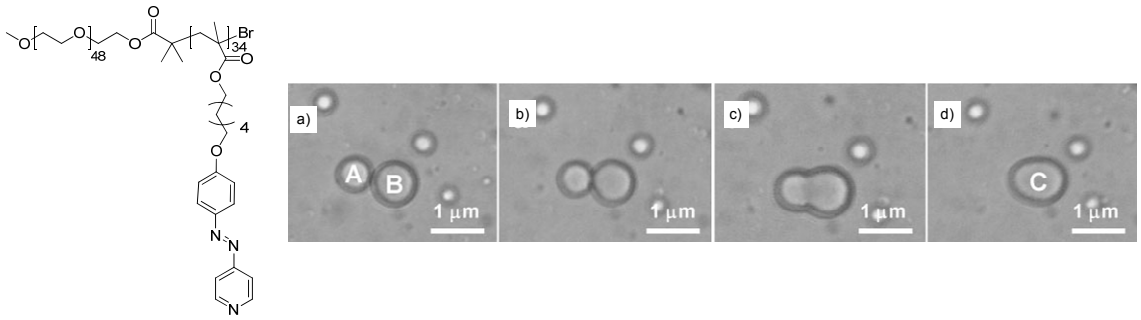

Figure 1.27 *Chemical structure an amphiphilic BC composed of PEG and an azopyridine poly(methacrylate) (left) and optical micrographs of the self-assemblies in a 55:45 H_2O:THF mixture under UV irradiation for different times (right): a) 0s, b) 2s, c) 4s, and d) 6s*[138]

Recently, a series of amphiphilic LDBCs composed of PEG of different molecular weights and dendrons based on bisMPA functionalised at the periphery with 4-cyanoazobenzene moieties have been studied in our research group.[99] A diversity of aqueous assemblies (cylindrical, sheet-like micelles and tubular micelles, as well as polymer vesicles) were exhibited by tuning the length of the hydrohophilic block as well as the generation of the dendron (**Figure 1.28**). Polymeric self-assemblies were observed for hydrophilic/hydrophobic ratios ranging from 67/33 to 20/80. As the size of the hydrophobic dendritic block was increased, a morphological transition from cylindrical micelles to sheet-like micelles and eventually to polymeric vesicles was observed. In order to study the photoreponsive behaviour of the vesicles, they were irradiated with UV light and distortion of the vesicles was found due to *trans*-to-*cis* isomerisation of azobenzene. These experimental observations have been recently supported by simulation studies.[153] Sheng and coworkers employed mesoscopic simulations to study the self-assemblies formed by these azobenzene LDBCs. By varying polymer concentration and lengths of the blocks, morphological phase diagrams and internal structures of the resulting aggregates were obtained (**Figure 1.29**). These simulations also proved that upon UV irradiation, an increase of the membrane permeability takes place. This increase of the permeability is mainly caused by the structural change of the azobenzene layer and makes these systems potentially useful as controlled delivery systems.

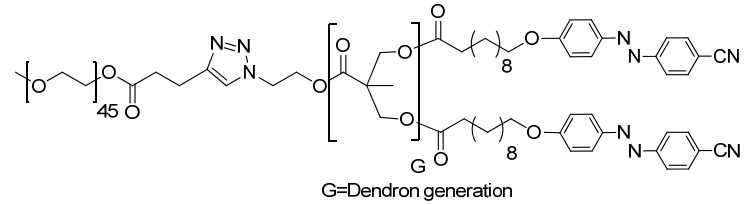

G	Phobic/Philic Ratio (wt%)
1	33/67
2	50/50
3	67/33
4	80/20

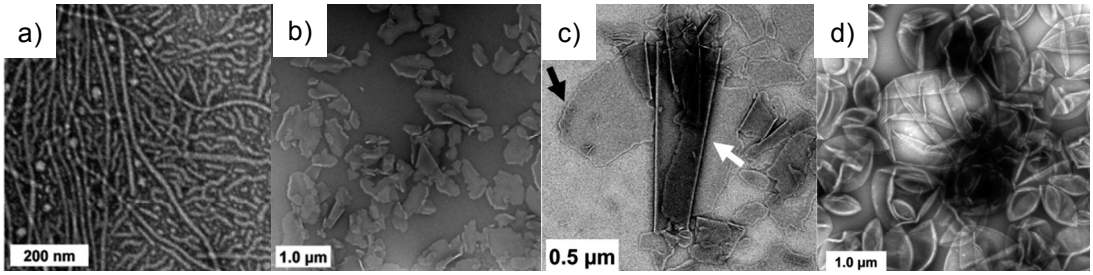

Figure 1.28 *Chemical structure of the azobenzene containing LDBC (top) and TEM images of the different self-assemblies in water (bottom): a) nanofibers, b) sheet-like aggregates, c) tubular micelles (indicated by the white arrow) in coexistence with sheet-like micelles (indicated the black arrow), d) polymeric vesicles.*[99] *G=generation of the dendron being* 2^n *the number of peripheral photochromic units*

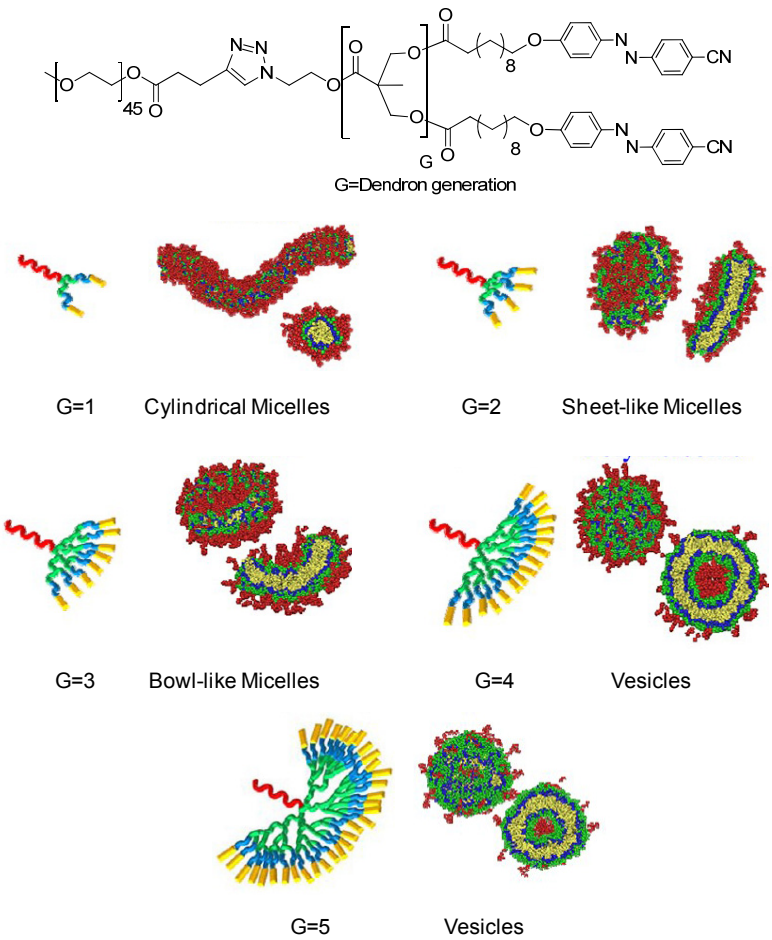

Figure 1.29 *Simulation results of the self-assemblies derived from the LDBC first described by del Barrio et al. in selective solvents (Image adapted from ref.153)*

Closely related amphiphilic LDBCs were also reported by Shi *et al.* by combining PEG and different generations of 4-octyloxyazobenzene poly(amido amine) (PPI) dendrons where this generation dependent self-assembling behaviour was also observed (**Figure 1.30**).[100] These authors reported on the reversible photoinduced *trans*-to-*cis* isomerisation in solution but not on the photoresponse of the aqueous self-assemblies.

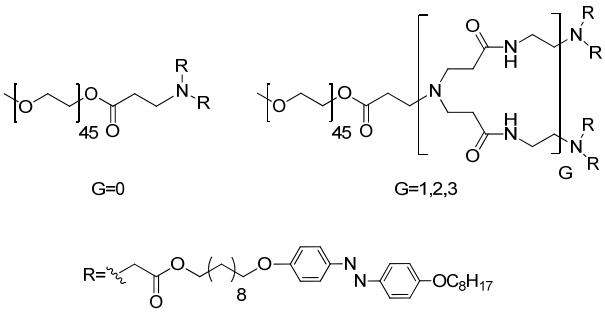

G	Phobic/Philic Ratio (wt%)
0	33/67
1	52/48
2	70/30
3	82/18

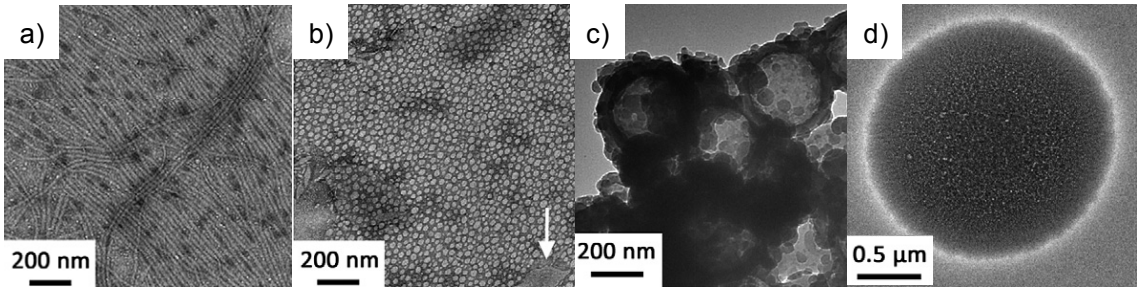

Figure 1.30 *Chemical structure of the amphiphilic LDBCs reported by Shi et al. (top) and TEM images of the different self-assemblies in a 17:83 dioxane:water mixture(bottom): a) nanofibers, b) nanospheres in coexistence with nanosheets (indicated by the white arrow) c) polymeric vesicles and d) large micelles*[100]

1.4 Photoresponsive Surfaces

Responsive smart surfaces have recently attracted significant attention because of their associated interesting applications such as biosensors, intelligent membranes or microfluidic devices.[154-156] During the last years, the study of surfaces with controllable wettability has emerged as a major focus of interest in responsive surface field,[155] especially photoresponsive surfaces prepared from inorganic oxides and/or photoresponsive organic molecules.[157-160]

Photoresponsive organic surfaces are based on photochromic moieties such as azobenzene, spiropyrans, fulgides among others.[157,161] The photoresponsive moieties are usually incorporated in a suitable platform, usually a small molecule or a polymer, to form self-assembled monolayers (SAMs) or polymer based surfaces. SAMs are spontaneously formed by adsorption of an active surfactant into solid surfaces. Thiol and silane derivates are examples of two widely used organic groups to functionalise inorganic surfaces. The photoswitching of SAM modified surfaces is normally based on chemical or conformational changes of the photoresponsive group. As an example, Rosario *et al*. reported photoresponsive surfaces by covalently bound spiropyran to a glass surface.[162] The surface modification was carried out by reaction of the corresponding organic silanes with silicate surfaces to form Si-O-Si bonds. The relatively nonpolar spiropyran can be reversibly switched to a polar, zwitterionic merocyanine isomer that has a much larger dipole moment by UV light, and back again by visible light (**Figure 1.31**). The light induced changes observed in the surface energy were correlated to the switching of the surface bound spiropyran molecule between polar and nonpolar forms by means of fluorescence spectroscopy.

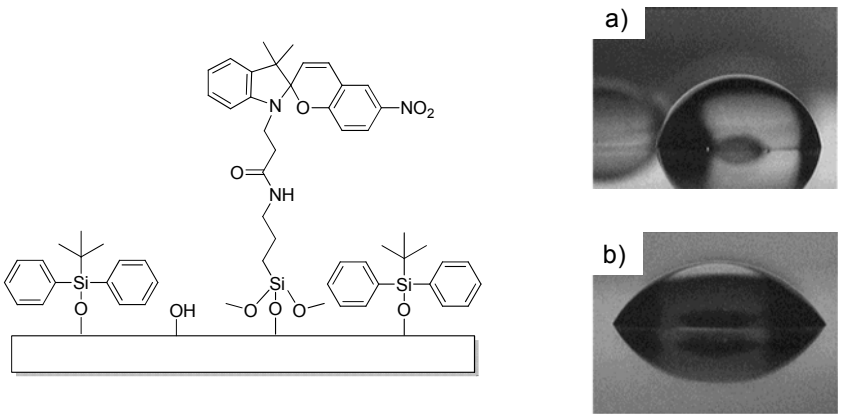

Figure 1.31 *Spiropyran functionalised surface and the behaviour of a water droplet a) under Vis irradiation and b) under UV* irradiation[162]

On the other hand, polymer films can be prepared on substrate surfaces using several deposition techniques as well as chemical reactions. One of the simplest techniques of applying thin films onto substrates is either casting or spin coating of a polymer solution. As an example, spiropyrane photoresponsive polymeric films were prepared by Sumaru and coworkers.[163] A polymer blend of an spiropyran containing polymer and PMMA was dissolved in 1,2-dichloroethane and poured onto a glass substrate, which had been hydrophobicised with dichlorodimethylsilane and dried in air for 3 days. Due to the photocontrolled change in the polarity of the surface, a reversible cell adhesion control was achieved.

1.4.1 Azobenzene Functionalised Surfaces

Azobenzene functionalised surfaces have also attracted much attention. As mentioned, the modification the dipole moment of the molecule due to *trans*-to-*cis* isomerisation gives the possibility to prepare surfaces with photocontrolled wettability (**Scheme 1.19**).

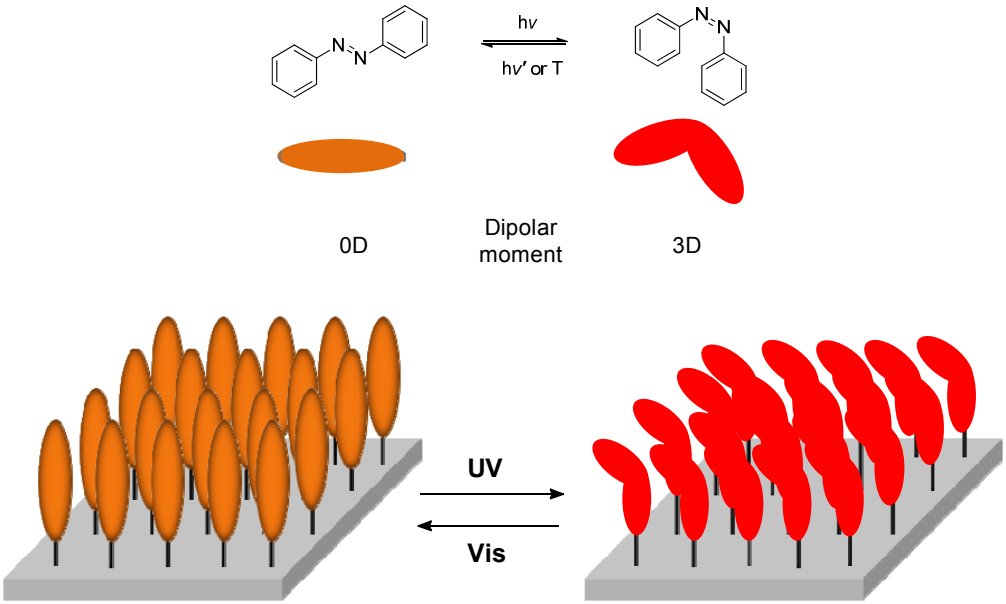

Scheme 1.19 *Photoinduced isomerisation of azobenzene moieties in a surface*

Pioneering studies on photoresponsive azobenzene surfaces were reported by Ichimura and coworkers using a flat surface modified with a calix[4]resorcinarene containing four pendant azobenzene units that was irradiated with a gradient in light intensity achieving light driven motion of liquids (**Figure 1.32**).[164,165] The asymmetrical irradiation caused a gradient in the surface free energy because of the photosiomerisation azobenzene moieties generating CA hysteresis on both edges of the droplet. This induced tension led to a directional motion of the droplet.

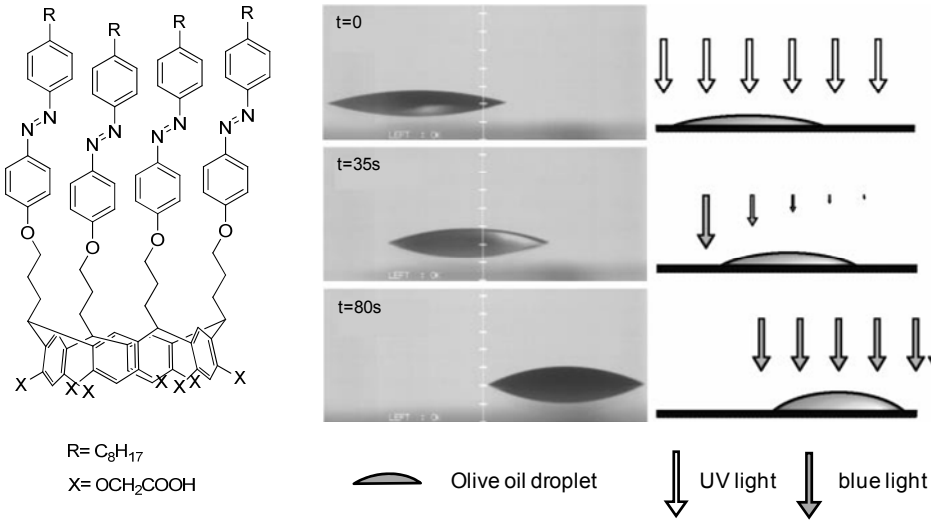

Figure 1.32 *Chemical structure of the azobenzene containing calix[4]resorcinareno reported by Ichimura and coworkers and light driven motion of an olive oil droplet under asymmetrical irradiation*[164]

Selected examples in compact monolayers containing azobenzene moieties prepared on silicon substrates were described by Delorme *et al*. as well as Hamelmann *et al.* (**Figure 1.33**).[166,167] These photoresponsive surfaces were prepared either by covalent grafting of azobenzene moieties onto a surface previously functionalised with an isocyanate monolayer or direct grafting of silane containing azobenzene. These studies provided evidence of controlled photoisomerisation of the azobenzene moieties in the surface and subsequently a photocontrolled change in the CA of the surface.

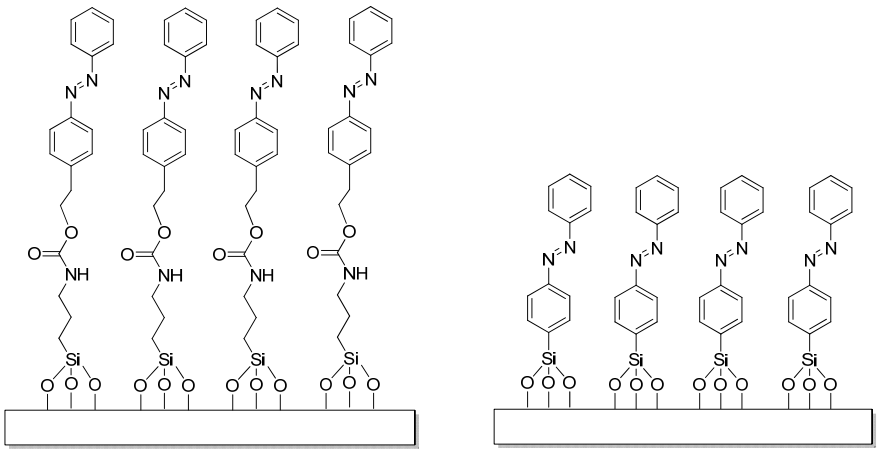

Figure 1.33 *Azobenzene functionalised surfaces prepared by covalent grafting of azobenzene moieties*[166,167]

Recently, rough surfaces with a good photoresponsiveness fabricated via layer-by-layer deposition were also reported. For example, Zhou *et al.* prepared a switchable surface changing from a slippery to a sticky state when the azocompound assumes *trans* or *cis* conformation, respectively (**Figure 1.34**).[168] The coating consists of a siloxane elastomer containing trifluoromethoxy azobenzene moieties. Cho *et al.* also prepared fluorinated azobenzene modified nanoporous substrates.[169] Upon UV irradiation, the surface was reversibly switched between superhydrophobic and superhydrophilic states. These studies evidenced that the presence of nanostructures strongly enhanced the wettability changes resulting from azobenzene isomerisation in comparison with monolayers. This improvement could be attributed to a increase in the available space for the isomerisation in the case of rough surfaces.

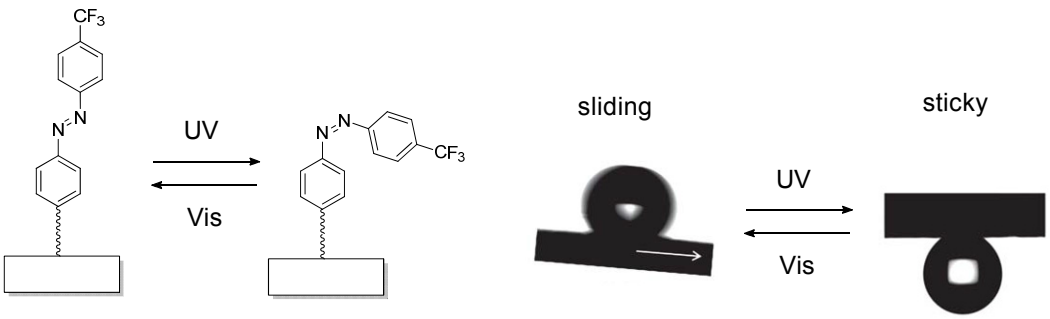

Figure 1.34 *Azobenzene functionalised surfaces containing trifluoromethoxy-azobenzene moieties (left) and the shape of a water droplet upon UV and Vis irradiation (right)*[168-169]

References

1 Gil, E. S.; Hudson, S. M. Stimuli-reponsive polymers and their bioconjugates. *Progress in Polymer Science* **2004**, 29, 1173-1222.

2 Stuart, M. A.; Huck, W. T.; Genzer, J.; Müller, M.; Ober, C.; Stamm, M.; Sukhorukov G. B.; Szleifer, I.; Tsukruk, V. V.; Urban, M.; Winnik, F.; Zauscher, S.; Luzinov, I.; Minko, S. Emerging applications of stimuli-responsive polymer materials. *Nature Materials* **2010**, 9, 101-113.

3 Liu, F.; Urban, M. W. Recent advances and challenges in designing stimuli-responsive polymers. *Progress in Polymer Science* **2010**, 35, 3-23.

4 Roy, D.; Cambre, J. N.; Sumerlin, B. S. Future perspectives and recent advances in stimuli-responsive materials. *Progress in Polymer Science* **2010**, 35, 278-301.

5 Shibaev, V.; Bobrovsky, A.; Boiko, N. Photoactive liquid crystalline polymer systems with light-controllable structure and optical properties. *Progress in Polymer Science* **2003**, 28, 729-836.

6 Berkovic, G.; Krongauz, V.; Weiss, V. Spiropyrans and Spirooxazines for Memories and Switches. *Chemical Reviews* **2000**, 100, 1741-1754.

7 Lenoble, C.; Becker, R. S. Photophysics, photochemistry, and kinetics of photochromic fulgides. *The Journal of Physical Chemistry* **1986**, 90, 2651-2654.

8 Ilge, H.-D.; Sühnel, J.; Khechinashvili, D.; Kaschke, M. Photochemistry of phenylfulgides XXII: Competing ultrafast radiationless deactivation, E—Z isomerization and electrocyclic ring-closure reactions. *Journal of Photochemistry* **1987**, 38, 189-203.

9 Yun, C.; You, J.; Kim, J.; Huh, J.; Kim, E. Photochromic fluorescence switching from diarylethenes and its applications. *Journal of Photochemistry and Photobiology C: Photochemistry Reviews* **2009**, 10, 111-129.

10 Natansohn, A.; Rochon, P. Photoinduced motions in azo-containing polymers. *Chemical Reviews* **2002**, 102, 4139-4175.

11 Rau, H. *Photochemistry and Photophysics*. Vol. II 119-141 (CRC Press, 1990).

12 Ono, H.; Kowatari, N.; Kawatsuki, N. Holographic grating generation in thick polymer films containing azo dye molecules. *Optical Materials* **2001**, 17, 387-394.

13 Lu, Y.; Lei, H.; Pan, Q.; Liu, Z.; Rempel, G. L. Holographic coherence tomography for measurement of three-dimensional refractive-index space. *Optics Letters* **2002**, 27, 1102-1104.

14 Bian, S.; Kuzyk, M. G. Real-time holographic reflection gratings in volume media of azo-dye-doped poly(methyl methacrylate). *Optics Letters* **2002**, 27, 1761-1763.

15 Xie, P.; Zhang, R. Liquid crystal elastomers, networks and gels: advanced smart materials. *Journal of Materials Chemistry* **2005**, 15, 2529-2550.

16 Dingemans, T. J.; Madsen, L. A.; Zafiropoulos, N. A.; Lin, W.; Samulski, E. T. Uniaxial and biaxial nematic liquid crystals. *Philosophical Transactions of the Royal Society A* **2006**, 364, 2681-2696.

17 Hvilsted, S., Andruzzi, F., Kulinna, C., Siesler, H. W. & Ramanujam, P. S. Novel Side-Chain Liquid Crystalline Polyester Architecture for Reversible Optical Storage. *Macromolecules* **1995**, 28, 2172-2183.

18 Sánchez, C.; Alcalá S, A.; Hvilsted, S.; P.S., R. Biphotonic holographic gratings in azobenzene polyesters: Surface relief phenomena and polarization effects. *Applied Physics Letters* **2000**, 77, 1440-1442.

19 Zebger, I.; Rutloh, M.; Hoffmann, U.; Stumpe, J.; Siesler, H. W.; Hvilsted, S. Photoorientation of a liquid crystalline polyester with azobenzene side groups. 1. Effects of irradiation with linearly polarized blue light. *Journal of Physical Chemistry A* **2002**, 106, 3454-3462.

20 Nuyken, O.; Weidner, R. in *Chromatography/Foams/Copolymers* Vol. 73/74 *Advances in Polymer Science* Ch. 4, 145-199 (Springer Berlin Heidelberg, 1986).

21 Hallensleben, M.; Weichart, B. Photoresponsive polymers. *Polymer Bulletin* **1989**, 22, 553-556.

22 Jagur-Grodzinski, J. Preparation of functionalized polymers using living and controlled polymerizations. *Reactive & Functional Polymers* **2001**, 49, 1-54.

23 Braunecker, W. A.; Matyjaszewski, K. Controlled/living radical polymerization: Features, developments, and perspectives. *Progress in Polymer Science* **2007**, 32, 93-146.

24 Matyjaszewski, K.; Xia, J. Atom Transfer Radical Polymerization. *Chemical Reviews* **2001**, 101, 2921-2990.

25 Ouchi, M.; Terashima, T.; Sawamoto, M. Transition Metal-Catalyzed Living Radical Polymerization: Toward Perfection in Catalysis and Precision Polymer Synthesis. *Chemical Reviews* **2009**, 109, 4963-5050.

26 Matyjaszewski, K. Atom Transfer Radical Polymerization (ATRP): Current Status and Future Perspectives. *Macromolecules* **2012**, 45, 4015-4039.

27 Li, M.-H.; Keller, P.; Grelet, E.: Auroy, P. Liquid-Crystalline Polymethacrylates by Atom-Transfer Radical Polymerization at Ambient Temperature. *Macromolecular Chemistry and Physics* **2002**, 203, 619-626.

28 Jin, M.; Xin Yang, Q.; Lu, R.; Hua Xu, T.; Ying Zhao, Y. Syntheses of bisazo-containing polymethacrylates using atom transfer radical polymerization and the photoalignment behavior. *Journal of Polymer Science Part A: Polymer Chemistry* **2004**, 42, 4237-4247.

29 Moad, G.; Barner-Kowollik, C. in *Handbook of RAFT Polymerization* 51-104 (Wiley-VCH Verlag GmbH & Co. KGaA, 2008).

30 Moad, G.; Rizzardo, E.; Thang, S. H. Living Radical Polymerization by the RAFT Process – A Second Update. *Australian Journal of Chemistry* **2009**, 62, 1402-1472.

31 Rodriguez, F. J.; Sánchez, C.; Villacampa, B.; Alcalá, R.; Cases, R.; Millaruelo, M.; Oriol, L. Fast and stable recording of birefringence and holographic gratings in an azo-polymethacrylate using a single nanosecond light pulse. *The Journal of Chemical Physics* **2005**, 127, 204706-204713.

32 Rodriguez, F. J.; Sánchez, C.; Villacampa, B.; Alcalá, R.; Cases, R.; Millaruelo, M.; Oriol, L. Red light induced holographic storage in an azobenzenepolymethacrylate at room temperature. *Optical Materials* **2006**, 28, 480.

33 Xu, J.; Zhang, W.; Zhou, N.; Zhu, J.; Cheng, Z.; Xu, Y.; Zhu, X. Synthesis of azobenzene-containing polymers via RAFT polymerization and investigation on intense fluorescence from aggregates of azobenzene-containing amphiphilic diblock copolymers. *Journal of Polymer Science Part A: Polymer Chemistry* **2008**, 46, 5652-5662.

34 Gao, J.; Sun, Y.; Zhou, J.; Zheng, Z.; Chen, H.; Su, W.; Zhang, Q. Preparation of Ag nanoparticles termini-protected side-chain liquid crystalline azobenzene polymers by RAFT polymerization. *Journal of Polymer Science Part A: Polymer Chemistry* **2007**, 45, 5380-5386.

35 Zhang, Y.; Cheng, Z.; Chen, X.; Zhang, W.; Wu, J.; Zhu, J.; Zhu, X. Synthesis and Photoresponsive Behaviors of Well-Defined Azobenzene-Containing Polymers via RAFT Polymerization. *Macromolecules* **2007**, 40, 4809-4817.

36 Wang, X.; Kumar, J.; Tripathy, S. K. Epoxy-Based Nonlinear Optical Polymers from Post Azo Coupling Reaction. *Macromolecules* **1997***,* 30, 219-225*.*

37 Kang, E.-H.; Liu, X.; Sun, J.; Shen, J. Robust Ion-Permselective Multilayer Films Prepared by Photolysis of Polyelectrolyte Multilayers Containing Photo-Cross-Linkable and Photolabile Groups. *Langmuir* **2006**, 22, 7894-7901.

38 Royes, J; Rebolé, J.; Custardoy, L.; Gimeno, N.; Oriol, L.; Tejedor, R.M.; Piñol, M. Preparation of side-chain liquid crystalline Azopolymers by CuAAC postfunctionalization using bifunctional azides: Induction of chirality using circularly polarized light. *Journal of Polymer Science Part A: Polymer Chemistry* **2012**, 50, 1579-1590.

39 Wu, L.; Tuo, X.; Cheng, H.; Chen, Z.; Wang, X. Synthesis, Photoresponsive Behavior, and Self-Assembly of Poly(acrylic acid)-Based Azo Polyelectrolytes. *Macromolecules* **2001**, 34, 8005-8013.

40 Kolb, H. C.; Finn, M. G.; Sharpless, K. B. Click chemistry: Diverse chemical function from a few good reactions. *Angewandte Chemie-International Edition* **2001**, 40, 2004-2021.

41 Meldal, M.; Tornøe, C. W. Cu-Catalyzed Azide−Alkyne Cycloaddition. *Chemical Reviews* **2008**, 108, 2952-3015.

42 Hoyle, C. E.; Bowman, C. N. Thiol–Ene Click Chemistry. *Angewandte Chemie International Edition* **2010**, 49, 1540-1573.

43 Hoyle, C. E.; Lowe, A. B.; Bowman, C. N. Thiol-click chemistry: a multifaceted toolbox for small molecule and polymer synthesis. *Chemical Society Reviews* **2010**, 39, 1355-1387.

44 Kade, M. J.; Burke, D. J.; Hawker, C. J. The power of thiol-ene chemistry. *Journal of Polymer Science Part A: Polymer Chemistry* **2010**, 48, 743-750.

45 Ramachary, D. B.; Barbas, C. F. Towards Organo-Click Chemistry: Development of Organocatalytic Multicomponent Reactions Through Combinations of Aldol, Wittig, Knoevenagel, Michael, Diels–Alder and Huisgen Cycloaddition Reactions. *Chemistry – A European Journal* **2004**, 10, 5323-5331.

46 Binder, W. H.; Sachsenhofer, R. 'Click' chemistry in polymer and materials science. *Macromolecular Rapid Communications* **2007**, 28, 15-54.

47 Fournier, D.; Hoogenboom, R.; Schubert, U. S. Clicking polymers: a straightforward approach to novel macromolecular architectures. *Chemical Society Reviews* **2007**, 36, 1369-1380.

48 Kempe, K.; Krieg, A.; Becer, C. R.; Schubert, U. S. "Clicking" on/with polymers: a rapidly expanding field for the straightforward preparation of novel macromolecular architectures. *Chemical Society Reviews* **2012**, 41, 176-191.

49 Ishiguro, M.; Sato, D.; Shishido, A.; Ikeda, T. Bragg-Type Polarization Gratings Formed in Thick Polymer Films Containing Azobenzene and Tolane Moieties†. *Langmuir* **2007**, 23, 332-338.

50 Saishoji, A.; Sato, D.; Shishido, A.; Ikeda, T. Formation of Bragg Gratings with Large Angular Multiplicity by Means of the Photoinduced Reorientation of Azobenzene Copolymers. *Langmuir* **2007**, 23, 320-326.

51 Czapla, S.; Ruhmann, R.; Rübner, J.; Zschuppe, V.; Wolff, D. New copolymethacrylates with azo-chromophores in the side chain. *Die Makromolekulare Chemie* **1993**, 194, 243-250.

52 Angiolini, L.; Benelli, T.; Giorgini, L.; Salatelli, E. Optically Active Photochromic Polymers with Three-Arm Star Structure by Atom Transfer Radical Polymerization. *Macromolecules* **2006**, 39, 3731-3737.

53 Savic, R.; Luo, L. B.; Eisenberg, A.; Maysinger, D. Micellar nanocontainers distribute to defined cytoplasmic organelles. *Science* **2003**, 300, 615-618.

54 Riess, G. Micellization of block copolymers. *Progress in Polymer Science* **2003**, 28, 1107-1170.

55 Letchford, K.; Burt, H. A review of the formation and classification of amphiphilic block copolymer nanoparticulate structures: micelles, nanospheres, nanocapsules and polymersomes. *European Journal of Pharmaceutics and Biopharmaceutics* **2007**, 35, 259-269.

56 Smart, T.; Lomas, T.; Massignani, M.; Flores-Merino, M.V.; Ruiz-Perez, L.; Battaglia, G. Block copolymer nanostructures. *Nano Today* **2008**, 3, 38-46.

57 Kim, J. K.; Yang, S. Y.; Lee, Y.; Kim, Y. Functional nanomaterials based on block copolymer self-assembly. *Progress in Polymer Science* **2010**, 35, 1325-1349.

58 Discher, D. E.; Eisenberg, A. Polymer vesicles. *Science* **2002**, 297, 967-973.

59 Tian, Y.; Watanabe, K.; Kong, X.; Abe, J.; Iyoda, T. Synthesis, Nanostructures, and Functionality of Amphiphilic Liquid Crystalline Block Copolymers with Azobenzene Moieties. *Macromolecules* **2002**, 35, 3739-3747.

60 Yang, J.; Levy, D.; Deng, W.; Keller, P.; Li, M. H. Polymer vesicles formed by amphiphilic diblock copolymers containing a thermotropic liquid crystalline polymer block. *Chemical Communications* **2005**, 4345-4347.

61 Forcen, P.; Oriol, L.; Sánchez, C.; Alcalá, R.; Hvilsted, S.; Jankova, K.; Loos, J. Synthesis, characterization and photoinduction of optical anisotropy, in liquid crystalline diblock azo-copolymers. *Journal of Polymer Science Part a-Polymer Chemistry* **2007**, 45, 1899-1910.

62 Forcen, P.; Oriol, L.; Sánchez, C.; Rodríguez, F. J.; Alcalá, R. Methacrylic azopolymers for holographic storage: A comparison among different polymer types. *European Polymer Journal* **2007**, 43, 3292-3300.

63 Gimeno, S.; Forcén, P.; Oriol, L.; Piñol, M.; Sánchez, C.; Rodríguez, F. J..; Alcalá, R.; Jankova, K.; Hvilsted, S. Photoinduced optical anisotropy in azobenzene methacrylate block copolymers: Influence of molecular weight and irradiation conditions. *European Polymer Journal* **2009**, 45, 262-271.

64 Deng, W. *et al.* Azobenzene-Containing Liquid Crystal Triblock Copolymers: Synthesis, Characterization, and Self-Assembly Behavior. *Macromolecules* **2008**, 41, 2459-2466.

65 Cui, L.; Zhao, Y.; Yavrian, A.; Galstian, T. Synthesis of Azobenzene-Containing Diblock Copolymers Using Atom Transfer Radical Polymerization and the Photoalignment Behavior. *Macromolecules* **2003**, 36, 8246-8252.

66 Hackel, M.; Kador, L.; Kropp, D.; Frenz, C.; Schmidt, H. W. Holographic gratings in diblock copolymers with azobenzene and mesogenic side groups in the photoaddressable dispersed phase. *Advanced Functional Materials* **2005**, 15, 1722-1727.

67 Chen, W.; Wei, X.; Balazs, A. C.; Matyjaszewski, K.; Russell, T. P. Phase Behavior and Photoresponse of Azobenzene-Containing Polystyrene-block-poly(n-butyl methacrylate) Block Copolymers. *Macromolecules* **2011**, 44, 1125-1131.

68 Su, W.; Han, K.; Luo, Y.; Wang, Z.; Li, Y.; Zhang, Q. Formation and Photoresponsive Properties of Giant Microvesicles Assembled from Azobenzene-Containing Amphiphilic Diblock Copolymers. *Macromolecular Chemistry and Physics* **2007**, 208, 955-963.

69 Su, W.; Luo, Y.; Yan, Q.; Wu, S.; Han, K.; Zhang, Q.; Gu, Y.; Li, Y. Photoinduced fusion of micro-vesicles self-assembled from azobenzene-containing amphiphilic diblock copolymers. *Macromolecular Rapid Communications* **2007**, 28, 1251-1256.

70 Adams, J.; Gronski, W. LC Side Chain AB-Blockcopolymers with an Amorphous A-Block and a Liquid Crystalline B-Block. *Makromol. Chem., Rapid Commun.* **1989**, 10, 553.

71 Berges, C.; Gimeno, N.; Oriol, L.; Piñol, M.; Forcén, P.; Sánchez, C.; Alcalá, R. Photoinduced optical anisotropy in azobenzene containing block copolymer–homopolymer blends. Influence of microstructure and molecular weight. *European Polymer Journal* **2012**, 48, 613.

72 Bosman, A. W.; Janssen, H. M.; Meijer, E. W. About Dendrimers: Structure, Physical Properties, and Applications. *Chemical Reviews* **1999**, 99, 1665-1688.

73 Grayson, S. M.: Fréchet, J. M. J. Convergent Dendrons and Dendrimers: from Synthesis to Applications. *Chemical Reviews* **2001**, 101, 3819-3868.

74 Tomalia, D. A.; Fréchet, J. M. J. in *Dendrimers and Other Dendritic Polymers* 1-44 (John Wiley & Sons, Ltd, 2002).

75 Newkome, G. R.; Moorefield, C. N.; Vögtle, F. in *Dendrimers and Dendrons* i-xii (Wiley-VCH Verlag GmbH & Co. KGaA, 2004).

76 Momotake, A.; Arai, T. Synthesis, excited state properties, and dynamic structural change of photoresponsive dendrimers. *Polymer* **2004**, 45, 5369-5390.

77 Momotake, A.; Arai, T. Photochemistry and photophysics of stilbene dendrimers and related compounds. *Journal of Photochemistry and Photobiology C: Photochemistry Reviews* **2004**, 5, 1-25.

78 Deloncle, R.; Caminade, A.-M. Stimuli-responsive dendritic structures: The case of light-driven azobenzene-containing dendrimers and dendrons. *Journal of Phochemistry and Photobioloby C: Photochemistry Reviews* **2010**, 11, 25-45.

79 Archut, A.; Vögtle, F.; De Cola, L.; Azzellini, G. C,; Balzani, V.; Ramanujam, P. S.; Berg, R. H. Azobenzene-Functionalized Cascade Molecules: Photoswitchable Supramolecular Systems. *Chemistry – A European Journal* **1998**, 4, 699-706.

80 Weener, J. W.; Meijer, E. W. Photoresponsive Dendritic Monolayers. *Advanced Materials* **200**, 12, 741-746.

81 Vögtle, F.; Gorka, M.; Hesse, R.; Ceroni, P.; Maestri, M.; Balzani, V. Photochemical and photophysical properties of poly(propylene amine) dendrimers with peripheral naphthalene and azobenzene groups. *Photochemical & Photobiological Sciences* **2002**, 1, 45-51.

82 Alcalá, R.; Giménez, R.; Oriol, L.; Piñol, M.; Serrano, J. L.; Villacampa, B.; Viñuales, A. I. Synthesis, Characterization, and Induction of Stable Anisotropy in Liquid Crystalline Photo-addressable PPI Dendrimers. *Chemistry of Materials* **2006**, 19, 235-246.

83 Wiwattanapatapee, R.; Lomlim, L.; Saramunee, K. Dendrimers conjugates for colonic delivery of 5-aminosalicylic acid. *Journal of Controlled Release* **2003**, 88, 1-9.

84 Cheon, K. S.; Kazmaier, P. M.; Keum, S. R.; Park, K. T.; Buncel, E. Azo-functionalized dendrimers. *Canadian Journal of Chemistry* **2004**, 82, 551-566.

85 Gitsov, I.; Wooley, K. L.; Frechet, J. M. J. NOVEL POLYETHER COPOLYMERS CONSISTING OF LINEAR AND DENDRITIC BLOCKS. *Angewandte Chemie-International Edition in English* **1992**, 31, 1200-1202.

86 Gitsov, I. Hybrid linear dendritic macromolecules: From synthesis to applications. *Journal of Polymer Science Part A: Polymer Chemistry* **46**, 5295-5314, doi:10.1002/pola.22828 (2008).

87 Wurm, F. & Frey, H. Linear–dendritic block copolymers: The state of the art and exciting perspectives. *Progress in Polymer Science* **2008**, 36, 1-52.

88 van Hest, J. C. M.; Delnoye, D. A. P.; Baars, M. W. P. L.; van Genderen, M. H. P.; Meijer, E. W. Polystyrene-Dendrimer Amphiphilic Block Copolymers with a Generation-Dependent Aggregation. *Science* **1995**, 268, 1592-1595.

89 Iyer, J.; Fleming, K.; Hammond, P. T. Synthesis and solution properties of new linear-dendritic diblock copolymers. *Macromolecules* **1998**, 31, 8757-8765.

90 Leduc, M. R.; Hawker, C. J.; Dao, J.; Frechet, J. M. J. Dendritic initiators for "living" radical polymerizations: A versatile approach to the synthesis of dendritic-linear block copolymers. *Journal of the American Chemical Society* **1996**, 118, 11111-11118.

91 Mecerreyes, D.; Dubois, P.; Jérôme, R.; Hedrick, J. L.; Hawker, C. J. Synthesis of dendritic–linear block copolymers by living ring-opening polymerization of lactones and lactides using dendritic initiators. *Journal of Polymer Science Part A: Polymer Chemistry* **1999**, 37, 1923-1930.

92 Richez, A.; Belleney, J.; Bouteiller, L.; Pensec, S. Synthesis and MALDI-TOF analysis of dendritic-linear block copolymers of lactides: Influence of architecture on stereocomplexation. *Journal of Polymer Science Part A: Polymer Chemistry* **2006**, 44, 6782-6789.

93 Gitsov, I.; Wooley, K. L.; Hawker, C. J.; Ivanova, P. T.; Frechet, J. M. J. Synthesis and Properties of Novel Linear-Dendritic Block Copolymers- Reactivity of Dendritic Macromolecules towards Linear Polymers. *Macromolecules* **1993**, 26, 5621-5627.

94 Malenfant, P. R. L.; Groenendaal, L.; Frechet, J. M. J. Well-defined triblock hybrid dendrimers based on lengthy oligothiophene cores and poly(benzyl ether) dendrons. *Journal of the American Chemical Society* **1998**, 120, 10990-10991.

95 Gitsov, I.; Frechet, J. M. J. Novel Nanoscopic Architectures. Linear-Globular ABA Copolymers with Polyether Dendrimers as A Blocks and Polystyrene as B Block. *Macromolecules* **1994**, 27, 7309-7315.

96 Hua, C.; Peng, S.-M.; Dong, C.-M. Synthesis and characterization of linear-dendron-like poly(epsilon-caprolactone)-b-poly(ethylene oxide) copolymers via the combination of ring-opening polymerization and click chemistry. *Macromolecules* **2008**, 41, 6686-6695.

97 del Barrio, J.; Oriol, L.; Alcala, R.; Sanchez, C. Azobenzene-Containing Linear-Dendritic Diblock Copolymers by Click Chemistry: Synthesis, Characterization, Morphological Study, and Photoinduction of Optical Anisotropy. *Macromolecules* **2009**, 42, 5752-5760.

98 Del Barrio, J., Oriol, L., Alcala, R. & Sanchez, C. Photoresponsive Poly(methyl methacrylate)-b-Azodendron Block Copolymers Prepared by ATRP and Click Chemistry. *Journal of Polymer Science Part A: Polymer Chemistry* **2010**, 48, 1538-1550.

99 Del Barrio, J. *et al.* Self-Assembly of Linear-Dendritic Diblock Copolymers: From Nanofibers to Polymersomes. *Journal of the American Chemical Society* **2010**, 132, 3762-3769.

100 Shi, Z.; Lu, H.; Chen, Z.; Cheng, R.; Chen, D. Rational design, syntheses, characterization and solution behavior of amphiphilic azobenzene-containing linear-dendritic block copolymers. *Polymer* **2012**, 53, 359-369.

101 Shi, Z.; Chen, D.; Lu, H.; Wu, B.; Ma, J.; Cheng, R.; Fang J.; *Chen X.* Self-assembled hierarchical structure evolution of azobenzene-containing linear-dendritic liquid crystalline block copolymers. *Soft Matter* **2012**, 8, 6174-6184.

102 Higashihara, T.; Hayashi, M.; Hirao, A. Synthesis of well-defined star-branched polymers by stepwise iterative methodology using living anionic polymerization. *Progress in Polymer Science* **2011**, 36, 323-375.

103 Khanna, K.; Varshney, S.; Kakkar, A. Miktoarm star polymers: advances in synthesis, self-assembly, and applications. *Polymer Chemistry* **2010**, 1, 1171-1185.

104 Altintas, O.; Vogt, A. P.; Barner-Kowollik, C.; Tunca, U. Constructing star polymers via modular ligation strategies. *Polymer Chemistry* **2012**, 3, 34-45.

105 Durmaz, H. *et al.* Multiarm Star Block and Multiarm Star Mixed-Block Copolymers via Azide-Alkyne Click Reaction. *Journal of Polymer Science Part A: Polymer Chemistry* **2010**, 48, 99-108.

106 Altintas, O.; Hizal, G.; Tunca, U. ABC-type hetero-arm star terpolymers through “Click” chemistry. *Journal of Polymer Science Part A: Polymer Chemistry* **2006**, 44, 5699-5707.

107 Zhang, Y.; Li, C.; Liu, S. One-pot synthesis of ABC miktoarm star terpolymers by coupling ATRP, ROP, and click chemistry techniques. *Journal of Polymer Science Part A: Polymer Chemistry* **2009**, 47, 3066-3077.

108 He, X.; Sun, W.; Yan, D.; Liang, L. Novel ABC2-type liquid-crystalline block copolymers with azobenzene moieties prepared by atom transfer radical polymerization. *European Polymer Journal* **2008**, 44, 42-49.

109 Wang, Y.; Lin, S.; Zang, M.; Xing, Y.; He, X.; Lin, J.; Chen T. Self-assembly and photo-responsive behavior of novel ABC2-type block copolymers containing azobenzene moieties. *Soft Matter* **2012**, 8, 3131-3138.

110 Sun, W.; He, X.; Gao, C.; Liao, X.; Xie, M.; Lin, S.; Yanc, D. Novel amphiphilic and photo-responsive ABC 3-miktoarm star terpolymers: synthesis, self-assembly and photo-responsive behavior. *Polymer Chemistry* **2013**, 4, 1939-1949.

111 Ostroverkhova, O.; Moerner, W. E. Organic Photorefractives: Mechanisms, Materials, and Applications. *Chemical Reviews* **2004**, 104, 3267-3314.

112 Matharu, A. S.; Jeeva, S.; Ramanujam, P. S. Liquid crystals for holographic optical data storage. *Chemical Society Reviews* **2007**, 36, 1868-1880.

113 Juodkazis, S.; Mizeikis, V.; Misawa, H. in *Photoresponsive Polymers I* Vol. 213 *Advances in Polymer Science* (eds SethR Marder & Kwang-Sup Lee) Ch. 122, 157-206 (Springer Berlin Heidelberg, 2008).

114 Hvilsted, S.; Sanchez, C.; Alcala, R. The volume holographic optical storage potential in azobenzene containing polymers. *Journal of Materials Chemistry* **2009**, 19, 6641-6648.

115 Audorff, H.; Kreger, K.; Walker, R.; Haarer, D.; Kador, L.; Schmidt, H.-W. Holographic gratings and data storage in azobenzene-containing block copolymers and molecular glasses. *Advanced in Polymer Science* **2010**, 228, 59-121.

116 Bruder, F.-K.; Hagen, R.; Rölle, T.; Weiser, M.-S.; Fäcke, T. From the Surface to Volume: Concepts for the Next Generation of Optical–Holographic Data-Storage Materials. *Angewandte Chemie International Edition* **2011**, 50, 4552-4573.

117 Cumpston, B. H. Ananthavel, S. P.; Barlow, S.; Dyer, D.L.; Ehrlich, J.E.; Erskine, L. L.; Heikal, A. A.; Kuebler, S. M.; Lee, I.-Y.; McCord-Maughon, D.; Qin, J.; Röckel, H.; Rumi, M.; Wu, X.-L.; Marder, S.R.; Perry J.W. Two-photon polymerization initiators for three-dimensional optical data storage and microfabrication. *Nature* **1999**, 398, 51-54.

118 Strickler, J. H.; Webb, W. W. 3-Dimensional Optical-Data Storage in Refractive media by 2-Photon Point Excitation. *Optics Letters* **1991**, 16, 1780-1782.

119 Holme, N. C. R.; Ramanujam, P. S.; Hvilsted, S. Photoinduced anisotropy measurements in liquid-crystalline azobenzene side-chain polyesters. *Applied Optics* **1996**, 35, 4622-4627.

120 Sánchez, C.; Alcalá, R.; Hvilsted, S.; Ramanujam, P. S. High diffraction efficiency polarization gratings recorded by biphotonic holography in an azobenzene. *Applied Physics Letters* **2001**, 78, 3944.

121 Lee, M.-J.; Jung, D.-H.; Han, Y.-K. Photo-responsive Polymers and their Applications to Optical Memory. *Molecular Crystals and Liquid Crystals* **2006**, 444, 41-50.

122 Bieringer, T.; Wuttke, R.; Haarer, D.; Geßner, U.; Rübner, J. Relaxation of holographic gratings in liquid-crystalline side chain polymers with azo chromophores. *Macromolecular Chemistry and Physics* **1995**, 196, 1375-1390.

123 Yu, H.; Naka, Y.; Shishido, A.; Ikeda, T. Well-Defined Liquid-Crystalline Diblock Copolymers with an Azobenzene Moiety: Synthesis, Photoinduced Alignment and their Holographic Properties. *Macromolecules* **2008**, 41, 7959-7966.

124 Yu, H.; Ikeda, T. Photocontrollable Liquid-Crystalline Actuators. *Advanced Materials* **2011**, 23, 2149-2180.

125 Finkelmann, H.; Nishikawa, E.; Pereira, G. G.; Warner, M. A New Opto-Mechanical Effect in Solids. *Physical Review Letters* **2001**, 87, 015501.

126 Li, M. H.; Keller, P.; Li, B.; Wang, X.; Brunet, M. Light-Driven Side-On Nematic Elastomer Actuators. *Advanced Materials* **2003**, 15, 569-572.

127 Kondo, M.; Yu, Y. L.; Ikeda, T. How does the initial alignment of mesogens affect the photoinduced bending behavior of liquid-crystalline elastomers? *Angewandte Chemie-International Edition* **2006**, 45, 1378-1382.

128 Yu, Y.; Nakano, M.; Ikeda, T. Photomechanics: Directed bending of a polymer film by light. *Nature* **2003**, 425, 145-145.

129 Nagano, S; Koizuka, Y; Murase, T; Sano, M; Shinohara, Y; Amemiya, Y ; Seki, T. Synergy Effect on Morphology Switching: Real-Time Observation of Photo-Orientation of Microphase Separation in a Block Copolymer. *Angewandte Chemie-International Edition* **2012**, 21, 5884-5888.

130 Yu, H.; Iyoda, T.; Ikeda, T. Photoinduced Alignment of Nanocylinders by Supramolecular Cooperative Motions. *Journal of the American Chemical Society* **2006**, 128, 11010-11011.

131 Morikawa, Y.; Kondo, T.; Nagano, S.; Seki, T. Photoinduced 3D Ordering and Patterning of Microphase-Separated Nanostructure in Polystyrene-Based Block Copolymer. *Chemistry of Materials* **2007**, 19, 1540-1542.

132 Adams, M. L.; Lavasanifar, A.; Kwon, G. S. Amphiphilic block copolymers for drug delivery. *Journal of Pharmaceutical Sciences* **2003**, 92, 1343-1355.

133 Blanazs, A.; Armes, S. P.; Ryan, A. J. Self-Assembled Block Copolymer Aggregates: From Micelles to Vesicles and their Biological Applications. *Macromolecular Rapid Communications* **2009**, 30, 267-277.

134 Tyrrell, Z. L.; Shen, Y. Q.; Radosz, M. Fabrication of micellar nanoparticles for drug delivery through the self-assembly of block copolymers. *Progress in Polymer Science* **2010**, 35, 1128-1143.

135 Gohy, J.-F.; Zhao, Y. Photo-responsive block copolymer micelles: design and behavior. *Chemical Society Reviews* **2013**. DOI: 10.1039/C3CS35469E

136 Wang, G.; Tong, X.; Zhao, Y. Preparation of azobenzene-containing amphiphilic diblock copolymers for light-responsive micellar aggregates. *Macromolecules* **2004**, 37, 8911-8917.

137 Ravi, P. Sin, S. L.; Gan, L. H.; Gan, Y.Y.; Tam, K.C.; Xia, X. L.; Hu, X. New water soluble azobenzene-containing diblock copolymers: synthesis and aggregation behavior. *Polymer* **2005**, 46, 137-146.

138 Lin, L.; Yan, Z.; Gu, J.; Zhang, Y.; Feng, Z.; Yu, Y. UV-Responsive Behavior of Azopyridine-Containing Diblock Copolymeric Vesicles: Photoinduced Fusion, Disintegration and Rearrangement. *Macromolecular Rapid Communications* **2009**, 30, 1089-1093.

139 Tang, X. D.; Gao, L. C.; Fan, X. H.; Liang, X. C.; Zhou, Q. F. Self-Assembly and Photoresponsivity Property of Amphiphilic ABA Triblock Copolymers Containing Azobenzene Moieties in Dilute Solution. *Macromolecular Chemistry and Physics* **2009**, 210, 1556-1562.

140 Feng, Z.; Lin, L.; Yan, Z.; Yu, Y. L. Dual Responsive Block Copolymer Micelles Functionalized by NIPAM and Azobenzene. *Macromolecular Rapid Communications* **2010**, 31, 640-644.

141 Jochum, F. D.; Theato, P. Thermo- and light responsive micellation of azobenzene containing block copolymers. *Chemical Communications* **2010**, 46, 6717-6719.

142 Boissiere, O.; Han, D.; Tremblay, L.; Zhao, Y. Flower micelles of poly(N-isopropylacrylamide) with azobenzene moieties regularly inserted into the main chain. *Soft Matter* **2011**, 7, 9410-9415.

143 Wang, D.; Wang, X. Amphiphilic azo polymers: Molecular engineering, self-assembly and photoresponsive properties. *Progress in Polymer Science* **2013**, 38, 271-301.

144 Jin, Q.; Liu, G.; Ji, J. Micelles and reverse micelles with a photo and thermo double-responsive block copolymer. *Journal of Polymer Science Part A: Polymer Chemistry* **2010**, 48, 2855-2861.

145 Huang, C.-Q.; Wang, Y.; Hong, C.-Y.; Pan, C.-Y. Spiropyran-Based Polymeric Vesicles: Preparation and Photochromic Properties. *Macromolecular Rapid Communications* **2011**, 32, 1174-1179.

146 Yan, B.; He, J.; Ayotte, P.; Zhao, Y. Optically Triggered Dissociation of Kinetically Stabilized Block Copolymer Vesicles in Aqueous Solution. *Macromolecular Rapid Communications* **2011**, 32, 972-976.

147 Kotharangannagari, V. K.; Sánchez-Ferrer, A.; Ruokolainen, J.; Mezzenga, R. Photoresponsive Reversible Aggregation and Dissolution of Rod–Coil Polypeptide Diblock Copolymers. *Macromolecules* **2011**, 44, 4569-4573.

148 Goodwin, A. P.; Mynar, J. L.; Ma, Y. Z.; Fleming, G. R.; Frechet, J. M. J. Synthetic micelle sensitive to IR light via a two-photon process. *Journal of the American Chemical Society* **2005**, 127, 9952-9953.

149 Mynar, J. L.; Goodwin, A. P.; Cohen, J. A.; Ma, Y.; Fleming, G. R.; Fréchet, J. M. J. Two-photon degradable supramolecular assemblies of linear-dendritic copolymers. *Chemical Communications* **2007**, 2081-2082.

150 Katz, J. S.; Zhong, S.; Ricart, B. G.; Pochan, D. J.; Hammer, D. A.; Burdick, J. A. Modular Synthesis of Biodegradable Diblock Copolymers for Designing Functional Polymersomes. *Journal of the American Chemical Society* **2010**, 132, 3654-3655.

151 Wang, D.; Ren, H.; Wang, X.; Wang, X. Amphiphilic Diblock Copolymers Functionalized with Strong Push−Pull Azo Chromophores: Synthesis and Multi-Morphological Aggregation. *Macromolecules* **2008**, 41, 9382-9388.

152 Zhang, L.; Eisenberg, A. Multiple Morphologies of "Crew-Cut" Aggregates of Polystyrene-b-poly(acrylic acid) Block Copolymers. *Science* **1995**, 268, 1728-1731.

153 Lin, Y.-L.; Chang, H.-Y.; Sheng, Y.-J.; Tsao, H.-K. Photoresponsive Polymersomes Formed by Amphiphilic Linear–Dendritic Block Copolymers: Generation-Dependent Aggregation Behavior. *Macromolecules* **2012**, 45 , 7143–7156.

154 Russell, T. P. Surface-responsive materials. *Science* **2002**, 297, 964-967.

155 Sun, T. L.; Feng, L.; Gao, X. F.; Jiang, L. Bioinspired surfaces with special wettability. *Accounts of Chemical Research* **2005**, 38, 644–652.

156 Grunze, M. Surface science - Driven liquids. *Science* **1999**, 283, 41-42.

157 Mendes, P. M. Stimuli-responsive surfaces for bio-applications. *Chemical Society Reviews* **2008**, 37, 2512-2529.

158 Wang, R.; Hashimoto, K.; Fujishima, A.; Chikuni, M.; Kojima, E.; Kitamura, A.; Shimohigoshi, M.; Watanabe, T. Light-induced amphiphilic surfaces. *Nature* **1997**, 388, 431-432 (1997).

159 Nakajima, A.; Hashimoto, K.; Watanabe, T. Transparent Superhydrophobic Thin Films with Self-Cleaning Properties. *Langmuir* **2000**, 16, 7044-7047.

160 Sun, R.-D.; Nakajima, A.; Fujishima, A.; Watanabe, T.; Hashimoto, K. Photoinduced Surface Wettability Conversion of ZnO and TiO2 Thin Films. *The Journal of Physical Chemistry B* **2001**, 105, 1984-1990.

161 Wang, S.; Song, Y.; Jiang, L. Photoresponsive surfaces with controllable wettability. *Journal of Photochemistry and Photobiology C: Photochemistry Reviews* **2007**, 8, 18-29.

162 Rosario, R.; Gust, D.; Hayes, M.; Jahnke, F.; Springer, J.; Garcia J. A. Photon-modulated wettability changes on spiropyran-coated surfaces. *Langmuir* **2002**, 18, 8062-8069.

163 Edahiro, J.; Sumaru, K.; Tada, Y.; Ohi, K.; Takagi, T.; Kameda, M.; Shinbo, T.; Kanamori, T.; Yoshimi, Y. In Situ Control of Cell Adhesion Using Photoresponsive Culture Surface. *Biomacromolecules* **2005**, 6, 970-974.

164 Ichimura, K.; Oh, S. K.; Nakagawa, M. Light-driven motion of liquids on a photoresponsive surface. *Science* **2000**, 288, 1624-1626.

165 Oh, S. K., Nakagawa, M. & Ichimura, K. Photocontrol of liquid motion on an azobenzene monolayer. *Journal of Materials Chemistry* **2002**, 12, 2262-2269.

166 Delorme, N.; Bardeau, J. F.; Bulou, A.; Poncin-Epaillard, F. Azobenzene-containing monolayer with photoswitchable wettability. *Langmuir* **2005**, 21, 12278–12282.

167 Hamelmamm, F.; Heinzmann, U.; Siemling, U.; Bretthauer, F.; der Bruggen, J. V. Light-stimulated switching of azobenzene-containing self-assembled monolayers. *Applied Surface Science* **2004**, 222, 1-5.

168 Liu, X.; Cai, M.; Liang, Y.; Zhou, F.; Liu, W. Photo-regulated stick-slip switch of water droplet mobility. *Soft Matter* **2011**, 7, 3331-3336.

169 Lim, H. S.; Han, J. T.; Kwak, D.; Jin, M.; Cho, K. Photoreversibly switchable superhydrophobic surface with erasable and rewritable pattern. *Journal of the American Chemical Society* **2006**, 128, 14458-14459.

CHAPTER 2

Linear-Dendritic Block Copolymers for Optical Applications

Published in *Polymer* **2012**, 53, 4604-4613

2.1 Introduction and Aims

Photoresponsive polymers having azobenzene moieties in the side chain have been widely studied as smart materials in the field of optical applications. Most of these applications are based on the azobenzene molecular reorientation induced by irradiation with LPL.[1-7] In particular, azobenzene containing polymers have been actively investigated as volume holographic optical storage media, which has been briefly described in Chapter 1. The reason behind is that azopolymers are easy to fabricate, good quality thin films can be obtained with an initial isotropic distribution of the chromophores, and after irradiation with LPL a large birefringence can be created. However, volume holography requires of thick films of azopolymers as was noted before, and BC architecture brings about the opportunity of reducing the azobenzene content within the film maintaining the photoinduced cooperative motions into the microsegregated phases.

Most of the azobenzene BCs reported for optical applications are linear-linear diblock copolymers where the non-absorbing block is either PMMA[8,9] or PS.[10,11] These BCs are efficiently prepared by controlled radical polymerization techniques that allowed a good control over the polymerization process although the number of azobenzene chromophores by macromolecule is difficult to accurately control. Recently, a series of photoresponsive linear-dendritic block copolymers (LDBCs) with azobenzene units was described by our research group. These LDBCs were synthesised by coupling the first four generations of dendritic aliphatic polyesters based on bis-MPA functionalised at the periphery with 4-cyanoazobenzene moieties to either PEG or PMMA as linear segments.[12-14] In these studies, it was found that using PEG in a LDBC based on the dendron having sixteen azobenzene units (fourth-generation) a stable photoinduced anisotropy was achieved by irradiating at 488 nm. However, PEG is not appropriate for optical applications due to its high crystallinity and low glass transition. Optical applications better require amorphous linear blocks and in this way, PMMA was used which confers processability and transparency to the LDBCs although photoinduced anisotropy was lower than in PEG-azodendron LDBCs.

To extend the study about the influence of the linear block on the properties of LDBCs, the investigation of new series of LDBCs containing a poly(ethyl methacrylate) (PEMA) or PS linear block linked to a liquid crystalline aliphatic polyester dendron functionalised with sixteen cyanoazobenzene moieties as planned, as well as the analogous with PMMA as reference (**Figure 2.1**). The main aim of this work was then the preparation and characterisation of these LDBCs for the subsequent study of the optical properties of films processed from these materials. It should be noticed that the dendron used in the synthesis of these materials has a 6-azidohexyl group at the focal point in contrast to the 2-azidoethyl group used in previous work.[12] This structural change was merely motivated because it implies the manipulation of 6-azido-1-hexanol, instead of the more dangerous 2-azido-1-ethanol (very recently Polymer Factory started the commercialisation of dendrons having the same azidohexyl group at the focal point). PEMA was selected because it has a chemical structure that is closely related to that of PMMA but has a lower T_g. PS, which is easily synthesised by ATRP, was investigated because it has a similar T_g to PMMA but different polarity than PMMA and it is aromatic in character as the azobenzene, which should have influence on the microphase segregation properties. As mentioned, the LDBC having a PMMA linear block of similar degree of polymerization was synthesised as reference to establish straight comparisons.

This work was carried out in collaboration with the Department of Condensed Matter Physics. Morphological and optical studies of the LDBCs were performed in the laboratories of the group of Prof. Rafael Alcalá.

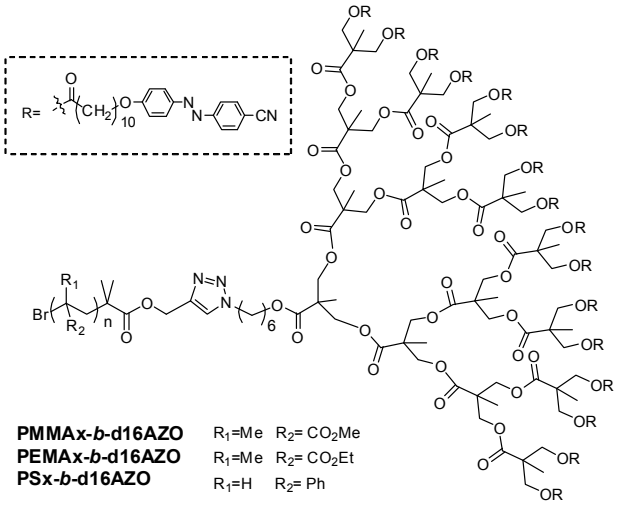

Figure 2.1 *Chemical structure of the proposed LDBCs*

2.2 Tasks and Methods

- Synthesis of the dendritic block consisting of a fourth-generation polyester dendron based on the bis-MPA acid functionalised with sixteen 4-cyanoazobenzene moieties linked through a decamethylenic spacer and an azido functional group at the focal point.

- Synthesis of alkyne functionalised PMMA, PEMA and PS having two different average molecular weights of approx. 10000 and 20000 g/mol by ATRP.

- Synthesis of the proposed LDBCs accomplished by coupling of preformed blocks using CuAAC (**Figure 2.2**).

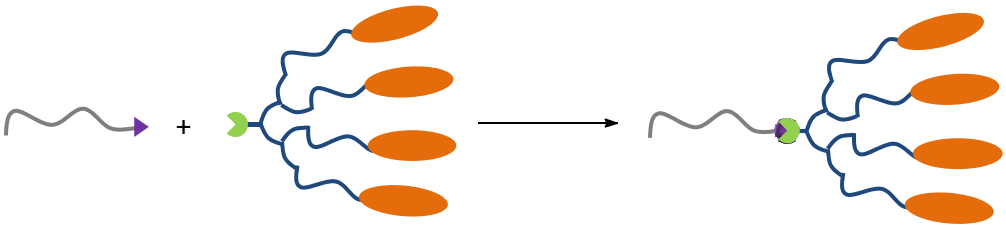

Figure 2.2 *Synthetic approach for the synthesis of the LDBCs*

- Structuctural characterisation of the building blocks and by FTIR, NMR, MS as well as elemental. Thermal characterisation using POM, TGA and DSC.

- Morphological characterisation of the LDBCs in bulk by TEM and optical studies of the LDBCs (carried out by the group of Prof. Rafael Alcalá).

2.3. Results and Discussion

2.3.1 Synthesis and Characterisation

The LDBCs were obtained by coupling an alkyne terminated linear blocks - PMMA, PEMA or PS- and the azide functionalised azodendron by CuAAC as it is shown in **Scheme 2.1**. This implies the synthesis of two separated blocks containing the azido and alkyne complementary functional groups. As noted above, the azido group was introduced at the focal point of the dendritic block and the alkyne in one of the end groups of the linear polymeric chain.

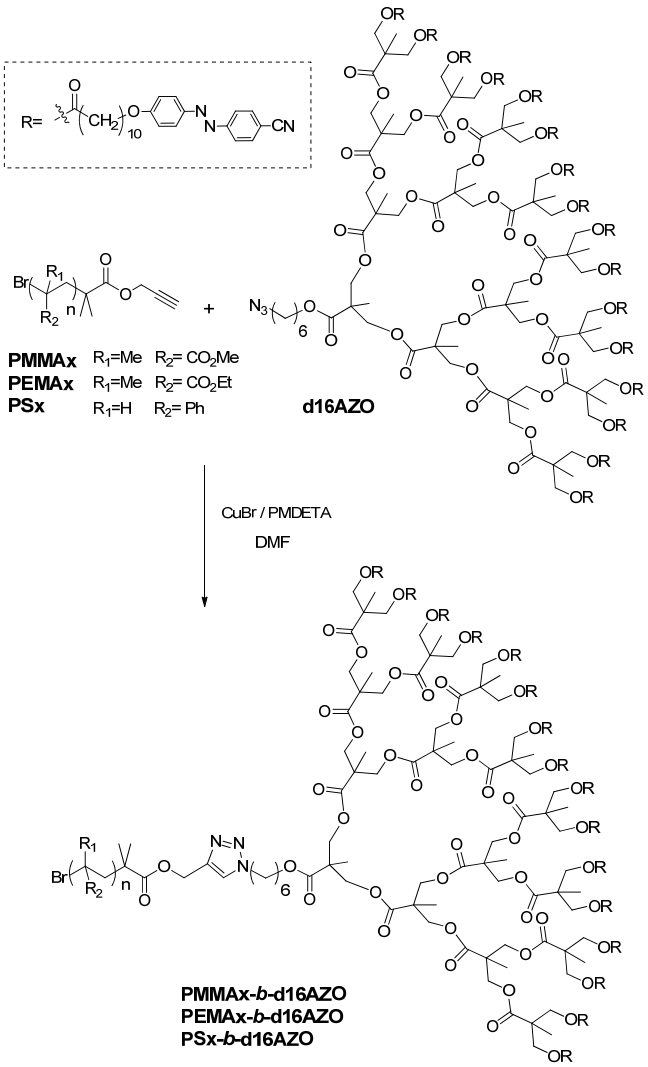

Scheme 2.1 *Synthesis of the investigated LDBCs*

The azido functionalised polyester dendron was synthesised according to a well known double stage convergent approach using bis-MPA as starting material which it is summarised in **Scheme 2.2**.[15] This strategy allows the preparation of the fourth generation dendron in high yields by alternating two efficient reactions, i.e esterification reaction and acetonide deprotection. The esterification reactions were performed using *N,N*-dicyclohexylcarbodiimide (DCC) and 4-(dimethylamino)pyridinium *p*-toluenesulfonate (DPTS) as catalyst obtaining relatively high yields. Deprotection of acetonide groups was carried out by employing the common acid resin Dowex® in a quantitative manner. Thus, the hydroxyl goups of bis-MPA were protected by reaction with 2,2-dimethoxypropane giving compound (**1**). Protected bis-MPA (**1**) was then esterified using 6-azidohexanol (**2**) to give compound (**3**), which rendered the azido derivative (**4**) after deprotection of the hydroxyl groups. The subsequent reaction of compound (**4**) with the protected bis-MPA (**1**) in a 1:2 stoichiometric ratio, and acetal deprotection, gives the second generation dendron generation (**6**) having an azido group in the focal point. On the other hand, the carboxylic group of the bis-MPA was protected using benzyl bromide to yield compound (**7**), that reacts with protected bis-MPA (**1**) to give the second-generation dendron (**9**) once the benzyl ester was deprotected. In the final step, the esterification of dendron (**6**) with dendron (**9)** in a 1:4 stoichiometric ratio gives the target azido functionalised dendron (**d16OH)** after deprotection of the hydroxyl groups.

Finally, the target azobenzene functionalised dendron (**d16AZO**) was obtained by esterification of the hydroxyl groups at the periphery with an excess of 11-[4-(4'-cyanophenylazo)phenyloxy]undecanoic acid (**AZO**) (synthetic details of **AZO** are given in the Experimental section) using DCC (**Scheme 2.3**). Evolution of the reaction was followed by MALDI-TOF MS until and the reaction was mantained until fully functionalisation of the dendron was observed. The product was purified by column chromatography and **d16AZO** was obtained in 55% yield.

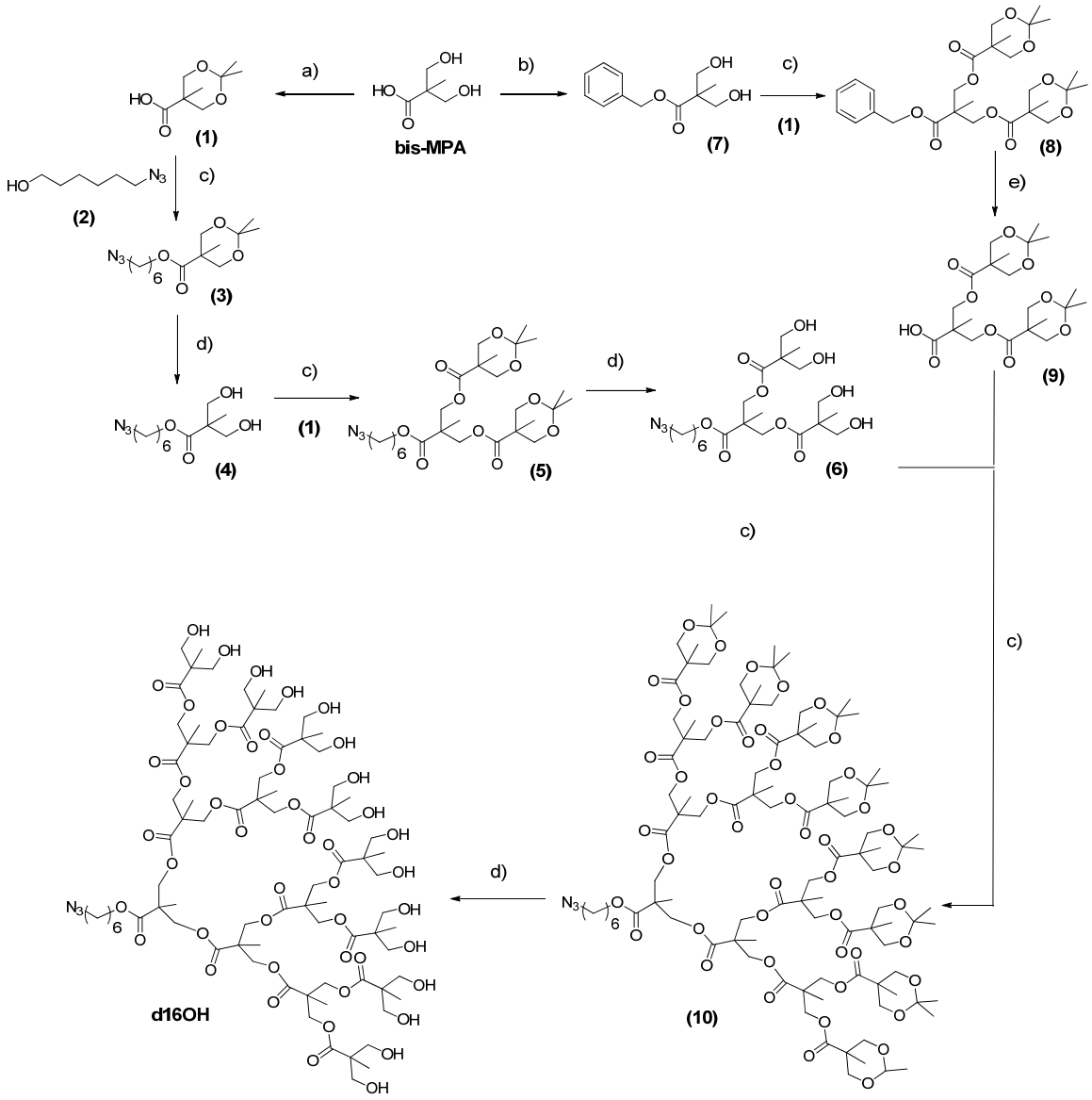

Scheme 2.2 *Synthesis of the fourth generation polyester dendron bearing an azide group in the focal point: a) 2,2-dimethoxypropane, TsOH, acetone, b) BnBr, KOH, DMF, c) DCC/DPTS, CH_2Cl_2, d) Dowex®, CH_3OH and e) Pd(C) 20%, AcOEt*

For the preparation of the alkyne functionalised linear chains, ATRP was selected as polymerization method (**Scheme 2.4**). Alkyne functionality can be introduced in either by utilizing functionalised initiators or a postpolymerization end group modification (bromine substitution in the case of ATRP). While the first procedure ensures complete functionalisation of all polymer chains, in the latter incomplete functionalisation due to the lost of the bromine group in the ATRP may occur. Following the strategy reported by van Hest and coworkers,[16]

an initiator with a trimethylsilyl protected alkyne group was prepared by esterification of α-bromoisobutyryl bromide with trimethylsilyl propargyl alcohol and employed for ATRP.

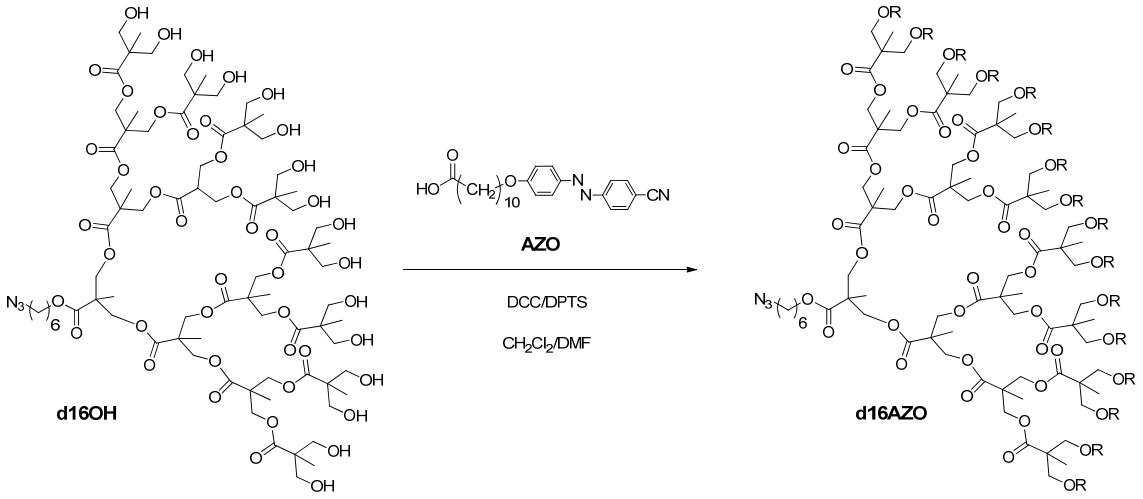

Scheme 2.3 *Synthesis of the azobenzene containing dendron (**d16AZO**)*

Linear blocks of PMMA, PEMA and PS with two different average molecular weights of approx. 10000 and 20000 g/mol were prepared. The polymerizations were performed in bulk at 90ºC (PMMA and PEMA) or 110ºC (PS) and employing CuBr and *N,N,N',N'',N''*- pentamethyldiethylenetriamine (PMDETA) as the catalyst system, according to procedures reported in the literature for PMMA and PS.[13,17] Polymerization times were adjusted to obtain different molecular weights. Number average molecular weights, M_n, of the linear blocks were determined by end group analysis of the TMS ended polymers by ^{1}H-NMR using the relative integral of the –Si(CH_3)$_3$ and –COOCH_3 of PMMA, –COOCH_2– of PEMA or aromatic protons of PS. **Figure 2.3** shows the ^{1}H-NMR of **PEMA2-TMS** indicating the signals used for M_n calculation. All data are gathered in **Table 2.1**. Molecular weight distribution were also determined by size exclusion chromatography (SEC) using PMMA standars in the case of PMMA and PEMA and PS standards for PS. SEC traces of linear blocks showed monomodal molar mass distributions. Low polydispersities ($Đ_M$

<1.1) were determined for PMMA and PS homopolymers and slightly higher ($Đ_M$ ≈1.2) for PEMA ones. This increment in the molecular weight distribution of PEMA could arise from uncontrolled termination processes.[18] In general, average molecular weights obtained by ^{1}H-NMR and SEC are very similar except for PEMA, although it should be taken account that data are referenced to PMMA standards. Finally, the trimethylsilyl protected alkyne functionalised linear blocks were deprotected with tetrabutylammonium fluoride (TBAF). Molecular masses of the deprotected polymers were also studied by SEC and the results are, as expected, very similar to those for the protected precursors.

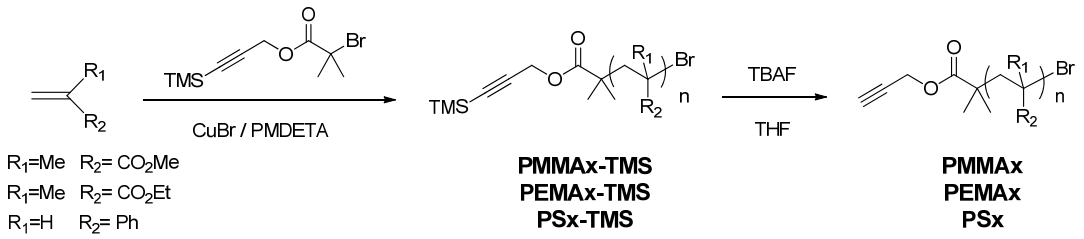

Scheme 2.4 *Synthesis of the alkyne terminated linear homopolymers (see Table 2.1 for the corresponding M_n)*

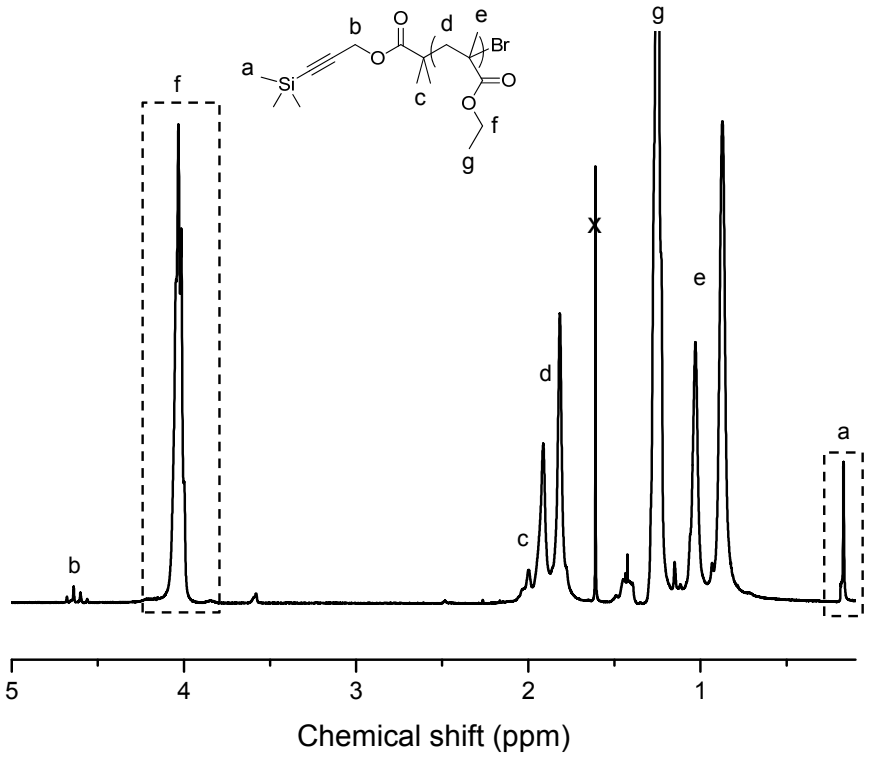

Figure 2.3 *^{1}H-RMN spectrum of the **PEMA2-TMS** in $CDCl_3$ (400 MHz) showing the signals used for M_n calculation*

***Table 2.1**. Molecular weight of the synthesised polymers*

Polymer	M_n	M_n [c]	$Đ_M$ [c]
PMMA1-TMS	10300[a]	11800	1.05
PMMA1	-	12100	1.04
PMMA2-TMS	19800[a]	19100	1.05
PMMA2	-	20200	1.04
PEMA1-TMS	9120[a]	11500	1.26
PEMA1	-	11800	1.22
PEMA2-TMS	18240[a]	23600	1.16
PEMA2	-	22800	1.20
PS1-TMS	10504[a]	10900	1.04
PS1	-	11100	1.04
PS2-TMS	20488[a]	19100	1.05
PS2	-	19500	1.05
PMMA1-b-d16AZO	18417[b]	16200	1.08
PMMA2-b-d16AZO	27917[b]	21600	1.09
PEMA1-b-d16AZO	17237[b]	20900	1.14
PEMA2-b-d16AZO	26357[b]	32400	1.19
PS1-b-d16AZO	18621[b]	16700	1.08
PS2-b-d16AZO	28695[b]	23500	1.08

[a] Number average molecular weight (M_n) calculated by ^{1}H-NMR (see text). [b] Calculated by the sum of the linear block M_n calculated by ^{1}H-NMR and the molecular weight of d16AZO. [c]M_n and $Đ_M$ of PMMA and PEMA homopolymers and their corresponding BCs were determined by SEC using PMMA standars. M_n and $Đ_M$ of PS homopolymers and their corresponding BCs were determined by SEC using PS standars.

In the final synthetic step, the azido functionalised dendritic block and the alkyne functionalised polymers were coupled by CuAAC using DMF as solvent and CuBr and PMDETA as the catalytic system (**Scheme 2.1**). A slight excess of the alkyne ended linear block was employed to ensure the completeness of the reaction and was eventually removed using an azido functionalised polystyrene resin. The efficiency of the coupling was asserted by SEC analysis. For PMMA and PEMA containing LDBCs, evidence of residual azodendron was not observed in SEC traces. This was not the case of PS containing LDBCs, where a very small peak corresponding to residual azodendron was detected in the SEC curve that indicates a less effective coupling (**Figure 2.4a**). Therefore, preparative SEC was used in order to purify completely the LDBC. **Figure 2.4b** collects the SEC curves corresponding to the precursor blocks and the **PS2-*b*-d16AZO** once purified. As can be observed, CuAAC coupling of the precursor blocks gives rise to a shift of the molar mass distribution peak towards lower retention times that indicates LDBC formation. Further evidence for the formation of the BCs was gained from the IR spectra, as can be seen for **PS2-*b*-d16AZO** in **Figure 2.5** as a representative example, where the band at 2100 cm^{-1} due to the azido group of the azodendron has disappeared upon coupling. The ^{1}H-NMR spectra of the LDBCs also confirm the coupling, as is shown in **Figure 2.6** for **PEMA1-*b*-d16AZO** as an example. Relative integration of azobenzene aromatic protons signals and the corresponding ones to the linear block protons (–COOCH_3 of PMMA at 3.60 ppm, –COOCH_2 of PEMA at 4.02 ppm or aromatic protons of the PS at 6.50 ppm) is in good agreement with the LDBCs structure, and confirms that there is not excess of any of the blocks. Furthermore, new peaks corresponding to the formed triazol ring appeared at 8.56 ppm (see peak labelled as '*o*' in **Figure 2.6**), and at 5.15 and 4.10 ppm corresponding to the methylenic protons linked to it (see protons '*n*' and '*p*' labelled in **Figure 2.6**).

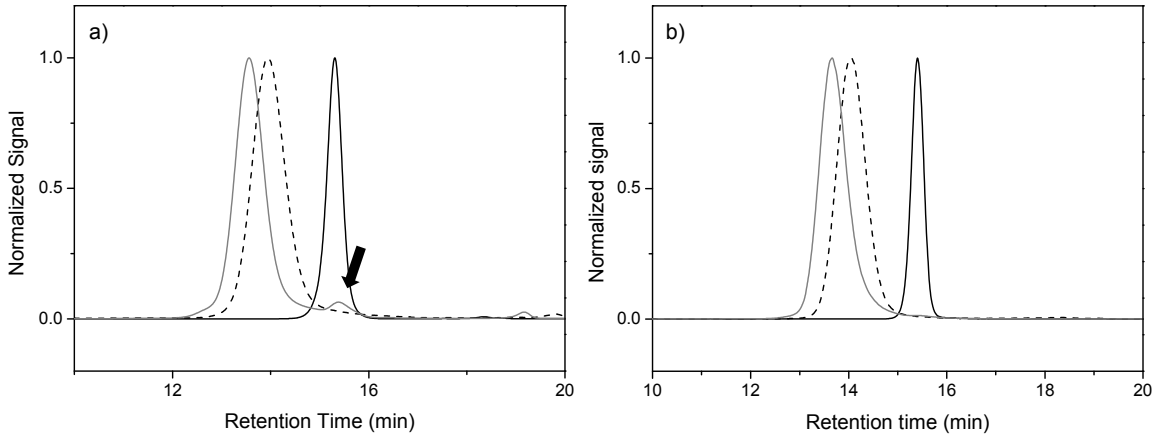

Figure 2.4 *SEC traces of* ***d16AZO*** *(black line) and* ***PS2*** *(dashed line) and* ***PS2-b-d16AZO*** *(grey line): a) before and b) after purification*

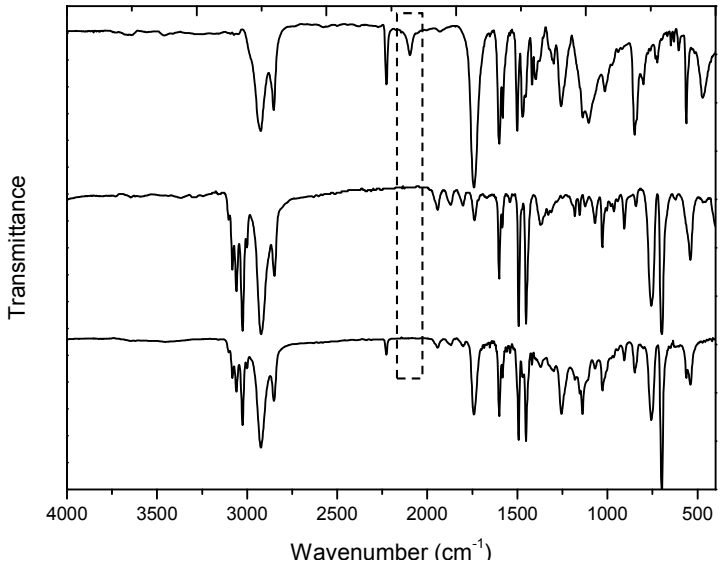

Figure 2.5 *FT-IR spectra in KBr of the LDBC* ***PS2-b-d16AZO*** *and the corresponding azodendron* ***d16AZO*** *and linear block* ***PS2*** *(bottom to top)*

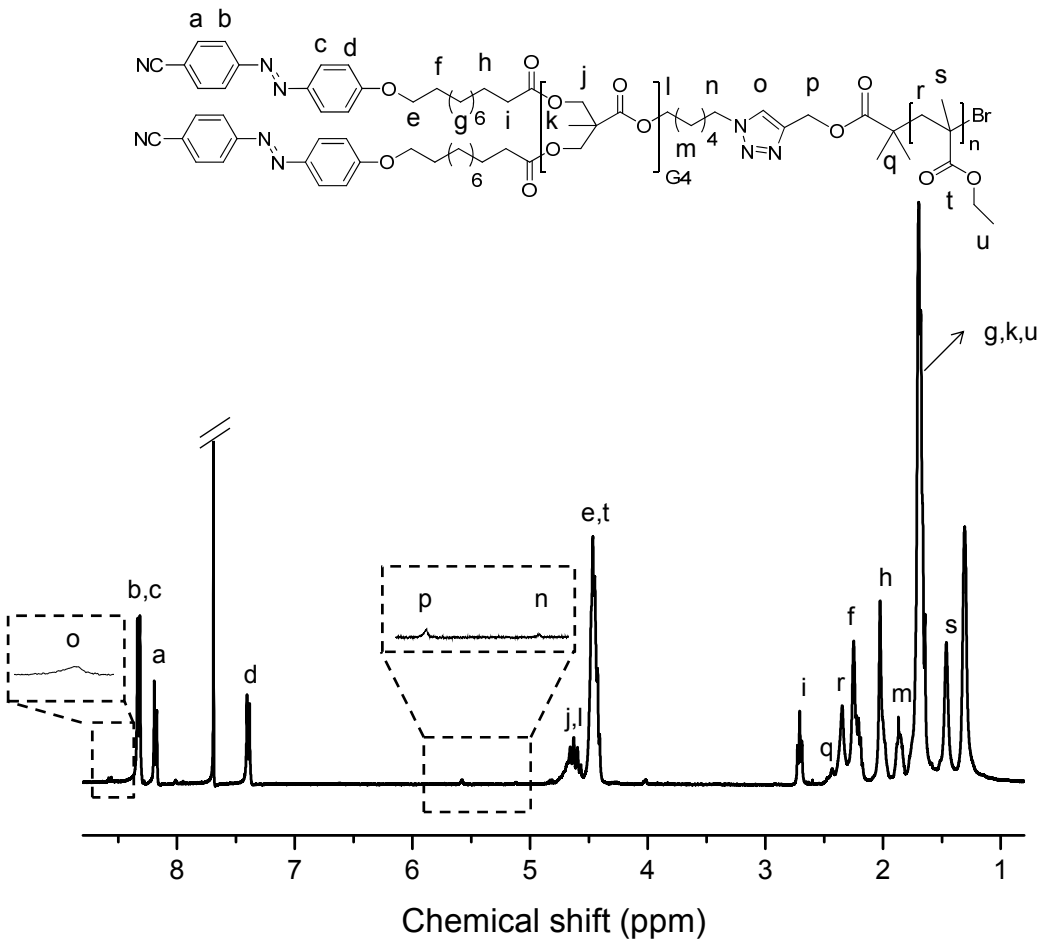

Figure 2.6 *^{1}H-RMN spectrum of the* ***PEMA1-b-d16AZO*** *in $CDCl_3$ (400 MHz) showing the signals used for M_n calculation*

2.3.2 Thermal Characterisation and Morphological Study

Thermal stability of the LDBCs as well as of the isolated blocks was studied by thermogravimetric analysis (TGA) under nitrogen atmosphere up to 600ºC using powdered samples. Weight losses associated to the presence of residual solvents or water were not detected. From the TGA curves, significant differences were observed for PMMA, PEMA and PS containing LDBCs (**Table 2.2**). PMMA and PEMA LDBCs showed major weight losses associated to sample decomposition above 315ºC. PS imparted superior thermal stability with major weight losses associated to sample decomposition above 390ºC.

Thermal transitions were studied by combining differential scanning calorimetry (DSC) and polarised optical microscopy (POM). Relevant data are collected in **Table 2.2**. The azodendron **d16AZO** is a vitreous material that exhibits a mesomorphic phase above glass transition, T_g. The DSC curve of the azodendron **d16AZO** presented a glass transition at 22ºC and a peak at 141ºC corresponding to a mesophase-to-isotropic transition (**Figure 2.7**). POM images of the azodendron showed fan shaped textures characteristic of a smectic A mesophase as can be seen in **Figure 2.8a.** The linear blocks were essentially amorphous materials. DSC curves showed a clear baseline jump corresponding to the glass transition with T_g values of around 115ºC for PMMA, 70ºC for PEMA and 100ºC for PS.

The investigated LDBCs exhibited DSC curves where two glass transitions were detected indicating microphase segregation of blocks. The lowest T_g, at 33-34ºC, corresponds to the glass transition of the azodendron block even if the calculated values are slightly higher (about 10ºC) than that of **d16AZO**. The highest T_g corresponds to the linear block and calculated values are also slightly higher than those of the corresponding homopolymers. All the LDBCs showed a peak corresponding to the mesophase-to-isotropic transition. The comparison between DSC curves of the azodendron, a linear block **PS-2** and the corresponding LDBC **PS2-*b*-d16AZO** is shown in **Figure 2.7**. For PMMA LDBCs, the higher T_g (at around 115ºC) overlaps the mesophase-to-isotropic transition. PEMA containing LDBCs circumvent this problem due to the lower T_g (at around 70ºC) of the linear block. All these LDBCs show liquid crystalline behaviour, although under POM they exhibited poorly defined textures which do not allow a clear identification of the mesophase (**Figure 2.8b**).

Table 2.2. *Thermal properties of the LDBCs and their building blocks*

	TGA[a]	DSC[b]			
Polymer	T_d	$T_{g(1)}$	$T_{g(2)}$	T_i	ΔH_i
d16AZO	313	22	-	141	78.8
PMMA1	342	-	115	-	-
PMMA2	361	-	113	-	-
PEMA1	252	-	69	-	-
PEMA2	271	-	66	-	-
PS1	390	-	97	-	-
PS2	390	-	98	-	-
PMMA1-*b*-d16AZO	341	32	116[c]	135[c]	63.4[c]
PMMA2-*b*-d16AZO	354	36	116[c]	134[c]	67.4[c]
PEMA1-*b*-d16AZO	326	33	70	134	64.9
PEMA2-*b*-d16AZO	317	33	76	133	69.4
PS1-b-d16AZO	392	34	102	134	34.6
PS2-*b*-d16AZO	393	34	102	141	39.7

[a] T_d (in ºC): decomposition temperature associated to mass lost calculated by TGA at the onset point in the weight loss curve. [b] Transition temperatures and enthalpies were determined by DSC from the second heating scan (10ºC/min): T_g = glass transition; T_i = isotropisation; ΔH_i= enthalpy associated to isotropisation. [c] Data cannot be calculated accurately. Mesophase-to-isotropic transition was overlapped with $T_{g(2)}$

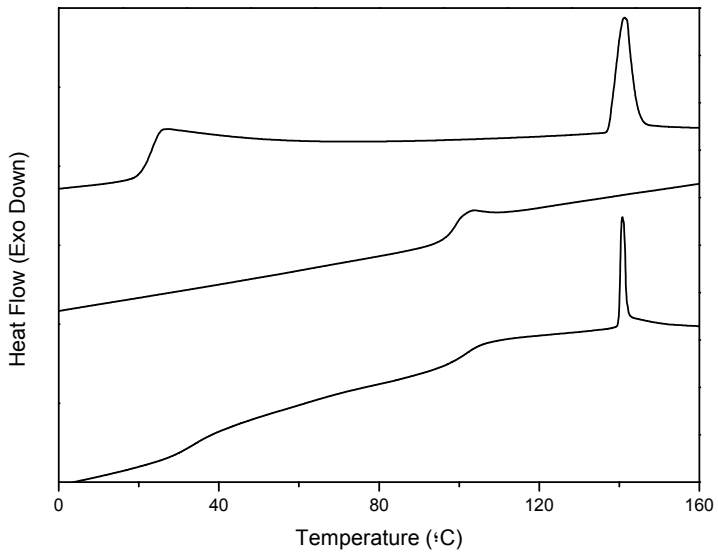

Figure 2.7 *DSC traces recorded at 10ºC/min corresponding to the second heating of* ***PS2****,* ***d16AZO*** and the corresponding LDBC ***PS2-b-d16AZO*** *(from top to bottom)*

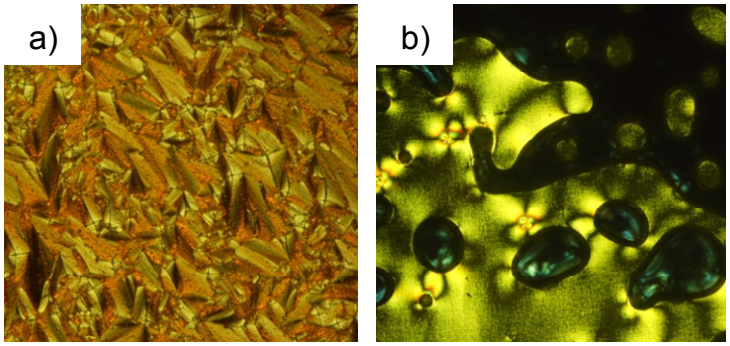

Figure 2.8 *POM images of* ***d16AZO*** *and* ***PEMA1-b-d16AZO*** *taken at 75ºC on cooling from the isotropic state*

The microphase segregation pointed by the DSC study was also confirmed by TEM in the study carried by the group of Prof. Alcalá. Small pellets of the LDBCs were prepared by heating the powdery polymers at 180ºC for about 2 min and subsequent fast cooling to room temperature. Pellets were then annealed for 1h at 140ºC and fast cooled again to room temperature. It was corroborated that longer annealing times at 140ºC does not introduce any significant change in the nanostructure. Then, thin slices (of about 100 nm thick) were cut from the pellets using a ultramicrotome, put on copper grids and

stained with RuO_4. TEM images show a lamellar nanostructure for all the compounds. As an example, **Figure 2.9** shows the nanostructure corresponding to three LDBCs containing different linear block.

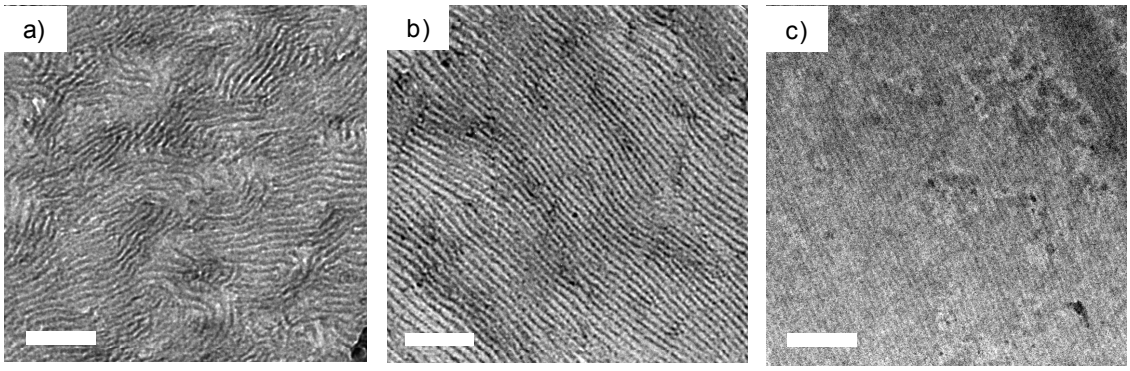

Figure 2.9 *TEM bright field micrographs of LDBCs: a)* ***PMMA1-b-d16AZO,*** *b)* ***PEMA1-b-d16AZO*** *and c)* ***PS1-b-d16AZO.*** *The size of the white bar is 200 nm*

Photoinduced anisotropy of LDBCs polymeric films has been studied by birefringence and dichroism measurements by the group of Prof. Alcalá. Although all the LDBCs showed a lamellar structure, they present very different photoinduced anisotropy. Low response has been obtained for the two BC containing PS while the two containing PMMA show a much higher response. In the case of PEMA compounds, different behaviour has been observed in **PEMA1-*b*-d16AZO** and in **PEMA2-*b*-d16AZO**.

2.4 Conclusions

A series of LDBCs composed of a linear block, and a dendritic block functionalised at the periphery with cyanoazobenzene units has been synthesised by the direct coupling of the preformed blocks.

Alkyne functionalised PMMA, PEMA and PS were first synthesised by ATRP and employed as the linear block. A dendron having sixteen peripheral 4-cyanoazobenzene photoresponsive units and a 6-azidohexyl chain in the focal point was coupled to the linear segment by CuAAC. This coupling was especially efficient in the case of the polymethacrylic derivatives.

All LDBCs exhibited liquid crystalline properties as well as a good thermal stability. T_g of PEMA derivatives was significant lower in comparison to PMMA one. DSC curves pointed to microphase segregation in all cases, which was also confirmed by TEM (lamellar microstructures).

2.5 Experimental Section

Materials

Methyl methacrylate, ethyl methacrylate and styrene (Aldrich, 99%) were passed through a basic alumina column, stored over CaH_2, and vacuum distilled before use. CuBr was used as received and handled in a dry box. All other commercially available reagents were purchased from Aldrich and used as received without further purification. The ATRP inititator 3-(trimethylsilyl)prop-2-ynyl 2-bromo-2-methylpropanoate and the azide functionalised PS resin were prepared according to literature procedures.[16,19]

2.5.1 Experimental Details for the Synthesis of the Azido Functionalised Fourth Generation Dendron (d16OH)

General Procedure for Esterification Reactions

The selected alcohol and acid, and DPTS were dissolved in dry dichloromethane (DCM). The reaction flask was flushed with argon, and a solution of DCC in dichloromethane was dropwise added. The mixture was stirred at room temperature for several hours under argon atmosphere. The formed white precipitate was filtered off and the solvent removed under vacuum. The crude product was purified by flash column chromatography on silica gel.

Synthesis and Characterisation of Isopropylidene-2,2-bis(methoxy) propionic acid (1)

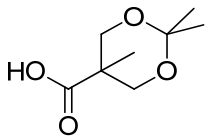

(1)

Bis-MPA (15.00 g, 111.83 mmol), 2,2-dimethoxypropane (20.6 mL, 167.74 mmol) and *p*-toluenesulfonic acid monohydrate (1.06 g, 5.59 mmol) were dissolved in acetone (75 mL). The reaction mixture was stirred for 2 h at room

temperature. Then, the catalyst was neutralised by adding a NH_3:EtOH (50:50) solution (approximately 1 mL) and the solvent was removed under vacuum. The residue was then dissolved in DCM (250 mL) and washed with water. The organic phase was dried over magnesium sulphate, filtered and the solvent was evaporated to give a white powder. Yield: 80%. IR (KBr), ν (cm^{-1}): 3360, 1718, 1706, 1225. ^{1}H-NMR ($CDCl_3$, 400MHz) δ (ppm): 4.18 (d, *J*=12.0 Hz, 2H), 3.68 (d, *J*=12.0 Hz, 2H), 1.45 (s, 3H), 1.42 (s, 3H), 1.21 (s, 3H). ^{13}C-NMR ($CDCl_3$, 100 MHz) δ (ppm): 179.7, 98.4, 65.9, 41.7, 25.4, 21.7, 18.3.

Synthesis and Characterisation of 6-azidohexan-1-ol (2)

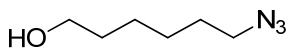

(2)

Sodium azide (6.42 g, 98.81 mmol) was added to a solution of 6-chlorohexan-1-ol (4.50 g, 32.93 mmol) in *N*,*N*-dimethylformamide (DMF) (20 mL). The mixture was stirred at 120°C for 24 h and then cooled to room temperature. The crude was diluted with diethyl ether, washed with water (3×75 mL), the organic layer dried over magnesium sulphate, filtered and evaporated to obtain 6-azidohexan-1-ol **(2)** as a colourless oil. Yield: 90%. IR (NaCl), ν (cm^{-1}): 3340, 2096, 1266. ^{1}H-NMR ($CDCl_3$, 400MHz) δ (ppm): 3.65 (t, *J*=6.5 Hz, 2H), 3.27 (t, *J*=6.9 Hz, 2H), 1.68-1.55 (m, 4H), 1.43-1.39 (m, 4H). ^{13}C-NMR ($CDCl_3$, 100 MHz) δ (ppm): 62.8, 51.4, 32.6, 28.8, 26.6, 25.3.

Synthesis and Characterisation of 6-azidohexyl 2,2,5-trimethyl-1,3-dioxane-5-carboxylate (3)

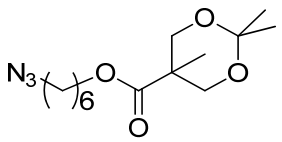

(3)

Compound **(3)** was prepared according to the described general esterification procedure by employing 6-azidohexan-1-ol **(2)** (3.18 g, 22.20 mmol), isopropylidene-2,2-bis(methoxy)propionic acid **(1)** (4.25 g, 24.40 mmol), DPTS (2.88 g, 9.77 mmol) and DCC (6.05 g, 29.28 mmol) in dry DCM (25 mL). The crude product was purified by flash column chromatography on silica gel, eluted with hexane, gradually increasing polarity to ethyl acetate/hexane (1:9) to yield

(3) as a colourless viscous oil. Yield: 75%. IR (NaCl), ν (cm^{-1}): 2097, 1728, 1257. ^{1}H-NMR ($CDCl_3$, 400MHz) δ (ppm): 4.18 (d, *J*=11.8 Hz, 2H), 4.15 (t, *J*=6.6 Hz, 2H), 3.64 (d, *J*=11.8 Hz, 2H), 3.27 (t, *J*= 6.9 Hz, 2H), 1.70-1.52 (m, 4H), 1.45-1.36 (m, 4H), 1.43 (s, 3H), 1.39 (s, 3H), 1.18 (s, 3H). ^{13}C-NMR ($CDCl_3$, 100 MHz) δ (ppm): 175.8, 98.4, 66.0, 64.7, 51.3, 41.8, 28.7, 28.4, 26.3, 25.4, 24.6, 22.7, 18.7.

Synthesis and Characterisation of 6-azidohexyl 2,2-di(hidroxyethyl) propanoate (4)

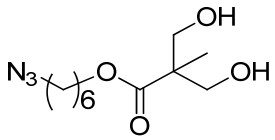

(4)

DOWEX-50-X2 resin (1.10 g) was added to a solution of compound **(3)** (4.50 g, 17.35 mmol) in methanol (40 mL). The mixture was stirred for 3 h at room temperature. Then the resin was filtered off and the solvent removed under vacuum to give **(4)** as a colourless viscous oil. Yield: 94%. IR (NaCl), ν (cm^{-1}): 3400, 2097, 1725, 1240. ^{1}H-NMR ($CDCl_3$, 400MHz) δ (ppm): 4.16 (t, *J*=6.6 Hz , 2H), 3.90 (d, *J*=11.2 Hz, 2H), 3.71 (d, *J*=11.2 Hz, 2H), 3.27 (t, *J*= 6.8 Hz, 2H), 1.75-1.67 (m, 2H), 1.67-1.56 (m, 2H), 1.47-1.36 (m, 4H), 1.05 (s, 3H). ^{13}C-NMR ($CDCl_3$, 100 MHz) δ (ppm): 176.0, 99.9, 68.5, 64.9, 51.2, 49.0, 28.6, 28.3, 26.3, 25.4, 17.1.

Synthesis and Characterisation of Compound (5)

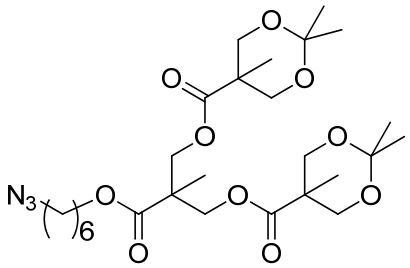

(5)

Compound **(5)** was prepared according to the described general esterification procedure by employing 6-azidohexyl 2,2-di(hidroxyethyl) propanoate **(4)** (3.67 g, 14.16 mmol), isopropylidene-2,2-bis(methoxy)propionic acid **(1)** (5.18 g, 29.73 mmol), DPTS (1.67 g, 5.66 mmol) and DCC (7.30 g, 35.38 mmol) in dry

DCM (50 mL). The crude product was purified by flash column chromatography on silica gel, eluted with hexane, gradually increasing polarity to ethyl acetate/hexane (2:8). Compound **(5)** was obtained as a colourless viscous oil. Yield: 70%. IR (NaCl), ν (cm^{-1}): 2097, 1737, 1219. ^{1}H-NMR ($CDCl_3$, 400MHz) δ (ppm): 4.27 (s, 4H), 4.09 (d, *J*=11.9 Hz, 4H), 4.06 (t, *J*=6.7 Hz, 2H), 3.56 (d, *J*=11.9 Hz, 4H), 3.21 (t, *J*= 6.9 Hz, 2H), 1.70-1.52 (m, 4H), 1.38-1.29 (m, 4H), 1.36 (s, 6H), 1.30 (s, 6H), 1.22 (3H), 1.09 (s, 6H). ^{13}C-NMR ($CDCl_3$, 100 MHz) δ (ppm): 173.5, 172.6, 98.1, 65.9, 65.3, 65.1, 51.3, 46.7, 42.0, 28.7, 28.4, 26.3, 25.5, 25.0, 22.2, 18.5, 17.7. MALDI-TOF MS (matrix: α-cyano-4-hydroxycinnamic acid, m/z): 594.3 $[M+Na]^+$.

Synthesis and Characterisation of Compound (6)

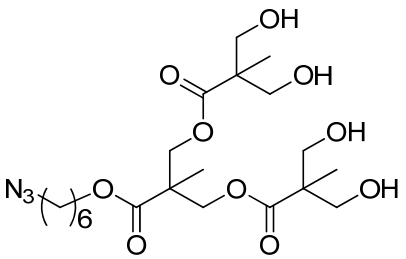

(6)

DOWEX-50-X2 resin (1.20 g) was added to a solution of compound **(5)** (5.05 g, 10.22 mmol) in methanol (50 mL) in a 250 mL round bottom flask. The mixture was stirred for 8 h at room temperature. Then, the resin was filtered off and the filtrate was removed under vacuum to give compound **(6)** as a colourless viscous oil. Yield: 97 %. IR (NaCl), ν (cm^{-1}): 3300, 2101, 1731, 1242. ^{1}H-NMR ($CDCl_3$, 400MHz) δ (ppm): 4.46 (d, *J*=11.1 Hz, 2H), 4.28 (d, *J*=11.1 Hz, 2H), 4.15 (t, *J*=6.6 Hz, 2H), 3.92-3.83 (m, 4H), 3.76-3.67 (m, 4H), 3.28 (t, *J*= 6.8 Hz, 2H), 1.70-1.52 (m, 4H), 1.45-1.36 (m, 4H), 1.31 (s, 3H), 1.05 (s, 6H). ^{13}C-NMR ($CDCl_3$, 100 MHz) δ (ppm): 175.1, 173.0, 68.2 ,65.4, 64.8, 51.3, 49.6, 46.3, 28.7, 28.4, 26.3, 25.5, 18.1, 17.1. MALDI-TOF MS (matrix: α-cyano-4-hydroxycinnamic acid, m/z): 514.2 $[M+Na]^+$.

Synthesis and Characterisation of Benzyl 2,2-di(hidroxyethyl)propanoate (7)

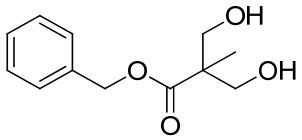

(7)

Bis-MPA (10.00 g, 74.55 mmol), and KOH (4.81 g, 85.73 mmol) were dissolved in DMF (50 mL). The mixture was heated at 100 °C for 1 h and benzyl bromide (10.6 mL, 89.46 mmol) was added then. After stirring for 15 h at 100 °C, DMF was evaporated off using a rotary evaporator. The residue was dissolved in DCM (200mL) and washed with water. Organic solvent was evaporated and the crude product was recrystallised from hexane/dicholoromethane (1:1). Yield: 60 %. IR (KBr), ν (cm^{-1}): 3360, 1706, 1606, 1499, 1226. ^{1}H-NMR ($CDCl_3$, 400MHz) δ (ppm): 7.45-7.28 (m, 5H), 5.20 (s, 2H), 3.93 (d, *J*= 11.3 Hz, 2H), 3.73 (d, *J*=11.3 Hz, 2H), 2.98 (s, 2H), 1.08 (s, 3H). ^{13}C-NMR ($CDCl_3$, 100 MHz) δ (ppm): 175.7, 135.6, 128.6, 128.3, 127.8, 68.1, 66.6, 49.2, 17.1.

Synthesis and Characterisation of Compound (8)

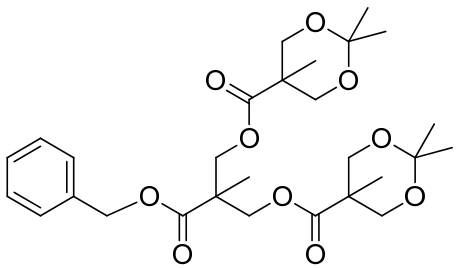

(8)

Compound **(8)** was prepared according to the described general esterification procedure by employing compound **(1)** (10.11 g, 58.06 mmol), compound **(7)** (6.20 g, 27.64 mmol), DPTS (3.25 g, 11.06 mmol) and DCC (14.26 g, 69.12 mmol) in dry DCM (80 mL). The crude product was purified by flash column chromatography on silica gel, eluted with hexane, gradually increasing the polarity to ethyl acetate/hexane (8:2). Compound **(8)** was obtained as a colourless viscous oil. Yield: 63%. IR (NaCl), ν (cm^{-1}): 1738, 1259. ^{1}H-NMR ($CDCl_3$, 400MHz) δ (ppm): 7.42-7.32 (m, 5H), 5.12 (s, 2H), 4.44 – 4.25 (m, 4H), 4.11 (d, *J* = 11.9 Hz, 4H), 3.58 (d, *J* = 11.6 Hz, 4H), 1.41 (s, 6H), 1.34 (s, 6H), 1.30 (s, 3H), 1.09 (s, 6H). ^{13}C-NMR ($CDCl_3$, 100 MHz) δ (ppm): 173.5, 171.8,

135.5, 128.6, 128.5, 128.3, 98.1, 66.0, 65.9, 64.8, 46.9, 46.7, 42.1, 25.2, 22.1, 18.5, 17.7. MALDI-TOF MS (matrix: dithranol, m/z): 559.3 $[M+Na]^+$.

Synthesis and Characterisation of Compound (9)

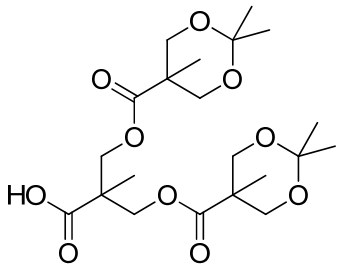

(9)

The compound **(8)** (4.00 g, 7.52 mmol) was dissolved in ethyl acetate and Pd/C (10%) (0,40 g) was added. Then the flask was evacuated from air and filled with H_2. After 4 h of stirring at room temperature, the catalyst was filtered off using Celite® and carefully washed with ethyl acetate. The solvent was evaporated and the product was obtained as a viscous oil. Yield: 98%. IR (NaCl), ν (cm^{-1}): 3300, 1742, 1258. ^{1}H-NMR ($CDCl_3$, 400MHz) δ (ppm): 4.35 (s, 4H), 4.17 (d, *J*=11.1 Hz, 4H), 3.63 (d, *J*= 11.9 Hz, 4H), 1.42 (s, 6H), 1.36 (s, 6H), 1.32 (s, 3H), 1.15 (s, 6H).^{13}C-RMN ($CDCl_3$, 100 MHz) δ (ppm): 173.6, 175.43, 98.2, 66.9, 66.0, 65.4, 46.8, 42.1, 25.1, 22.1, 18.5, 17.7. MALDI-TOF MS (matrix: α-cyano-4-hydroxycinnamic acid, m/z): 469.2 $[M+Na]^+$.

Synthesis and Characterisation of Compound (10)

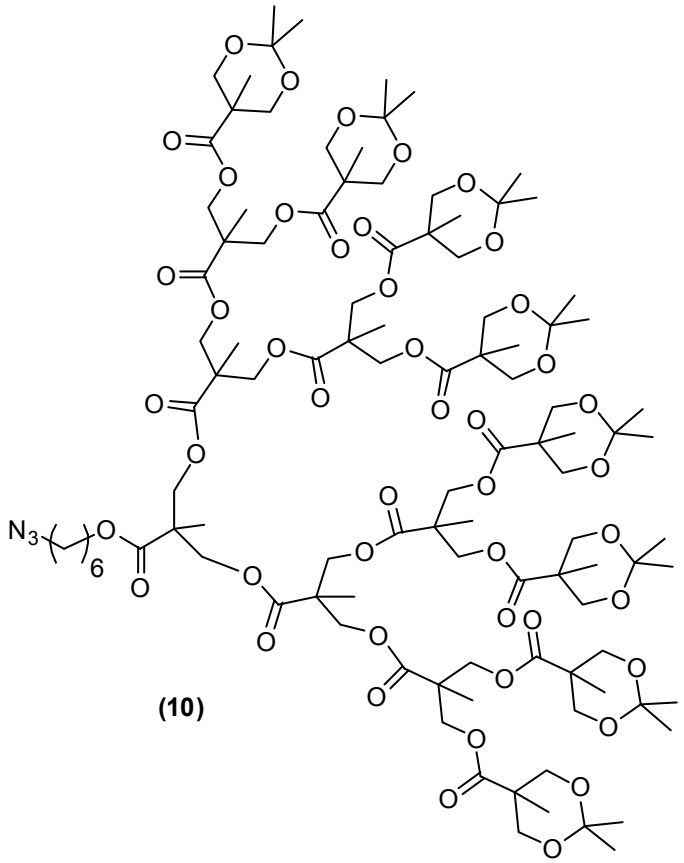

(10)

Compound (**10)** was prepared according to the general esterification procedure described from compound **(6)** (2.20 g, 4.48 mmol), compound **(9)** (12.00 g, 26.88 mmol), DPTS (5.27 g, 17.92 mmol) and DCC (6.01 g, 29.12 mmol) dissolved in dry DCM (80 mL). The crude product was purified by liquid chromatography on silica gel, eluted with hexane, gradually increasing to ethyl acetate/hexane (8:2). The product was obtained as colourless viscous oil. Yield: 63%. IR (NaCl), ν (cm^{-1}): 2097, 1725, 1259. ^{1}H-NMR ($CDCl_3$, 400MHz) δ (ppm): 4.37-4.20 (m, 30H) 4.14 (d, *J*=11.9 Hz, 16H), 4.11 (t, *J*=6.8 Hz, 2H), 3.62 (d, *J*=11.9 Hz, 16H), 3.28 (t, *J*=6.8Hz, 2H), 1.70-1.52 (m, 8H), 1.41 (s, 24H), 1.35 (s, 24H), 1.28-1.21 (m, 21H), 1.14 (s, 24H). ^{13}C-NMR ($CDCl_3$, 100 MHz) δ (ppm): 173.5, 171.8, 98.1, 66.0, 65.9, 64.8, 46.9, 46.7, 42.1, 25.2, 22.1, 18.5, 17.7. MALDI-TOF MS (matrix: α-cyano-4-hydroxycinnamic acid, m/z): 2205.1 $[M-H]^+$.

Synthesis and Characterisation of d16OH

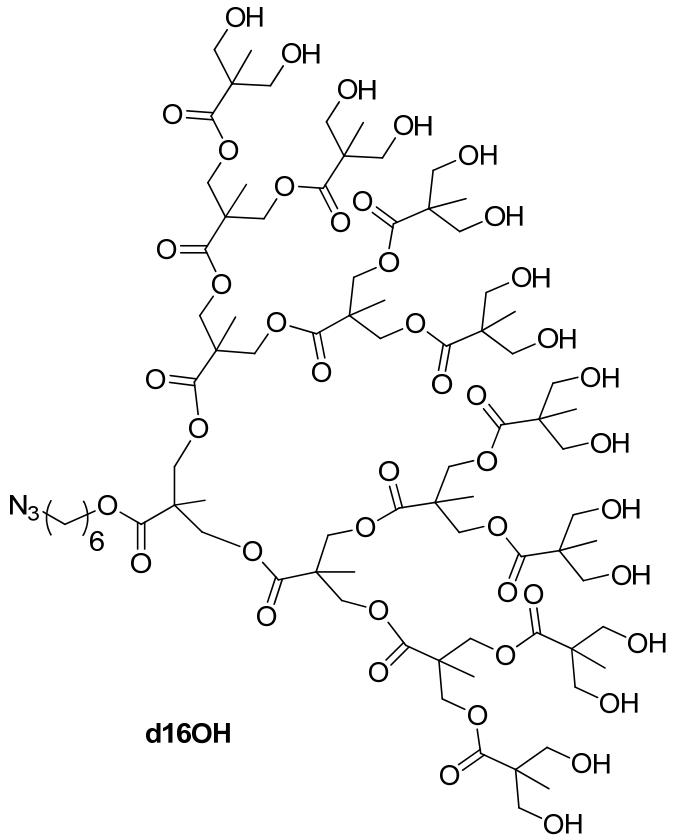

DOWEX-50-X2 resin (0.20 g) was added to a solution of compound **(10)** (1.00 g, 0.46 mmol) in methanol (10 mL). The mixture was stirred for 18 h at room temperature. Then the resin was filtered off and the solvent eliminated under vacuum to give **d16OH** as a colourless viscous oil. Yield: 97 %. IR (KBr), ν (cm^{-1}): 3400, 2099, 1729, 1239. ^{1}H-NMR (DMSO-d_6, 400MHz) δ (ppm): 4.65 (t, *J*=5.3Hz, 16H), 4.30-4.02 (m, 30H), 3.50-3.27 (m, 34H), 1.61-1.55 (m, 2H), 1.55-1.47 (m, 2H), 1.36-1.32 (m, 4H), 1.20 (s, 3H). 1.17 (s, 6H), 1.15 (s, 12H), 1.00 (s, 24H). ^{13}C-NMR ($CDCl_3$, 100 MHz) δ (ppm): 173.9, 171.7, 63.7, 63.6, 50.6, 50.2, 46.2, 28.0, 27.7, 25.7, 24.8, 17.1, 16.6. MALDI-TOF MS (matrix: dithranol, m/z): 1884.1 $[M+H]^+$.

2.5.2 Experimental Details for the Synthesis of 11-[4-(4'-cyanophenylazo) phenyloxy]undecanoic acid (AZO)

Synthesis and Characterisation of 4-(4'-hydroxyphenyazo)benzonitrile (11)

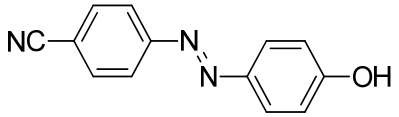

(11)

A mixture of 4-aminobenzonitrile (10.00 g, 84.60 mmol) and HCl 6M (40 mL) was cooled into an ice bath. A 2.5 M $NaNO_2$ solution (50 mL, 84.60 mmol) was added dropwise to the mixture and it was kept stirring in the ice bath. Then, a solution of phenol (7.10 g, 84.60 mmol) in 2 M NaOH (75 mL) was carefully added. The product was precipitated upon addition of HCl until neutral pH and it was purified by flash column chromatography on silica gel using DCM as an eluent. The product was obtained as a yellow powder. Yield: 65%. IR (KBr), ν (cm^{-1}): 3300, 2240, 1606, 1586, 1503, 1219, 844. ^{1}H-NMR ($CDCl_3$, 400MHz) δ (ppm): 7.95-7.91 (m, 4H), 7.81-7.79 (m, 2H), 6.98-6.96 (m, 2H), 5.33 (s, 1H). ^{13}C-NMR ($CDCl_3$, 100 MHz) δ (ppm): 133.1, 125.6, 123.0, 115.9.

Synthesis and Characterisation of Methyl 11-[4-(4'-cyanophenylazo) phenyloxy]undecanoate (12)

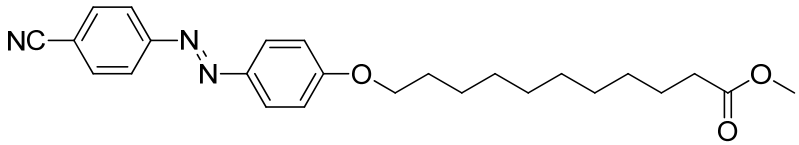

(12)

A solution of 4-(4'-hydroxyphenyazo)benzonitrile **(11)** (6.90 g, 30.90 mmol), methyl 11-bromoundecanoate (9.50 g, 34.05 mmol) in butanone (80 mL) was prepared. 18-Crown-6 ether (0.05 g) and potassium carbonate (5.10 g, 37.11 mol) were added. The suspension was stirred and heated under reflux for 24 h. Then, it was filtered and concentrated. The crude product was purified by flash column chromatography on silica gel using DCM as eluent. The product was obtained as a yellow powder. Yield: 65%. IR (KBr), ν (cm^{-1}): 2233, 1730, 1602, 1583, 1500, 1251, 863. ^{1}H-NMR ($CDCl_3$, 400MHz) δ (ppm): 7.95-7.93 (m, 4H),

7.80-7.72 (m, 2H), 7.02-7.00 (m, 2H), 4.06 (t, 2H, *J*=6.6 Hz), 3.67 (s, 3H), 2.31 (t, 2H, *J*=7.6 Hz), 1.85-1.78 (m, 2H), 1.69-1,53 (m, 4H), 1.51-1.41 (m, 2H), 1.39-1.17 (m, 8H). ^{13}C-NMR ($CDCl_3$, 100 MHz) δ (ppm): 174.8, 161.3, 146.9, 133.1, 125.5, 123.1, 118.6, 114.8, 68.1, 51.1, 33.8, 29.4, 28.8, 25.6, 24.6.

Synthesis and Characterisation of 11-[4-(4'-cyanophenylazo)phenyloxy] undecanoic acid (AZO)

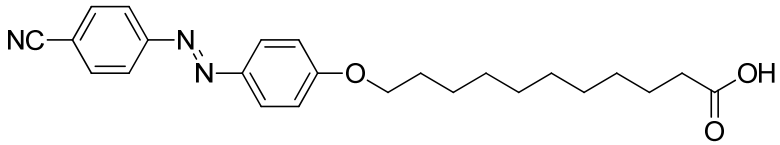

(AZO)

An aqueous solution of KOH (1.5 g, 15 mL) was added to a solution of methyl 11-[4-(4'-cyanophenylazo)phenyloxy]undecanoate **(12)** (8.00 g, 19.03 mmol) in ethanol and butanone (120 mL and 40 mL, respectively). The mixture was stirred and heated under reflux for 1 h. Then, the crude product was precipitated by addition of HCl until pH 2 and it was recovered by filtration. The product was recrystallised from ethanol. Yield: 70%. IR (KBr), ν (cm^{-1}): 3300, 2242, 1714, 1600, 1580, 1499, 1255, 851. ^{1}H-NMR (DMSO-d_6, 400MHz) δ (ppm): 8.05-8.03 (m, 2H), 7.97-7.92 (m, 4H), 7.16-7.13 (m, 2H), 4.08 (t, *J*=6.4 Hz, 2H), 2.18 (t, *J*=7.2 Hz, 2H), 1.78-1.69 (m, 2H), 1.52-1.44 (m, 2H), 1.44-1.36 (m, 2H), 1.34-1.17 (m, 10H). ^{13}C-NMR (DMSO-d_6, 100 MHz) δ (ppm): 174.5, 162.4, 154.1, 145.9, 133.7, 125.2, 122.8, 118.5, 115.2, 112.4, 68.1, 33.6, 28.9, 28.8, 28.7, 28.5, 28.4, 25.4, 24.4.

2.5.3 Synthesis and Characterisation of the Azodendron d16AZO

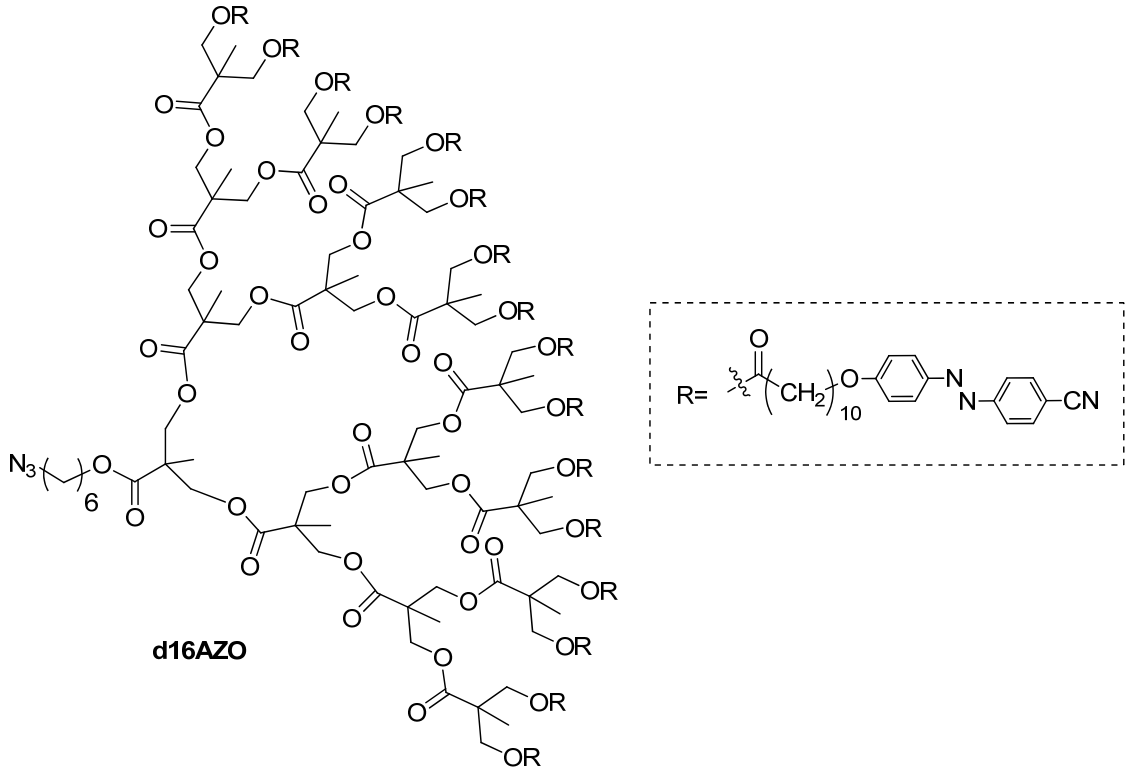

d16OH (0.75 g, 0.70 mmol), 11-[4-(4'-cyanophenylazo) phenyloxy]undecanoic acid **(AZO)** (3.11 g, 7.64 mmol) and DPTS (1.87 g, 6.36 mmol), were dissolved in a mixture of DCM (40 mL) and DMF (15 mL). The reaction flask was flushed with argon, and DCC (1.73 g, 8.40 mmol) was added. The mixture was stirred at room temperature for 48 h under argon atmosphere. The white precipitate formed was filtered off, and the solvent was evaporated. The crude product was purified by flash column chromatography on silica gel and eluted with DCM, gradually increasing the polarity to ethyl acetate:DCM (1:10). The target azodendron was obtained as a red powdery solid. Yield: 55%. IR (KBr), ν (cm^{-1}): 2227, 2096, 1741, 1600, 1582, 1501, 1257, 859. ^{1}H-NMR ($CDCl_3$, 400MHz) δ (ppm): 7.93-7.91 (m, 64H), 7.79-7.77 (m, 32H), 7.00-6.98 (m, 32H), 4.36-4.11 (m, 62H), 4.02 (t, *J*=6.5 Hz, 32H), 3.29 (t, *J*=6.7 Hz, 2H), 2.31 (t, *J*=7.5 Hz 32H), 1.81-1.78 (m, 32H), 1.64-1.56 (m, 32H), 1.50-1.40 (m, 36H), 1.39-1.24 (m, 209H). ^{13}C-NMR ($CDCl_3$, 100 MHz) δ (ppm): 173.1, 172.0, 162.6, 154.7, 146.6, 133.1, 125.4, 123.0, 118.6, 114.8, 113.2, 68.4, 64.7, 46.3, 34.0, 29.6, 29.5, 29.4, 29.3, 29.2, 26.0, 24.8, 17.8. MS ($MALDI^+$, dithranol) m/z: 8116.9

$[M-H]^+$. Anal. Calc for $C_{465}H_{565}N_{51}O_{78}$: C, 68.82; H, 6.97; N, 8.81. Found: C, 68.34; H, 7.22; N, 8.64.

2.5.4 Experimental Details for the Synthesis of the Linear Blocks

PMMA, PEMA and PS were synthesised by ATRP using 3-(trimethylsilyl)prop-2-ynyl 2-bromo-2-methylpropanoate,[16] an initiator with a protected alkyne function that was subsequently deprotected (refer to **Scheme 2.4**).

PMMA Polymerization

Methyl methacrylate (18.70 g, 0.19 mol), PMDETA (200 µL, 0.9 mmol), CuBr (134.3 mg, 0.9 mmol) and the initiator (260.2 mg, 0.9 mmol) were added to a Schlenk tube. The reaction mixture was degassed by three freeze-pump-thaw cycles and flushed with argon. The polymerization was carried out in a thermostated oil bath at 90ºC. After 5 min for **PMMA1-TMS** or 10 min for **PMMA2-TMS** the polymerization mixture was diluted with THF, passed through a column of neutral alumina to remove the catalyst and precipitated into methanol. The polymer was dried in a vacuum oven at 40ºC.

PEMA Polymerization

Ethyl methacrylate (13.76 g, 0.12 mol), PMDETA (144.1 µL, 0.7 mmol), CuBr (99.1 mg, 0.7 mmol) and the initiator (190.2 mg, 0.7 mmol) were added to a Schlenk tube. The reaction mixture was degassed by three freeze-pump-thaw cycles and flushed with argon. The polymerization was carried out in a thermostated oil bath at 90ºC. After 3 min for **PEMA1-TMS** or 8 min for **PEMA2-TMS** the polymerization mixture was diluted with THF, passed through a column of neutral alumina to remove the catalyst and precipitated into hexane. The polymer was dried in a vacuum oven at 40ºC.

PS Polymerization

Styrene (13.59 g, 0.14 mol), PMDETA (and 21.3 µL, 0.1 mmol), CuBr (14.6 mg, 0.1 mmol) and the initiator (28.3 mg, 0.1 mmol) were added to a Schlenk tube.

The reaction mixture was degassed by three freeze-pump-thaw cycles and flushed with argon. The polymerization was carried out in a thermostated oil bath at 110ºC. After 45 min for **PS1-TMS** or 4 h for **PS2-TMS** the polymerization mixture was diluted with THF, passed through a column of neutral alumina to remove the catalyst and precipitated into methanol. The polymer was dried in a vacuum oven at 40ºC.

General Procedure of Alkyne Deprotection

A 0.01 M solution of the protected alkyne-terminated polymer in THF was prepared and a five-fold excess of 1.0 M solution of TBAF in THF with respect to trimethylsilyl group (TMS) was added dropwise. The reaction mixture was stirred overnight at room temperature and the product was precipitated into cold methanol. The alkyne-ended linear polymer was dried at 40ºC under vacuum for 48 h.

Characterisation Data for PMMA1: IR (KBr), ν (cm^{-1}): 1728, 1240, 1150. ^{1}H-NMR ($CDCl_3$, 400MHz) δ (ppm): 4.68-4.58 (m), 3.59 (s), 2.06-1.75 (m), 1.48-1.38 (m), 1.26-1.13 (m), 1.10-0.80 (m). Anal. Calc: C, 59.98%; H, 8.05% Found: C, 60.30%; H, 7.89. SEC: M_n= 12100, $Đ_M$ =1.04 (PMMA standars).

Characterisation Data for PMMA2: IR (KBr), ν (cm^{-1}): 1729, 1242, 1147. ^{1}H-NMR ($CDCl_3$, 400MHz) δ (ppm): 4.65-4-52(m), 3.60 (s), 2.07-1.72 (m), 1.50-1.35 (m), 1.26-1.13 (m), 1.09-0.70 (m). Anal. Calc: C, 59.98%; H, 8.05% Found: C, 59.20%; H, 7.80%. SEC: M_n= 20200, $Đ_M$ =1.04 (PMMA standars)

Characterisation Data for PEMA1: IR (KBr), ν (cm^{-1}): 1728, 1269, 1146. ^{1}H-NMR ($CDCl_3$, 400MHz) δ (ppm): 4.60-4.36 (m), 4.02 (q, *J*=6.7 Hz), 2.10-1.70 (m), 1.34-1.10 (m), 1.10-0.80 (m). Anal. Calc: C, 63.14%; H, 8.83% Found: C, 63.34 %; H, 9.13 %. SEC: M_n= 11800, $Đ_M$ =1.22 (PMMA standars).

Characterisation Data for PEMA2: IR (KBr), ν (cm^{-1}): 1729,1272, 1147. ^{1}H-NMR ($CDCl_3$, 400MHz) δ (ppm): 4.60-4.36 (m), 4.02 (q, *J*=6.7 Hz), 2.10-1.70 (m), 1.24-1.10 (m), 1.10-0.80 (m). Anal. Calc: C, 63.14%; H, 8.83% Found: C, 63.42 %; H, 9.08 %. SEC: M_n = 22800, $Đ_M$ =1.20 (PMMA standars).

Characterisation Data for PS1: IR (KBr), ν (cm^{-1}): 1601, 1493, 756, 698. ^{1}H-NMR ($CDCl_3$, 400MHz) δ (ppm): 7.36-6.89 (m), 6.85-6.30 (m), 4.60-4.36 (m), 4.08-4.01 (m) , 2.29 (s), 2.05-1.65 (m) 1.62-0.85 (m). Anal. Calc: C, 92.26%; H, 7.74% Found: C, 91.99 %; H, 7.89 %. SEC: M_n = 11100, $Đ_M$ =1.04 (PS standars).

Characterisation Data for PS2: IR (KBr), ν (cm^{-1}): 1601, 1492, 756, 697. ^{1}H-NMR ($CDCl_3$, 400MHz) δ (ppm): 7.36-6.89 (m), 6.85-6.30 (m), 4.60-4.36 (m), 4.08-3.98 (m), 2.29 (s), 2.03-1.65 (m) 1.63-0.85 (m). Anal. Calc: C, 92.26%; H, 7.74% Found: C, 91.81 %; H, 7.98 %. SEC: M_n = 19500, $Đ_M$ =1.05 (PS standars).

2.5.5 Experimental Details for the Preparation of LDBCs

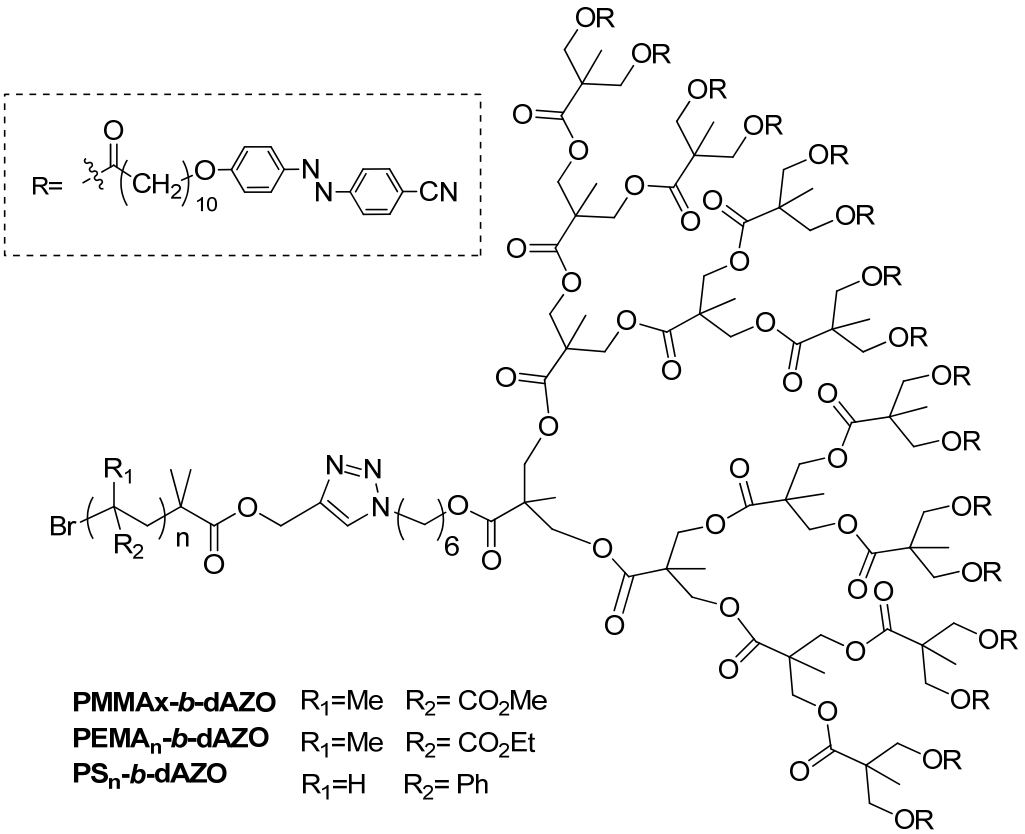

General Procedure for Coupling Reactions

Azodendron **d16AZO**, 1.2 fold excess of alkyne functionalised polymer and two-fold excess of CuBr were placed into a Schlenk tube. Two-fold excess of PMDETA and deoxygenated DMF (around 1 mL per 100 mg of polymer) were added with an argon-purged syringe, and the flask was further degassed by three freeze-pump-thaw cycles and flushed with argon. The reaction mixture was stirred at 40ºC for 72 h. Then, an azido functionalised resin was added under argon flow in order to remove the excess of the alkyne functionalised polymer and the reaction mixture was stirred for further 24 h. The resin was filtered off, the mixture diluted with THF and then passed through a short column of neutral alumina. The solvent was partially evaporated and the resulting polymer solution carefully precipitated into cold methanol.

Characterisation Data for PMMA1-*b*-d16AZO: IR (KBr), ν (cm^{-1}): 2228, 1727, 1601, 1582, 1500, 1256, 1141, 849. ^{1}H-NMR ($CDCl_3$, 400MHz) δ (ppm): 7.91-7.89 (m), 7.76-7.64 (m), 7.56 (s), 6.98-6.95(m), 5.15-5.11(m), 4.71-4.68 (m), 4.36-4.11 (m), 4.01 (t), 3.59 (s) 2.28 (t), 2.10-1.70 (m),1.65-1.48 (m), 1.47-1.34 (m), 1.34-1.10 (m), 1.10-0.80 (m). Anal. Calc: C, 62.47 %; H, 7.69 %; N, 3.88 % Found: C, 62.71 %; H, 7.38 %; N, 3.53 %.

Characterisation Data for PMMA2-*b*-d16AZO: IR (KBr), ν (cm^{-1}): 2228, 1728, 1600, 1582, 1499 (Ar), 1265, 1146, 852. ^{1}H-NMR ($CDCl_3$, 400MHz) δ (ppm): 7.91-7.89 (m), 7.76-7.64 (m), 7.55 (s), 6.98-6.95 (m), 5.14-5.11 (m), 4.36-4.11 (m), 3.99 (t), 3.60 (s), 2.28 (t), 2.10-1.70 (m),1.65-1.48 (m), 1.47-1.34 (m), 1.34-1.10 (m), 1.10-0.80 (m). Anal. Calc: C, 62.34 %; H, 7.68 %; N, 2.47 % Found: C, 62.63 %; H, 7.41 %; N, 2.11 %.

Characterisation Data for PEMA1-*b*-d16AZO: IR (KBr), ν (cm^{-1}): 2227 1727, 1600, 1582, 1501, 1257, 1141, 851. ^{1}H-NMR ($CDCl_3$, 400MHz) δ (ppm): 7.91-7.89 (m), 7.76-7.64 (m), 7.56 (s), 6.98-6.95 (m), 5.15-5.11(m), 4.71-4.68 (m), 4.36-4.11 (m), 4.09-3.91 (m), 2.28 (t), 2.10-1.70 (m),1.65-1.48 (m), 1.47-1.34 (m), 1.34-1.10 (m), 1.10-0.80 (m). Anal. Calc: C, 64.49 %; H, 8.39 %; N, 2.10 % Found: C, 64.92 %; H, 7.95 %; N, 2.67%.

Characterisation Data for PEMA2-*b*-d16AZO: IR (KBr), ν (cm^{-1}): 2228, 1728, 1601, 1583, 1501, 1265, 1145, 858. ^{1}H-NMR ($CDCl_3$, 400MHz) δ (ppm): 7.91-7.89 (m), 7.76-7.64 (m), 7.55 (s), 6.98-6.95 (m), 5.14-5.11 (m), 4.36-4.11 (m), 4.09-3.91 (m), 2.28 (t), 2.10-1.70 (m),1.65-1.48 (m), 1.47-1.34 (m), 1.34-1.10 (m), 1.10-0.80 (m). Anal. Calc: C, 64.51 %; H, 8.33 %; N, 2.29 % Found: C, 64.06 %; H, 7.97 %; N, 1.99%.

Characterisation Data for PS1-*b*-d16AZO: IR (KBr), ν (cm^{-1}): 2227, 1741, 1600, 1582, 1493, 1255, 848, 757, 698. ^{1}H-NMR ($CDCl_3$, 400MHz) δ (ppm): 7.91-7.89 (m), 7.77-7.64 (m), 7.51-6.89 (m), 6.85-6.30 (m), 4.36-4.11 (m), 4.00 (t), 2.28 (t), 1.97-1.63 (m), 1.63-0.89 (m). Anal. Calc: C, 82.30 %; H, 7.42 %; N, 3.74 % Found: C, 82.68 %; H, 7.43 %; N, 3.59 %.

Characterisation Data for PS2-*b*-d16AZO. IR (KBr), ν (cm^{-1}): 2227, 1741, 1600, 1582, 1493, 1256, 848, 756, 698. ^{1}H-NMR ($CDCl_3$, 400MHz) δ (ppm): 7.91-7.89 (m), 7.77-7.64 (m), 7.51-6.89 (m), 6.85-6.30 (m), 4.36-4.11 (m), 4.01 (t), 2.28 (t), 1.97-1.63 (m), 1.63-0.89 (m). Anal. Calc: C, 85.37 %; H, 7.52 %; N, 2.59 % Found: C, 85.68 %; H, 7.90 %; N, 2.07%.

References

1 Ivanov, S.; Ivanov S.; Yakovlev I.; Kostromin S.; Shibaev V.; Läsker L.; Stumpe J.; Kreysig D. Laser-Induced Birefringence in Homeotropic Films of Photochromic Comb-Shaped Liquid-Crystalline Copolymers with Azobenzene Moieties at Different Temperatures. *Makromolekulare Chemie-Rapid Communications* **1991**, 12, 709-715.

2 Ichimura, K. Photoalignment of liquid-crystal systems. *Chemical Reviews* **2000**, 100, 1847-1873.

3 Hagen, R.; Bieringer, T. Photoaddressable polymers for optical data storage. *Advanced Materials* **2001**, 13, 1805-1810.

4 Natansohn, A.; Rochon, P. Photoinduced motions in azo-containing polymers. *Chemical Reviews* **2002**, 102, 4139-4175.

5 Zhao, Y.; Ikeda, T. *Smart light-responsive materials : azobenzene-containing polymers and liquid crystals*. (Wiley-Interscience, **2009**).

6 Ikeda, T.; Ube, T. Photomobile polymer materials: from nano to macro. *Materials Today* **2011**, 11, 480-487.

7 Yu, H.; Ikeda, T. Photocontrollable Liquid-Crystalline Actuators. *Advanced Materials* **2011**, 23, 2149-2180.

8 Forcen, P.; Oriol.L.; Sánchez, C.; Hvilsted, S.; Jankova, K.; Loos, J. Synthesis, characterization and photoinduction of optical anisotropy, in liquid crystalline diblock azo-copolymers. *Journal of Polymer Science Part a-Polymer Chemistry* **2007**, 45, 1899-1910.

9 Gimeno, S.; Forcén, P.; Oriol, L.; Piñol, M.; Sánchez, C.; Rodríguez, F.J.; Alcalá, R.; Jankova, K.; Hvilsted, S. Photoinduced optical anisotropy in azobenzene methacrylate block copolymers: Influence of molecular weight and irradiation conditions. *European Polymer Journal* **2009**, 45, 262-271.

10 Chen, W.; Wei, X.; Balazs, A.C.; Matyjaszewski, K.; Russell, T. P. Phase Behavior and Photoresponse of Azobenzene-Containing Polystyrene-block-poly(n-butyl methacrylate) Block Copolymers. *Macromolecules* **2011**, 44, 1125-1131.

11 Huang, C.-F.; Chen, W.; Russell, T.P.; Balazs, A.C.; Chang, F.-C.; Matyjaszewski, K. Synthesis of Photoisomerizable Block Copolymers by Atom Transfer Radical Polymerization. *Macromolecular Chemistry and Physics* **2009**, 210, 1484-1492.

12 del Barrio, J.; Oriol, L.; Alcala, R.; Sanchez, C. Azobenzene-Containing Linear-Dendritic Diblock Copolymers by Click Chemistry: Synthesis, Characterization, Morphological Study, and Photoinduction of Optical Anisotropy. *Macromolecules* **42**, 5752-5760.

13 Del Barrio, J.; Oriol, L.; Alcala, R.; Sanchez, C. Photoresponsive Poly(methyl methacrylate)-b-Azodendron Block Copolymers Prepared by ATRP and Click Chemistry. *Journal of Polymer Science Part A: Polymer Chemistry* **2010**, 48, 1538-1550.

14 del Barrio, J.; Oriol, L.; Sánchez, C.; Serrano, J.L.; Di Cicco, A.; Keller, P.; Li, M.H. Self-Assembly of Linear-Dendritic Diblock Copolymers: From Nanofibers to Polymersomes. *Journal of the American Chemical Society* **2010**, 132, 3762-3769.

15 Ihre, H.; Hult, A.; Frechet, J. M. J.; Gitsov, I. Double-stage convergent approach for the synthesis of functionalized dendritic aliphatic polyesters based on 2,2-bis(hydroxymethyl)propionic acid. *Macromolecules* **1998**, 31, 4061-4068.

16 Opsteen, J. A.; van Hest, J. C. M. Modular synthesis of block copolymers via cycloaddition of terminal azide and alkyne functionalized polymers. *Chemical Communications* **2005**, 57-59.

17 Durmaz, H.; Dag, A.; Erdogan, E.; Demirel, A. L.; Hizal,G.; Tunca, U. Multiarm Star Block and Multiarm Star Mixed-Block Copolymers via Azide-Alkyne Click Reaction. *Journal of Polymer Science Part A: Polymer Chemistry* **2010**, 48, 99-108.

18 Munoz-Molina, M. J.; Belderrain, T. R.; Perez, P. J. Efficient Atom-Transfer Radical Polymerization of Methacrylates Catalyzed by Neutral Copper Complexes. *Macromolecules* **2010**, 43, 3221-3227.

19 Lober, S.; Rodriguez-Loaiza, P.; Gmeiner, P. Click linker: Efficient and high-yielding synthesis of a new family of SPOS resins by 1,3-dipolar cycloaddition. *Organic Letters* **2003**, 5, 1753-1755.

CHAPTER 3

Amphiphilic Linear-Dendritic Block Copolymers: Self-assembly and Photoresponse

Published in *Polym. Chem.* **2013**, 4, 2246-2254

3.1 Introduction and Aims

As it was described in Chapter 1, one of the most important features of amphiphilic BCs is their ability to undergo spontaneous phase separation in solution forming different supramolecular structures of nanoscale dimensions, such as spheres, rods, lamellae or vesicles.[1-3] Among all the different morphologies, polymeric vesicles, also known as polymersomes, are of particular interest as drug nanocontainers. Polymer vesicles originate from closing bilayers forming a central aqueous compartment which is enclosed by an amphiphilic copolymer bilayer membrane.[4] The hydrophobic chains create the wall membrane stabilised by the hydrophilic chains forming internal and external coronas (**Figure 3.1**).

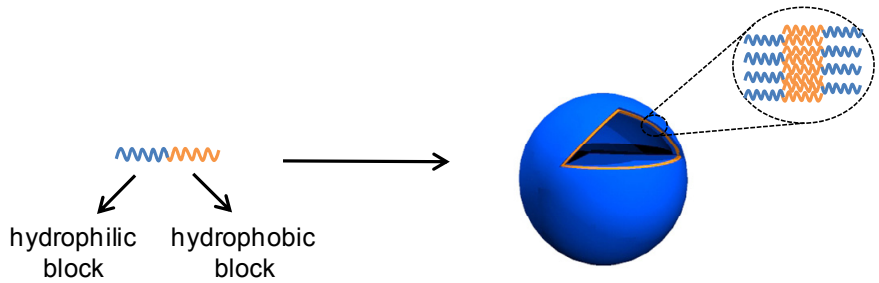

Figure 3.1 *Schematic representation of a polymeric vesicle*

Because of their internal hydrophilic cavities and robust hydrophobic membranes, vesicles can physically store both hydrophobic and hydrophilic compounds. The hydrophilic molecules will be encapsulated within the aqueous interior and hydrophobic molecules will be integrated within the membrane. The methods of loading the molecules into the polymersomes are diverse.[5] Hydrophobic compounds can be solubilised into the vesicle bilayer by diffusion on stirring together with the vesicles suspension or by cooperative encapsulation during the self-assembly process. Hydrophilic molecules can be directly encapsulated during the vesicle formation. Depending on the properties of the hydrophobic block, vesicles might retain loaded molecules very long periods of time, from days to weeks.

The membrane regulates transport of molecules between the inside and outside of the vesicle and its properties can be easily designed and tailored on varying the structural and chemical features of the BCs to include a range of desirable functions which make them useful in various technologies.[6] For instance, modification of the coronas might determine the surface characteristics of the vesicles and hence their interactions with the environment. But also, the incorporation of stimuli sensitive groups into the membrane wall might activate the delivery of cargo molecules on demand.[5]

In this context, our research group studied a diversity of aqueous assemblies (cylindrical micelles, sheet-like micelles, tubular micelles, as well as polymer vesicles) exhibited by a series of amphiphilic LDBCs composed of PEG of different molecular weights and dendrons based on bisMPA functionalised at the periphery with 4-cyanoazobenzene moieties. In particular, vesicles were observed for the LDBC consisting of a fourth generation dendron with sixteen 4-cyanoazobenzene units and a 2000 g/mol linear PEG.[7] The proposed model for these vesicles consists of a bilayer organisation for the azobenzene groups packing in the hydrophobic domains with internal and external PEG coronas. In order to check the photoresponse of these vesicles, they were irradiated with UV light to induce *trans*-to-*cis* isomerisation of the azobenzene located in the inner part of the bilayer. Nevertheless, morphological changes of the vesicles were only achieved by irradiation with intense UV light (**Figure 3.2**). It is well recognised the strong tendency of 4-cyanoazobenzenes towards antiparallel dipolar interactions[8,9] and it has been described that for highly and densely packed azobenzene moieties the fast and highly efficient *trans*-to-*cis* isomerisation is hindered.[10,11] Consequently, disruption of the membrane formed by such densely packed arrangements of 4-cyanoazobenzene might be restricted.

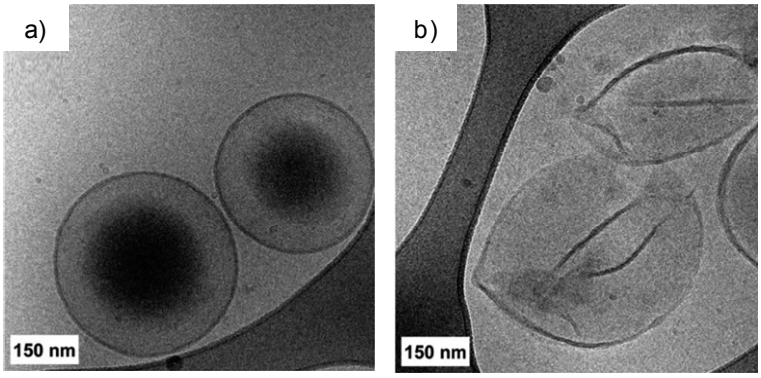

Figure 3.2 *Cryo-TEM images of cyanoazobenzene containing vesicles before (a) and after (b) irradiation for 35 min at 360 nm and 150 mW/cm^2*

Due to the potential of vesicles as controlled delivery systems, the aim of this work is the preparation of new LDBCs able to self-assembly into polymeric vesicles which can act as light controlled delivery nanocarriers upon irradiation with low intensity UV light. The use of low intensity UV irradiation limits possible undesired side photochemical process as well as the damage of the organic structures when exposed to UV irradiation. For that purpose, the fourth generation of azodendrons derived from bisMPA and PEG of 2000 g/mol average molecular weight as the linear block has been selected (**Figure 3.3**). The cyano group at the *para*- position of the azobenzene moiety of the previously mentioned materials has been substituted by an alkoxy one. This substituents should have a lower tendency to antiparallel and dense arrangements. Furthermore, alkoxy *para*-substituents increase the difference in polarity between the *trans* and the *cis* isomers compared to the cyano one and, as it was above recognised, this facilitates the disruption of self-assemblies under UV irradiation.[12]

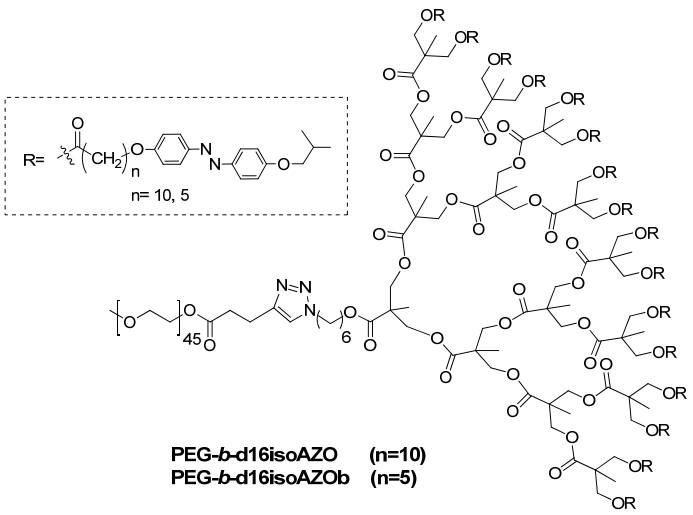

Figure 3.3 *Chemical structure of the proposed LDBCs*

3.2 Tasks and Methods

- Synthesis of the blocks consisting of a fourth generation polyester dendron based on the bisMPA acid functionalised with sixteen 4-alkoxyazobenzene moieties linked through different spacers and an azido functional group at the focal point.

- Synthesis of alkyne functionalised PEG 2000 g/mol as linear block.

- Synthesis of the target LDBCs approached by a coupling the preformed blocks using the CuAAC reaction (**Figure 3.4**).

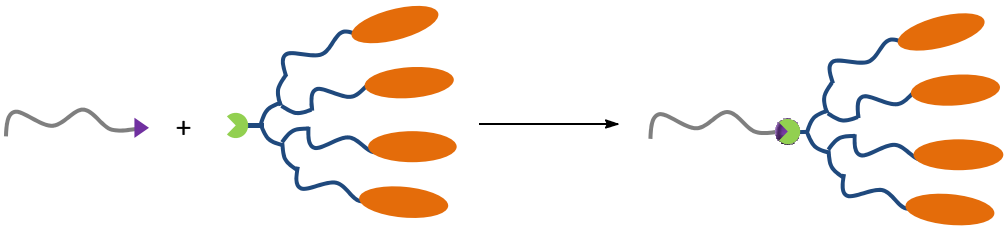

Figure 3.4 *Synthetic approach for the synthesis of the LDBCs*

- Structural characterisation of the building blocks and derived LDBCs by FTIR, NMR, MS as well as elemental analysis. Thermal characterisation using POM, TGA and DSC.

- Self-assembly of the LDBCs in water.

- Morphological study of the self-assemblies in water by electron microscopy: TEM and Cryo-TEM.

- Study of the photoresponsive behaviour of the self-assemblies in water.

- Study of the encapsulation and photoinduced release of hydrophobic and hydrophilic fluorescent probes.

3.3. Results and Discussion

3.3.1 Synthesis and Characterisation of the Amphiphilic Block Copolymers

The synthesis of the amphiphilic LDBCs was carried out by using the same coupling strategy presented in Chapter 2 where a fourth generation of bisMPA based dendron with an azido group at the focal point and functionalised at the periphery with azobenzene units was 'click' coupled to a previously synthesised alkyne terminated PEG chain (**Scheme 3.1**).

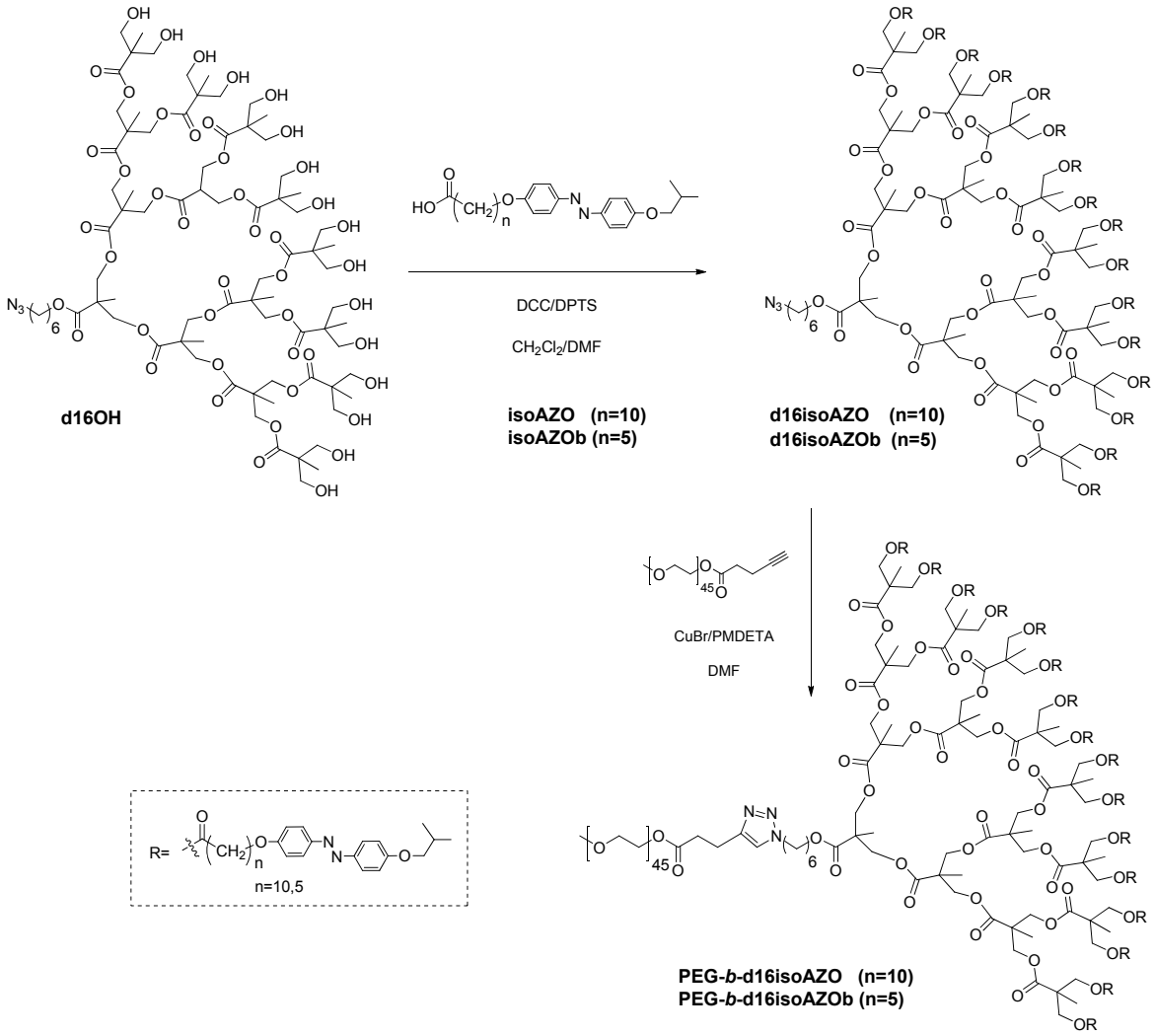

Scheme 3.1 *Synthesis of the aimed LDBCs starting from d16OH described in Chapter 2*

The synthesis of the azido functionalised dendron having sixteen hydroxyl groups (**d16OH)** was described in the Experimental section in Chapter 2. The 4-alkoxyazobenzene unit was attached to the periphery of the dendron **d16OH** by an esterification reaction between its hydroxyl groups and the appropriate acids using the DCC/DPTS system. In a first attempt, esterification of **d16OH** with 11-[4-(4'-methyloxy-phenylazo)phenyloxy] undecanoic acid was approached but the sequential incorporation of 4-methyloxyazobenzene units during the course of the reaction decreased the solubility of the resulting dendron causing its precipitation from the reaction medium and preventing the complete functionalisation of the hydroxyl groups at dendron periphery. This result contrast with the solubility exhibited by dendrons functionalised with analogous cyanobenzene moieties. Therefore, the 4-methyloxy substituent was replaced by the 4-isobutyloxy one while keeping the decamethylenic spacer. Nevertheless, a shorter flexible chain was also introduced that should decrease the hydrophobicity of the dendrons and influence the self-assembly process. For this purpose, two acids having the 4-isobutyloxyazobenzene photoactive unit and a decamethylenic (**isoAZO**) or a pentamethylenic (**isoAZOb**) flexible spacer were synthesised according to **Scheme 3.2** using previously reported synthetic methods.[13] Esterification of **d16OH** with 4-isobutyloxyazobenzene derivates, **isoAZO** and **isoAZOb**, rendered the corresponding dendrons, **d16isoAZO** and **d16isoAZOb** in 30-40% yield. Evidence for the complete functionalisation of the periphery of the dendrons was provided by several techniques. The MALDI-TOF mass spectra showed the expected ion peaks (see MALDI spectrum of **d16isoAZOb** in **Figure 3.7b** as an example). The ^{1}H-NMR spectra of the azodendrons are fully consistent with the proposed chemical structures. As an example, the ^{1}H-NMR spectrum of **d16isoAZO** is shown in **Figure 3.5**. Relative integration between the signals corresponding to the aromatic protons of the azobenzene units and the signal corresponding to the methylene unit linked to the azide group, CH_2-N_3 at 3.27 ppm (labelled as '*a*' in **Figure 3.5**) also confirmed the complete functionalisation of the periphery of the dendron.

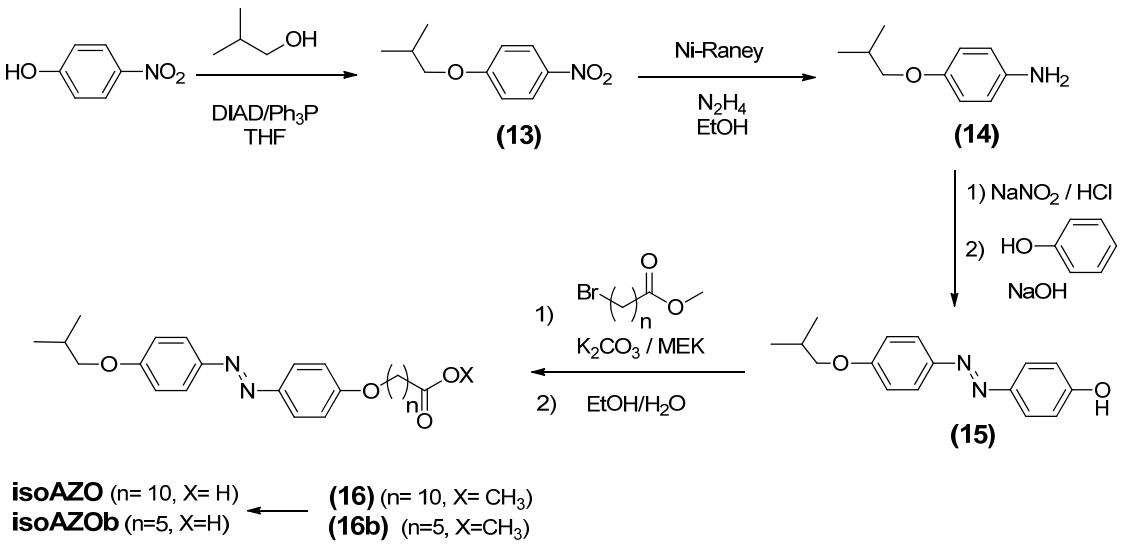

Scheme 3.2 *Synthesis of 4-isobutyloxyazobenzene derivates* ***isoAZO*** *and* ***isoAZOb***

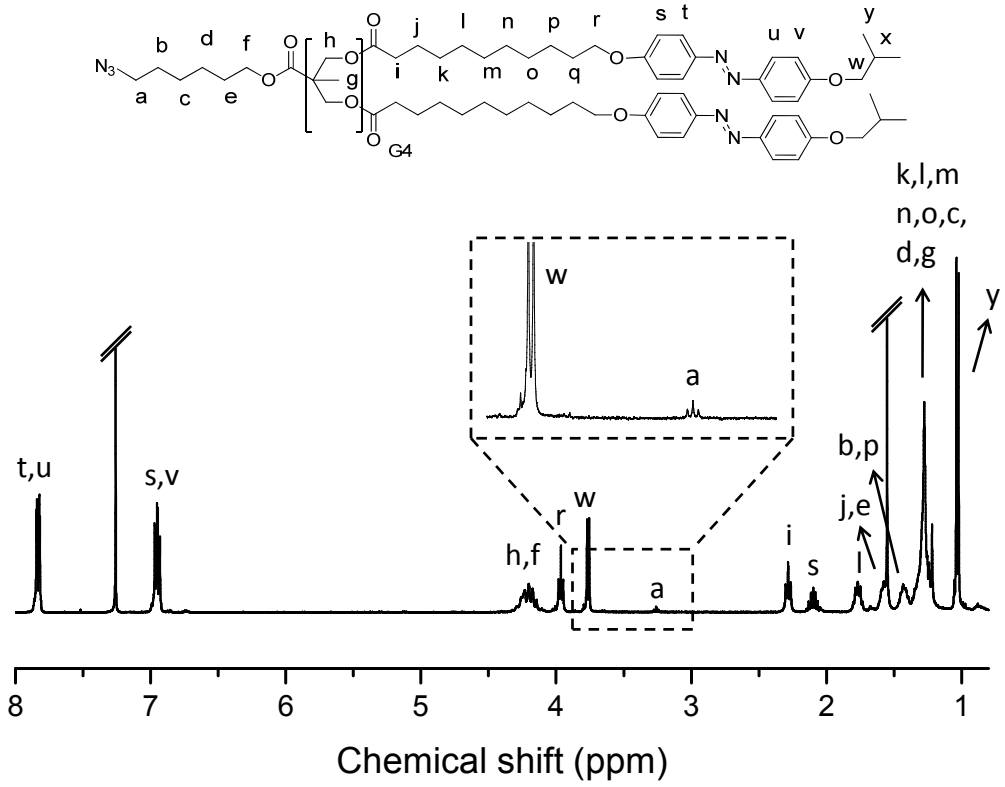

Figure 3.5 *^{1}H-NMR spectrum of* ***d16isoAZO*** *in $CDCl_3$ (400MHz)*

The alkyne-terminated PEG of 2000 g/mol average molecular weight was prepared by postpolymerisation modification of commercial monomethyl polyethylenglycol monomethyl ether. Thus, the end functional polymer was prepared by esterification of the PEG block with 4-pentynoic acid using DCC and DPTS.[14] Incoporporation of the alkyne group was corroborated by ^{1}H-NMR (**Figure 3.6**). Relative integration of the signal corresponding to the methoxy group of PEG at 3.36 (labelled as '*a*') and the signal at 2.60-2.50 ppm (labelled as '*d*' and '*e*') evidenced complete functionalisation.

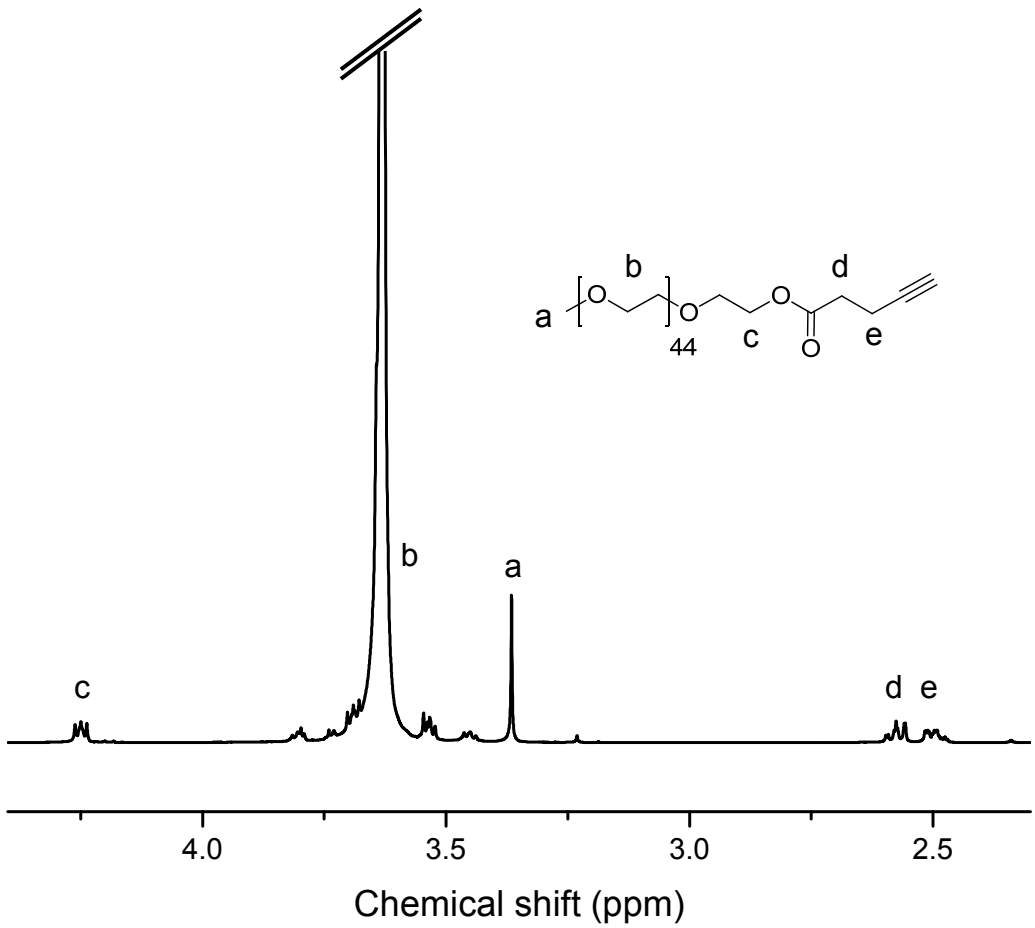

Figure 3.6 *^{1}H-NMR spectrum of alkyne functionalised PEG in $CDCl_3$ (400MHz)*

The preformed blocks, alkyne functionalised PEG and azobenzene containing dendrons (**d16isoAZO** and **d16isoAZOb)**, were coupled in the last synthetic step to form the amphiphilic LDBCs **PEG-*b*-d16isoAZO** and **PEG-*b*-d16isoAZOb**. The efficiency of the coupling was corroborated by SEC and

MALDI-TOF MS in order to check the presence of the original blocks. However, residual traces of the non coupled blocks were not detected. The SEC curves corresponding to the LDBCs were monomodal and the narrow molecular weight distribution was maintained on coupling, while the molecular peak was slightly shifted towards lower retention times compared to that of the separated blocks as an indication of the effective coupling of the blocks (**Figure 3.7a**). In the MALDI-TOF spectra of the LDBCs evidences of the dendron or the linear blocks were not observed and their polidispersities are similar to the original PEG linear block (**Figure 3.7b**). Further evidence for the formation of the BCs was gained from the IR spectra where the band at 2100 cm^{-1} due to the azide functionality of the azodendron completely disappeared (**Figure 3.8**).

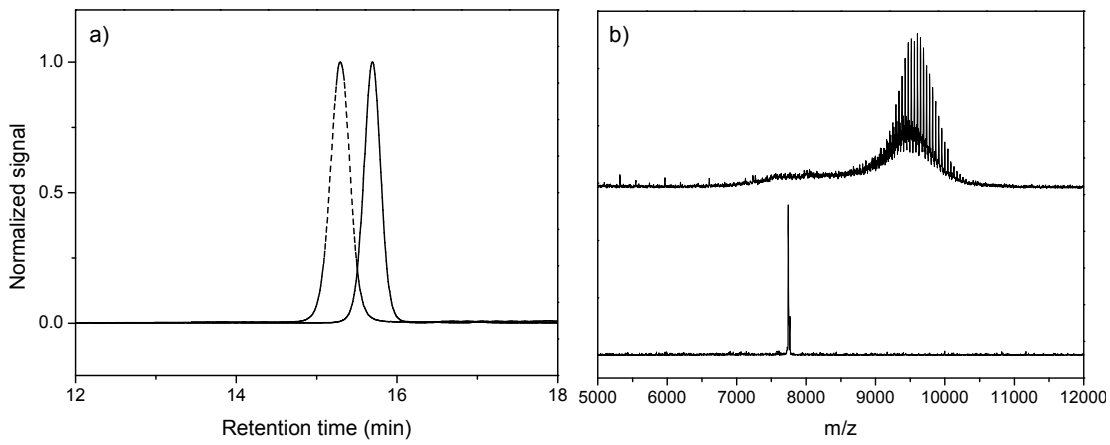

Figure 3.7 *a) SEC traces of* ***PEG-b-d16isoAZOb*** *(dot line) and* ***d16isoAZOb*** *(straight line). b) MALDI-TOF mass spectra of* ***PEG-b-d16isoAZOb*** *(top) and* ***d16isoAZOb*** *(bottom)*

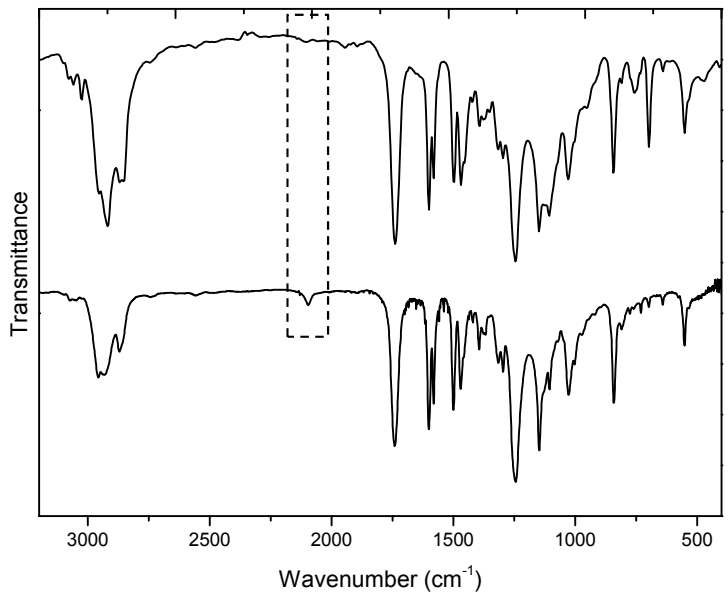

Figure 3.8 *FTIR spectra of* ***PEG-b-d16isoAZO*** *(top) and the corresponding azodendron* ***d16isoAZO*** *(bottom)*

Details of the average molecular weights exhibited by the studied compounds are given in **Table 3.1**. LDBCs average molecular weights calculated by MALDI-TOF fairly agree with expected values taken into account the molecular weight of the PEG block (MALDI-TOF) and the dendron. However, the values calculated by SEC using PS standards are underestimated. This phenomena has been observed previously for other types of LDBCs and can be attributed to the smaller hydrodynamic volume of these copolymers.[15]

Table 3.1*. Molecular weight of the synthesised polymers*

Polymer	M_n [a]	M_n [b]	M_n [c]	$Đ_M$ [c]	**philic/phobic ratio[d]**
PEG-*b*-d16isoAZO	10840	10681	9900	1.01	18/82
PEG-*b*-d16isoAZOb	9718	9539	9000	1.01	21/79

[a] Number average molecular weight (M_n) calculated as the sum of the molecular weight of the PEG block (M_n=1970 calculated by mass spectrometry) and the dendritic blocks (MW= 8870 g/mol for **d16isoAZO** and MW=7748 g/mol for **d16isoAZOb**). [b] M_n were calculated by MALDI-TOF. [c] M_n and polydispersity ($Đ_M$) were determined by SEC using PS standards. [d] Hydrophilic/ hydrophobic ratio was calculated considering the linear block (PEG) as the hydrophilic part and the azobenzene-containing dendritic block as the hydrophobic part.

^{1}H-NMR also confirmed the expected structures. **Figure 3.9** depicts the ^{1}H-NMR spectrum of **PEG-b-d16isoAZOb** as an example. Relative integration of azobenzene aromatic protons signals and the corresponding ones to the PEG linear block protons at 3.65-3.50 ppm is in good agreement with the linear-dendritic BCs structure. Furthemore, the signal corresponding to the methylene unit linkes to the azide, CH_2-N_3, at 3.27 ppm, disappeared and two new peaks appeared at 2.97 and 2.73 ppm (labelled as '*e*' and '*d*'), which are related with triazol ring formation.

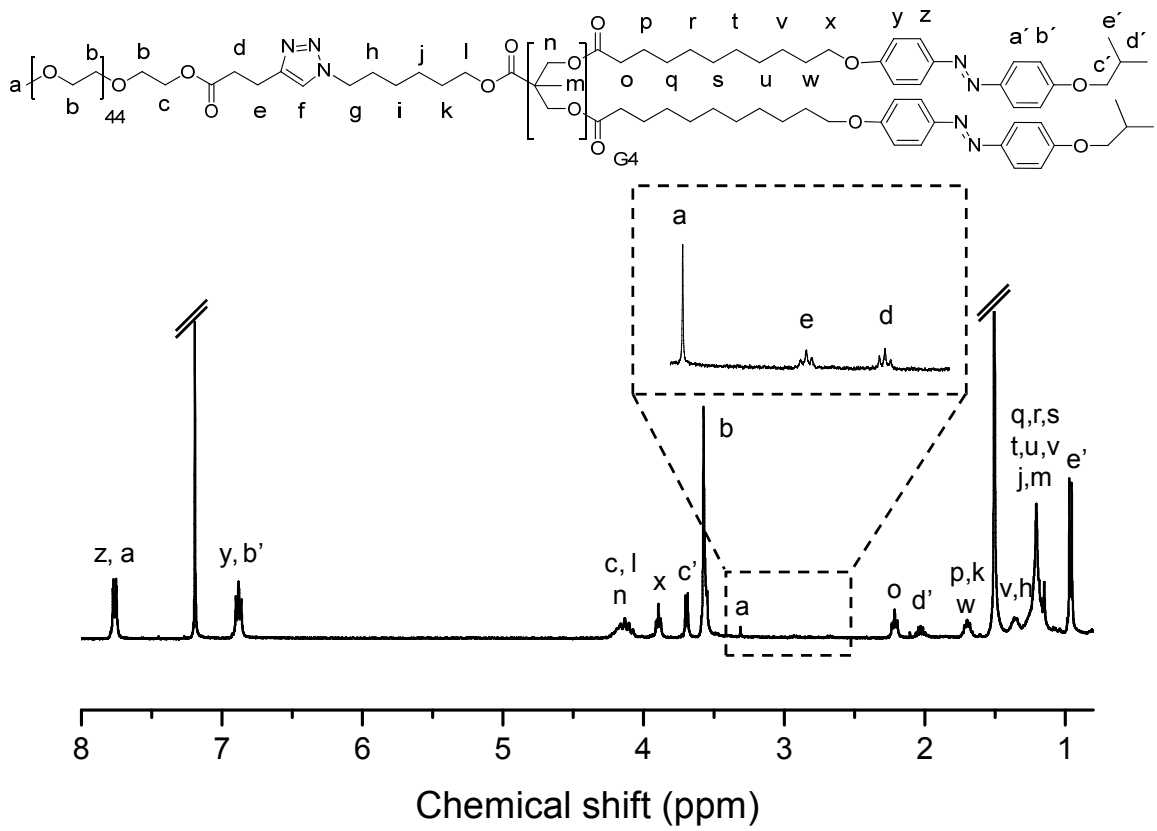

Figure 3.9 *^{1}H-NMR spectrum* ***PEG-b-d16isoAZO*** *in $CDCl_3$ (400MHz)*

The thermal stability of the azodendrons and the LDBCs was studied by TGA using powdered samples. All the samples exhibited a good thermal stability up to 250ºC, with the onset of decomposition detected above 300ºC, being the stability of the BCs slightly higher than that of the corresponding azodendrons. Futhermore, no volatile residues were detected in all the studied samples.

The thermal transitions of the dendrons and LDBCs were studied by POM and DSC (**Table 3.2**, **Figure 3.10**). In the case of POM, the materials were first heated to the isotropic state in a heating stage to have a common thermal history and then analysed. The results were compared with the DSC curves at 10ºC/min scan rate. In the case of **d16isoAZO,** when it was cooled rom the isotropic state, the appearance of birefringent textures associated to the development of a smectic A mesophase were observed by POM. By DSC, the isotropic-to-mesophase transition temperature was detected at 92ºC followed by an exothermic peak at 79ºC corresponding to the crystallisation of the sample.

***Table 3.2**. Thermal properties of the azodendrons and LDBCs*

	TGA[a]	DSC[b]			
Dendrons and LDBCs	T_d	T_{I-M}	ΔH_{I-M}	T_C	ΔH_C
d16isoAZO	328	92	68	79	247
PEG-*b*-d16isoAZO	357	-	-	84	422
d16isoAZOb	323	55	-[c]	51	107[c]
PEG-*b*-d16isoAZOb	338	-	-	62	83

[a] T_d (in ºC): decomposition temperature associated to mass loss calculated by TGA at the onset point in the weight loss curve. [b] T_{I-M} (in ºC) and ΔH_{I-M} (in kJ per mole of polymer chain): isotropic-to-mesophase transition temperature and associated enthalpy. T_C (in ºC) and ΔH_C (in kJ per mole of polymer chain): crystallisation temperature and associated enthalpy. M_n of polymer chain used to calculate enthalpy values was determined by MALDI-TOF. Data calculated from the first cooling scan recorded at 10ºC/min. [c] Crystallisation and isotropic-to-mesophase transition peaks are overlapped. Enthalpy was calculated including the area of the two peaks, ΔH_{I-M} and ΔH_C.

The study of **d16isoAZOb** under POM did not give evidence of mesomorphism and only crystallisation of the isotropic liquid was observed upon cooling. However, on the DSC cooling curve a small peak at 55ºC was registered before crystallisation at 51ºC, which may be indicative of a narrow interval of

mesophase. Its identification by POM is hindered due to the high viscosity of the sample and its proximity to the crystallisation.

In relation to the behaviour of the LDBCs, both **PEG-*b*-d16isoAZO** and **PEG-*b*-d16isoAZOb** were crystalline in nature and the occurrence of mesomorphism was discarded by POM and DSC studies. By DSC, the crystallisation peak of the PEG block about 20ºC was not observed and upon cooling only the crystallisation process corresponding to the azodendron domains was detected at 84 ºC for **PEG-*b*-d16isoAZO** and at 62ºC for **PEG-*b*-d16isoAZOb**. **PEG-*b*-d16isoAZO** crystallisation peak exhibits a little shoulder which could be related to an isotropic-to-mesophase very close the crystallisation process. Restricted PEG crystallisation has been also observed for LDBC when PEG is the minor component.[16]

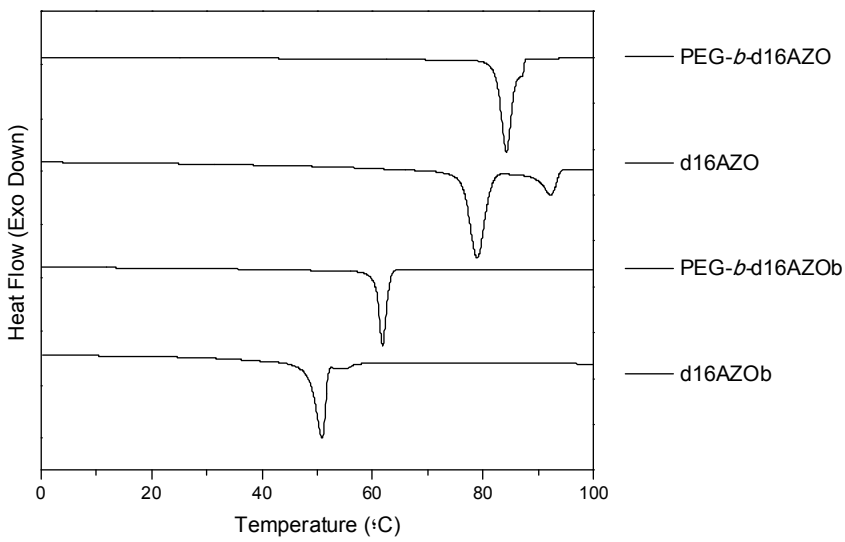

Figure 3.10 *DSC traces of the dendrons and the corresponding LDBC at 10ºC/min corresponding to the first cooling*

3.3.2 Self-assembly of the Linear-Dendritic Azobenzene Block Copolymers in Water

Self-assembled structures of the LDBCs were prepared by the solvent switch (or co-solvent) method using THF-water. The process was followed by measuring the loss of intensity of transmitted light due to scattering (turbidimetry) when pass from a solution to a micellar dispersion. The two LDBCs were first dissolved in THF which is a good a solvent for both blocks. Then water, which is non solvent for the hydrophobic block, was slowly added to the solution while the turbidity of the mixture was monitored as a function of the water content (**Figure 3.11**). When a critical water content was reached a sudden increase in turbidity occurred indicating that polymer self-assembly starts. At this point the hydrophilic block tends to shield the hydrophobic block apart from the solvent. The self-assembly process sacrifices the entropy of the single chains, but prevents a larger enthalpy penalty resulting from energetically unfavourable hydrophobe-water interactions.[4] Once turbidity reached an almost constant value, the resulting dispersion was dialyzed against water to remove the organic solvent as it is described in the Experimental Section.

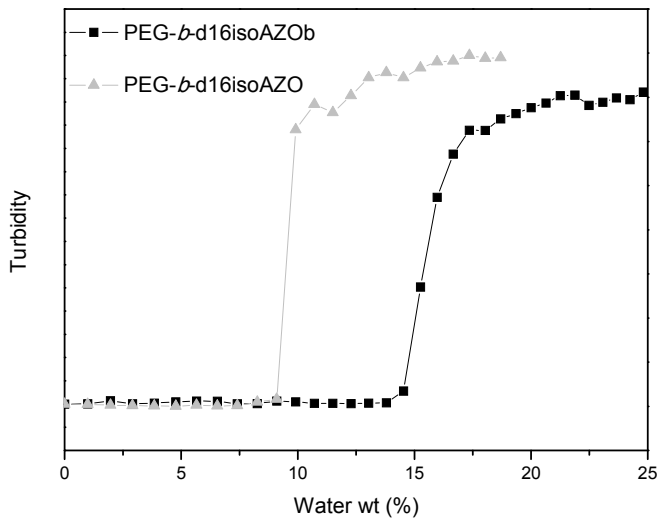

Figure 3.11 *Turbidity plot of the LDBCs THF solution versus amount of water added*

Unfortunately, for **PEG-*b*-d16isoAZO** a precipitate was obtained by removing the organic solvent through dialysis which points to the collapse of the self-

assemblies in water. In the case of **PEG-*b*-d16isoAZOb**, a stable water suspension of self-assemblies was eventually obtained using the same procedure. The hydrophilic/hydrophobic balance is responsible of this behaviour and put in evidence the influence of the structural design on the preparation of polymeric vesicles.

The morphology of the stable self-assemblies of **PEG-*b*-d16isoAZOb** was first investigated by TEM on dried samples stained with uranyl acetate (see Experimental Section for further details). In fact, the TEM images confirmed the formation of vesicular self-assemblies with a deflated appearance because of dehydration in the procedure of the sample preparation (**Figure 3.12a**).

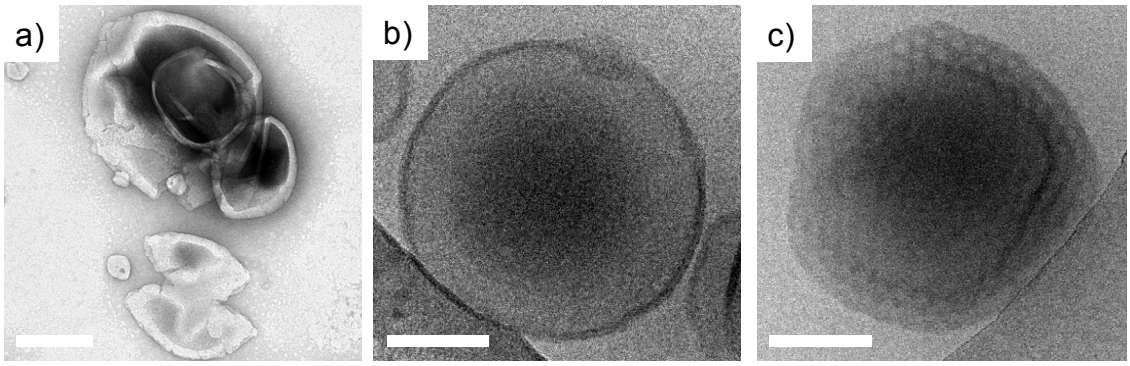

Figure 3.12 *a) TEM image of* ***PEG-b-d16isoAZOb*** *non-irradiated vesicles. Cryo-TEM images of* ***PEG-b-d16isoAZOb*** *vesicles before b) and after c) irradiation for 1 h at 365 nm and 2.6 mW/cm^2. The length of the scale bar corresponds to 200 nm in a) and 100 nm in b) and c)*

The aqueous suspension **PEG-*b*-d16isoAZOb** vesicles were also analyzed by Cryo-TEM (**Figure 3.12b**). In this case, the sample was vitrified in liquid ethane at –170ºC, and images were obtained with liquid nitrogen cooling without the need of staining. Spherical vesicles were observed with dark regions corresponding to the aromatic azobenzene moieties that form the hydrophobic membrane. The vesicle diameter was in the range 250-450 nm and the thickness of the membrane around 8 nm, which fits well with a bilayer arrangement of the azodendrons as was previously reported for analogous azobenzene containing LDBCs.[7] Size of the vesicles was also evaluated by dynamic light scattering (DLS) (see below **Figure 3.16** before irradation). The

mean hydrodynamic diameter (D_h) was found to be 365 nm, which is in good agreement with Cryo-TEM observations.

The critical aggregation concentration (CAC) of **PEG-*b*-d16isoAZOb** in water was determined by fluorescence spectroscopy using Nile Red as a polarity sensitive probe.[17-20] In water, Nile Red exhibits a weak emission at 660 nm (with excitation at 550 nm) due to excimer formation but if the dye is located in a more hydrophobic environment its emission is blue shifted and the intensity increases dramatically.[20] The self-assembly of this LDBCs produces a hydrophobic environment into which Nile Red can enter and the CAC can be determined by recording the fluorescence intensity as a function of the LDBC concentration.

It has to be emphasise that Nile Red was also chosen because the excitation/emission wavelengths of this particular probe are separated from the wavelengths required to induce the *trans*-to-*cis* photoisomerisation of the azobenzene. Besides, the intrinsic fluorescence emission of the vesicles with excitation at 365 nm (maximum absorption wavelength of azobenzene), was discarded.[21]

Samples of **PEG-*b*-d16isoAZOb** were stirred together with Nile Red at room temperature overnight and the emission spectra of Nile Red were registered from 560 to 700 nm (see Experimental Section for further details). As expected, the fluorescence spectra show that the emission intensity increases on increasing the concentration of **PEG-*b*-d16isoAZOb**. At low concentrations of **PEG-*b*-d16isoAZOb**, the weak fluorescence intensity indicates that Nile Red is preferentially in water and, therefore, few micellar self-assemblies are present. At higher concentrations, the emission intensity increases indicating that Nile Red is located in a more hydrophobic environment as a consequence of being encapsulated by the polymer self-assemblies. The relationship between fluorescence intensity (maximum) and logarithm of the **PEG-*b*-d16isoAZOb** concentration is non-linear and the onset point corresponds to the CAC (**Figure 3.13**). The observed onset point corresponded to a concentration of 35 µg/mL, which is comparable with CAC values reported for other LDBC self-assemblies.[19,22]

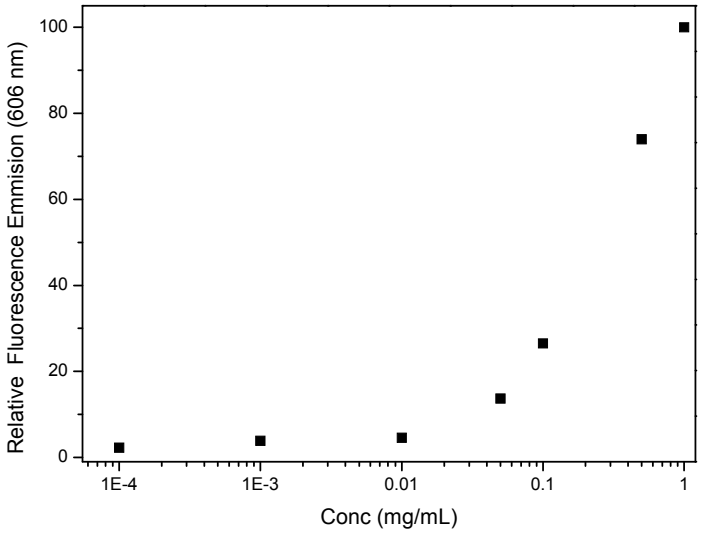

Figure 3.13 *Fluorescence intensity of Nile Red at 606 nm (λ_{exc} = 550 nm) versus* ***PEG-b-d16isoAZOb*** *concentration (mg/mL)*

3.3.3 Light Responsive Behaviour of the Vesicles

In order to study the photoresponse of the **PEG-*b*-d16isoAZOb** vesicles, the UV-vis spectra of both a solution of the LDBC in chloroform and the vesicles suspension in water were first recorded (**Figure 3.14a**). The spectra of **PEG-*b*-d16isoAZOb** in solution was characterised by two absorption bands corresponding to the *trans*-isomer, a strong one centred at 360 nm attributed to the π-π* transition and a weak one at about 450 nm corresponding to n-π* transition.

The spectrum of the vesicles showed a large broadening and a hypsochromic shift of the π-π* band (**Figure 3.14a**). The absorption maximum shifted down to 320 nm which indicates the dominant formation of H-aggregates of azobenzene units. Furthermore two shoulders at higher wavelengths were observed, one at 360 nm which corresponds to the value determined for the non-aggregated *trans*-azobenzene and the other at 375 nm which is characteristic of the formation of J-aggregates.

Exposure of the vesicles to UV irradiation, 365 nm and 2.6 mW/cm^2, caused significant spectral changes (**Figure 3.14b**). A remarkably decreasing of π-π* absorbance was observed accompanied by a notably increase of the

absorbance at 450 nm that can be attributed to the photo-isomerisation of the *trans*- to the *cis*-azobenzene. After 30 min of light exposure only slight changes were further detected in the UV-vis spectrum. When the irradiated suspension of the vesicles was kept in the dark, after 2 h the spectrum gradually started to recover its initial shape due to the slow thermal back isomerisation *cis*-to-*trans*. Although the thermal isomerisation is slow (hours) it can be readily accelerated by exposure to visible light. Thus, the vesicles (previously irradiated at 365 nm) were irradiated at 450 nm (**Figure 3.15**). After 10 min, absorbance at around 360 nm increased which can be attributed to the back *cis*-to-*trans* photoisomerisation. After 1 h, the spectrum almost recovered the initial shape.

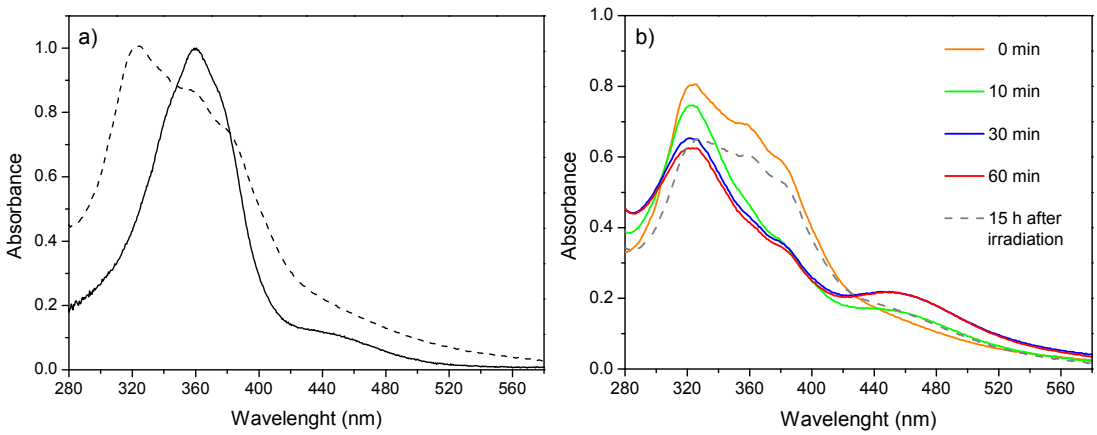

Figure 3.14 *a) UV-Vis spectra* ***of PEG-b-d16isoAZOb*** *in a 5x10^{-6} M solution in $CHCl_3$ (straight line) and a water suspension of* ***PEG-b-d16isoAZOb*** *vesicles (dashed line). b) UV-Vis spectra of* ***PEG-b-d16isoAZOb*** *irradiated vesicles (concentration of 1 mg/mL) for different times at 365 nm and 2.6 mW/cm^2*

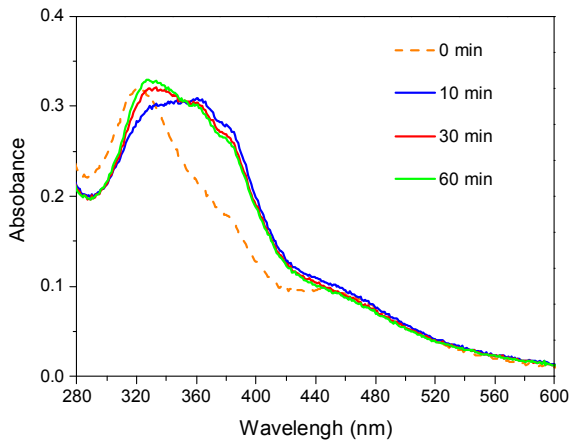

Figure 3.15 *UV-Vis spectra of* ***PEG-b-d16isoAZOb*** *irradiated vesicles (concentration of 1 mg/mL) at different times at 450 nm (0 min correspond to vesicles previously irradiated at 365 nm for 30 min)*

The irradiated samples were also studied by DLS and Cryo-TEM in order to study the modification on the particle dimension and morphology. For these studies the vesicles were irradiated for 1h at 365 nm and then measured. By DLS measurements a permanent change of the vesicles size upon irradiation was observed with a mean D_h of 270 nm determined after irradiation (**Figure 3.16**). The D_h was evaluated immediately upon irradiation and after 24 h of irradiation and no evolution of the D_h was found evidencing an irreversible morphological change. The Cryo-TEM image of the irradiated sample after 15 h shows deformed vesicles with a distorted membrane in contrast to the non-irradiated samples (**Figure 3.12c**). Therefore, the experiments suggest remarkable changes in the morphology of **PEG-*b*-d16isoAZOb** vesicles before and after UV irradiation as a consecuence of the azobenzene photoisomerisation.

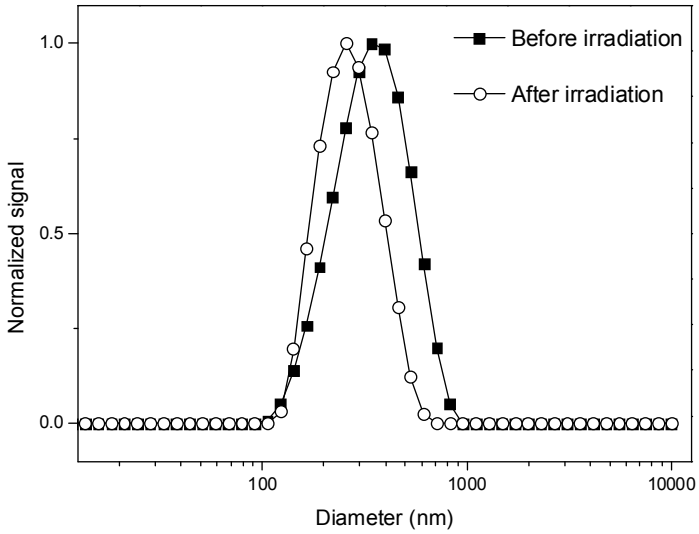

Figure 3.16 *DLS measurements of a water suspension of* ***PEG-b-d16isoAZOb*** *vesicles before and after UV light irradiation at 365 nm and 2.6 mW/cm^2*

For the sake of comparison, vesicles of LDBC functionalised with 4-cyanoazobenzene were irradiated under the same conditions of low intensity used in this work. Recording of the UV data at different irradiation times indicated that *trans*-to-*cis* isomerisation took place to a lesser extent (**Figure 3.17a**). Substantial changes were not observed in the mean D_h determined by DLS upon irradiation (**Figure 3.17b**). Therefore, under the same experimental

conditions, changes on vesicles containing 4-cyanoazobenzene units were only moderate. We can assume that the higher tendency towards aggregation and the higher polarity of the *trans* 4-cyanoazobenzene might hinder an effective disruption of the photochromic bilayer shell.

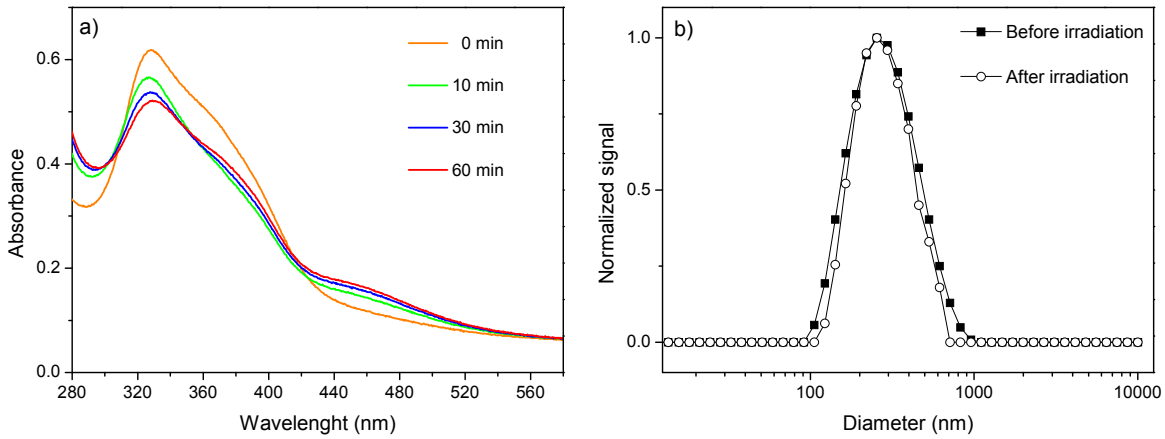

Figure 3.17 *a) UV-Vis spectra and b) dynamic light scattering measurements of the 4-cyanoazobenene-containing vesicles (concentration of 1 mg/mL) irradiated for different times at 365 nm and 2.6 mW/cm^2*

3.3.4 Encapsulation and Photoinduced Release of Molecular Probes

The potential of the vesicles as light responsive nanocontainers was investigated by encapsulation and subsequent release of fluorescent probes. Since molecules of interest can be trapped either in the hydrophilic hollow cavity or in the hydrophobic membrane of the vesicle, the ability to encapsulate both Nile Red and Rhodamine B, which are respectively of hydrophobic and hydrophilic nature, was tested.

Encapsulation of Nile Red was already demonstrated in the determination of the CAC. Because of its hydrophobic nature, Nile Red should be retained in the hydrophobic region of the vesicle, i.e. in the membrane formed by the photo-responsive azobenzene block, rather than in the internal compartment of the vesicle.[23] Thereof, Red Nile was encapsulated by difussion stirring an aqueous vesicle suspension of 1 mg/mL concentration in Nile Red 10^{-6} M. The suspension was stirred overnight to reach the equilibrium before fluorescence was measured. The emission spectra of Nile Red were registered from 560 to

700 nm while exciting at 550 nm. Nile Red exhibits an strong fluorescence revealing that the probe has been encapsulated.

The suspension of the loaded vesicles was irradiated with 365 nm UV light, 2.6 mW/cm^2, and the fluorescence of Nile Red was recorded at different exposure times. Upon irradiation, an abruptly decrease on the initial fluorescence intensity at 606 nm was observed (**Figure 3.18**). This change in fluorescence upon UV light exposure indicates that the environment of the probe becomes less hydrophobic. A *priori* this can be reasonably related to the disruption of the vesicle membrane and subsequent release of Nile Red into water due to *trans*-to-*cis* isomerisation of azobenzene. But also, the *trans*-to-*cis* isomerisation of the azobenzene brings about a change in the polarity of membrane which becomes more hydrophilic and this can also explain the decrease on the fluorescence intensity of the Nile Red without its complete releasing into water. When the irradiated vesicles were kept in the dark the fluorescence intensity was slowly and partially recovered. Therefore, because the slow back thermal *cis-to-trans* relaxation of azobenzene takes place the fluorescence intensity should increases again because the recovery of a more hydrophobic environment within the membrane.[24]

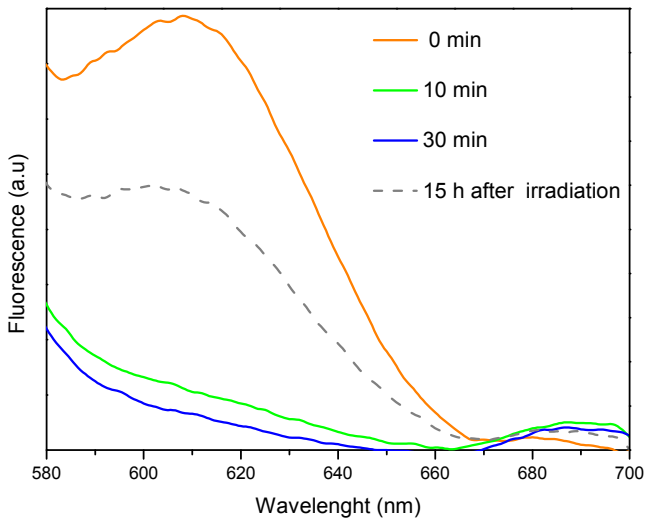

Figure 3.18 *Emission spectra of the Nile Red encapsulated vesicles of* ***PEG-b-d16isoAZOb*** *recorded after irradiating at 365 nm and 2.6 mW/cm^2 for different time intervals*

To gain more information on whether or not the photoinduced increase of membrane permeation takes place, vesicles were loaded with Rhodamine B dye and confocal microscopy was used for monitoring the process. Rhodamine B exhibits emission at 575 nm when excitation with 554 nm light which do not overlap with absorption bands of azobenzene. Due to its hydrophilic nature, Rhodamine B should be loaded in the hydrophilic internal cavity of the vesicle. In this case, vesicles were formed in THF by slowly addition of an aqueous solution of Rhodamine B following the self-assembling process by turbidity analysis (see experimental section for further details).[25] The vesicles were dialysed against water to remove THF as well as the non-encapsulated Rhodamine B. Dye encapsulation was confirmed by confocal microscopy images where fluorescence dots in a dark background were observed (**Figure 3.19a**).

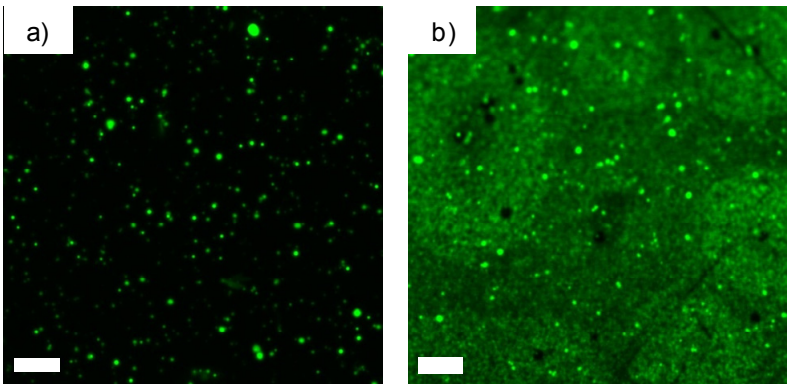

Figure 3.19 *Fluorescence microscopy images of the water supension of loaded* ***PEG-b-d16isoAZOb*** *vesicles before a) and after b) irradiation for 1 h at 365 nm and 2.6 mW/cm^2. The length of the scale bar corresponds to 5 µm*

After irradiation at 365 nm for 1h, fluorescent dots were still visible by fluorescence microscopy but also a fluorescent background was observed due to Rhodamine B release from the interior of the vesicles to the aqueous media (**Figure 3.19b**). These experiments indicate that under UV illumination the vesicle membrane became permeable to the loaded fluorescent probe. The persistence of fluorescent dots after 1 h irradiation might be due to the fact that some of the vesicles are still unaffected by irradiation but more likely it can be due to only partial release of the encapsulated dye. A continuous permeation

through the membrane of the encapsulated Rhodamine B occurs on exposure due to its deformation but, reassembly (at least partially) of the vesicle membrane on the dark due to thermal *cis*-to-*trans* back isomerisation limits the release. Recent simulation studies pointed out that despite the release of hydrophilic substance starts as soon as the vesicles are exposed to light, the membrane permeation does not enhance suddenly.[26]

3.4 Conclusions

Novel photoresponsive amphiphilic LDBCs have been prepared that include 4-isobutyloxyazobenzene moieties at the dendritic block as the photo-active units and PEG as the linear hydrophilic block. As it was proved in analogous materials based on 4-cyanoazobenzene, it has been found that combining the fourth generation of a bis-MPA based 4-isobutyloxyazodendron with PEG of Mn=2000 g/mol stable vesicles are produced. However, these polymeric self-assemblies are only achieved when the incorporation of the alkoxy terminal chain is compensated by reducing the length of the methylenic linker used to attach the azobenzene to the periphery of the dendron. This structural modification (4-isobutyloxyazobenzene incorporation) does not significantly alter self-assembly in solution but what is more valuable it facilitates the disruption of azobenzene aggregates of the membrane on exposing the vesicles to low intensity UV light when compared to its 4-cyanoazobenzene counterparts.

It has been demonstrated by fluorescence spectroscopy that these vesicles are able to load both hydrophobic and hydrophilic molecules and that under conditions of low intensity UV illumination *trans*-to-*cis* isomerisation of azobenzene occurs causing a distortion of the bilayer membrane increasing its permeability to loaded fluorescent probe. Therefore, the light stimulated delivery process of encapsulate dyes has been proved.

3.5 Experimental Section

Materials

The fourth-generation polyester dendron (**d16OH**) was prepared according to the procedure described in Chapter 2. CuBr was used as received and handled in a dry box. All other reagents were purchased from Sigma-Aldrich and used as received without further purification.

3.5.1 Experimental Details for the Synthesis of 4-isobutyloxyazobenzene derivatives

Synthesis and Characterisation of 4-isobutyloxynitrobenzene (13)

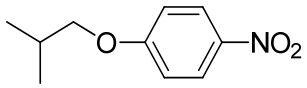

(13)

2-Methyl-1-propanol (5.33 g, 71.90 mmol), *p*-nitrophenol (10.05 g, 71.90 mmol), and diisopropylazadicarboxylate (14.53 g, 71.90 mmol) were dissolved in dry THF (50 mL) under argon atmosphere and cooled into an ice-water bath. Then, a solution of triphenylphosphine (18.85 g, 71.90 mmol) in dry THF (25 mL) was added dropwise with stirring. The mixture was stirred at room temperature overnight, the solvent was evaporated and the residue dissolved in DCM. The solution was washed twice with a saturated Na_2CO_3 solution, twice with water, and then with brine. The organic phase was dried, concentrated, and purified by flash column chromatography on silica gel using hexane/ethyl acetate (8:2) as eluent. Yield: 80%. IR (KBr), ν (cm^{-1}): 1592, 1519, 1501, 1344, 1268, 1112, 845. ^{1}H-NMR ($CDCl_3$, 400MHz) δ (ppm): 8.21-8.18 (m, 2H), 6.96-6.93 (m, 2H), 3.81 (d, *J*=6,5 Hz, 2H), 2.07-2.13 (m, 1H), 1.05 (d, *J*= 6,7 Hz, 6H). ^{13}C-NMR ($CDCl_3$, 100 MHz) δ (ppm): 164.3, 140.8, 125.9, 114.4, 75.1, 28.1, 19.1.

Synthesis and Characterisation of 4-isobutyloxyaniline (14)

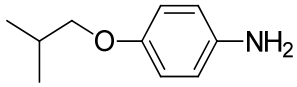

(14)

Hydrazine monohydrate (98%, 3.5 mL, 71.71 mmol) was added dropwise to a solution of the nitrobenzene derivative **(13)** (7.00 g, 35.85 mmol) in ethanol (70 mL). After the solution was heated to 40 °C, activated Raney nickel was added and the mixture stirred until no further reaction was observed. The resulting mixture was filtered off of the Raney nickel, and ethanol was removed under reduced pressure. The crude was dissolved in diethyl ether (60 mL), washed with water and brine, and dried over anhydrous magnesium sulphate. The solvent was distilled off giving the aniline as a yellow oil that was used without further purification. Yield: 90%. IR (KBr), ν (cm^{-1}): 3433, 3358, 1592, 1236, 1036, 823. ^{1}H-NMR ($CDCl_3$, 400MHz) δ (ppm): 6.75-6.73 (m, 2H), 6.65-6.62 (m, 2H), 3.64 (d, *J*=6,5 Hz, 2H), 3,40 (s broad, 2H), 2.04-2.11 (m, 1H), 1.00 (d, *J*= 6,7 Hz, 6H). ^{13}C-NMR ($CDCl_3$, 100 MHz) δ (ppm): 152.5, 139.8, 116.5, 115.6, 75.2, 28.3, 19.3.

Synthesis and Characterisation of 4-isobutyloxy-4'-hydroxyazobenzene (15)

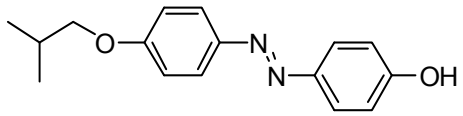

(15)

A mixture of aniline **(14)** (5.21 g, 31.50 mmol) and HCl 6M (15 mL) was cooled into an ice bath. A 2.5 M sodium nitrite solution (20 mL, 31.50 mmol) was added dropwise to the mixture and it was kept stirring in the ice bath. Then, a solution of phenol (2.96 g, 31.50 mmol) in 2 M NaOH (25 mL) was carefully added. The product was precipitated upon addition of HCl until neutral pH and it was purified by flash column chromatography on silica gel using DCM as an eluent. The product was obtained as a yellow powder. Yield: 65%. IR (KBr), ν (cm^{-1}): 3137, 1599, 1586, 1503, 1261, 1149, 839. ^{1}H-NMR ($CDCl_3$, 400MHz) δ (ppm): 7.87-7.85 (m, 4H), 7.84-7.82 (m, 4H), 3.81 (d, 2H, *J*=6,5 Hz), 2.07-2.13 (m, 1H),

1.05 (d, 6H, *J*= 6,7 Hz). ^{13}C-NMR ($CDCl_3$, 100 MHz) δ (ppm): 161.4, 157.6, 146.8, 124.6, 124.4, 115.8, 114.7, 74.7, 28.3, 19.3.

Synthesis and Characterisation of Methyl 11-[4-(4'-isobutyloxyphenylazo) phenyloxy]undecanoate (16a)

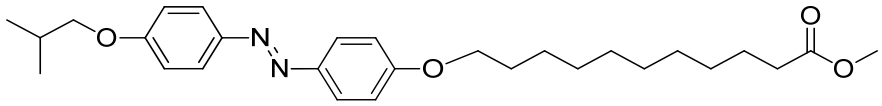

(16a)

A solution of 4-isobutyloxy-4'-hydroxyazobenzene **(15)** (2.05 g, 7.40 mmol), methyl 11-bromoundecanoate (2.48 g, 8.88 mmol) in butanone (40 mL) was prepared. 18-Crown-6 ether (0.05 g) and potassium carbonate (2.05 g, 14.79 mol) were added. The suspension was stirred under reflux for 24 h. Then, it was filtered and concentrated. The crude product was purified by flash column chromatography on silica gel using DCM as eluent. The product was obtained as a yellow powder. Yield: 75%. IR (KBr), ν (cm^{-1}): 1739, 1592, 1580, 1465, 1242, 845. ^{1}H- NMR ($CDCl_3$, 400MHz) δ (ppm): 7.87-7.85 (m, 4H), 6.94-6.92 (m, 4H), 4.03 (t, *J*=6.4 Hz, 2H), 3.80 (d, J=6,5 Hz, 2H), 3.69 (s, 3H), 2.30 (t, *J*=7.4 Hz, 2H), 2.09-2.14 (m, 1H), 1.88-1.75 (m, 2H), 1-67-1,56 (m, 2H), 1.37-1,21 (m, 12H), 1.05 (d, *J*= 6,7 Hz, 6H). ^{13}C-NMR ($CDCl_3$, 100 MHz) δ (ppm): 174.8, 161.3, 146.9, 124.3, 114.6, 74.6, 68.3, 51.4, 34.1, 29.4, 29.3, 29.2, 29.1, 28.3, 26.0, 24.9, 19.2.

Synthesis and Characterisation of Methyl 6-[4-(4'-isobutyloxyphenylazo) phenyloxy]hexanoate (16b)

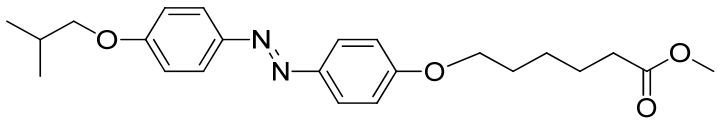

(16b)

The product was obtained following the procedure described for **(16a)** using methyl 6-bromohexanoate. Yield: 88%. IR (KBr), ν (cm^{-1}): 1741, 1601, 1580, 1497, 1242, 843. ^{1}H-NMR ($CDCl_3$, 400MHz) δ (ppm): 7.84-7.82 (m, 4H), 7.00-6.98 (m, 4H), 4.04 (t, *J*=6.4 Hz, 2H), 3.81 (d, *J*=6,5 Hz, 2H), 3.69 (s, 3H), 2.37 (t, *J*=7.4 Hz, 2H), 2.07-2.13 (m, 1H), 1.88-1.81 (m, 2H), 1.76-1.69 (m, 2H), 1.57-

1.49 (m, 2H), 1.05 (d, *J*= 6,7 Hz, 6H). ^{13}C-NMR ($CDCl_3$, 100 MHz) δ (ppm): 175.0, 161.3, 160.9, 146.9, 124.3, 114.6, 114.6, 74.6, 67.9, 51.53, 33.9, 28.9, 28.3, 25.6, 24.7, 19.3.

Synthesis and Characterisation of 11-[4-(4'-isobutyloxyphenylazo) phenyloxy]undecanoic acid (isoAZO)

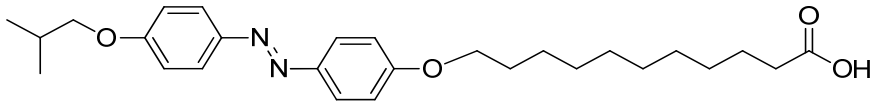

(isoAZO)

An aqueous solution of potassium hydroxide (0.9g, 9mL) was added to a solution of methyl 11-[4-(4'-isobutyloxyphenylazo)phenyloxy]undecanoate **(17a)** (6g, 15.05 mmol) in ethanol (60 mL). The mixture was stirred and heated under reflux for 1 h. Then, the crude product was precipitated by addition of HCl until pH 2 and it was recovered by filtration. The product was recrystallised from ethanol. Yield: 85%. IR (KBr), ν (cm^{-1}): 3300, 1714, 1601, 1579, 1499, 1241, 846.^{1}H-NMR ($CDCl_3$, 400MHz) δ (ppm): 7.86-7.84 (m, 4H), 7.00-6.98 (m, 4H), 4.02 (t, *J*=6.4 Hz, 2H), 3.79 (d, *J*=6,5 Hz, 2H), 2.33 (t, *J*=7.4 Hz, 2H), 2.05-2.11 (m, 1H), 1.86-1.73 (m, 2H), 1.64-1.59 (m, 2H), 1.48-1.43 (m, 2H), 1.34-1.21 (m, 10H), 1.04 (d, *J*= 6,7 Hz, 6H). ^{13}C-NMR ($CDCl_3$, 100 MHz) δ (ppm): 173.9, 161.6, 147.3, 124.4, 114.5, 74.6, 68.3, 34.1, 29.4, 29.3, 29.2, 28.3, 26.0, 24.8, 19.2.

Synthesis and Characterisation of 6-[4-(4'-isobutyloxyphenylazo) phenyloxy]hexanoic acid (isoAZOb)

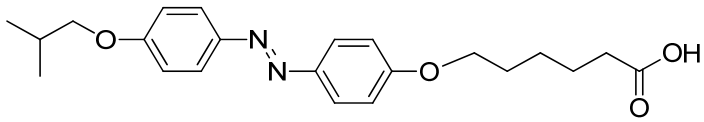

(isoAZOb)

The product was obtained following the procedure descibed for **isoAZO** by using methyl 6-[4-(4'-isobutyloxyphenylazo)phenyloxy]hexanoate **(16b)**. Yield: 80%. IR (KBr), ν (cm^{-1}): 3300, 1708, 1693, 1601, 1580, 1501, 1240, 843. ^{1}H-NMR ($CDCl_3$, 400MHz) δ (ppm): 7.87-7.85 (m, 2H), 6.94-6.92 (m, 2H), 4.06 (t, *J*=6.4 Hz. 2H), 3.81 (d, *J*=6,5 Hz, 2H), 2.37 (t, *J*=7.4 Hz, 2H), 2.08-2.14 (m, 1H), 1.88-1.81 (m, 2H), 1.76-1.69 (m, 2H), 1.57-1.49 (m, 2H), 1.05 (d, *J*= 6,7 Hz,

6H). ^{13}C-NMR ($CDCl_3$, 100 MHz) δ (ppm): 174.4, 161.0, 146.9, 124.3, 114.7, 74.7, 67.9, 33.6, 28.9, 28.3, 25.6, 24.4, 19.3.

3.5.2 Experimental Details for the Synthesis of the Azodendrons

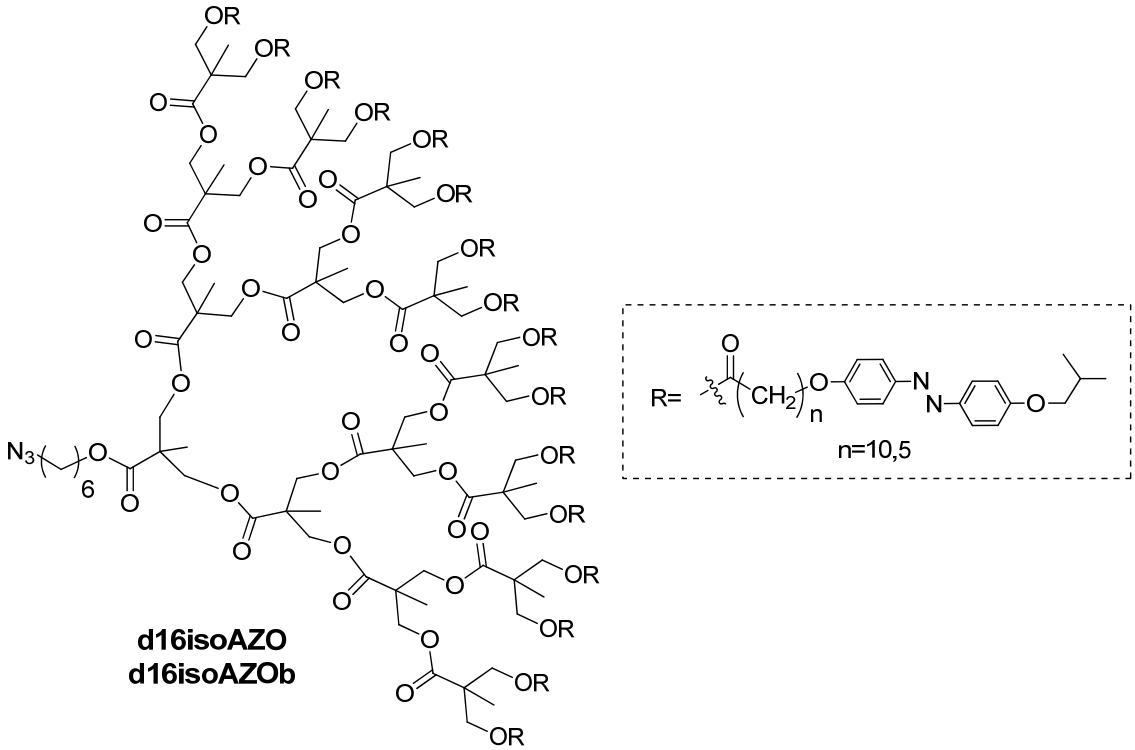

General Procedure

d16OH (n mmol), **isoAZO** or **isoAZOb** (1.2 x 16 n mmol) and DPTS (16 n mmol) were dissolved in a mixture of DCM and DMF 5:1 (around 20 mL per 200 mg of **d16OH**) The reaction flask was flushed with argon, and DCC (1.32 x 16 n mmol) was added. The mixture was stirred at room temperature for 48 h under argon atmosphere. The white precipitate formed was filtered off, and the solvent evaporated. The crude product was purified by liquid chromatography on silica gel and eluted with DCM, gradually increasing the polarity to 1:10 ethyl acetate:DCM. Azodendrons were obtained as a red powder. Yield: 30-40 %.

Characterisation Data for d16isoAZO: IR (KBr), ν (cm^{-1}): 2097, 1742, 1601, 1581, 1500, 1242, 1147, 843. ^{1}H-NMR ($CDCl_3$, 400MHz) δ (ppm): 7.85-7.82 (m, 64H), 6.98-6.92 (m, 64H), 4.30-4.16 (m, 62H) 3.96 (t, *J*=6.3 Hz, 32H), 3.76

(d, *J*=6,5 Hz, 32H), 3.26 (t, *J*=6.8 Hz, 2H), 2.28 (t, *J*=7.5 Hz, 32H), 2.12-1.08 (m, 16H), 1.82-1.77 (m, 32H), 1.68-1.62 (m, 34H), 1.48-1.43 (m, 34H), 1.35-1.10 (m, 209H), 1.03 (d, *J*= 6,7 Hz, 96H). ^{13}C-NMR (100 MHz, $CDCl_3$) δ (ppm): 173.1, 161.1, 146.9, 124.3, 114.6, 114.6, 74.6, 68.2, 33.9, 29.6, 29.5, 29.3, 28.2, 26.0, 24.8, 19.2. (MALDI$^+$, dithranol) m/z: 8890.6 $[M+Na]^+$. Anal. Calc for $C_{513}H_{709}N_{35}O_{94}$: C, 69.46%; H, 8.06 %; N, 5.53 %. Found: C, 69.36 %; H, 8.36 %; N, 5.56%.

Characterisation Data for d16isoAZOb: IR (KBr), ν (cm^{-1}): 2096, 1741, 1601, 1581, 1500, 1244, 1148, 842. ^{1}H-NMR ($CDCl_3$, 400MHz) δ (ppm): 7.83-7.80 (m, 64H), 6.96-6.90 (m, 64H), 4.30-4.16 (m, 62H) 3.93 (t, *J*=6.3 Hz, 32H), 3.74 (d, *J*=6,5 Hz, 32H), 3.21 (t, *J*=6.8 Hz, 2H), 2.32 (t, *J*=7.5 Hz, 32H), 2.10-2.07 (m, 16H) 1.78-1.73 (m, 32H), 1.62-1.54 (m, 34H), 1.47-1.38 (m, 34H), 1.36-1.10 (m, 49H), 1.03 (d, *J*= 6,7 Hz, 96H). ^{13}C-NMR ($CDCl_3$, 100 MHz) δ (ppm): 172.8, 172.1, 161.3, 161.0, 147.3, 146.9, 124.3, 114.5, 74.6, 67.9, 64.8, 46.4, 33.9, 28.9, 28.3, 28.3, 25.6, 24.6, 19.2, 17.9. (MALDI$^+$, dithranol) m/z: 7771.1 $[M+Na]^+$. Anal. Calc for $C_{433}H_{549}N_{35}O_{94}$: C, 67.12 %; H, 7.14 %; N, 6.33 %. Found: C, 67.69 %; H, 6.87 %; N, 5.98%.

3.5.3 Experimental Details for the Synthesis of the Linear Block

Synthesis and Characterisation of Alkyne Functionalised Polyethylene glycol (PEG) [14]

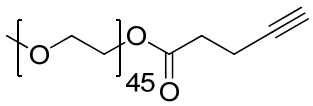

(PEG)

Polyethylenglycol mono ethyl ether (M_n=2000 g/mol) (4.30 g, 2.15 mmol), 4-pentynoic acid (0.26 g, 2.65 mmol) and DPTS (0.11 g, 0.90 mmol) were dissolved in DCM (25 mL) and coleed in an ice bath. The reaction flask was flushed with argon and DCC (0.59 g, 2.86 mmol) was added. The mixture was kept in the ice-water bath for 10 min and then stirred overnight under an argon atmosphere at room temperature. The white precipitate (*N,N*'-dicyclohexylurea) was filtered off and the solution precipitated into a large volume of cold diethyl ether. The target product was then filtered and dried under vacuum. Yield: 90

%. IR (KBr), ν (cm^{-1}): 3260, 2881, 1962, 1730, 1475, 1285. ^{1}H-NMR ($CDCl_3$, 400MHz) δ (ppm): 4.34 (t, *J* = 4.6 Hz, 2H), 3.70-3.54 (m, 178H), 3.36 (s, 3H), 2.61-2.53 (m, 2H), 2.52-2.44 (m, 2H), 1.97 (t, *J* = 2.3 Hz, 1H).

3.5.4 Experimental Details for the Synthesis of the LDBCs

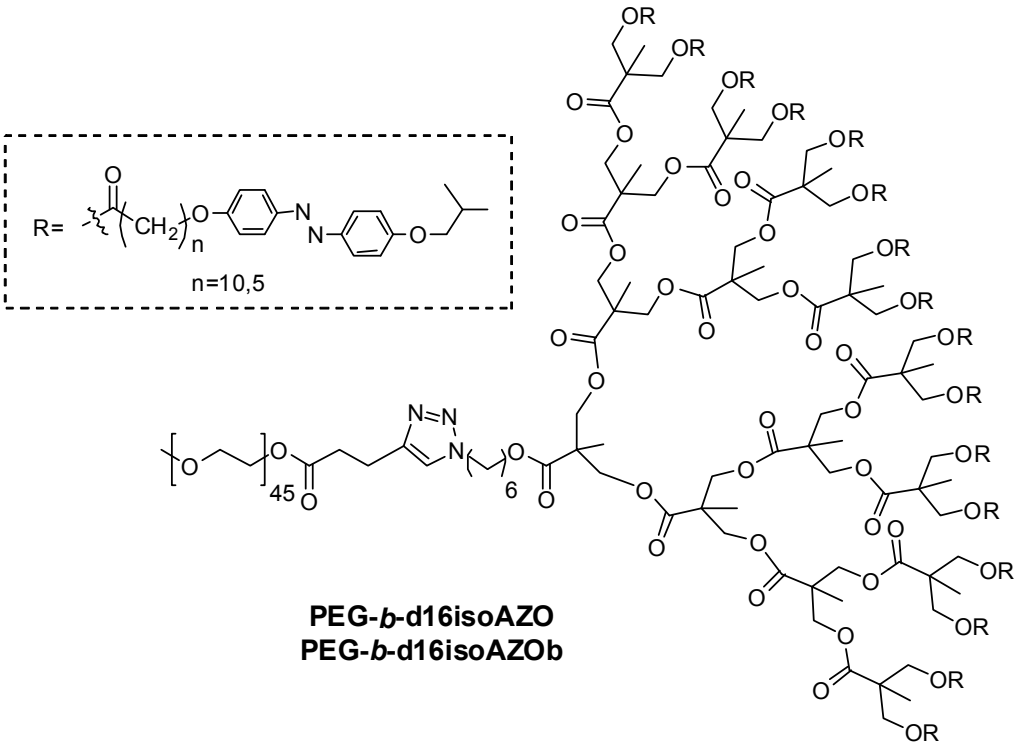

General Procedure for the Coupling Reaction

Azodendron **d16AZO**, 1.2-fold excess of alkyne-functionalised PEG and two-fold excess of CuBr were placed into a Schlenk tube. Two-fold excess of PMDETA and deoxygenated DMF (around 1 mL per 100 mg of polymer) were added with an argon-purged syringe, and the flask was further degassed by three freeze-pump-thaw cycles and flushed with argon. The reaction mixture was stirred at 40ºC for 72 h. The reaction mixture was stirred under an argon atmosphere at room temperature for 72 h. The mixture was diluted with THF and then passed through a short column of alumina. The solvent was partially evaporated and the resulting polymer solution was carefully precipitated of cold ethanol. Yield: 75-80%.

Characterisation Data for PEG-b-d16isoAZO: IR (KBr), ν (cm^{-1}): 1741, 1602, 1581, 1499, 1243, 1148, 843. ^{1}H-NMR ($CDCl_3$, 400MHz) δ (ppm): 7.85-7.82 (m, 64H), 7.52 (s, 1H), 6.98-6.92 (m, 64H), 4.30-4.16 (m, 64H) 3.96 (t, *J*=6.3 Hz, 32H), 3.76 (d, *J*=6,5 Hz, 32H), 3.65-3.50 (m, 178H), 3.38 (s, 3H), 2.97 (t, *J*=6.5 Hz, 2H), 2.73 (t, *J*=6.5 Hz, 2H), 2.28 (t, *J*=7.5 Hz, 32H), 2.12-2.08 (m, 16H) 1.82-1.77 (m, 32H), 1.68-1.62 (m, 34H), 1.48-1.43 (m, 34H), 1.35-1.10 (m, 209H), 1.03 (d, *J*= 6,7 Hz, 96H). Anal. Calc: C, 66.73 %; H, 8.19 %; N, 4.47 %. Found: C, 66.28 %; H, 8.59 %; N, 5.05 %.

Characterisation Data for PEG-b-d16isoAZOb: IR (KBr), ν (cm^{-1}): 1739, 1601, 1581, 1498, 1245, 1148, 843. ^{1}H-NMR ($CDCl_3$, 400MHz) δ (ppm): 7.83-7.80 (m, 64H), 7.52 (s, 1H), 6.96-6.90 (m, 64H), 4.30-4.16 (m, 64H) 3.93 (t, *J*=6.3 Hz, 32H), 3.74 (d, *J*=6,5 Hz, 32H), 3.65-3.50 (m, 178H), 3.38 (s, 3H), 2.97 (t, *J*=6.5 Hz, 2H), 2.73 (t, *J*=6.5 Hz, 2H), 2.32 (t, *J*=7.5 Hz, 32H), 2.10-2.07 (m, 16H) 1.78-1.73 (m, 32H), 1.68-1.62 (m, 34H), 1.48-1.43 (m, 34H), 1.35-1.10 (m, 49H), 1.03 (d, *J*= 6,7 Hz, 96H). Anal. Calc: C, 64.57%; H, 7.50 %; N, 4.98 %. Found: C, 64.09 %; H, 7.72 %; N, 4.63%.

3.5.5 General Procedures

Preparation of the Vesicles

For the preparation of the self-assemblies, a solution of 5mg/mL of the amphiphilic BC in THF was prepared and Milli-Q water was gradually added while measuring the absorbance at 650nm in the UV-Vis spectrophotometer as a means of monitoring turbidity (scattering). When a constant value was reached, the mixture was dialyzed against water to remove the organic solvent using a Spectra/Por® dialysis membrane (MWCO 1000) during 3 days. Water suspensions of the vesicles with a concentration around 2 mg/mL were obtained.

Determination of the Critical Agregation Concentration (CAC*)*

Critical aggregation concentration (CAC) was determined by fluorescence spectroscopy using Nile Red as the probe as follows: 119 µL of a solution of Nile Red in DCM (5×10^{-6} M) was added into a series of flasks and then the solvent evaporated. Afterwards, a water suspension of vesicles of concentration ranging from 1.0×10^{-4} to 1.0 mg /mL was added to each flask. The vesicles suspensions were prepared by diluting the former 2 mg/mL vesicle suspension. In each flask a final concentration of 1.0×10^{-6} M of Nile Red was reached. These solutions were stirred overnight to reach equilibrium before fluorescence was measured. The emission spectra of Nile Red were registered from 560 to 700 nm while exciting at 550 nm.

Loading of Rhodamine B into the Vesicle

In order to encapsulate the dye, vesicles formation was carried out following the same procedure described for the polymer vesicles but using a solution of Rhodamine B in Milli-Q water.[25] The copolymer was first dissolved in THF and a solution of Rhodamine B was gradually added to induce the self-assembly into vesicles. The charge ratio was 1:5 (mol copolymer/mol dye). Self-assembly was followed by monitoring the turbidity and once prepared the encapsulated vesicles, the mixture was then dialyzed against water to remove THF and non-encapsulated Rhodamine B.

Preparation of Samples for TEM Inspection

5 µL of a 0.5 mg/mL water dispersion of self-assemblies was applied to a TEM grid. Water of the sample was removed by capillarity using filter paper. Then, the sample was stained with uranyl acetate and the grid was dried overnight under vacuum.

Preparation of Samples for Cryo-TEM Inspection

5µL of a 2 mg/mL water dispersion of self-assemblies were applied to a suitable grid and then rapidly frozen in liquid ethane.

Confocal Microscopy Sample Preparation

5µL of a 2 mg/mL water dispersion of self-assemblies with encapsulated Rhodamine B were applied to a glass slide and a cover slip was placed on the top of the sample. The edges were sealed to avoid solvent evaporation during measurement.

Irradiation Experiments

A 1000 W mercury lamp Oriel was used as the light source for the photoisomerisation of the azobenzenes. Light was passed through a IR water filter (10 cm) and a cut-off filter (λ = 365 nm). The samples were placed at a distance of 40 cm from the light source in quartz cuvettes at room temperature. Power lamp was measured by using a calibrated photodiode sensor Newsport model 818-UV.

References

1 Letchford, K.; Burt, H. A review of the formation and classification of amphiphilic block copolymer nanoparticulate structures: micelles, nanospheres, nanocapsules and polymersomes. *European Journal of Pharmaceutics and Biopharmaceutics* **2007**, 65, 259-269.

2 Blanazs, A.; Armes, S.P.; Ryan, A.J. Self-Assembled Block Copolymer Aggregates: From Micelles to Vesicles and their Biological Applications. *Macromolecular Rapid Communications* **2009**, 30, 267-277.

3 Smart, T.; Lomas, T.; Massignani, M.; Flores-Merino, M.V.; Ruiz-Perez, L.; Battaglia, G. Block copolymer nanostructures. *Nano Today* **2008**, 3, 38-46.

4 Mai, Y.; Eisenberg, A. Self-assembly of block copolymers. *Chemical Society Reviews* **2012**, 41, 5969-5985.

5 Meng, F. H.; Zhong, Z. Y.; Feijen, J. Stimuli-Responsive Polymersomes for Programmed Drug Delivery. *Biomacromolecules* **2009**, 10, 197-209.

6 Jin, Q.; Liu, G.; Liu, X.; Ji, J. Photo-responsive supramolecular self-assembly and disassembly of an azobenzene-containing block copolymer. *Soft Matter* **2010**, 6, 5589-5595.

7 del Barrio, J.; Oriol, L.; Sánchez, C.; Serrano, J.L.; Di Cicco, A.; Keller, P.; Li, M.H. Self-Assembly of Linear-Dendritic Diblock Copolymers: From Nanofibers to Polymersomes. *Journal of the American Chemical Society* **2010**, 132, 3762-3769.

8 Zebger, I.; Rutloh, M.; Hoffmann, U.; Stumpe, J.; Siesler, H.W.; Hvilsted, S. Photoorientation of a liquid crystalline polyester with azobenzene side groups. 1. Effects of irradiation with linearly polarized blue light. *Journal of Physical Chemistry A* **2002**, 106, 3454-3462.

9 Han, M.; Hara, M. Intense fluorescence from light-driven self-assembled aggregates of nonionic azobenzene derivative. *Journal of the American Chemical Society* **2005**, 127, 10951-10955.

10 Cao, H.; Jiang, J.; Zhu, X.; Duan, P.; Liu, M. Hierarchical co-assembly of chiral lipid nanotubes with an azobenzene derivative: optical and chiroptical switching. *Soft Matter* **2011**, 7, 4654-4660.

11 Xiang, Y.; Xue, X.; Zhu, J.; Zhang, Z.; Zhang, W.; Zhoua, N.;Xiang, X.Z. Fluorescence behavior of an azobenzene-containing amphiphilic diblock copolymer. *Polymer Chemistry* **2010**, 1, 1453-1458.

12 Tong, X.; Wang, G.; Soldera, A.; Zhao, Y. How can azobenzene block copolymer vesicles be dissociated and reformed by light? *Journal of Physical Chemsitry B* **2005**, 109, 20281-20287.

13 del Barrio, J.; Oriol, L.; Alcala, R.; Sanchez, C. Azobenzene-Containing Linear-Dendritic Diblock Copolymers by Click Chemistry: Synthesis, Characterization, Morphological Study, and Photoinduction of Optical Anisotropy. *Macromolecules* **2009**, 42, 5752-5760.

14 Tsarevsky, N. V.; Bencherif, S. A.; Matyjaszewski, K. Graft Copolymers by a Combination of ATRP and Two Different Consecutive Click Reactions. *Macromolecules* **2007**, 40, 4439-4445.

15 Peng, S.-M.; Chen, Y., Hua, C.; Dong, C.-M. Dendron-like Polypeptide/Linear Poly(ethylene oxide) Biohybrids with Both Asymmetrical and Symmetrical Topologies Synthesized via the Combination of Click Chemistry and Ring-Opening Polymerization. *Macromolecules* **2008**, 42, 104-113.

16 Shi, Z.; Chen, D.; Lu, H.; Wu, B.; Ma, J.; Cheng, R.; Fangb, J.; Chen, X. Self-assembled hierarchical structure evolution of azobenzene-containing linear-dendritic liquid crystalline block copolymers. *Soft Matter* **2012**, 8, 6174-6184.

17 Goodwin, A. P.; Mynar, J. L.; Ma, Y. Z.; Fleming, G. R.; Frechet, J. M. J. Synthetic micelle sensitive to IR light via a two-photon process. *Journal of the American Chemical Society* **2005**, 127, 9952-9953.

18 Cui, Q. L.; Wu, F. P.; Wang, E. J. Novel amphiphilic diblock copolymers bearing acid-labile oxazolidine moieties: Synthesis, self-assembly and responsive behavior in aqueous solution. *Polymer* **2011**, 52, 1755-1765.

19 Mynar, J. L.; Goodwin, A. P.; Cohen, J. A.; Ma, Y.; Fleming J. R.; Fréchet J.M.J. Two-photon degradable supramolecular assemblies of linear-dendritic copolymers. *Chemical Communications* **2007**, 2081-2082.

20 Ferreira, S. A.; Coutinho, P. J. G.; Gama, F. M. Self-Assembled Nanogel Made of Mannan: Synthesis and Characterization. *Langmuir* **2010**, 26, 11413-11420.

21 Qi, B.; Zhao, Y. Fluorescence from an azobenzene-containing diblock copolymer micelle in solution. *Langmuir* **2007**, 23, 5746-5751.

22 Chang, Y.; Kwon, Y. C.; Lee, S. C.; Kim, C. Amphiphilic linear PEO-dendritic carbosilane block copolymers. *Macromolecules* **2000**, 33, 4496-4500.

23 Shobha, J.; Srinivas, V.; Balasubramanian, D. Differetial-Modes of Incorporation of Probe Molecules in Micelles and in Bilayer Vesicles. *Journal of Physical Chemistry* **1989**, 93, 17-20.

24 Feng, Z.; Lin, L.; Yan, Z.; Yu, Y. L. Dual Responsive Block Copolymer Micelles Functionalized by NIPAM and Azobenzene. *Macromolecular Rapid Communications* **2010**, 31, 640-644.

25 Hernandez-Ainsa, S.; Barbera, J.; Marcos, M.; Serrano, J. L. Nanoobjects coming from mesomorphic ionic PAMAM dendrimers. *Soft Matter* **2011**, 7, 2560-2568.

26 Lin, Y.-L.; Chang, H.-Y.; Sheng, Y.-J.; Tsao, H.-K. Photoresponsive Polymersomes Formed by Amphiphilic Linear–Dendritic Block Copolymers: Generation-Dependent Aggregation Behavior. *Macromolecules* **2012**, 7143-7156.

CHAPTER 4

Amphiphilic Linear-Dendritic Block Copolymers using Azobenzene-Aliphatic Codendrons: Self-assembly and Photoresponse

Published in *Macromolecules* **2013** (accepted)

4.1 Introduction and Aims

It has already been emphasised the increasingly interest in the preparation of stimuli-responsive polymeric nanoparticles for on demand delivery.[1-10] From them, polymer vesicles created using synthetic amphiphilic block copolymers represent excellent candidates for new nanocarriers as they offer the benefit of simultaneous encapsulation of hydrophilic compounds in their aqueous cavities and the insertion of hydrophobic compounds in their membranes. Polymer vesicles have similar structure to lipid vesicles with the advantage of superior stability and toughness but in addition offer numerous possibilities of tailoring physical and chemical properties. By variation of block length, chemical structure, hydrophobic/hydrophilic ratio, architecture or implementing additional functionalities, parameters such as the size, membrane integrity, permeation or responsiveness to stimuli can be modified.[11-13]

We have focused our interest in light-responsive LDBC that can form polymeric vesicles in water when an appropriate hydrophilic-hydrophobic balance is reached. As already discussed in the previous chapter, amphiphilic LDBCs composed of a fourth generation of the azodendron based on bis-MPA having sixteen peripheral azobenzene units coupled to a PEG segment of 2000 number average molecular weight generate stable vesicles in water.[14] These vesicles can entrap small hydrophobic and hydrophilic molecules that can be released upon UV-irradiation. The photoresponsive behaviour of the vesicles was initially demonstrated from LDBC having 4-cyanoazobenzene units using a high intensity UV lamp. In the previous chapter, we showed that the incorporation of sixteen 4-isobutyloxyazobenzene units at the surface of the dendron facilitates the effectively light induced disruption of the membrane, as lower intensity of light illumination is required. The vesicles were used to encapsulate both hydrophobic and hydrophilic molecules and, under conditions of low intensity UV irradiation, the distortion of the membrane increased its permeability to the entrapped molecules.

In this chapter, the chemical composition of the dendritic block is varied by incorporating 4-isobutyloxyazobenzene and hydrocarbon chains in different proportions randomly distributed at the periphery of the dendron. The purpose

of this structural modification is to decrease the azobenzene content altering the interactions in the inner membrane and to investigate its possible influence in the uptake/release usin fluorescent probes. Specifically, three different codendrons derived from the fourth generation dendrons of bis-MPA statistically functionalised with 4-isobutyloxyazobenzene (**isoAZOb**) and alkyl chains (**C18**) in 3:1, 1:1 and 1:3 molar ratio (that correspond to 75/25, 50/50 and 25/75 molar percentages of isoAZOb/C18) were proposed (**Figure 4.1**).

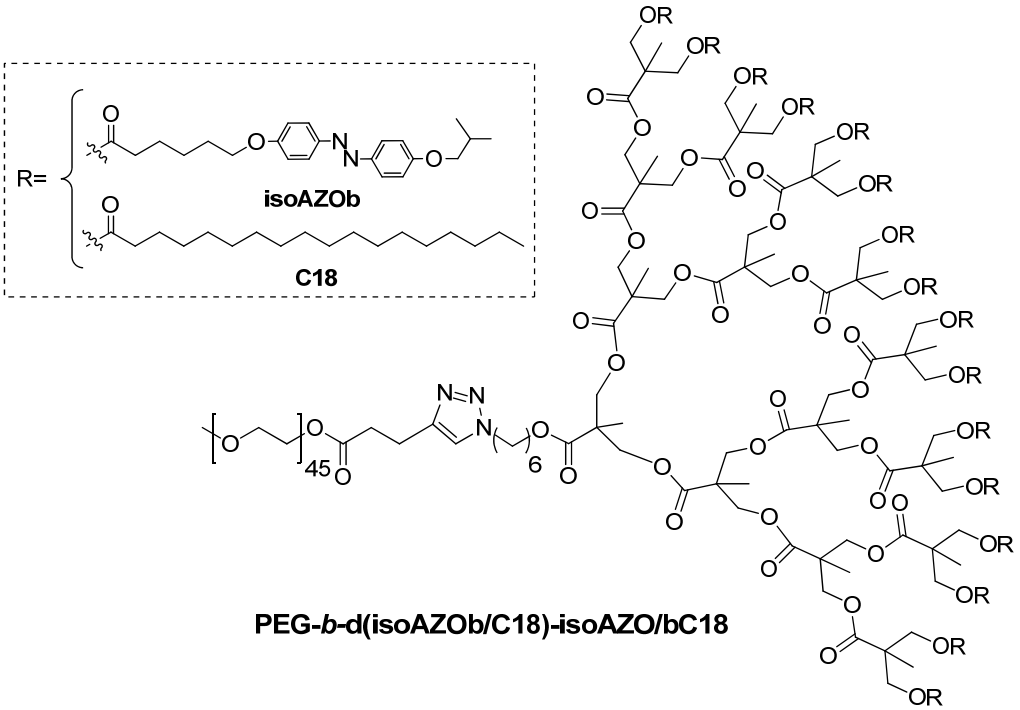

LDBC	isoAZOb units	C18 units	isoAZOb/C18
PEG-b-d(isoAZOb/C18)-75/25	12	4	75/25
PEG-b-d(isoAZOb/C18)-50/50	8	8	50/50
PEG-b-d(isoAZOb/C18)-25/75	4	12	25/75

Figure 4.1 *Schematic representation of the LDBCs with a statistitical cofunctionalisation of the dendron periphery*

Tasks in this chapter are analogous to the described in the previous one. The materials were accomplished by the same synthetic approach (**Figure 4.2**) and characterised using similar techniques in order to compare the results with the LDBC having sixteen azobenzene moieties used as reference.

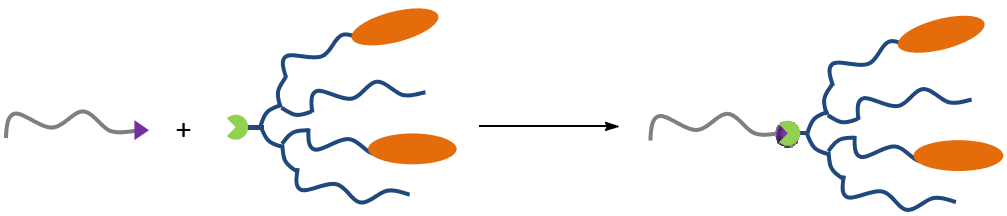

Figure 4.2 *Synthetic approach for the synthesis of the LDBCs*

4.2 Results and discussion

4.2.1 Synthesis and Characterisation of the Amphiphilic Block Copolymers

The target amphiphilic LDBCs with a statistical functionalisation were prepared following the coupling strategy described in Chapter 3. In this case, the dendron **d16OH** was esterified with a mixture of 4-isobutyloxyazobenzene carboxylic acid **isoAZOb** and stearic acid (**C18**) using DCC/DPTS (see Experimental Section). Three different proportions of both acids were fed in the esterification reaction being 75/25, 50/50 and 25/75 the molar percentages of isoAZOb/C18 used (**Scheme 4.1**).

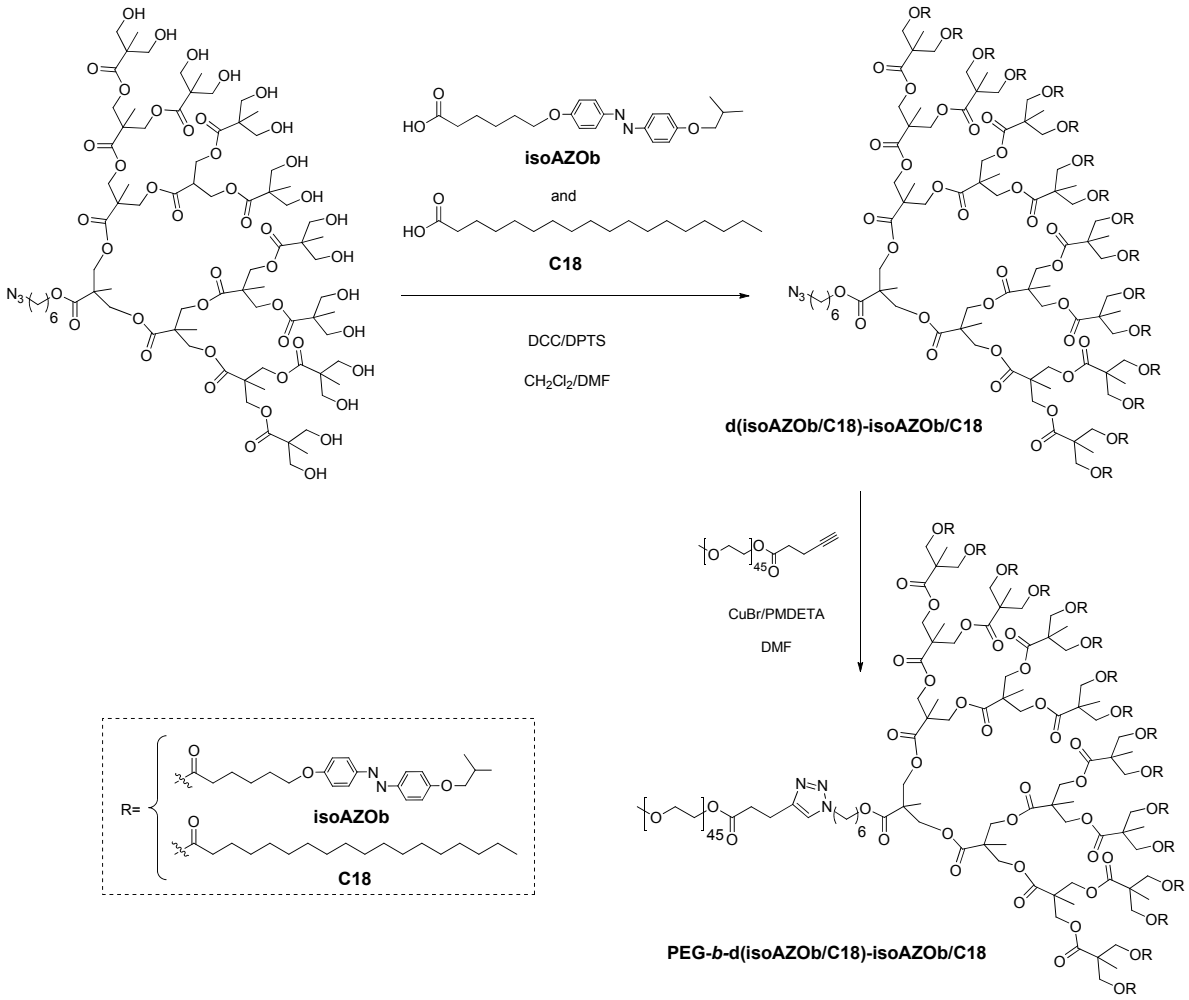

Scheme 4.1 *Synthesis of the investigated LDBCs*

Different analytical techniques were used to gain full information about the resulting composition of these codendrons. As expected, several peaks were registered in the MALDI-TOF mass spectra corresponding to a distribution of codendrons with different composition. The mass spectra showed a statistical functionalisation of the periphery of the dendron, being the most intense peaks the corresponding to fully substituted codendrons (**Figure 4.3**). However, peaks corresponding to codendrons with fifteen functionalised groups were also detected at lower masses. The maximum of this distribution (**Table 4.1**) corresponds to codendrons with a functionalisation equal or similar to the acids' ratio feed on the esterification reaction. Accordingly, for **d(isoAZOb/C18)-75/25** the maximum of this distribution corresponds to fully functionalised condendron containing 12 isoAZOb units and 4 alkyl chains (12isoAZOb/4C18 composition) at the sixteen peripheral positions, for **d(isoAZOb/C18)-50/50** there is a similar population of codendrons with 8isoAZOb/8C18 and 9isoAZOb/7C18 compositions and for **d(isoAZOb/C18)-25/75** the majority corresponds to 4isoAZOb/12C18 composition.

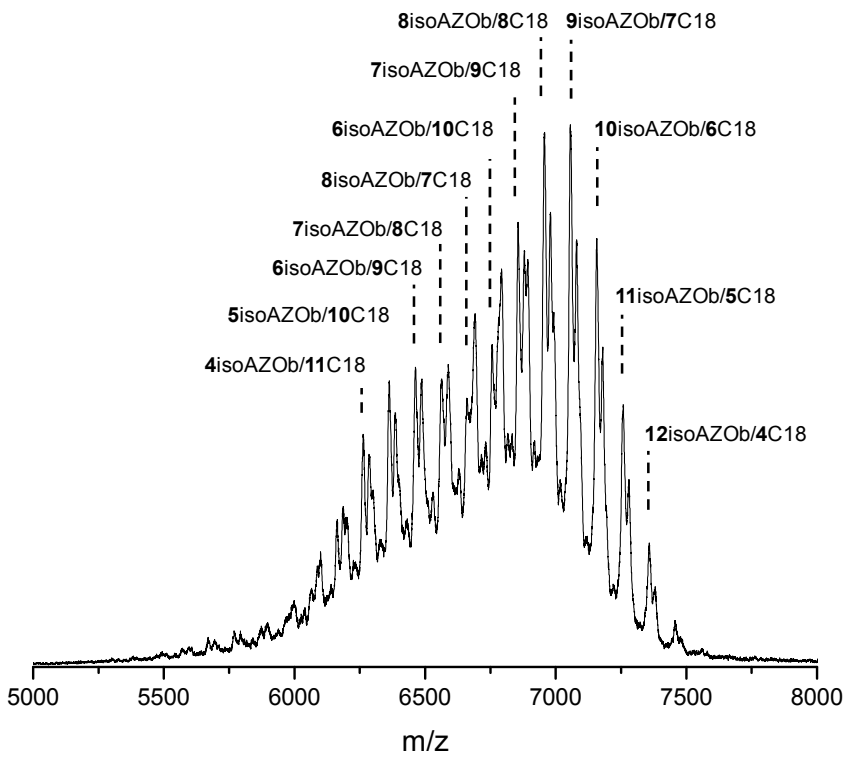

Figure 4.3 *MALDI-TOF spectrum of* ***d(isoAZOb/C18)-50/50*** *codendron as an example. Assigned peaks correspond to the protonated species* $[M\text{-}H]^+$*, although* $[M\text{-}Na]^+$ *are also detected*

Table 4.1 *Molecular weight and composition of the synthesised condendrons and LDBCs.*

Codendrons and LDBCs	M_n[a]	M_n[b]	M_n[c]	$Đ_M$[c]	isoAZOb/C18 ratio[d]	philic/phobic ratio[e]
d(isoAZOb/C18)-75/25	7349	7350	6300	1.01	72/28	-
d(isoAZOb/C18)-50/50	6948	6949	6500	1.02	47/53	-
d(isoAZOb/C18)-25/75	6548	6549	6000	1.03	31/69	-
PEG-*b*-d(isoAZOb/C18)-75/25	9319	9100	8600	1.02	-	79/21
PEG-*b*-d(isoAZOb/C18)-50/50	8918	8800	8400	1.02	-	78/22
PEG-*b*-d(isoAZOb/C18)-25/75	8518	8400	8000	1.03	-	76/24

[a] For the codendrons, molecular weight was calculated from the feed isoAZOb/C18 ratio. For LDBCs, the theoretical molecular weight is given as the sum of the molecular weight of the PEG block (M_n=1970) and the theoretical molecular weight of the dendritic block. [b] Molecular weights obtained by MALDI-TOF. Data of the dendrons corresponding to the most intense peak of the protonated species $[M-H]^+$ in dendron distributions (see MALDI-TOF spectra in **Figure 4.3**). [c] M_n and $Đ_M$ were calculated by SEC using PS standards. [d] isoAZOb/C18 ratio calculated by ^{1}H-NMR. [e] Hydrophilic/ hydrophobic ratio was calculated considering the linear block (PEG) as the hydrophilic part and the dendritic block as the hydrophobic one.

^{1}H-NMR spectroscopy was employed to study the average isoAZOb/C18 composition by relative integration of azobenzene aromatic protons signals and the corresponding to the methylenic protons (-CH_2-CO) of the functional units at the periphery (See **Figure 4.4** as an example). The calculated isoAZOb/C18 ratios are in fair agreement with the expected ones.

Alkyne functionalised PEG[15] and azido functionalised codendrons were finally coupled to give the corresponding LDBCs **PEG-*b*-d(isoAZOb/C18)-75/25**, **PEG-*b*-d(isoAZOb/C18)-50/50** and **PEG-*b*-d(isoAZOb/C18)-25/75**. Again, the CuAAC reaction was carried out in DMF and using CuBr and PMDETA as the catalytic system. A slight excess of the PEG block was used in order to facilitate the completeness of the coupling reaction that was easily removed by precipitation of the LDBC in ethanol.

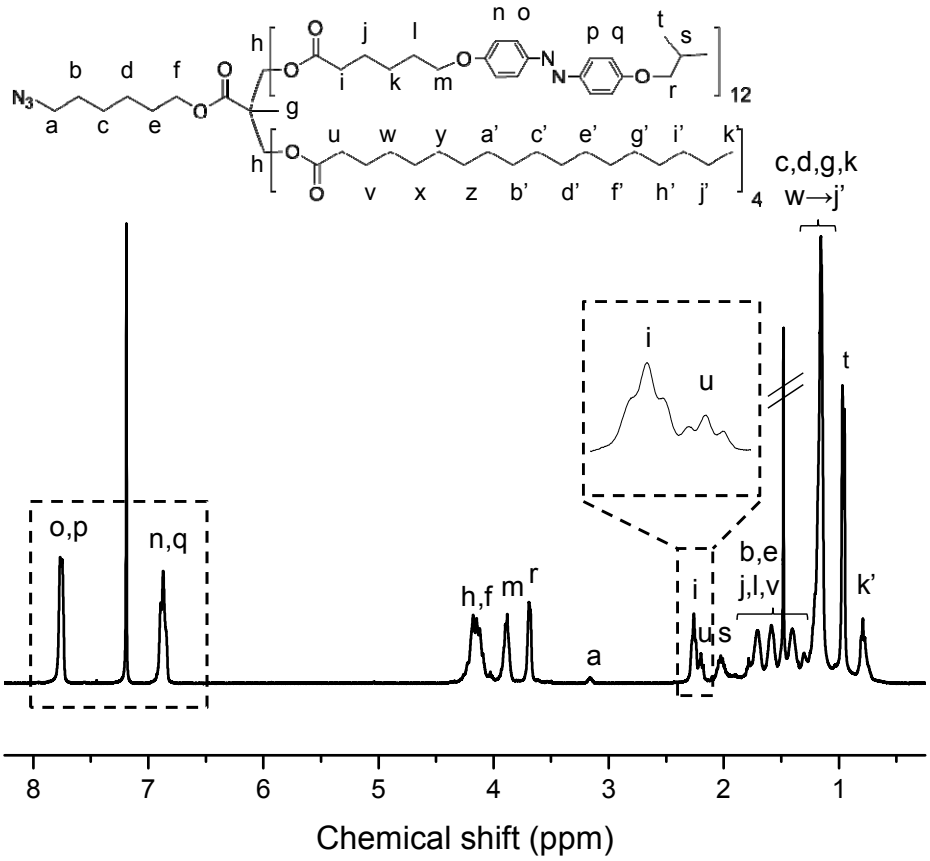

Figure 4.4 *^{1}H-NMR spectrum of* ***d(isoAZOb/C18)-75/25*** *showing the signals used to composition calculation in $CDCl_3$ (400 MHz)*

The efficiency of the coupling was corroborated by different techniques. First, the IR spectra confirmed the reaction of the azide and alkyne terminal groups. As an example in **Figure 4.5** the IR spectra of a dendron precursor block and the LDBC derivative were compared. As can be seen, the signal corresponding to the azide group, located at 2100 cm^{-1}, disappeared due to the coupling reaction. Furthermore, the absence of residual traces of non coupled blocks was corroborated by SEC and MALDI-TOF mass spectrometry, as it can be observed in the examples gathered in **Figure 4.6**. What is more, the relative integration of azobenzene aromatic protons signals and the corresponding ones to the linear PEG block protons at 3.70-3.55 ppm (labelled as '*b*' in **Figure 4.7**) in the ^{1}H-NMR spectra also confirmed the expected structures.

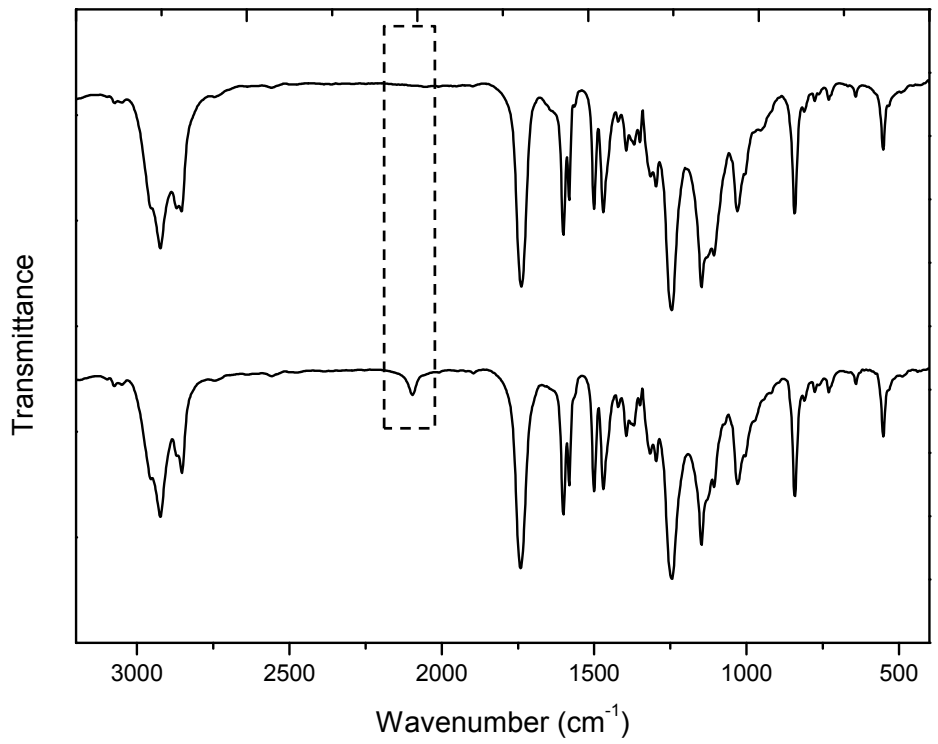

Figure 4.5 *FTIR spectra of* ***d(isoAZOb/C18-75/25*** *(bottom) and* ***PEG-b-d(isoAZOb/C18-75/25*** *(top)*

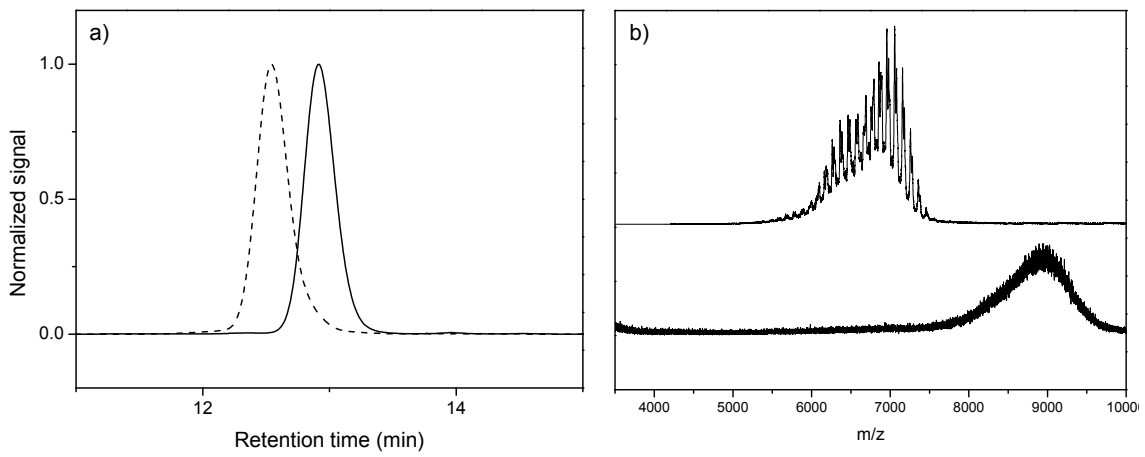

Figure 4.6 *a) SEC traces of* ***d(isoAZOb/C18)-50/50*** *(straight line) and* ***PEG-b-d(isoAZOb/C18)-50/50*** *(dashed line) b) MALDI-TOF mass spectra of* ***d(isoAZOb/C18)-50/50*** *(top) and* ***PEG-b-d(isoAZOb/C18)-50/50*** *(bottom)*

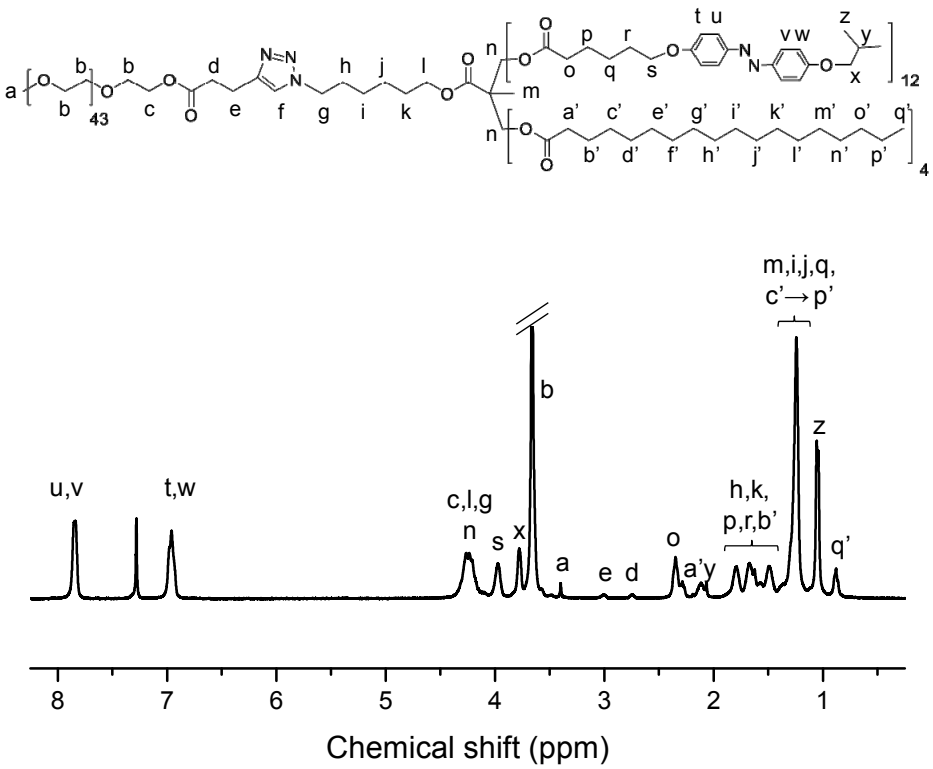

Figure 4.7. *^{1}H-NMR spectrum of* ***PEG-*b*-d(isoAZOb/C18)-75/25*** *in $CDCl_3$ (400MHz)*

LDBCs average molecular weights were calculated by MALDI-TOF and SEC. The values calculated by mass spectrometry are in good agreement with theoretical values. The values calculated by SEC using PS standards are slightly underestimated (**Table 4.1**) as can be expected.[16]

The thermal stability of the azodendrons and the LDBCs was analysed by TGA using powdered samples and the results main are presented in **Table 4.2**. All the samples exhibited a good thermal stability with the onset of decomposition above 320ºC. The stability of the LDBCs is around 30ºC higher than the corresponding codendrons. The thermal stability of the codendrons and the derived LDBCs is similar, even slightly higher, than the corresponding to the derivatives having sixteen azobenzene moieties linked to the periphery of the dendron, which were reported in previous chapter.

Table 4.2. *Thermal properties of the codendrons and derived LDBCs.*

	TGA [a]	DSC [b]	
Codendrons and LDBCs	T_d	T_c	ΔH_c
d(isoAZOb/C18)-75/25	331	36	128
d(isoAZOb/C18)-50/50	335	29	228
d(isoAZOb/C18)-25/75	327	29	258
PEG-*b*-d(isoAZOb/C18)-75/25	359	38	139
PEG-*b*-d(isoAZOb/C18)-50/50	365	32	173
PEG-*b*-d(isoAZOb/C18)-25/75	360	31	232

[a] T_d (in ºC): decomposition temperature associated to mass loss calculated by TGA, under nitrogen atmosphere (10ºC/min) at the onset point in the weight loss curve. [b] T_C (in ºC) and ΔH_C (in kJ per mole of polymer chain): crystallisation temperature and associated enthalpy calculated from the first cooling scan recorded at 10ºC/min. Molecular weight of the codendrons and M_n of polymer (determined by MALDI-TOF) were used to calculate enthalpy values.

The thermal transitions of the dendrons and BCs were studied by POM and DSC (**Table 4.2**, **Figure 4.8**). Upon cooling from the liquid isotropic state, in all cases crystallisation of the codendrons was detected at approx. 30ºC, as calculated by DSC but it was observed that the crystallisation temperature depends on the C18 content. While crystallisation of the dendron containing only 4-isobutyloxyazobenzene occurs at 51ºC, crystallisation of codendrons decreases to 36ºC for **d(isoAZOb/C18)-75/25** and to 29ºC for the lower isoAZOb/C18 contents, at the same time as crystallisation enthalpy increases. In the case of **d(isoAZOb/C18)-75/25**, the DSC cooling curve exhibits a small shoulder before crystallisation, which could be due to a narrow interval of mesophase analogous to the dendron containing 100% azobenzene, although this behaviour could not be corroborated by POM. The increase on the crystallinity content can be associated to the crystallisation of the alkyl chain as it has been reported for bis-MPA based hyperbranched polyesters containing terminal long alkyl chains.[17]

Similarly to the codendrons, LDBCs have tendency to crystallise. An exothermic crystallisation process was recorded on the DSC curves at 31-38ºC associated to the codendron block. Crystallisation of the PEG block, which should show at about 20ºC, was not visible. Again, on decreasing the azobenzene content the crystallisation temperature slightly decreases as the correlated crystallisation enthalpy increases. The crystallisation temperature for LDBC with only isoAZOb moieties was 62ºC.

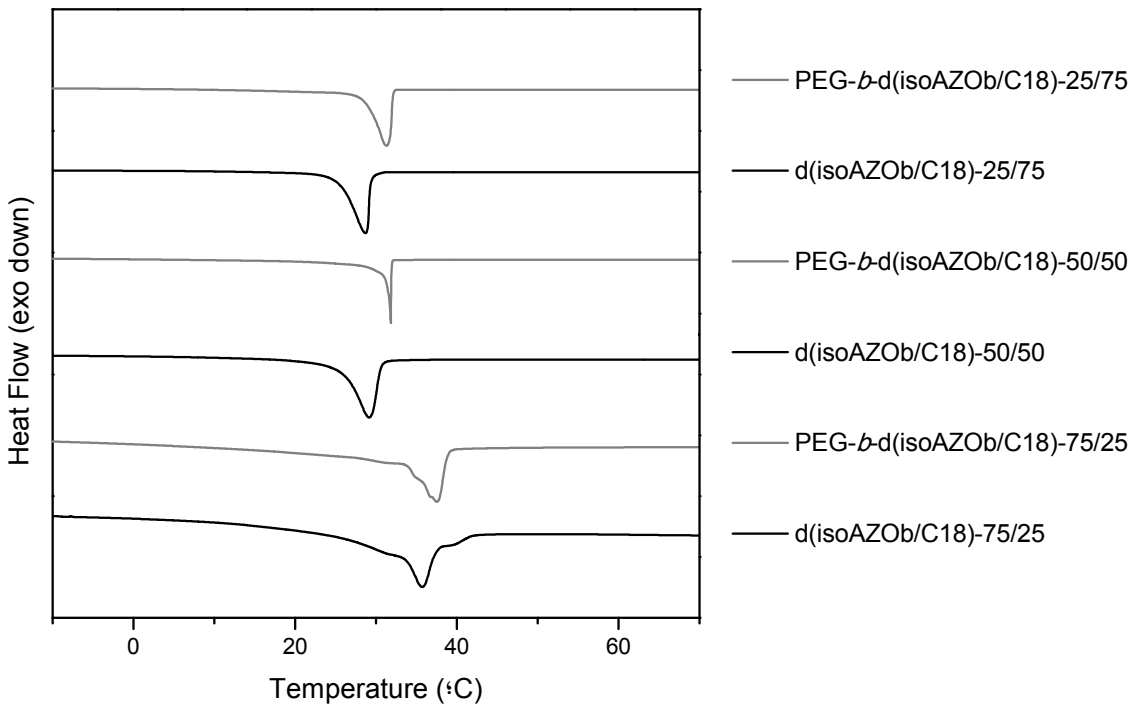

Figure 4.8 *DSC traces (10ºC/min) corresponding to the first cooling of the synthesised materials*

4.2.2 Self-assembly of the Linear-Dendritic Azobenzene Block Copolymers in Water

Vesicles were formed by the cosolvent method using THF and water and the process was followed by turbidimetry measurements (**Figure 4.9**). When water was gradually added to a solution of the LDBCs in THF, an abrupt increase of scattered light was observed which indicates that polymer chains started to associate due to hydrophobic interactions.

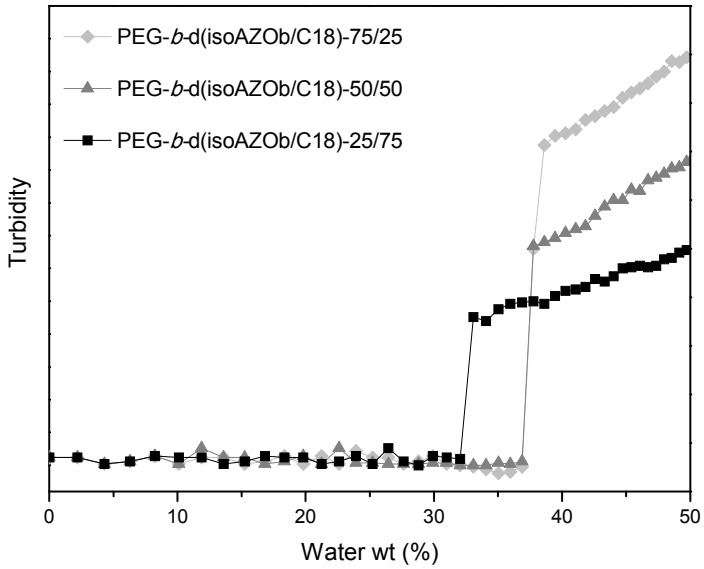

Figure 4.9 *Turbidity plot of the LDBCs THF solution versus amount of water added*

As in Chapter 3, Nile Red was equilibrated with the amphiphilic LDBCs at several concentrations in order to determine the CAC. **Figure 4.10** registers the emission intensity of Nile Red as a function of the concentration of **PEG-*b*-d(isoAZOb/C18)-50/50** in water. The relationship between the fluorescence and the concentration is non linear and the CAC of the three LDBCs in water was determined at the onset of the fluorescence intensity increase. Calculated CAC values were about 8-10 µg/mL. These CAC values for the investigated compounds, which incorporate aliphatic chains, are remarkably lower compared to the values calculated for LDBC containing only isoAZOb moieties (35 µg/mL). As the CAC is most commonly used to evaluate the stability of the self-

assemblies in aqueous solution, lower CAC values point to a stronger tendency for aggregation or, in other words, higher thermodynamic stability.[18]

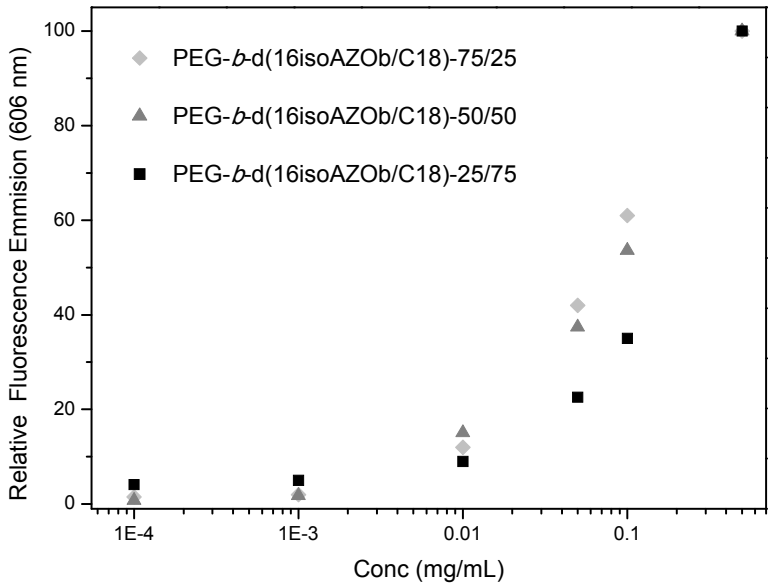

Figure 4.10 *Fluorescence intensity of Nile Red at 606 nm (λ_{exc} = 550 nm) versus BC concentration (mg/mL)*

The morphology of the self-assemblies was initially studied TEM using dried samples stained with uranyl acetate. The presence of vesicular self-assemblies, in general with a deflated appearance due to dehydration during sample preparation, was confirmed (**Figure 4.11a**). Vitrified samples of the self-assemblies without staining were also analysed by Cryo-TEM (**Figure 4.11b**). In this case, non disturbed vesicles were observed with a clear membrane that showed a distribution of diameters ranging from 70 to 300 nm for all the LDBCs. As was mentioned, the dark region of the membrane corresponds to the hydrophobic dendritic arrangement. The thickness of this inner part of the membrane was found to be around 8 nm fitting with a bilayer arrangement of the codendrons.[14]

DLS measurements were also performed. The mean hydrodynamic diameters (D_h) were found to be around 200-300 nm (**Table 5.3,** see **Figure 4.13** below), slightly smaller than the previous vesicles described, i.e 365 nm. On the other hand, a higher dispersity in the size of the self-asssemblies was also found by

employing codendrons as dendritic block rather than a monodisperse dendron only containing 4-isobutyloxyazobenzene moieties.

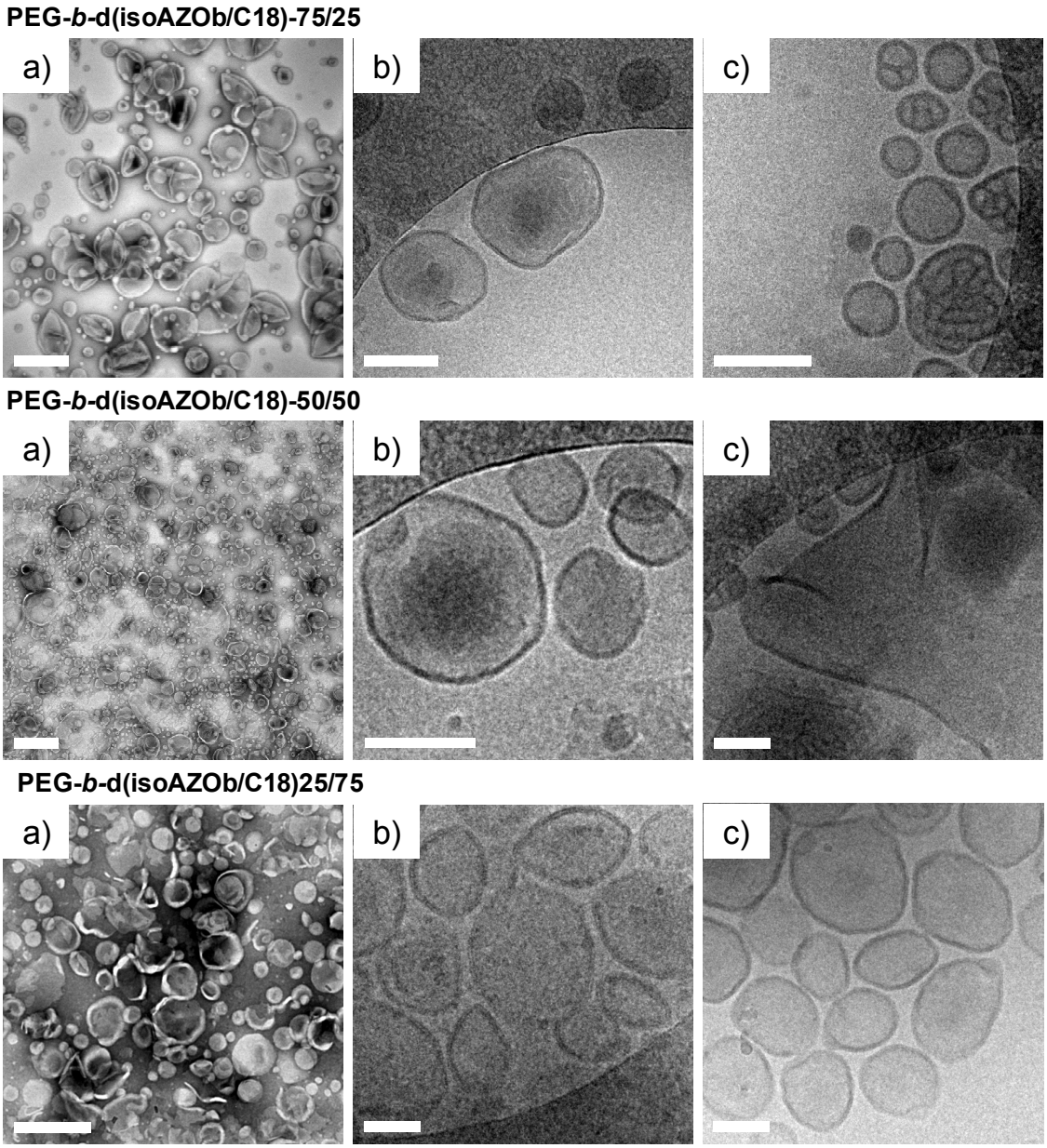

Figure 4.11 *a) TEM images of non-irradiated dried vesicles. Cryo-TEM images of the vesicles: b) before and c) after irradiation. The length of the scale bar corresponds to 200 nm in a) and 100 nm in b) and c)*

Table 5.3. *Mean hydrodynamic diameters (D_h) of the vesicles before and after irradiation.*

Vesicles	D_h (nm) Non-irradiated	D_h (nm) Irradiated
PEG-*b*-d(isoAZOb/C18)-75/25	195	178
PEG-*b*-d(isoAZOb/C18)-50/50	298	98/350[a]
PEG-*b*-d(isoAZOb/C18)-25/75	210	190

[a] *Bimodal size distribution with two maxima (see **Figure 4.13**)*

4.2.3 Light Responsive Behaviour of the Self-Assemblies

UV-Vis spectra of both LDBCs in an organic solution and the vesicles suspensions, 1mg/mL in water, were recorded and compared with that recorded for vesicles previously obtained in LDBCs only containing 4-isobutyloxyazobenzene moieties (100% of azobenzene functionalisation) at the periphery described in the previous chapter.

The solution spectra of all LDBCs exhibited two absorption bands corresponding to the *trans*-isomer, a strong one centred at 355 nm attributed to the π-π* transition and a weak one at about 450 nm corresponding to n-π* transition, as described for the LDBC **PEG-*b*-d16isoAZOb**.

As it can be seen in **Figure 4.12a** the spectra of **PEG-*b*-d(isoAZOb/C18)-75/25** vesicles presents an absorption maximum located at 320 nm similarly to the LDBCs with 100% azobenzene functionalisation, althought the last one exhibited a broader band. This maximum indicates the dominating formation of H-aggregates of azobenzene units. Two shoulders at 355 nm and 375 nm are also observed and attributed to non-aggregated *trans*-azobenzene and the presence of J-aggregates, respectively.

For **PEG-*b*-d(isoAZOb/C18)-50/50** and **PEG-*b*-d(isoAZOb/C18)-25/75** vesicles the spectrum are very similar and showed a clear narrowing of the π-π* band accompanied by a bathochromic shift of the maximum, from 320 to 335 nm, indicating a lower tendency to aggregation of the azobenzene moieties as can be expected from the dilution effect of the C18 alkyl chains.

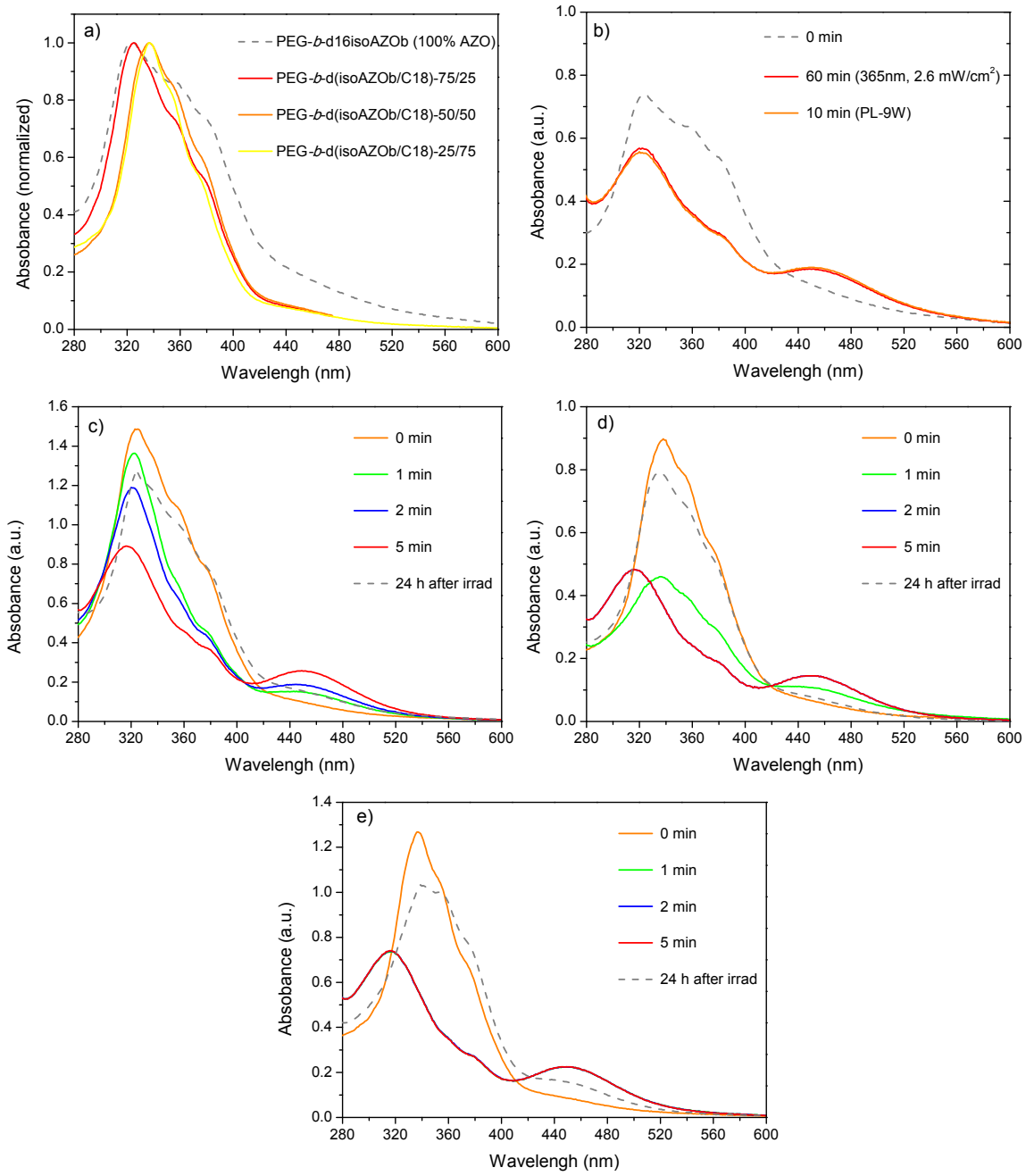

Figure 4.12 *a) Comparison of the UV-Vis spectra of water suspension vesicles of* ***PEG-b-d(isoAZOb/C18)-75/25, PEG-b-d(isoAZOb/C18)-50/50*** *and* ***PEG-b-d(isoAZOb/C18)-25/75*** *with the vesicles previously reported in Chapter 3 (****PEG-b-d16isoAZOb,*** *100% azobenzene functionalisation). b) Comparison of the UV-Vis spectra of irradiated* ***PEG-b-d16isoAZOb*** *vesicles described in Chapter 3 by employing different lamps. Evolution of the UV-Vis spectra of irradiated vesicles at different irradiation times: c)* ***PEG-b-d(isoAZOb/C18)-75/25,*** *d)* ***PEG-b-d(isoAZOb/C18)-50/50****, e)* ***PEG-b-d(isoAZOb/C18)-25/75***

Irradiation experiments described in Chapter 3 were performed with a 1000 W mercury lamp with a 10 cm IR water filter and a cut-off filter (λ = 365 nm). In this work, the lamp was substituted by a smaller and easier to handle lamp emitting at 350-400 nm (Philips PL-9W). Therefore, irradiation control experiments with the previous vesicles containing only isoAZOb moieties using the new UV light source getting similar results to those described before were achieved. As it can be observed in **Figure 4.12b**, under these new conditions, a photostationary state was reached only after 10 min irradatiation.

To demonstrate the sensitivity of the vesicles to UV-light, the suspensions of the three new LDBC in water were exposed to UV irradiation with the new lamp and evolution in the UV-vis spectra was followed (**Figure 4.12c-e**). In all cases, a notable decrease of π-π* band as well as an increase of the absorbance at 450 nm were observed indicating the presence of *cis*-azobenzene. For **PEG-*b*-d(isoAZOb/C18)-75/25** vesicles, no further changes were detected in the UV-vis spectrum after 5 min of irradiation indicating that a photostationary state was reached at this irradiation time. However, when the azobenzene content decreases, it was observed than the lower is AZO/C18 ratio of the dendritic block, the less is the time necessary to reach the photostationary state, being around 2 min for **PEG-*b*-d(isoAZOb/C18)-50/50** vesicles and around 1 min for **PEG-*b*-d(isoAZOb/C18)-25/75** vesicles. Thus, a faster and more efficient photoinduced isomerisation was achieved by decreasing azobenzene content in the codendrons. This fact could be related with a less dense packing and aggregation of azobenzene moieties. Once irradiated and maintained in the dark, the spectra of the vesicles were similar to the observed before irradiation due to the back *cis*-to-*trans* isomerisation.

Cryo-TEM microscopy (**Figure 4.11c**) and DLS measurements (**Table 5.3**) were carried out to gain further information about morphological changes occurred upon irradiation. The samples were studied immediately after irradiation for 5 min. For **PEG-*b*-d(isoAZOb/C18)-75/25** vesicles, a slight decrease in the D_h, i.e. from 195 to 178 nm, was detected (**Figure 4.13a**). Similarly to the vesicles of **PEG-*b*-d16isoAZOb** (100% azobenzene functionalisation), Cryo-TEM images showed deformed vesicles with a distorted membrane revealing that

trans-to-*cis* isomerisation provokes a notable morphological change of the vesicles. In the case of **PEG-*b*-d(isoAZOb/C18)-50/50**, cryo-TEM images showed drastic structural changes upon irradiation. An evident decrease in the number of vesicles accompanied by material without a clear morphology was observed (**Figure 4.11c**). By DLS a clear change in the distribution curve was detected appearing a new peak at smaller D_h (**Figure 4.13b**). This new distribution could explain the disarrangement of some of the self-assemblies observed by Cryo-TEM. By contrast, Cryo-TEM images show that **PEG-*b*-d(isoAZOb/C18)-25/75** vesicles retain the morphology after irradiation (**Figure 4.11c**), despite the modifications detected by UV-vis and only slight modifications were observed by DLS measurements after irradiation (**Figure 4.13c**).

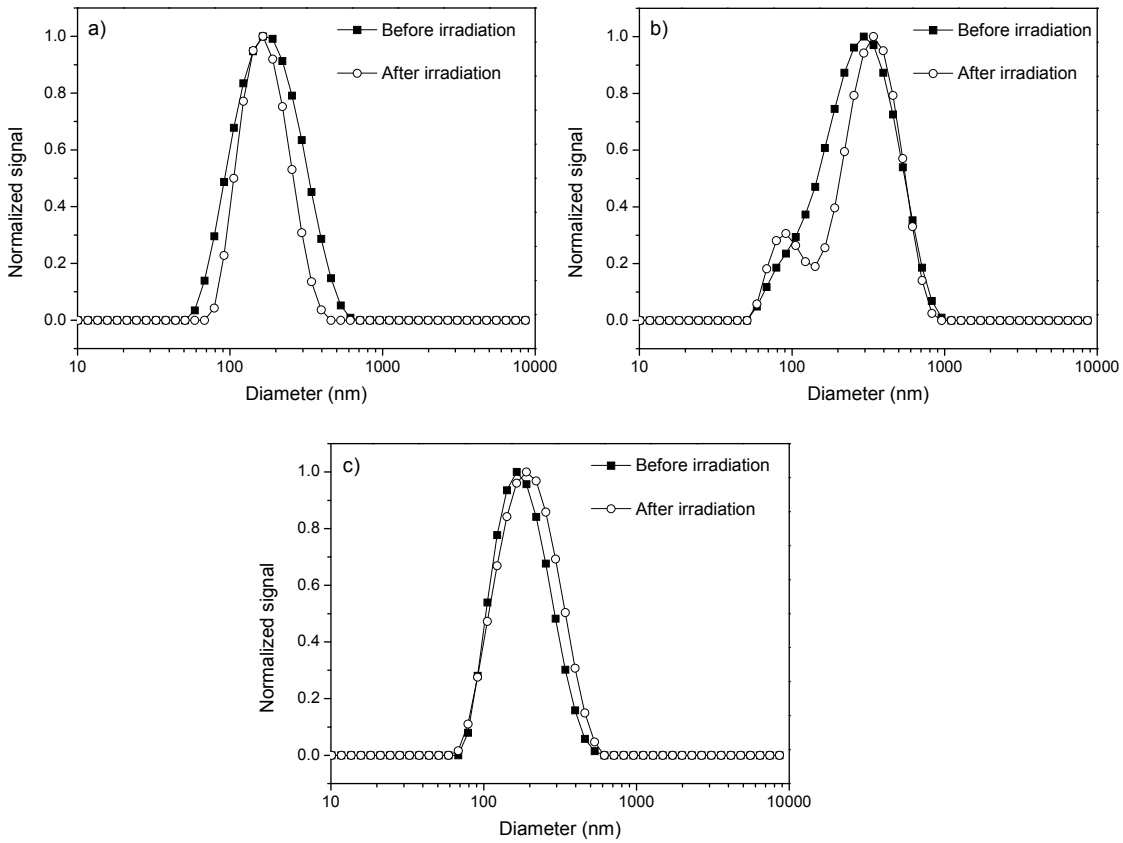

Figure 4.13 *Dynamic light scattering measurements of a water suspension vesicles before and after UV light irradiation: a)**PEG-b-d(isoAZOb/C18)-75/25,** b) **PEG-b-d(isoAZOb/C18)-50/50** and c) **PEG-b-d(isoAZOb/C18)-25/75***

4.2.4 Encapsulation and Photoinduced Release of Molecular Probes

To investigate the release of encapsulated molecules stimulated by the *trans*-to-*cis* photoisomerisation of the azobenzenes, Nile Red was first incorporated into the vesicles. Using an aqueous suspension of vesicles, 1 mg/mL, equilibrated with Nile Red, the fluorescence emission intensity was registered before, and upon UV irradiation at 365 nm to provoke *trans*-to-*cis* isomerisation. Before irradiation, an intense emission peak registered at 606 nm under excitation at 550 nm indicates that Nile Red is in a hydrophobic environment, at the inner part of the membrane.

Upon irradiation, the emission of Nile Red abruptly decreased in all cases (**Figure 4.14**). As mentioned, this decrease of the emission of the dye can be due to both Nile Red migration from the membrane to the aqueous media and to the increase in the polarity of the inner membrane due to the change in net dipole moment associated to *trans*-to-*cis* isomerisation. After standing the samples in the dark, and once thermal back *cis*-to-*trans* isomerisation took place according to the UV-vis spectra, Nile Red fluorescence was evaluated again. Nile Red emission in the samples was almost recovered to the initial value for **PEG-*b*-d(isoAZOb/C18)-25/75**, indicating that the fluorescent probe is again in an hydrophobic environment and consequently, the fluorescent probe mainly remains encapsulated. However, in the case of **PEG-*b*-d(isoAZOb/C18)-75/25** and **PEG-*b*-d(isoAZOb/C18)-50/50**, the initial Nile Red emission was not recovered at all and a weak emission band between 660 and 680 nm appeared. This new band can be related with the Nile Red excimer formation in water proving the light triggered release of the trapped probe to the aqueous environment. It is necessary to mention that in the case of the vesicles containing only azobenzene (described in the previous chapter) Nile Red emission was partially recovered on standing in the dark which might be related to a less efficient release of the fluorescence probes.

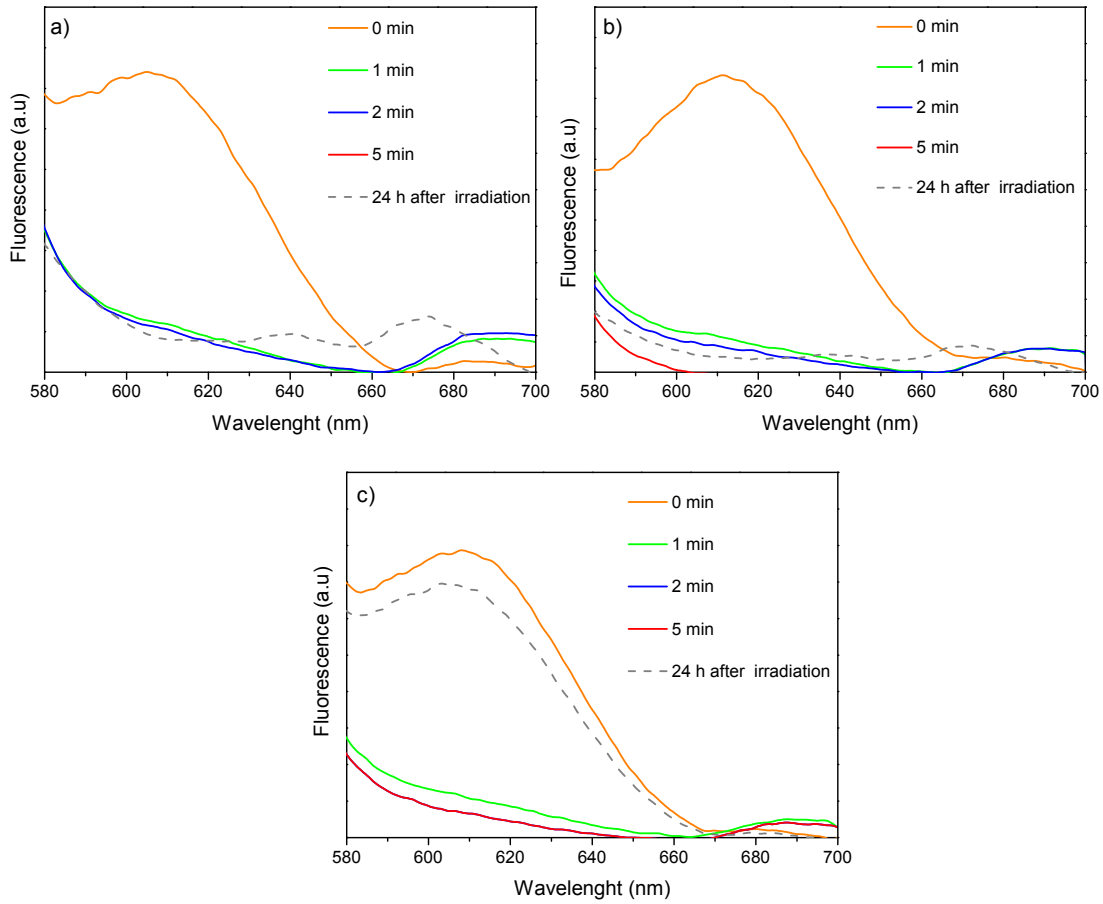

Figure 4.14 *Emission spectra of Nile Red encapsulated vesicles of a)* ***PEG-b-d(isoAZOb/C18)-75/25,*** *b)* ***PEG-b-d(isoAZOb/C18)-50/50*** *and c)* ***PEG-b-d(isoAZOb/C18)-25/75***

Encapsulation and photoinduced release of Rhodamine B was also investigated as a hydrophilic probe to be loaded at the internal cavity of the vesicle. Firstly, vesicles were formed in presence of a Rhodamine B solution and dialysed against water to remove the organic solvent and the non encapsulated dye. The Rhodamine B dialysed solution was analysed by fluorescence measurements to determine the quantity of dye molecules in the solution and consequently, the number of molecules encapsulated in the vesicles. It was found that in these conditions, vesicles were able to trap around 20 molecules of dye per LDBC molecule.

The evolution of the Rhodamine B release upon irradiation was investigated by confocal microscopy. Before irradiation, the green fluorescence due to the fluorescent dye is concentrated in some specific regions dispersed in a

nonfluorescent background due to the encapsulation of the dye in the polymeric vesicles (**Figure 4.15**). Once irradiated, the fluorescence of the polymeric dispersion was again measured by confocal microscopy. The appearance of a fluorescent background after irradiation was associated to the release of Rhodamine B.

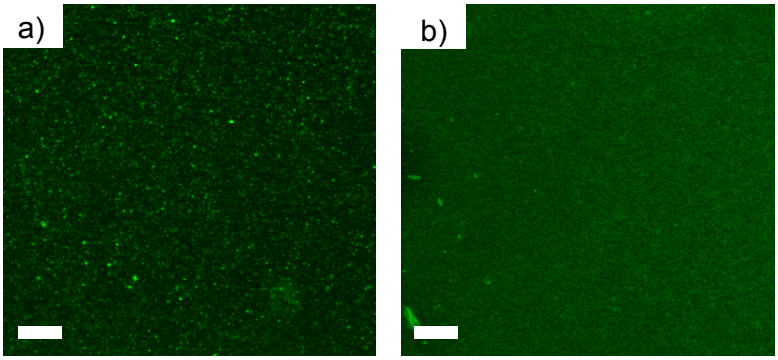

Figure 4.15 *Fluorescence microscopy images of the water suspension of loaded* ***PEG-b-d(isoAZOb/C18)-50/50*** *vesicles before a) and after b) irradiation for 5 min (350-400 nm, 9W) The length of the scale bar corresponds to 5 µm*

In an attempt to monitor the released dye *versus* the irradiation time, the intensity of the background fluorescence in the confocal images was measured after irradiating during different times. Values of fluorescence intensity were obtained averaging 200-250 randomly selected points of the background on the irradiated samples and comparing them with the corresponding value for non-irradiated samples. **Figure 4.16** shows the evolution of fluorescence intensity of the aqueous solution at different irradiation times.

The recorded data for **PEG-*b*-d(isoAZOb/C18)-25/75** revealed that almost not dye was released (fluorescence intensity is almost constant), which is in accordance with previous described results where no morphological change was detected by Cryo-TEM in the irradiated vesicles of this LDBC. Consequently, it could be concluded that for a high content of hydrocarbon chains, the membrane vesicles were not altered enough to allow the permeation and release of the encapsulated hydrophilic molecules despite isomerising the azobenzene moieties. However, for **PEG-*b*-d(isoAZOb/C18)-75/25** and **PEG-*b*-d(isoAZOb/C18)-50/50** vesicles, the intensity of the background fluorescence

increases on increasing the irradiation time. While a gradual increase of the emission intensity over irradiation time was observed for **PEG-*b*-d(isoAZOb/C18)-75/25** vesicles, a faster increase was found for **PEG-*b*-d(isoAZOb/C18)-50/50**. Data collected for **PEG-*b*-d(isoAZOb/C18)-75/25** show that Rhodamine B is gradually liberated upon irradiation and after 24 h in the dark leaking of the uploaded dye still persist. However, a complete release was achieved by irradiation during 2 minutes in the case of vesicles derived from **PEG-*b*-d(isoAZOb/C18)-50/50** which agrees with the vesicle collapsed observed by cryo-TEM.

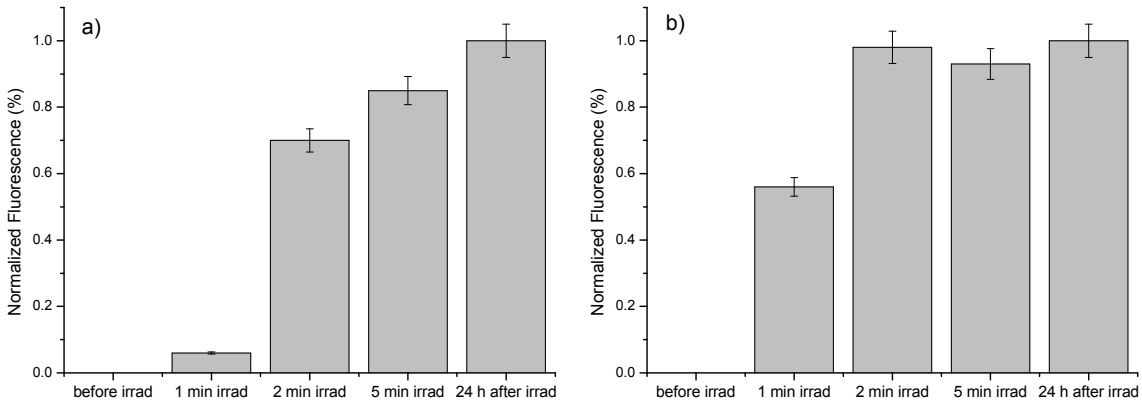

Figure 4.16 *Evolution of fluorescence intensity of the aqueous solution of Rhodamine B encapsulated vesicles of a)* ***PEG-b-d(isoAZOb/C18)-75/25*** *and b)* ***PEG-b-d(isoAZOb/C18)-50/50*** *at different irradiation times. The fluorescence value after 24 h of irradiation was considered as reference for normalisation*

4.3 Conclusions

Light responsive vesicles have been prepared from LDBCs with a PEG of 2000 g/mol average molecular weight and new codendrons containing different percentages of 4-isobutyloxyazobenzene and hydrocarbon chains randomly distributed at the periphery. It has been shown that dilution of azobenzene content using alkyl chains accelerates the *trans*-to-*cis* photoisomerisation process at the inner membrane probably by frustrating the aggregation tendency of the azobenzenes and providing higher mobility.

PEG-*b*-d(isoAZOb/C18)-75/25 vesicles show similar photoresponse to previously reported vesicles containing only azobenzene moieties linked to the periphery. UV irradiation induces an evident deformation in the membrane and consequently an increase on its permeability. In this case, the release of the internal cargo molecule is constant and progressive. Nevertheless, the release is improved with respect to the LDBC with only azobenzene moieties as demonstrated with of hydrophobic Nile Red molecules retained at the membrane.

For **PEG-*b*-d(isoAZOb/C18)-50/50** vesicles, *trans*-to-*cis* photoisomerisation causes important changes in the stability of the vesicles. Upon UV irradiation, large damages on the membrane of the vesicles are observed by cryo-TEM achieving fast release of the encapsulated probes.

When AZO content is diluted down to 25% in **PEG-*b*-d(isoAZOb/C18)-25/75**, the vesicles do not suffer any modification upon irradiation. The absence of significant changes in the irradiated samples could be due to the fact that the morphological change accompanied by the polarity change due to azobenzene isomerisation was not enough to provoke a deformation in the polymeric membrane and the subsequent release of the fluorescence probes.

Therefore, the dendritic block of LDBCs has been used as a suitable platform to incorporate chemical changes and alter the properties of inner part of the vesicle membrane. By adjusting AZO/C18, the photoresponsive properties of the vesicles and consequently the release rate can be tailored.

4.4 Experimental Section

Materials

Alkyne-functionalised **PEG**, the fourth-generation polyester dendron (**d16OH**) and 6-[4-(4'-isobutyloxyphenylazo)phenyloxy]hexanoic acid (**isoAZOb**) were prepared according to procedures previously described in Chapers 2 and 3. All other reagents were purchased from Sigma-Aldrich and used as received without further purification.

4.4.1 Synthesis and Characterisation of the Codendrons

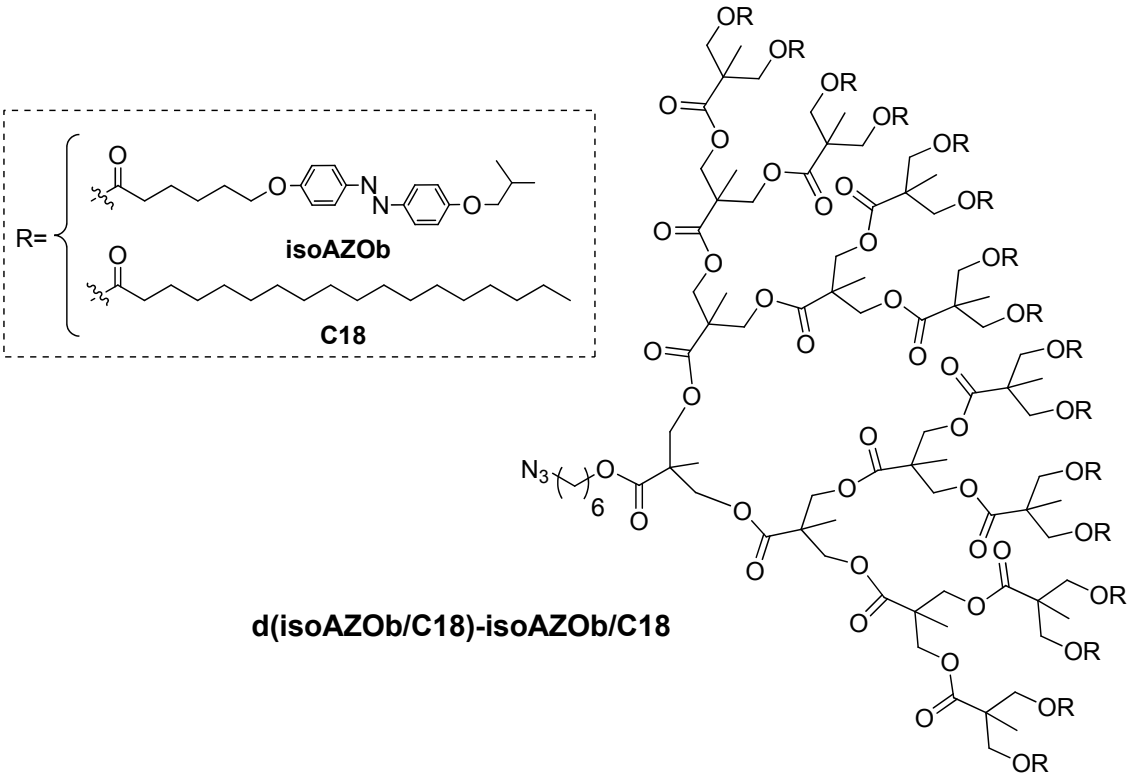

General procedure

d16OH (n mmol), 6-[4-(4'-isobutyloxyphenylazo)phenyloxy]hexanoic acid (**isoAZOb**) and stearic acid (**C18**) (1.2 x 16 n mmol) in the desired molar ratio (3:1, 1:1 or 1:3) and DPTS (16 n mmol) were dissolved in a mixture of DCM and DMF 5:1 (around 20 mL per 200 mg of **d16OH**) The reaction flask was flushed with argon, and DCC (1.32 x 16 n mmol) was added. The mixture was stirred at room temperature for 48 h under argon atmosphere. The white precipitate

formed was filtered off, and the solvent evaporated. The crude product was purified by liquid chromatography on silica gel and eluted with DCM, gradually increasing the polarity to 1:10 ethyl acetate:DCM. Azodendrons were obtained as an orange powder. Yield: 65-70 %.

Characterisation Data for d(isoAZOb/C18)-75/25: IR (KBr), ν (cm^{-1}): 2096, 1740, 1601, 1582, 1499, 1243, 1149, 844. ^{1}H-NMR (400 MHz, $CDCl_3$) δ (ppm): 7.8-7.80 (m), 6.96-6.90 (m), 4.3-4. (m) 3.93 (t, J=6.3 Hz), 3.74 (d, J=6,5 Hz), 3.25 (t, J=6.8 Hz), 2.33 (t, J=7.5 Hz), 2.27 (t, J=7.4 Hz), 2.15-2.04 (m) 1.84-1.73 (m), 1.70-1.59 (m), 1.52-1.41 (m), 1.40-1.13 (m), 1.03 (d, J= 6,8 Hz), 0.87 (t, J= 6,6 Hz). ^{13}C-NMR (100 MHz, $CDCl_3$) δ (ppm): 173.3, 172.8, 161.2, 161.0, 146.9, 146.8, 124.3, 114.6, 74.6, 67.9, 46.4, 33.8, 31.9, 29.8, 29.7, 29.6, 29.4, 28.9, 28.3, 25.6, 24.9, 24.6, 22.7, 19.2, 17.8, 14.1. Anal. Calc: C, 68.15 %; H, 7.98 %; N, 5.15 %. Found: C, 68.12 %; H, 8.24 %; N, 8.42 %.

Characterisation Data for d(isoAZOb/C18)-50/50: IR (KBr), ν (cm^{-1}): 2097, 1742, 1601, 1582, 1501, 1247, 1147, 840. ^{1}H-NMR (400 MHz, $CDCl_3$) δ (ppm): 7.85-7.82 (m), 6.98-6.91 (m), 4.34-4.06 (m) 3.96 (t, *J*=6.3 Hz), 3.77 (d, *J*=6,5 Hz), 3.25 (t, J=6.8 Hz), 2.34 (t, *J*=7.5 Hz), 2.27 (t, *J*=7.4 Hz), 2.16-2.06 (m) 1.84-1.73 (m), 1.72-1.62 (m), 1.60-1.42 (m), 1.40-1.13 (m), 1.03 (d, *J*= 6,8 Hz,), 0.86 (t, *J*= 6,6 Hz).^{13}C-NMR (100 MHz, $CDCl_3$) δ (ppm): 173.1, 172.8, 161.3, 161.0, 146.9, 146.8, 124.3, 114.6, 114.6, 74.6, 67.9, 64.8, 46.6, 46.3, 34.0, 33.8, 31.9, 29.7, 29.7, 29.6, 29.6, 29.4, 29.2, 28.9, 28.3, 25.6, 24.9, 24.6, 22.7, 19.2, 17.8, 17.5, 14.1. Anal. Calc: C, 69.32 %; H, 8.89 %; N, 3.83 %. Found: C, 69.62 %; H, 9.11 %; N, 3.99 %.

Characterisation Data for d(isoAZOb/C18)-25/75: IR (KBr), ν (cm^{-1}): 2096, 1742, 1601, 1582, 1500, 1247, 1148, 841. ^{1}H-NMR (400 MHz,$CDCl_3$) δ (ppm): 7.83-7.80 (m), 6.96-6.90 (m), 4.36-4.06 (m) 3.93 (t, *J*=6.3 Hz), 3.74 (d, *J*=6,5 Hz), 3.25 (t, *J*=6.8 Hz), 2.33 (t, *J*=7.5 Hz), 2.27 (t, *J*=7.4 Hz), 2.15.2.03 (m) 1.83-1.72 (m), 1.72-1.57 (m), 1.55-1.40 (m), 1.38-1.10 (m), 1.03 (d), 0.87 (t, J= 6,6 Hz). ^{13}C-NMR (100 MHz, $CDCl_3$) δ (ppm): 173.0, 172.7, 161.3, 161.0, 146.9, 146.9, 124.2, 114.6, 74.6, 67.9, 64.9, 46.7, 46.5, 34.0, 33.8, 31.7, 29.7, 29.6, 29.5, 29.4, 29.2, 29.0, 28.3, 25.5, 24.9, 24.6, 22.8, 19.2, 17.8, 17.6, 14.2. Anal.

Calc: C, 70.62 %; H, 9.93 %; N, 2.35 %. Found: C, 70.83 %; H, 9.87 %; N, 2.50 %.

4.4.2 Synthesis and Characterisation of the LDBCs

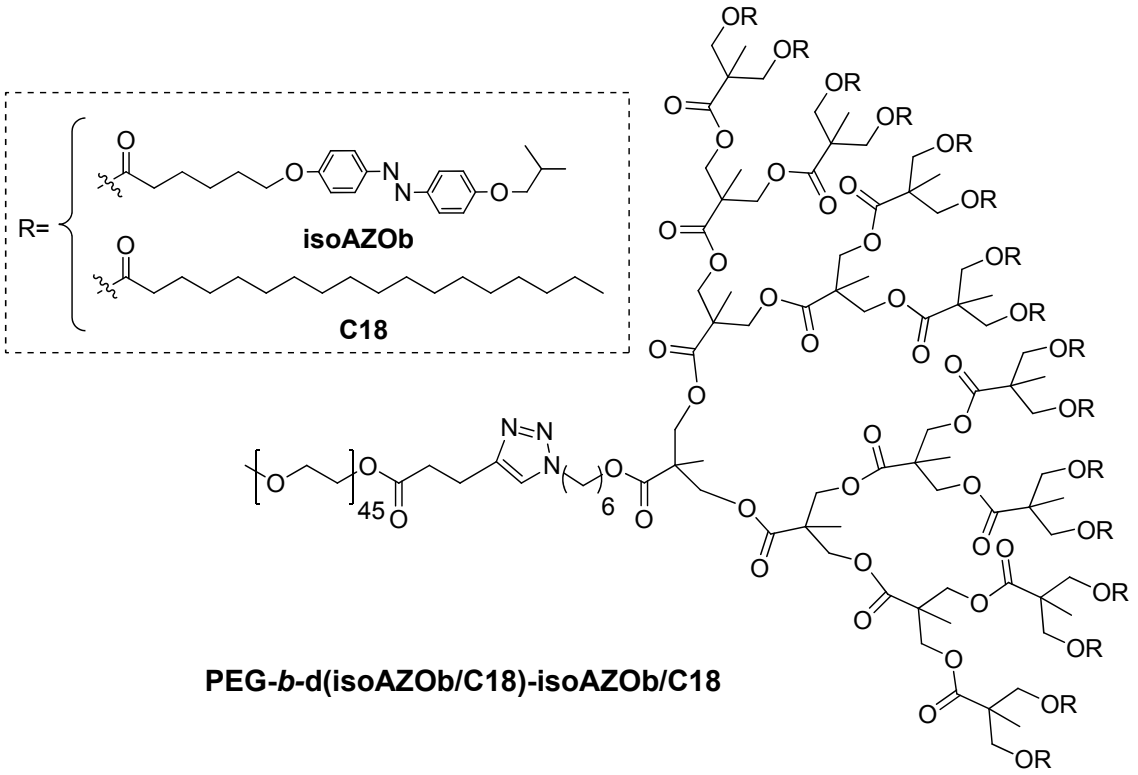

PEG-*b*-d(isoAZOb/C18)-isoAZOb/C18

General Procedure

The codendron (**d(isoAZOb/C18)-75/25, d(isoAZOb/C18)-50/50** or **d(isoAZOb/C18)-25/75**), 1.2-fold excess of alkyne-functionalised PEG and two-fold excess of CuBr were placed into a Schlenk tube. Two-fold excess of PMDETA and deoxygenated DMF (around 1 mL per 100 mg of polymer) were added with an argon-purged syringe, and the flask was further degassed by three freeze-pump-thaw cycles and flushed with argon. The reaction mixture was stirred at 40ºC for 72 h. The reaction mixture was stirred under an argon atmosphere at room temperature for 72 h. The mixture was diluted with THF and then passed through a short column of alumina. The solvent was partially evaporated and the resulting polymer solution was carefully precipitated into cold ethanol. Yield: 80-85%.

Characterisation Data for PEG-*b*-d(isoAZOb/C18)-75/25: IR (KBr), ν (cm^{-1}): 1737, 1601, 1581, 1500, 1246, 1148, 841. ^{1}H-NMR (400 MHz, $CDCl_3$) δ (ppm): 7.84-7.80 (m), 6.98-6.90 (m), 4.30-4.16 (m), 4.01-3.90 (m), 3.79-3.72 (m), 3.71-3.55 (m), 3.38 (s), 3.02-2.95 (m), 2.76-2.70 (m), 2.33 (t, *J*=7.5 Hz), 2.27 (m), 2.15-2.04 (m) 1.83-1.71 (m), 1.70-1.55 (m), 1.5.-1.39 (m), 1.36-1.13 (m), 1.03 (d, *J*= 6,8 Hz), 0.86 (t, *J*= 6,6 Hz). Anal. Calc: C, 65.32 %; H, 8.16 %; N, 4.02 %. Found: C, 65.03 %; H, 8.53 %; N, 4.25%.

Characterisation Data for PEG-*b*-d(isoAZOb/C18)-50/50: IR (KBr), ν (cm^{-1}): 1739, 1601, 1582, 1501, 1247, 1147, 841. ^{1}H-NMR (400 MHz, $CDCl_3$) δ (ppm): 7.83-7.80 (m), 6.98-6.92 (m), 4.30-4.10 (m), 4.02-3.92 (m), 3.80-3.73 (m), 3.71-3.54 (m), 3.38 (s), 3.01-2.97 (m), 2.75-2.69 (m), 2.33 (t, *J*=7.5 Hz), 2.27 (t, *J*=7.4 Hz), 2.14-2.03 (m) 1.86-1.73 (m), 1.72-1.61 (m), 1.60-1.42 (m), 1.40-1.10 (m), 1.03 (d, *J*= 6,8 Hz), 0.85 (t, *J*= 6,6 Hz). Anal. Calc: C, 66.05 %; H, 8.92 %; N, 2.96 %. Found: C, 65.80 %; H, 8.53 %; N, 2.58%.

Characterisation Data for PEG-*b*-d(isoAZOb/C18)-25/75: IR (KBr), ν (cm^{-1}): 1739, 1600, 1581, 1500, 1246, 1147, 842. ^{1}H-NMR (400 MHz, $CDCl_3$) δ (ppm): 7.84-7.80 (m), 6.98-6.90 (m), 4.30-4.12 (m), 4.04-3.96 (m), 3.80-3.73 (m), 3.72-3.55 (m), 3.38 (s), 3.02-2.97 (m), 2.74-2.70 (m), 2.33 (t, *J*=7.5 Hz), 2.27 (t, *J*=7.4 Hz), 2.12-2.02 (m) 1.86-1.72 (m), 1.70-1.61 (m), 1.60-1.42 (m), 1.40-1.13 (m), 1.04 (d, *J*= 6,8 Hz), 0.87 (t, *J*= 6,6 Hz). Anal. Calc: C, 66.94 %; H, 9.65 %; N, 1.79 %. Found: C, 66.50 %; H, 9.59 %; N, 2.08%.

4.4.3 General Procedures

Self-assemblies formation, determination of the critical aggregation concentration (CAC), encapsulation of the fluorescence probes as well as the sample preparation for the different microscopies techniques have been performed following the same procedures described in Chapter 3.

Irradiation Experiments

The water dispersions of self-assemblies were irradiated during with a compact mercury low-pressure fluorescent lamp Philips PL-S 9W emitting UV irradiation between 350 and 400 nm. The samples were placed at a distance of 10 cm from the light source in quartz cuvettes at room temperature. After irradiation, the water suspensions were kept in the dark.

References

1 Meng, F. H.; Zhong, Z. Y.; Feijen, J. Stimuli-Responsive Polymersomes for Programmed Drug Delivery. *Biomacromolecules* **2009**, 10 , 197-209.

2 Discher, D. E.; Eisenberg, A. Polymer vesicles. *Science* **2002**, 297, 967-973.

3 Discher, D. E. *et al.* Emerging applications of polymersomes in delivery: From molecular dynamics to shrinkage of tumors. *Progress in Polymer Science* **2007**, 32, 838-857.

4 Gohy, J.-F.; Zhao, Y. Photo-responsive block copolymer micelles: design and behavior. *Chemical Society Reviews* **2013**. DOI: 10.1039/C3CS35469E

5 Gil, E. S.; Hudson, S. M. Stimuli-reponsive polymers and their bioconjugates. *Progress in Polymer Science* **2004**, 29, 1173-1222.

6 Stuart, M. A.; Huck, W. T.; Genzer, J.; Müller, M.; Ober, C.; Stamm, M.; Sukhorukov G. B.; Szleifer, I.; Tsukruk, V. V.; Urban, M.; Winnik, F.; Zauscher, S.; Luzinov, I.; Minko, S. Emerging applications of stimuli-responsive polymer materials. *Nature Materials* **2010**, 9, 101-113.

7 Pasparakis, G.;Vamvakaki, M. Multiresponsive polymers: nano-sized assemblies, stimuli-sensitive gels and smart surfaces. *Polymer Chemistry* **2011**, 2, 1234-1248.

8 Schumers, J.-M.; Fustin, C.-A.; Gohy, J.-F. Light-Responsive Block Copolymers. *Macromolecular Rapid Communications* **2010**, 31, 1588-1607.

9 Li, M.-H.; Keller, P. Stimuli-responsive polymer vesicles. *Soft Matter* **2009**, 5, 927-937.

10 Roy, D.; Cambre, J. N.; Sumerlin, B. S. Future perspectives and recent advances in stimuli-responsive materials. *Progress in Polymer Science* **2010**, 35, 278-301.

11 Tanner, P.; Baumann, P.; Enea, R.; Onaca, O.; Palivan, C.; Meier, W. Polymeric Vesicles: From Drug Carriers to Nanoreactors and Artificial Organelles. *Accounts of Chemical Research* **2011**, 44, 1039-1049.

12 Antonietti, M.; Förster, S. Vesicles and Liposomes: A Self-Assembly Principle Beyond Lipids. *Advanced Materials* **2003**, 15, 1323-1333.

13 Li, M. H.; Keller, P. Stimuli-responsive polymer vesicles. *Soft Matter* **2009**, 5, 927-937.

14 del Barrio, J.; Oriol, L.; Sánchez, C.; Serrano, J.L.; Di Cicco, A.; Keller, P.; Li, M.H. Self-Assembly of Linear-Dendritic Diblock Copolymers: From Nanofibers to Polymersomes. *Journal of the American Chemical Society* **2010**, 132, 3762-3769.

15 Tsarevsky, N. V.; Bencherif, S. A.; Matyjaszewski, K. Graft Copolymers by a Combination of ATRP and Two Different Consecutive Click Reactions. *Macromolecules* **2007**, 40, 4439-4445.

16 Peng, S.-M.; Chen, Y.; Hua, C.; Dong, C.-M. Dendron-like Polypeptide/Linear Poly(ethylene oxide) Biohybrids with Both Asymmetrical and Symmetrical Topologies Synthesized via the Combination of Click Chemistry and Ring-Opening Polymerization. *Macromolecules* **2008**, 42, 104-113.

17 Malmström, E.; Johansson, M.; Hult, A. The effect of terminal alkyl chains on hyperbranched polyesters based on 2,2-bis(hydroxymethyl)propionic acid. *Macromolecular Chemistry and Physics* **1996**, 197, 3199-3207.

18 Lavasanifar, A.; Samuel, J.; Kwon, G. S. Poly(ethylene oxide)-block-poly(l-amino acid) micelles for drug delivery. *Advanced Drug Delivery Reviews* **2002**, 54, 169-190.

CHAPTER 5

Miktoarm Star Polymers as an Alternative to Amphiphilic Block Copolymers

5.1 Introduction and Aims

The last decades have seen remarkable advances in the ability to prepare new polymeric architectures with improved control over molecular attributes to address the challenge of tailor made materials. Some authors proposed the term Macromolecular Engineering to refer to this challenge with high impact in the applications of the macromolecules.[1,2] Since structure and function are intimately related, subtle manipulation of functional groups and chain architecture might end in new materials with dramatically different properties. Indeed, synthetic tools are available to facilitate the access to macromolecules with precisely controlled architectures in terms of narrow molecular weight distribution, well defined branching, well defined monomer sequences or functionality. In this context, the primary goal on combining controlled radical polymerizations and highly efficient ligation techniques is to arrive at the required structure by the simplest, cleanest and most efficient approach possible.[3-6]

Star polymers are the simplest branched polymers consisting of several linear chains emanating from a central core. From star architectures, the relatively new miktoarm star polymers, also known as miktoarm polymers, are structures containing two or more arms with different chemical compositions and/or molecular weights.[7-10] The most common type of miktoarm stars are A_2B, A_3B, A_2B_2 and ABC types, where A, B and C are chemically different chains.[11] Miktoarm polymers are a challenge from a synthetic point of view but many reliable synthetic protocols have emerged that encouraged to pursue studies of their self-assembly and applications. The interest in miktoarm star polymers comes from the combination of virtually any type and number of polymer arms, including functional moieties, into a single unique architecture. In particular, amphiphilic miktoarm polymers containing both hydrophobic and hydrophilic arms, are expected to create nanostructures in water similarly to amphiphilic BCs.

As noted in the Chapter 1, only a few examples of azobenzene miktoarm polymers have been reported so far (see section 1.2.3.3). He and coworkers described a novel liquid crystalline miktoarm polymer, [PEG-PS-$(PMMAZO)_2$],

composed of poly(ethylene glycol) (PEG), poly(styrene) (PS) and an azobenzene side chain poly(methacrylate) (PMMAZO).[12,13] These polymers self-assembled into simple or large vesicles, which showed a shape deformation with an elongation along the polarised direction upon irradiation with LPL. Recently, the same authors have also reported similar photoresponsive ABC miktoarm terpolymers – (PEG)(PS)(PMMAZO) – composed of PEG, PS and an azobenzene side chain poly(methacrylate) (PMMAZO).[14] These terpolymers self-assembled into bowl shaped and multibowl shaped structures showing a photoinduced isomerisation behaviour influenced by different aggregation processes.

The current chapter presents the synthesis, self-assembly in water and photoresponsive behaviour of a novel amphiphilic miktoarm star polymer **$PAZO_{17}$-$(PEG_{12})_3$** of AB_3 type. The miktoarm polymer is composed of an azobenzene side chain poly(methacrylate) (**$PAZO_{17}$**) as the photoresponsive arm and three PEG arms of the same length (**Scheme 5.1**). By taking as a basis the results presented in previous chapters, 4-isobutyloxyazobenzene was used as the photoresponsive unit and a miktoarm having an approx. 80/20 hydrophobic/hydrophilic balance ratio was prepared seeking the formation of vesicular self-assemblies in water. The target degree of polymerization (DP) of **PAZO** was around 16, i.e similar to the azobenzene units incorporated in the previous fourth generation dendron described in chapter 3. Thus, in order to obtain the desired hydrophobic/hydrophilic ratio, three PEG arms of M_n=650 g/mol (DP=12) were employed. Once established the structural design of the macromolecule the synthesis was envisaged by a combination of controlled radical polymerization and ‘click chemistry’.

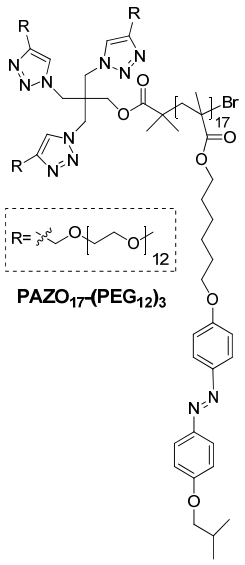

Figure 5.1 *Chemical structure of the investigated miktoarm star polymer*

5.2 Tasks and Methods

- Synthesis of a PEG star polymer macroinitiator containing an ATRP initiation site by coupling the preformed arms to a tetrafunctional core (**Figure 5.2**).

- Synthesis the proposed miktoarm star polymer by ATRP polymerization of an azomonomer using the PEG star macroinitiator (**Figure 5.2**).

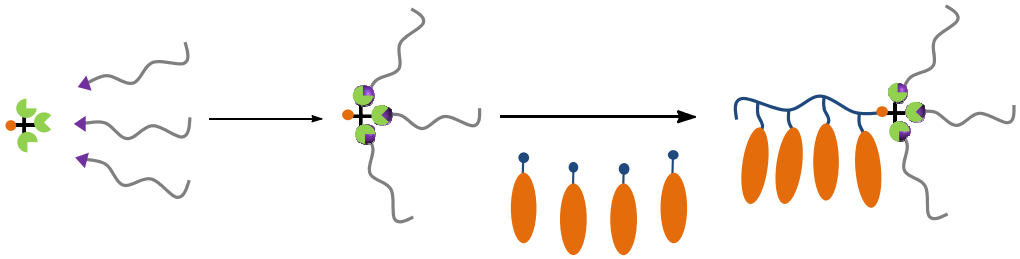

Figure 5.2 *Synthetic approach for the synthesis of the miktoarm star polymer*

- Structural characterisation of the miktoarm polymer and precursors by FTIR, NMR, MS. Thermal characterisation by using POM, TGA and DSC.

- Study of the self-assembly of the miktoarm polymer in water.

- Morphological study of the self-assemblies in water by TEM and cryo-TEM.

- Investigatio of the photoresponsive behaviour of the self-assemblies in water and studies of encapsulation and photoinduced release.

5.3 Results and Discussion

5.3.1 Synthesis and Characterisation of the Amphiphilic Miktoarm Star Polymer

The macromolecular structure of the target miktoarm star copolymer was prepared by a combination of CuAAC and CRP. Although several routes are possible, depending of the sequence of both types of reaction, we followed the three steps strategy collected in **Scheme 5.1**. As starting compound, a tetrafunctional core having three azide and a hydroxyl groups was used. Three end functionalised PEG arms were first coupled by CuAAC to the core and the remaining functional group was used for a subsequent polymerization reaction to grow the azobenzene containing arm by ATRP, eventually yielding the final miktoarm polymer.

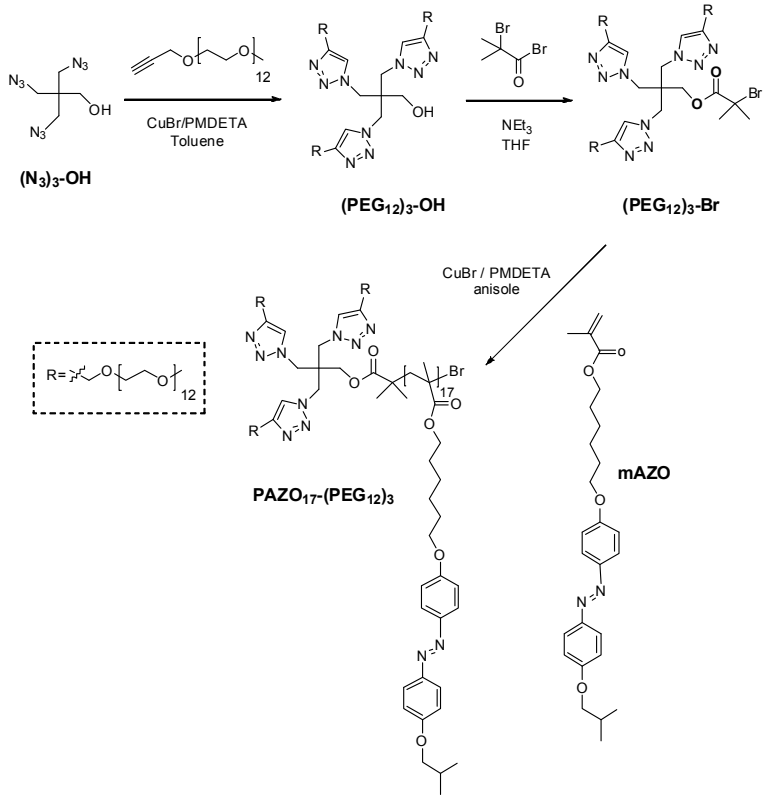

Scheme 5.1 *Synthesis of the PEG containing miktoarm polymer*

The tetrafunctional 2,2,2-tris(azidomethyl)ethanol core, **$(N_3)_3$-OH**, was prepared by substitution of the bromine groups of 2,2,2-tris(bromomethyl)ethanol by azide groups using a methodology previously reported.[15] Due to the high N/C ratio of this compound, it should be handled carefully (see Experimental Section). On the other hand, commercial PEG having one hydroxyl group was first etherified with propargyl bromide to obtain an alkyne terminated PEG[16] of M_n=650 g/mol, as was adequately confirmed by MALDI mass spectrometry (**Figure 5.3a**). PEG arms were coupled to **$(N_3)_3$-OH** triazido core by a CuAAC reaction using CuBr/PMDETA as catalytic system. A slight excess of the alkyne ended linear block was employed that was removed by precipitation into cold diethyl ether. The efficiency of the 'click' coupling and structure of the star **$(PEG_{12})_3$-OH** polymer was corroborated by MALDI mass spectrometry and ^{1}H-NMR. In the latter case, comparison of the integration the protons signals corresponding to PEG –CH_2O at 3.75-3.50 ppm– and the signals corresponding to the core were employed. **$(PEG_{12})_3$-OH** was then modified by esterification of the hydroxyl group with α-bromoisobutyryl bromide to include an ATRP initiation site into the remaining functionality of the core yielding the macroinitiator **$(PEG_{12})_3$-Br**. Again, the efficiency of the reaction as well as the average molecular weight (**Table 5.1**) were asserted by MALDI (**Figure 5.3b**), SEC and ^{1}H-NMR (**Figure 5.4**). Relative integration of the methyl groups signals of PEG (labelled as '*a*') and the corresponding methyl groups of the α-bromoisobutyl moiety (labelled as '*g*') evidenced successful incorporation of the ATRP initiation site.

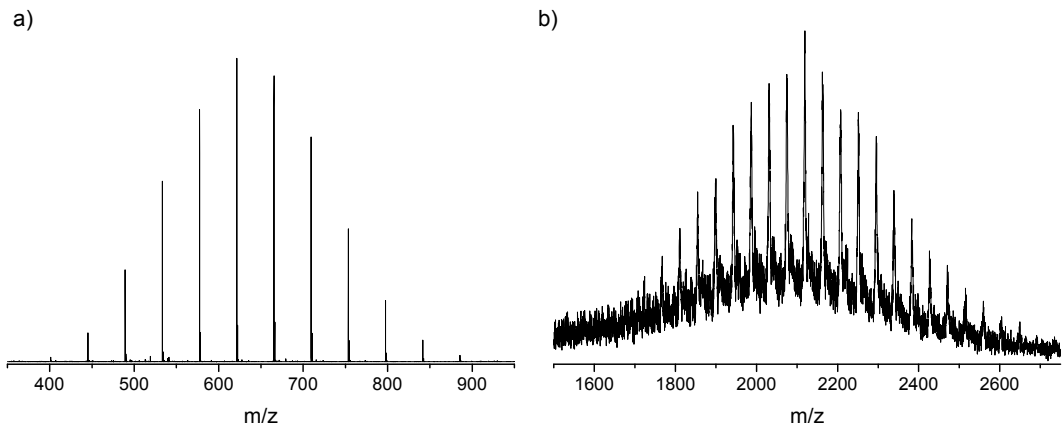

Figure 5.3 *MALDI-TOF mass spectra of a) alkyne functionalised PEG, b)* ***$(PEG_{12})_3$-Br***

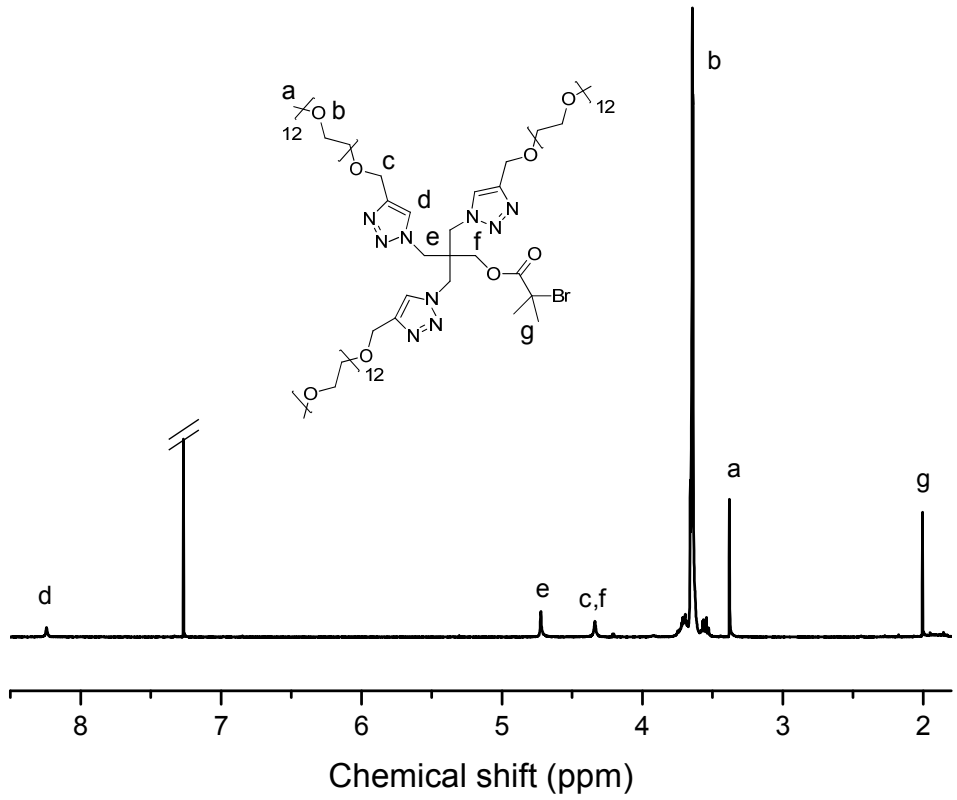

Figure 5.4 *^{1}H-NMR spectrum of* ***$(PEG_{12})_3$-Br*** *in $CDCl_3$ (250MHz)*

Table 5.1*. Molecular weight of the synthesised polymers*

Polymer	M_n [a]	M_n [b]	M_n [c]	$Đ_M$ [c]	Phobic/philic ratio[d]
$(PEG_{12})_3$-Br	2116	2154	2900	1.01	-
$PAZO_{17}$-$(PEG_{12})_3$	-	9608	9700	1.10	78/22

[a] M_n calculated by MALDI. [b] M_n calculated by ^{1}H-NMR (see text). [c] M_n and polydispersity ($Đ_M$) of the polymers were determined by SEC using PS standards. [d] Phobic/Philic ratio was calculated by considering PEG arms as the hydrophilic part and the rest as the hydrophobic part.

In the final step, the azobenzene methacrylate **mAZO** (details for the preparation of this monomer are given in the Experimental Section) was polymerised by ATRP from the **$(PEG_{12})_3$-Br** macroinitiator in anisole using CuBr/PMDETA as catalytic system at 80ºC. As this macroinitiator was not

employed before, the polymerization conditions were optimised in order to obtain an azopolymer with a polymerization degree around 16 (comparable with the previous described azobenzene functionalised dendrons). To study the kinetics, monomer conversion was determined *via* ^{1}H-NMR by relative integration of the vinyl protons, appearing at 6.10 and 5.55 ppm, and the aromatic protons corresponding to the azobenzene. Since monomer concentration at any time is given by

$[M] = [M]_0 - [M]_0 \text{ conversion} = [M]_0 (1- \text{conversion})$

$\ln([M]_0/[M])$ was calculated and plotted against the polymerization time. As it can be seen in **Figure 5.5a**, in the initial stages of the polymerization the corresponding relation was not initially linear indicating that the propagating radical concentration was non constant. However, a linear trend was found after 2 h. The average molecular weights measured by SEC increased linearly with monomer conversions, which is consistent with the polymerization proceeding in a controlled fashion (**Figure 5.5b**).

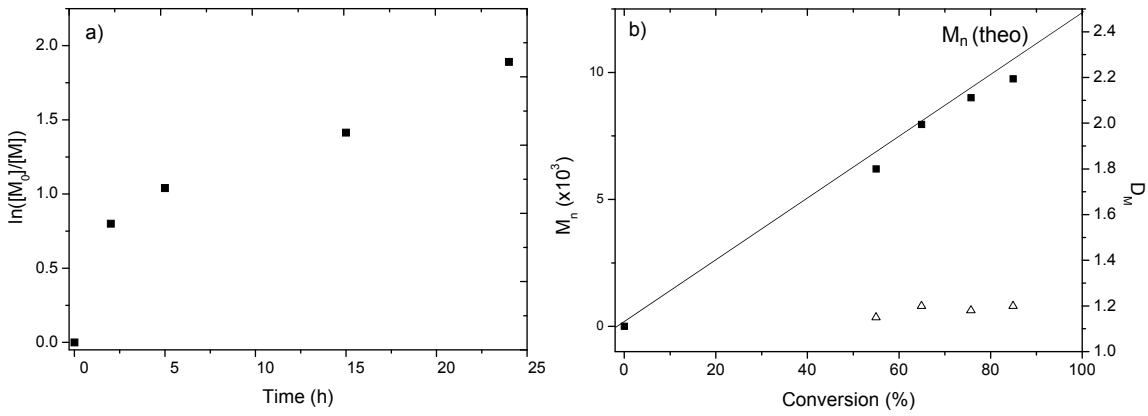

Figure 5.5 *a) Relationship of ln([M]$_0$/[M]) and monomer conversion with polymerization time and b) evolution of M_n and $Đ_M$ (SEC) with monomer conversion for the ATRP polymerization of* ***mAZO*** *in anisole at 80 ºC.*

Having evaluated the evolution of Mn vs conversion, time polymerization was set at 24 h. As noted before, the polymerization was performed in anisole using CuBr/PMDETA at 80ºC. ^{1}H-NMR spectroscopy was used to estimate the average number of azobenzene units per macromolecular chain (**Table 5.1**). The relative integration of the signal corresponding to the end groups –CH_3 of

the PEG arms at 3.37 ppm (labelled at '*a*' in **Figure 5.6**) and the signals corresponding to the aromatic protons of the repeating azobenzene unit gave 17 repeating units in average per polymer chain and consequently a molecular weight of 9608 g/mol. The molecular weight was also calculated by SEC using PS standards and it is good agreement with the value estimated by ^{1}H-NMR. **Figure 5.7** collects the SEC curves corresponding to the macroinitiator and the miktoarm polymer **PAZO$_{17}$-(PEG$_{12}$)$_3$**. As it can be observed, polymerization gives rise to a shift of the molecular weight distribution peak towards lower retention times where no residual macroinitiator was detected indicating that all the molecules contain the bromo group.

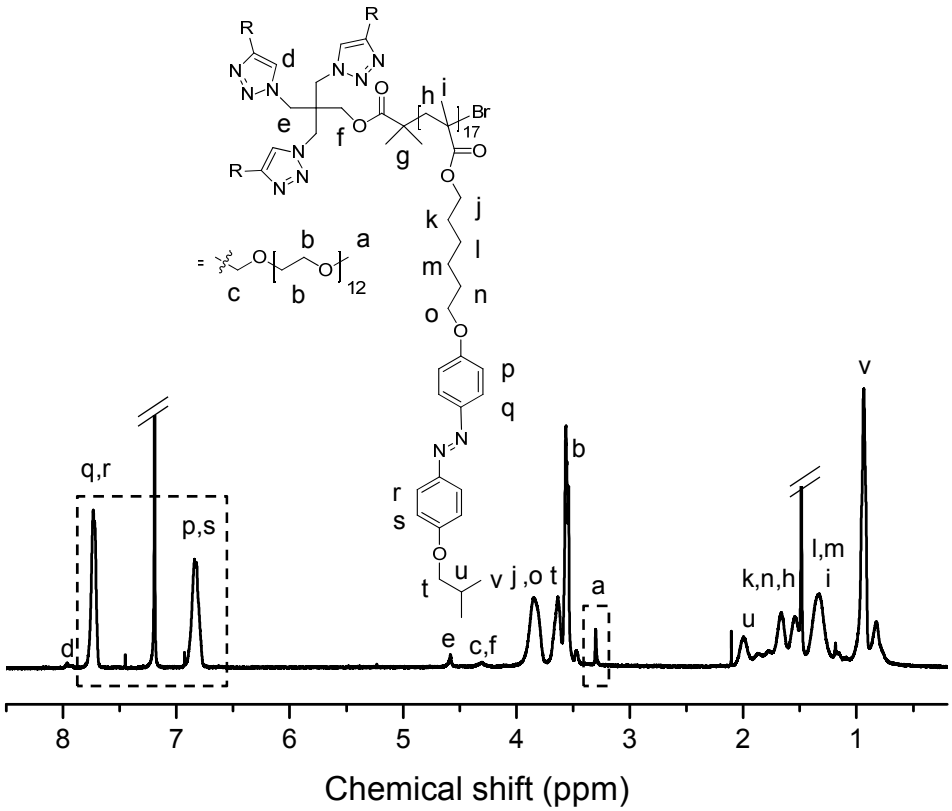

Figure 5.6 *^{1}H-NMR spectrum of* ***PAZO$_{17}$-(PEG$_{12}$)$_3$*** *in $CDCl_3$ (400MHz)*

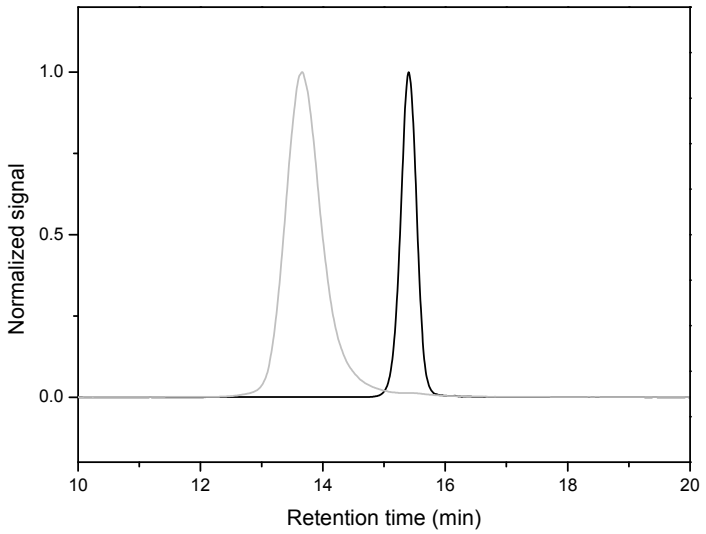

Figure 5.7 *SEC traces of the macroinitiator* ***(PEG$_{12}$)$_3$-Br*** *(black line) and the miktoarm polymer* ***PAZO$_{17}$-(PEG$_{12}$)$_3$*** *(grey line)*

The thermal stability was studied by TGA using a powdered sample. The miktoarm polymer exhibited a good thermal stability up to 300 ºC and no presence of volatile components (e.g. water, residual organic solvents, etc.) were detected (**Figure 5.8a**). The thermal transitions were studied by DSC and POM. By POM, a melting process was observed and no textures typical of mesomorphism were detected. DSC curve also revealed the crystalline character of the polymer (**Figure 5.8b**). The miktoarm polymer **PAZO$_{17}$-(PEG$_{12}$)$_3$** only presented a melting transition at around 110 ºC (10ºC/min) in the heating process and the subsequent crystallisation in the cooling scan at around 100ºC.

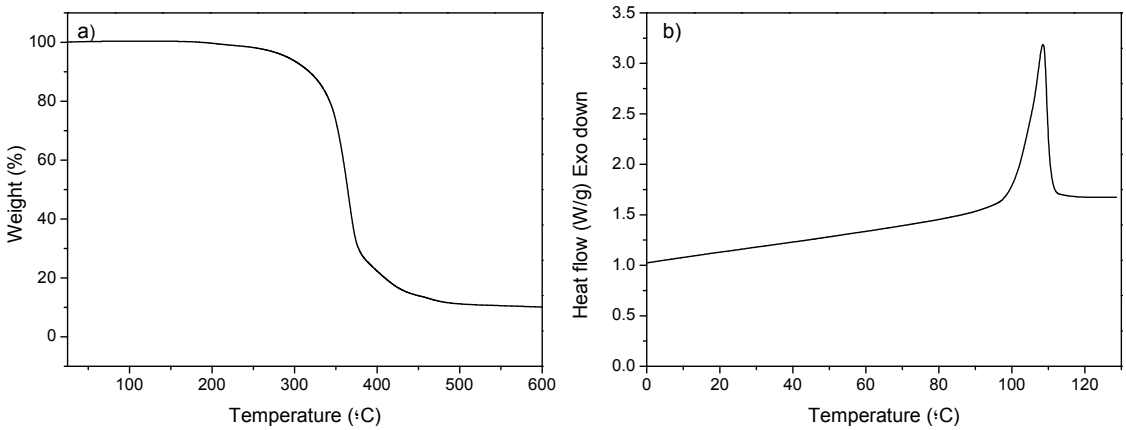

Figure 5.8 *a) TGA curve and b) DSC curve (10ºC/min) corresponding to the second heating of* ***PAZO$_{17}$-(PEG$_{12}$)$_3$*** *T_d: 315ºC, T_m: 108 ºC and ΔH_m: 155 kJ/mol*

5.3.2 Self-Assembly of the Miktoarm Polymer in Water

As was described in previous chapters, polymeric self-assemblies were prepared by adding water to a solution of the miktoarm polymer in THF and monitored by recording the turbidity (**Figure 5.9a**). Once the turbidity reached an almost constant value, the resulting dispersion was dialysed against water to remove the organic solvent. After dialysis, a stable dispersion was obtained, although precipitation of the sample was observed after storing for a few weeks.

CAC in water was determined using Nile Red following the procedure previously described in Chapter 3 and 4. The calculated CAC was about 40 µg/mL, which is similar to the value calculated for the LDBC of similar composition **PEG-*b*-d16AZOb** (35 µg/mL) described in Chapter 3 (**Figure 5.9b**).

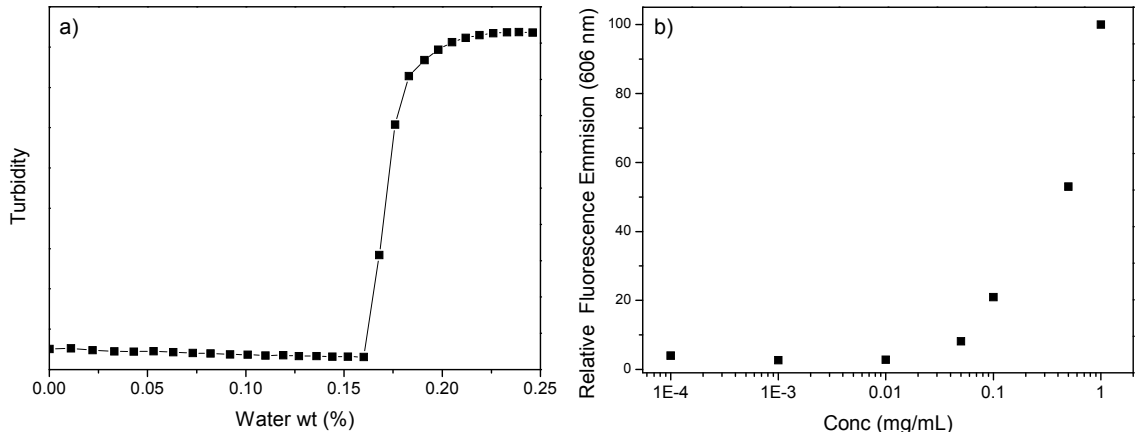

Figure 5.9 *a) Turbidity evolution of the miktoarm polymer THF solution as a function the amount of added water. b) Flurorescence intensity of Nile Red at 606 nm (λ_{exc} = 550 nm) versus miktoarm polymer concentration (mg/mL)*

The morphology of the **PAZO$_{17}$-(PEG$_{12}$)$_3$** self-assemblies was investigated by TEM on dried samples stained with uranyl acetate. It was found that the miktoarm polymer self-assembled into vesicles, which appear deflated because of sample drying (**Figure 5.10a**). Cryo-TEM images showed spherical vesicles with diameters ranging from 300 to 700 nm having a membrane thickness around 9 nm (**Figure 5.10b**). The size of the polymeric vesicles was additionally evaluated by DLS measurements providing a hydrodynamic diameter (D_h) of 640 nm, significantly larger than D_h values determined for LDBC vesicles ranging from 365 to 195 nm.

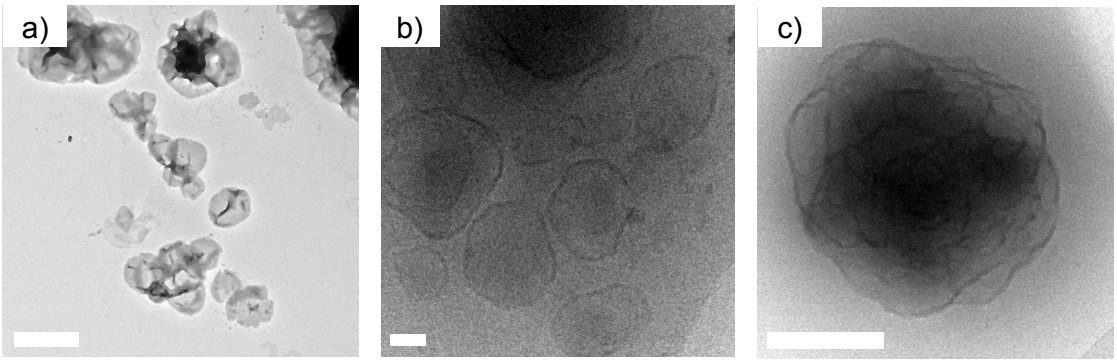

Figure 5.10 *TEM image of **PAZO$_{17}$-(PEG$_{12}$)$_3$** non irradiated vesicles. Cryo-TEM images of **PAZO$_{17}$-(PEG$_{12}$)$_3$** vesicles before b) and after c) irradiation for 5 min (350-400 nm, 9W). The length of the scale bar corresponds to 1 µm in a) and 200 nm in b) and c)*

5.3.3 Photoresponsive Behaviour of the Self-Assemblies

Initially, the UV-Vis spectra of both a miktoarm polymer isolution and the vesicles suspension in water where first recorded (**Figure 5.11a**). The spectrum in solution was characterised by two absorption bands corresponding to the *trans*-isomer, a strong one centred at 360 nm attributed to the π-π* transition and a weak one at about 450 nm corresponding to n-π* transition. The spectrum of the vesicles showed a broader π-π* transition due to aggregation of azobenzene moieties.

An aqueous suspension of **PAZO$_{17}$-(PEG$_{12}$)$_3$** vesicles of 1mg/mL concentration was irradiated with a mercury low pressure UV lamp (9W) emitting between 350 and 400 nm while recording the evolution of the UV-vis spectra (**Figure 5.11b**). During UV irradiation, a remarkable decrease on absorbance together with a hypsochromic shift of the π-π* transition took place accompanied by an increase of the absorbance at 450 nm corresponding to the n-π* transition. As noted in previous chapter, this change is attributed to the photoisomerisation of the *trans*-azobenzene to the *cis* isomer. After 5 min of irradiation, no further changes in the UV-vis spectra were detected indicating that a photostationary state was reached, similarly to **PEG-*b*-d(isoAZOb/C18)-75/25** vesicles described in the previous chapter. After 24 h in the dark, UV-vis spectra started to recover the initial shape due to thermal *cis*-to-*trans* back isomerisation.

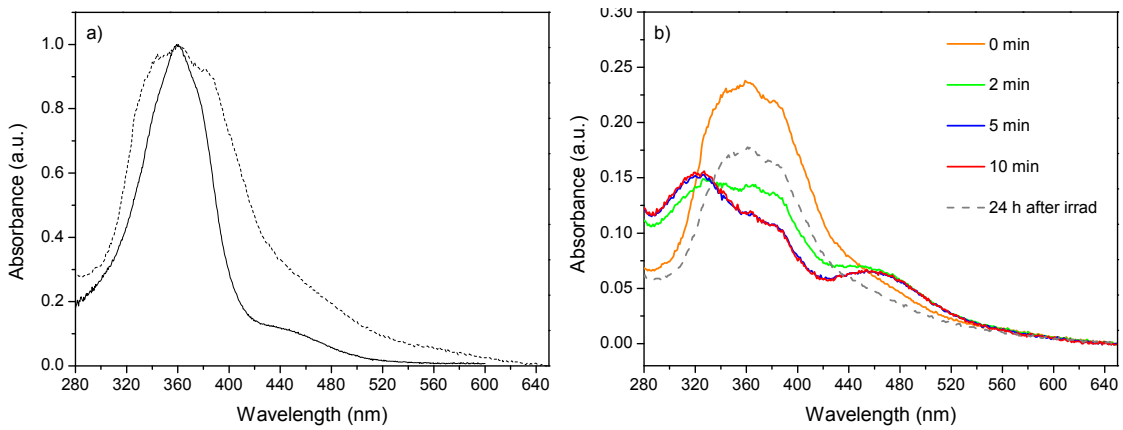

Figure 5.11 *a) UV-Vis spectra of* ***PEG-b-d16isoAZOb*** *in a 5x10^{-6} M solution in $CHCl_3$ (straight line) and a water suspension of* ***PAZO$_{17}$-(PEG$_{12}$)$_3$*** *vesicles (dashed line). b) UV-Vis spectra of* ***PAZO$_{17}$-(PEG$_{12}$)$_3$*** *irradiated vesicles (concentration of 1 mg/mL) for different times (350-400 nm, 9W)*

Cryo-TEM observation of the polymeric micelles in combination with DLS measurements were performed to gain information about morphological changes upon irradiation. The cryo-TEM image recorded after irradiation shows the presence of wrinkled vesicles (**Figure 5.10c**). Furthermore, a change of around 170 nm in the D_h was detected by DLS measurements (**Figure 5.12**) that reveal a D_h of 470 nm after irradiation. This change confirmed also the deformation of the vesicles upon irradiation. The D_h was evaluated after 24 h of irradiation and no evolution was found evidencing an irreversible morphological change.

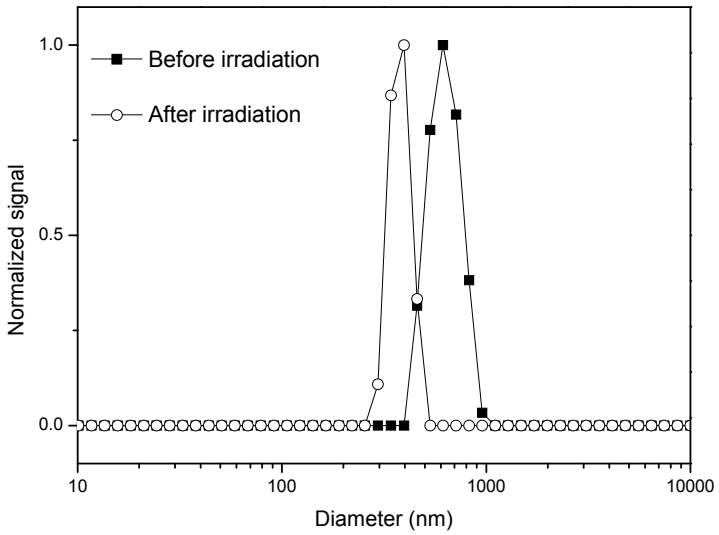

Figure 5.12 *DLS measurements of a water suspension of* ***PAZO$_{17}$-(PEG$_{12}$)$_3$*** *vesicles before and after UV light irradiation (5 min, 350-400 nm, 9W)*

5.3.4 Encapsulation and Photoinduced Release of Molecular Probes

Once corroborated that the vesicles of this polymer also exhibited photoresponse, encapsulation and release of fluorescent probes were also carried out. Firstly, Nile red was encapsulated in the vesicles and irradiated using the same conditions that in the previous experiments. Upon irradiation, a similar behaviour to LDBC **PEG-*b*-d16AZOb** described in Chapter 3 is observed as is collected in **Figure 4.13**. As mentioned, this decrease on the emission of the dye can be due to both Nile Red migration from the membrane

to the aqueous media and increase in the polarity of the inner membrane due to the change in net dipole moment associated to *trans*-to-*cis* isomerisation. After 24 h in the dark, Nile Red emission recovered the initial value indicating that the fluorescent probe is again in a hydrophobic environment and consequently, the fluorescent probe mainly remain encapsulated.

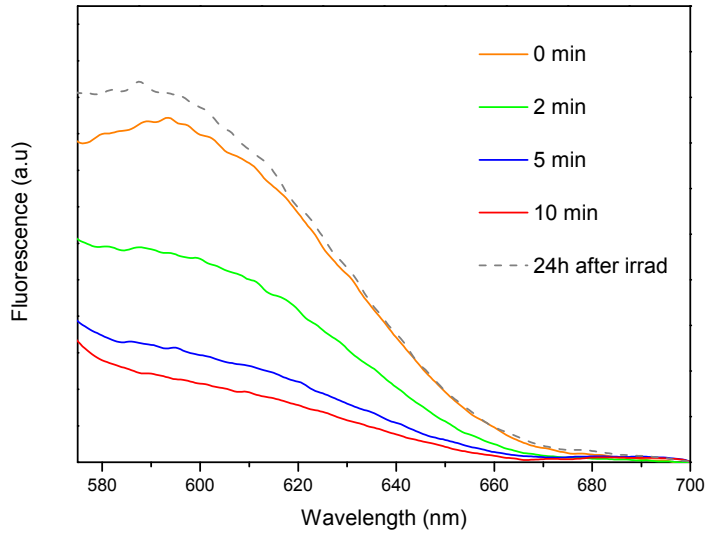

Figure 5.13 *Emission spectra of the Nile Red encapsulated micelles of* ***PAZO$_{17}$-(PDEAA$_{12}$)$_3$*** *(concentration of 1 mg/mL) recorded at different irradiation times*

Encapsulation and photoinduced release of Rhodamine B was also investigated using the same experimental procedure previously described. It was found that in these conditions, vesicles were able to trap around 45 molecules of dye per miktoarm polymer chain. This value is significantly higher than the previous obtained vesicles based on LDBC, of around 20 molecules of dye per LDBC molecule. These differences can be related with the different size of the vesicles and consequently with the available internal volume.

The evolution of the Rhodamine B release upon irradiation was investigated by confocal microscopy. **Figure 5.14a** display the fluorescence before irradiation with the dye concentrated in specific regions due to encapsulation. Upon irradiation, fluorescent dots were still visible by fluorescence microscopy but also a fluorescent background was observed due to Rhodamine B release from the interior of the vesicles to the aqueous media (**Figure 5.14b**). These

experiments proved once again that under UV illumination the vesicle membrane became permeable to the loaded fluorescent probe.

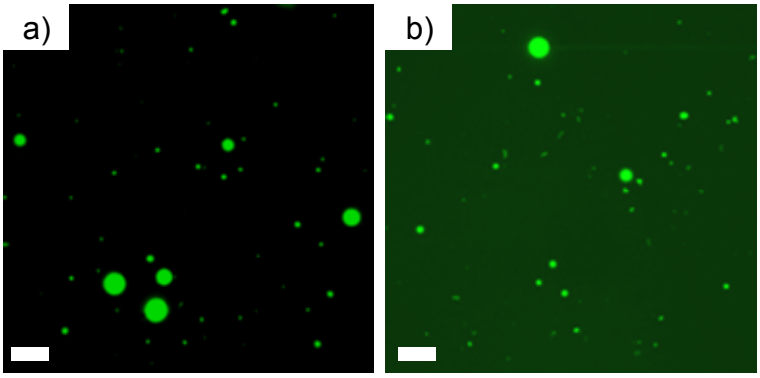

Figure 5.14 *Fluorescence microscopy images of the water suspension of loaded* ***PAZO$_{17}$-(PEG$_{12}$)$_3$*** *vesicles before a) and after b) irradiation for 5 min (350-400 nm, 9W). The length of the scale bar corresponds to 5 µm*

5.4 Conclusions

Combination of ATRP and CuAAC has been employed for the preparation of a novel miktoarm polymer **$PAZO_{17}$-$(PEG_{12})_3$**. Three alkyne functionalised PEG arms were first coupled by CuAAC to a tetrafunctional asymmetric core and subsequently used as macroinitiator for the polymerization of an azobenzene containing monomer. By fixing the length of the PEG arm and the reaction conditions, it was possible to adjust the phobic/philic ratio (78/22) of the final material.

As expected, the azobenzene containing miktoarm polymer synthesised was able to self-assemble into vesicles in water. Upon UV irradiation, deformed vesicles were observed by cryo-TEM evidencing a photoinduced morphological change. It has been demonstrated that these vesicles are able to load both hydrophobic and hydrophilic molecules. Upon UV irradiation, azobenzene isomerisation occurred and provoke the increase of the membrane permeability to loaded fluorescent probe.

5.5 Experimental Section

Materials

Experimental details for the synthesis of 4-isobutyloxy-4'-hydroxyazobenzene **(15)** are given in Chapter 3. CuBr was used as received and handle in a dry box. All other reagents were purchased from Sigma-Aldrich and used as received without further purification.

5.5.1 Experimental Details for the Synthesis of the Azomonomer (mAZO)

Synthesis and Characterisation of 6-[4-(4'-isobutyloxyphenylazo)-phenoxy]hexanol (17)

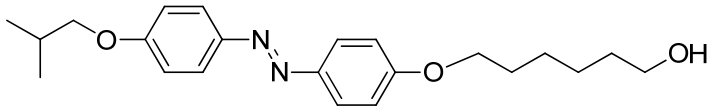

(17)

A solution of 4-isobutyloxy-4'-hydroxyazobenzene **(15)** (3.02 g, 11.10 mmol) and 6-chloro-1-hexanol (1.81 g, 13.30 mmol) in butanone (60 mL) was prepared. 18-Crown-6 (0.05 g) and potassium carbonate (3.15 g, 22.20 mol) were added. The suspension was stirred and heated under reflux for 24 h, then it was filtered and concentrated. The crude product was purified by flash column chromatography on silica gel using DCM as eluent. The product was obtained as a yellow powder. Yield: 60%. IR (KBr), ν (cm^{-1}): 3300, 1601, 1580, 1496, 1465, 1237, 844. ^{1}H-NMR ($CDCl_3$, 400MHz) δ (ppm): 7.87-7.85 (m, 4H), 6.94-6.92 (m, 4H), 4.03 (t, *J*=6.5 Hz, 2H), 3.80 (d, *J*=6.6 Hz, 2H), 3.65 (q, *J*=6.5 Hz, 2H), 2.12-2.03 (m, 1H), 1.88-1.75 (m, 2H), 1-67-1,56 (m, 2H), 1.37-1.21 (m, 4H), 1.05 (d, *J*= 6.7 Hz, 6H). ^{13}C-NMR ($CDCl_3$, 100 MHz) δ (ppm): 161.3, 146.9, 124.3, 114.7, 114.6, 74.7, 68.1, 62.9, 32.7, 29.2, 28.3, 25.9, 25.6, 19.3.

Synthesis and Characterisation of 6-[4-(4'-isobutyloxyphenylazo) phenoxy]hexyl methacrylate (mAZO)

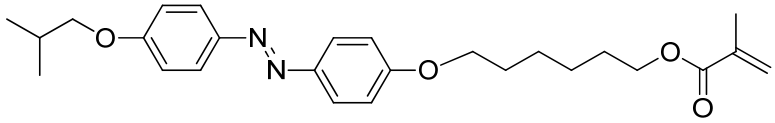

(mAZO)

A solution of 6-[4-(4'-isobutyloxyphenylazo)phenoxy]hexanol **(17)** (0.78 g, 2.20 mmol) and triethylamine (0.4 mL, 2.60 mmol) in dry THF (10 mL) was prepared. The solution was stirred and methacryloyl chloride (0.2 mL, 2.60 mmol) was added dropwise under argon atmosphere. The mixture was stirred and heated under reflux overnight. Then, it was filtered and concentrated. The crude product was purified by flash column chromatography on silica gel using DCM as eluent. The product was obtained as a yellow powder. Yield: 85%. IR (KBr), ν (cm^{-1}): 1702, 1637, 1602, 1580, 1500, 1470, 1240, 841. ^{1}H-NMR ($CDCl_3$, 400MHz) δ (ppm): 7.88-7.85 (m, 4H), 7.00-6.98 (m, 4H), 6.12-6.08 (m, 1H), 5.58-5.52 (m, 1H), 4.14 (t, *J*= 6.6 Hz, 2H), 4.04 (t, J= 6.4Hz, 2H), 3.80 (d, *J* = 6.6 Hz, 2H), 2.11-2.03 (m, 1H), 1.95 (dd, *J* = 1.5, 1.0 Hz, 3H), 1.90-1.78 (m, 2H), 1.80-1.67 (m, 2H), 1.37-1.21 (m, 4H), 1.05 (d, *J* = 6.7 Hz, 6H). ^{13}C- NMR ($CDCl_3$, 100 MHz) δ (ppm): 167.5, 161.3, 161.0, 146.9, 146.9, 136.5, 125.2, 124.3, 114.6, 114.6, 74.7, 68.1, 64.6, 29.1, 28.6, 28.3, 25.81, 25.7, 19.3, 18.3. Anal. Calc. for $C_{26}H_{34}N_2O_4$: C, 71.21 %; H, 7.81 %; N, 6.39 % Found: C, 71.13 %; H, 8.14 %; N, 6.34 %.

5.5.2 Experimental Details for the Synthesis of the Macroinitiator $(PEG_{12})_3$-Br

Synthesis and Characterisation of Alkyne Functionalised PEG[16]

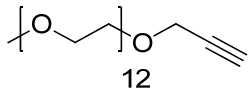

Polyethylene glycol mono methyl ether (15.00 g, 27.30 mmol) was dissolved in dry THF (200 mL) and the solution cooled into an ice-water bath. Then, sodium hydride (2.72 g, 55-65 wt%) was added and the solution stirred until no hydrogen gas was released. Propargyl bromide (4.5 mL g, 80 wt% in toluene) was added dropwise an the reaction mixture stirred at 0 ºC for 1 h and at room temperature overnight. The precipitated was filtered off and the solvent was removed under vacuum to yield the required product. Yield: 85%. IR (KBr), ν (cm^{-1}): 3245, 2112, 1960, 1456, 1248, 1105. ^{1}H-NMR (250 MHz, $CDCl_3$) δ (ppm): 4.21 (d, *J* = 2.4 Hz, 2H), 3.76-3.50 (m, 48H), 3.38 (s, 3H), 2.44 (t, *J* = 2.4 Hz, 1H).

Synthesis and Characterisation of 2,2,2-tris(azidomethyl)etanol $(N_3)_3$-OH[15]

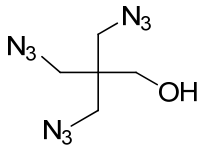

2,2,2-Tris(bromomethyl)etanol (2.00 g, 6.16 mmol) was dissolved in DMF (10 mL) and treated with sodium azide (1.22 g, 18.5 mmol) then heated to 120 °C for 17 h. The crude reaction mixture was cooled, an equivalent volume of water was added, the organic product was extracted into toluene (5x10mL), and DMF was back-extracted into brine. The organic solution was concentrated, but to no greater than 1 M in azide. **Caution!** Small organic azides should never be distilled to dryness. The final concentration of the triazide was determined by NMR (24 wt%). Yield: 86%. ^{1}H-NMR (250 MHz, CDCl3, toluene peaks omitted) δ (ppm): 3.49 (s ,2H), 3.33 (s, 6H).

Synthesis and Characterisation of $(PEG_{12})_3$-OH

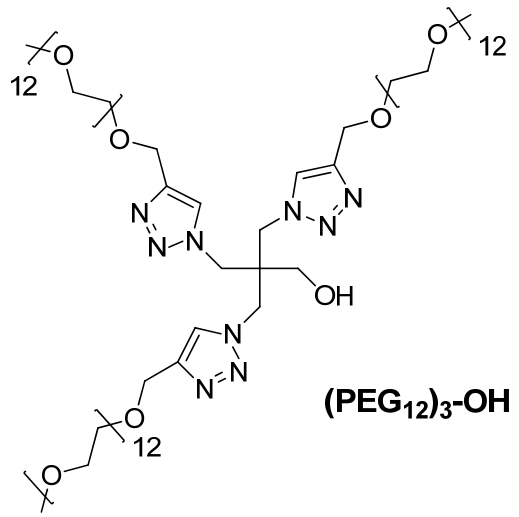

2,2,2-Tris(azidomethyl)ethanol **$(N_3)_3$-OH** (3.42 g, 3.80 mmol, 24 wt% in toluene) and alkyne functionalised PEG (9.00 g, 14.82 mmol) were placed into a Schlenk tube. PMDETA (160 µL, 0.76 mmol), CuBr (110.2 mg, 0.76 mmol) and deoxygenated toluene were added with an argon-purged syringe, and the flask was further degassed by three freeze-pump-thaw cycles and flushed with Argon. The reaction mixture was stirred at room temperature overnight. Then, the mixture was diluted with THF and passed through a short column of neutral alumina. The solvent was partially evaporated and the resulting polymer solution carefully precipitated into cold ethyl ether. Yield: 55%. IR (KBr), ν (cm^{-1}): 3500, 1959, 1456, 1249, 1106. ^{1}H-NMR (250 MHz, $CDCl_3$) δ (ppm): 8.23 (s, 3H), 4.72 (s, 6H), 4.33 (s, 6H), 3.75-3.50 (m, 146H), 3.37 (s, 9H), 3.02 (s, 1H).

Synthesis and Characterisation of $(PEG_{12})_3$-Br

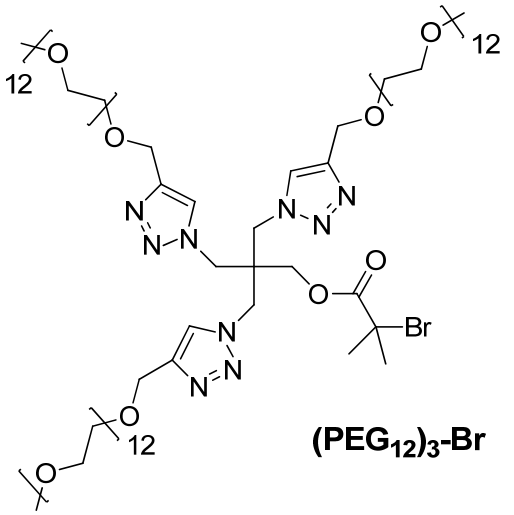

$(PEG_{12})_3$-Br

A solution of the polymer **$(PEG_{12})_3$-OH** (1.48 g, 0.76 mmol) in dry THF (20 mL) was prepared and cooled into an ice bath. The solution was stirred and triethylamine (0.5 mL, 3.80 mmol) and α-bromoisobutyryl bromide (0.4 mL, 3.80 mmol) were added dropwise under argon atmosphere. The mixture was stirred then at room temperature overnight and methanol (1mL) was added. The solution was filtered and the solvent was removed under vacuum. Yield: 70%. IR (KBr), ν (cm^{-1}): 1959, 1742, 1457, 1249, 1107. ^{1}H-NMR (250 MHz, $CDCl_3$) δ (ppm): 8.18 (s, 3H), 4.70 (s, 6H), 4.46 (s, 8H), 3.75-3.50 (m, 144H), 3.37 (s, 9H), 2.03 (s, 6H).

5.5.3 Experimental Details for the Synthesis of the Miktoarm Polymer ($PAZO_{17}$-$(PEG_{12})_3$)

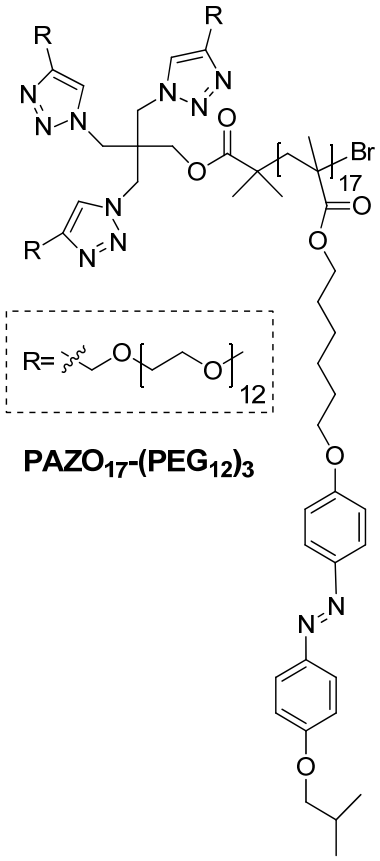

mAZO (200.0 mg, 456.3 μmol), **$(PEG_{12})_3$-Br** (42.1 mg, 20.2 μmol) and CuBr (2.8 mg, 20.2 μmol) were added to a Schlenk tube. PMDETA (4.0 μL, 20.2 μmol) and deoxygenated anisole (1mL) were added with an argon-purged syringe, and the flask was further degassed by three freeze-pump-thaw cycles and flushed with argon. The reaction mixture was stirred under an argon atmosphere at 80ºC for 24 h. The mixture was diluted with THF and then passed through a short column of alumina. The solvent was partially evaporated and the resulting polymer solution was carefully precipitated into cold methanol. Yield: 80% IR (KBr), v (cm^{-1}): 1727, 1600, 1581, 1500, 1247, 1147, 841. ^{1}H-NMR ($CDCl_3$, 400MHz) δ (ppm): 7.80-7.69 (m), 6.90-6.76 (m), 4.65 (s), 4.37 (s), 4.05-3.81 (m), 3.79-3.52 (m), 3.37 (s), 2.13-2.01 (m), 2.01-1.85 (m), 1.81-1.65 (m), 1.65-1.47 (m), 1.46-1.27 (m), 1.09-0.80 (m). M_n=9700 $Đ_M$ =1.10 (PS standars). Anal. Calc: C, 66.72 %; H, 7.93 %; N, 6.11 % Found: C, 67.21 %; H, 8.04 %; N, 6.26 %

5.5.4 General Procedures

The preparation of the vesicles, determination of the critical aggregation concentration (CAC) as well as the sample preparation for the different microscopies techniques has been performed following the same procedures described in Chapter 3. Irradiation experiments were carried out in the same conditions as Chapter 4 (Philips PL-S 9W, 350-400nm).

References

1 Matyjaszewski, K.; Tsarevsky, N. V. Nanostructured functional materials prepared by atom transfer radical polymerization. *Nature Chemistry* **2009**, 1, 276-288.

2 Sumerlin, B. S.; Vogt, A. P. Macromolecular Engineering through Click Chemistry and Other Efficient Transformations. *Macromolecules* **2010**, 43, 1-13.

3 Binder, W. H.; Sachsenhofer, R. 'Click' chemistry in polymer and materials science. *Macromolecular Rapid Communications* **2007**, 28, 15-54.

4 Binder, W. H.; Sachsenhofer, R. 'Click' chemistry in polymer and material science: An update. *Macromolecular Rapid Communications* **2008**, 29, 952-981.

5 Fournier, D.; Hoogenboom, R.; Schubert, U. S. Clicking polymers: a straightforward approach to novel macromolecular architectures. *Chemical Society Reviews* **2007**, 36, 1369-1380.

6 Kempe, K.; Krieg, A., Becer, C. R.; Schubert, U. S. "Clicking" on/with polymers: a rapidly expanding field for the straightforward preparation of novel macromolecular architectures. *Chemical Society Reviews* **2012**, 41, 176-191.

7 Khanna, K.; Varshney, S.; Kakkar, A. Miktoarm star polymers: advances in synthesis, self-assembly, and applications. *Polymer Chemistry* **2010**, 1, 1171-1185.

8 Higashihara, T.; Hayashi, M.; Hirao, A. Synthesis of well-defined star-branched polymers by stepwise iterative methodology using living anionic polymerization. *Progress in Polymer Science* **2011**, 36, 323-375.

9 Altintas, O.; Vogt, A. P.; Barner-Kowollik, C.; Tunca, U. Constructing star polymers via modular ligation strategies. *Polymer Chemistry* **2012**, 3, 34-45.

10 Jin, Q.; Liu, G.; Liu, X.; Ji, J. Photo-responsive supramolecular self-assembly and disassembly of an azobenzene-containing block copolymer. *Soft Matter* **2010**, 6, 5589-5595.

11 Hadjichristidis, N.; Pitsikalis, M.; Iatrou, H. in *Macromolecular Engineering* 909-972 (Wiley-VCH Verlag GmbH & Co. KGaA, 2007).

12 He, X.; Sun, W.; Yan, D.; Liang, L. Novel ABC2-type liquid-crystalline block copolymers with azobenzene moieties prepared by atom transfer radical polymerization. *European Polymer Journal* **2008**, 44, 42-49.

13 Wang, Y. Lin, S.; Zang, M.; Xing, Y.; He, X.; Lina, J.; Chen, Y. Self-assembly and photo-responsive behavior of novel ABC2-type block copolymers containing azobenzene moieties. *Soft Matter* **2012**, 8, 3131-3138.

14 Sun, W.; He, X.; Gao, C.; Liao, X.; Xie, M.; Lin, S.; Yan, D. Novel amphiphilic and photo-responsive ABC 3-miktoarm star terpolymers: synthesis, self-assembly and photo-responsive behavior. *Polymer Chemistry* **2013**, 4, 1939-1949.

15 Díaz, D. D.; Punna, S.; Holzer, P.; McPherson, A. K.;Sharpless, K. B.;Fokin, V. V.; Finn, M. G. Click chemistry in materials synthesis. 1. Adhesive polymers from copper-catalyzed azide-alkyne cycloaddition. *Journal of Polymer Science Part A: Polymer Chemistry* **2004**, 42, 4392-4403.

16 Zhang, X.; Chen, Z.; Würthner, F. Morphology Control of Fluorescent Nanoaggregates by Co-Self-Assembly of Wedge- and Dumbbell-Shaped Amphiphilic Perylene Bisimides. *Journal of the American Chemical Society* **2007**, 129, 4886-4887.

CHAPTER 6

Dual Responsive Miktoarm Star Polymers

Published in *Polym. Chem.* **2013**.

DOI: 10.1039/C3PY00576C

6.1 Introduction and Aims

BC micelles are simple spherical assemblies of amphiphilic copolymers that have core-shell type architecture (**Figure 6.1**). The hydrophobic parts of the polymer aggregate in the aqueous environment to form the core of the micelles and the hydrophilic parts form a water soluble corona that separates the core from the environment. The core of the micelles is a loading space that can accommodates hydrophobic molecules, as drugs, while the corona is a protective shell that ensures the water dispersibility of the micelles.[1-3] In that respect, amphiphilic block copolymer micelles have been widely explored for drug delivery as both the core and the corona can be chemically fine tuned to optimise the drug uptake/release.[4,5] Providing an adequate chemical design to incorporate stimuli-sensitive moieties, micelles are capable of undergoing changes in their physical properties upon exposure to external stimulus as pH value, temperature, additives or irradiation with light.[6]

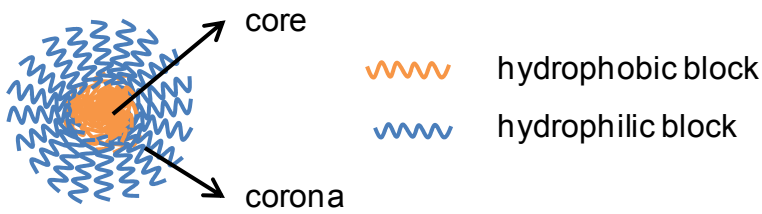

Figure 6.1 *Schematic representation of a polymeric micelle*

The solubility of certain polymers in water can be influenced by the temperature of the surrounding medium.[7-9] Most small molecules become increasingly soluble with rising temperature; however, the so-called thermoresponsive polymers have a sharp transition temperature at which they become either soluble or insoluble. When the transition is from a more soluble to a less soluble state, this temperature is known as the lower critical solution temperature (LCST). Conversely, if the transition is from a less soluble to a more soluble state this temperature is known as the upper critical solution temperature (UCST). The majority of research has focused on materials that display an LCST, mainly due to the derived advantages in the design of polymeric

biomaterials. The LCST behaviour is attributed to the interplay between the intermolecular polymer–water hydrogen bonding and intramolecular polymer-polymer interactions. Above the LCST macromolecules experience dehydration and collapse from a hydrated, extended coil to a hydrophobic globule. In general, most of non ionic water soluble polymers show LCST behaviour. This has been observed for poly(hydroxyethyl methacrylate) (PHEMA), poly(oligoethylene glycol methacrylate) (POEGMA), poly(*N,N*-dialkylaminoethyl methacrylates) (PDMAEMA and PDEAEMA) or poly(*N*-substituted acrylamide). Poly(*N*-isopropylacrylamide) (PNIPAM) is probably the most representative example of thermoresponsive polymers with a LCST near to body temperature.[7] Poly(*N,N*-diethylacrylamide) (PDEAA) is a structurally similar thermoresponsive polymer featuring an LSCT ranging from 25 to 35 ºC, close to room temperature.[10]

Thermoresponsive micelles assembled from amphiphilic block copolymers have been extensively studied. If the thermoresponsive component is combined with a hydrophilic polymer block then the polymer is molecularly dissolved below the LCST but, upon raising the temperature, the hydrophilic-hydrophobic switch results in micellar self-assembly with the thermoresponsive block forming the hydrophobic core. When the thermoresponsive component is combined with a hydrophobic block the polymer will form micelles with a thermoresponsive shell. Upon heating above the LCST the shell collapses resulting in the precipitation/gelation of the micelles.[11] Thermoresponsive micelles can be exploited as nanocontainers for controlled drug release.[12-14]

The area of micelles responsive to a single stimulus has been extended to micelles which show responsive behaviour to multiple stimuli as a way to better control their performance.[15] Of special importance are micelles responsive to temperature and light[16] and accordingly there have been several reports on temperature responsive polymers containing azobenzene moieties. Li et *al*. described the formation of micelles from a novel amphiphilic diblock copolymer composed of a PEG block and a hydrophobic block of a random azobenzene poly(methacrylate) and PNIPAM copolymer, (PEG-*b*-(PAZO-co-PNIPAM)) (**Figure 6.2a**).[17] The size of these micelles was dependent on temperature, while no disruption of the micelles was detected upon irradiation. Theato *et al*.

also reported a similar thermo and lightresponsive BC based on PEG and PNIPAM containing azobenzene moieties (**Figure 6.2b**) able to self-assemble in water forming micelles.[18] A temperature reversible formation as well as a light induced partial disruption of the micelles was found. In both examples, the photoresponsive moieties were included in the thermoresponsive block. A further example for dual-responsive micelles was reported by Zhao *et al.*[19] PNIPAM with azobenzene moieties inserted into the main chain was synthesised. The multiblock copolymer was able to self-assemble in cold water forming flower micelles. Upon UV irradiation, swelling of the vesicles was observed due to *trans*-to-*cis* isomerisation and the micelles collapsed upon heating above the LCST of PNIPAM.

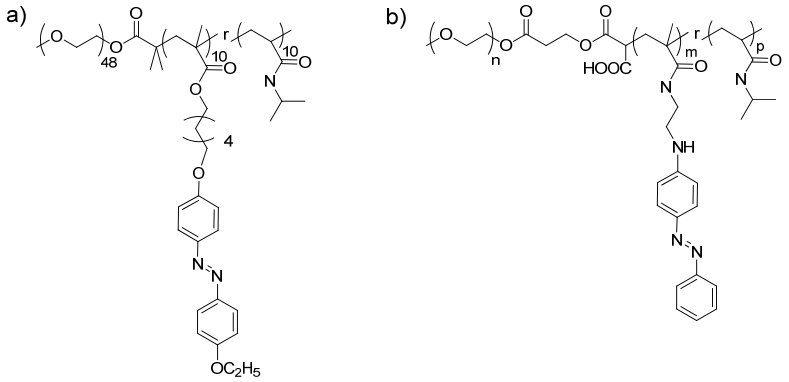

Figure 6.2 *Chemical structures of some examples of thermo and photoresponsive amphiphilic BCs: a) reported by Li et al.[17], b) reported by Theato et al.[18]*

In summary, all the thermo and photoresponsive amphiphilic BC reported so far are based on linear-linear diblock copolymers composed of a hydrophoilic block (PEG) and a hydrophobic responsive block composed of a copolymer containing azobenzene as well as thermoresponsive moieties.

The main goal approached on the current chapter was the preparation of novel thermoresponsive azobenzene miktoarm polymers AB_3 type having the thermo and photoresponsive moities located in different arms. The seleted miktoarm polymers, **PAZO$_{17}$-(PDEAA$_m$)$_3$**, are composed of an azobenzene poly(methacrylate) **PAZO$_{17}$** as the photoresponsive block and three arms containing poly(*N,N*-diethylacrylamide) (**PDEAA$_m$**), a thermoresponsive water

soluble polymer (**Figure 6.3**). The synthesis of the polymers was afforded by combining controlled radical polymerization, i.e. ATRP and RAFT polymerization, with CuAAC, as the way to obtain well-defined polymer structures with adjustable structural parameters. In order to assess the influence of the hydrophobic/hydrophilic ratio, PDEAA with three different average molecular weights were prepared leading to different miktoarm polymers with hydrophobic/hydrophilic ratios ranging from 56/44 to 26/74. The study additionally includes an exploration of thermo and photoresponsive properties of the materials.

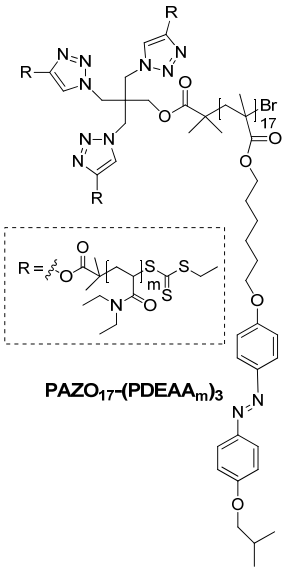

Figure 6.3 *Chemical structure of the investigated miktoarm star polymers*

6.2 Tasks and Methods

- Synthesis of the photoresponsive arm by ATRP polymerization of an azomonomer using an initiator containing three azido groups.

- Synthesis of the thermoresponsive arms consisting of alkyne functionalized PDEAA by RAFT polymerization.

- Coupling of the performed arms to obtain the target thermo and photoresponsive miktoarm star polymers of AB_3 type using CuAAC (**Figure 6.4**).

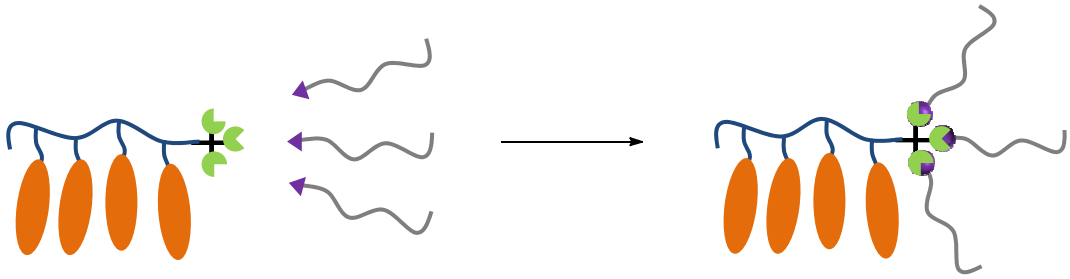

Figure 6.4 *Synthetic approach for the synthesis of the miktoarm star polymers*

- Structural characterisation of the miktoarm polymers (and their building blocks) by FTIR, NMR and elemental analysis. Thermal characterisation using POM, TGA and DSC.

- Self-assembly of the miktoarm polymers in water and morphological study of the self-assemblies in water by TEM

- Thermo and photoresponsive behaviour of the self-assemblies in water

- Encapsulation and thermo and photoinduced release of fluorescent probes

6.3 Results and Discussion

6.3.1 Synthesis and Characterisation of the Amphiphilic Miktoarm Star Polymers

The miktoarm star copolymers were prepared by a combination of controlled radical polymerizations (ATRP and RAFT were used) and CuAAC as it is collected in **Scheme 6.1**. ATRP was used to polymerize the azomonomer, **mAZO**, from an asymmetric tetrafunctionalised core, **$(N_3)_3$-Br**, giving an azobenzene polymethacrylate, **$(N_3)_3$-PAZO$_{17}$**, with three azido groups at the end. RAFT polymerization using a properly functionalised charge transfer reagent (CTA) with an alkyne function was used to prepare the thermoresponsive arms. Final coupling of the **$(N_3)_3$-PAZO$_{17}$** with the alkyne-terminated thermoresponsive arm through CuAAC leaves behind the target AB_3 miktoarm polymers.

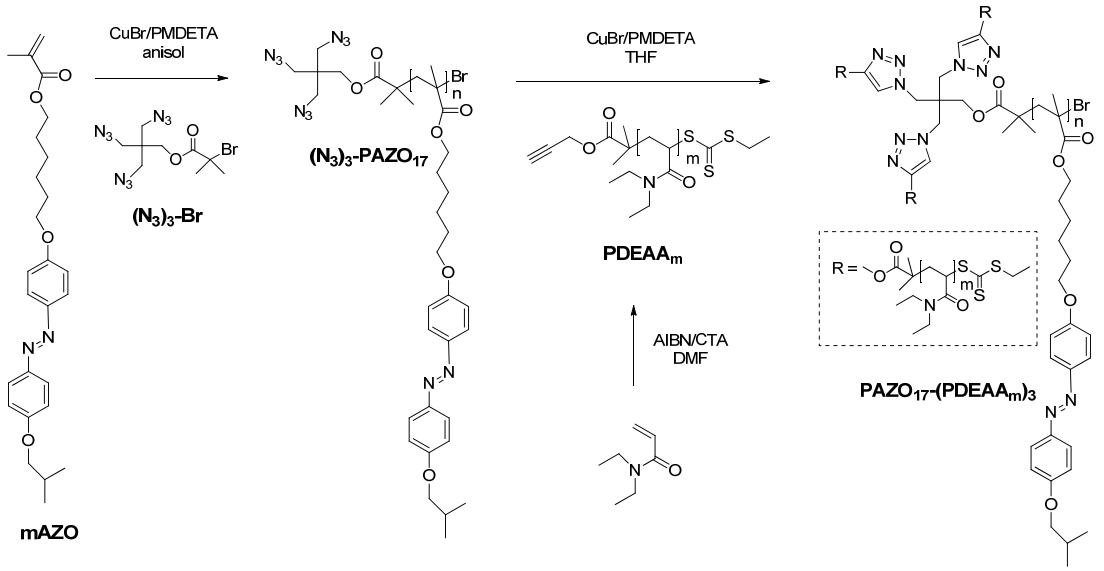

Scheme 6.1 *Synthesis of the investigated miktoarm star polymers*

As can be seen synthetic strategy is similar to that used in Chapter 5 but the sequence, polymerization and coupling, was reversed in order to modulate phobic/philic ratio maintaining the same photoresponsive block (in the previous chapter, commercial PEG arms of a predetermined M_n were first introduced).

Consequently, an appropriately functionalised azido initiator is required. In particular, starting from the same core, the tetrafunctional 2,2,2-tris(azidomethyl)ethanol core **$(N_3)_3$-OH**, a novel triazido ATRP initiator (**$(N_3)_3$-Br**) was prepared by an esterification reaction between **$(N_3)_3$-OH** and α-bromoisobutyryl bromide. This initiator was used to polymerize the azobencene methacrylate **mAZO** to render an azido functionalised polymer **$(N_3)_3$-PAZO$_{17}$**. ATRP was conducted in anisole at 80ºC using CuBr/PMDETA as the catalytic system. The average molecular weight of the polymer arm **$(N_3)_3$-PAZO$_{17}$** was deduced by end group analysis using ^{1}H-NMR spectroscopy: the relative integration of the signal corresponding to the end-group -CH_2-N_3 at 3.27 ppm (labelled at '*a*' in **Figure 6.5**) and the signals corresponding to the aromatic protons of the repeating azobenzene unit were used to calculate the polymerization degree, giving in average 17 repeating units per polymer chain as it is collected in **Table 6.1.**

Table 6.1 *Molecular weight the synthesised polymers*

Polymer	M_n [a]	M_n [b]	$Đ_M$ [b]	Phobic/philic ratio[c]
$(N_3)_3$-PAZO$_{17}$	7816	9900	1.18	--
PDEAA$_{14}$	2040	1700	1.18	--
PDEAA$_{22}$	3056	2400	1.14	--
PDEAA$_{55}$	7247	6300	1.11	--
PAZO$_{17}$-(PDEAA$_{14}$)$_3$	13936	14800	1.22	56/44
PAZO$_{17}$-(PDEAA$_{22}$)$_3$	16984	17400	1.10	46/54
PAZO$_{17}$-(PDEAA$_{55}$)$_3$	29557	26200	1.12	26/74

[a] M_n calculated by ^{1}H-NMR (see text). [b] M_n and polydispersity ($Đ_M$) of the polymers were determined by SEC using PS standards. [c] Phobic/Philic ratio was calculated by considering PDEAA arms as the hydrophilic part and the rest as the hydrophobic part.

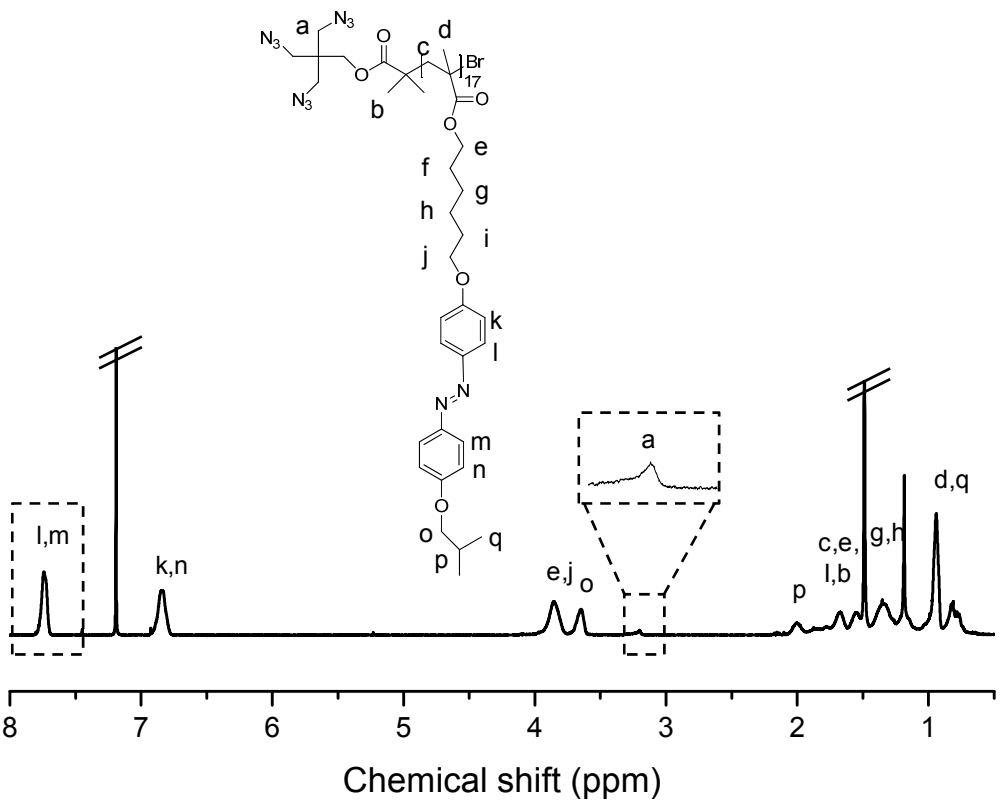

Figure 6.5 *^{1}H-NMR spectrum of* ***(N_3)$_3$-PAZO$_{17}$*** *in $CDCl_3$ (400MHz)*

Independently, three **PDEAA$_m$** polymers with different number average molecular weight were synthesised *via* RAFT polymerization using a suitable chain transfer agent (CTA) containing an alkyne group, according a method previously published.[20] The CTA was kindly provided by B. Schmidt (Macroarc group, KIT). For **PDEAA$_m$** polymers, the average molecular weight was also calculated by ^{1}H-NMR spectroscopy using the integral values corresponding to the terminal methylenic protons linked to the alkyne -CH_2-O-C≡C at 4.71 ppm (labelled as *'b'* in **Figure 6.6**) and the methylene linked to the amide functional group (-CH_2-N-CO- of the repeating unit at 3.5-3.0 ppm (labelled as *'f'* in **Figure 6.6**). In average, the target polymers contained m=14, 22 and 55 repeating units as it is collected in **Table 6.1.**

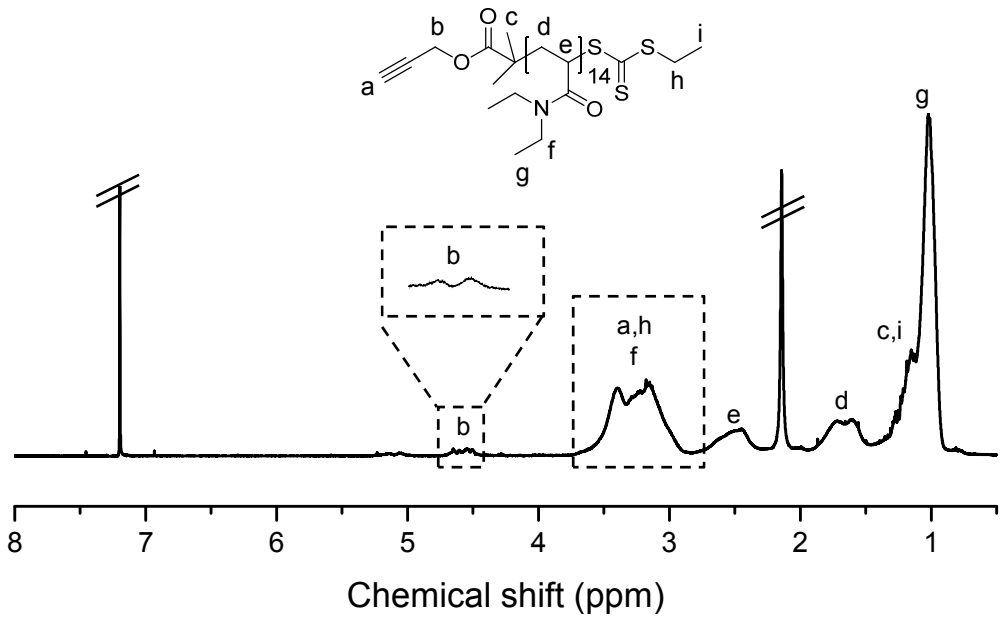

Figure 6.6 *^{1}H-NMR spectrum of* ***(PDEAA$_{14}$)$_3$*** *in $CDCl_3$ (400MHz)*

In the final step, the alkyne terminated **PDEAA$_m$** polymers were coupled with the azopolymer **(N$_3$)$_3$-PAZO$_{17}$** via a CuAAC to form the three target miktoarm polymers **PAZO$_{17}$-(PDEAA$_{14}$)$_3$**, **PAZO$_{17}$-(PDEAA$_{22}$)$_3$** and **PAZO$_{17}$-(PDEAA$_{55}$)$_3$**. An excess of the alkyne functionalised polymers was employed to ensure the completeness of the reaction. The excess of alkyne ended polymer was finally removed by using an azido functionalised polystyrene resin. The efficiency of the coupling reaction was assessed by SEC traces based on the unimodal distribution and the shift of the molecular weight distribution peak towards lower retention times that indicates miktoarm copolymer formation (**Figure 6.7a**). Further evidence for the miktoarm polymer formation was obtained from the IR spectra, where the band at 2100 cm^{-1} due to the azide functionality completely disappeared as it is observed in **Figure 6.7b**. The incorporation of the three **PDEAA** arms was confirmed by ^{1}H-NMR. The relative integration of azobenzene aromatic protons signals (photoresponsive block) and the corresponding ones to methylene groups linked to nitrogen at 3.50-3.00 ppm as well as the CH- group of the main chain of the **PDEAA** arms (thermoresponsive arms) were in good agreement with the proposed AB$_3$ structure in all the cases. **Figure 6.8** shows the ^{1}H-NMR spectrum of **PAZO$_{17}$-(PDEAA$_{14}$)$_3$** as an

example. The molecular weight of the miktoarms polymers were also calculated by SEC using PS standards and it is good agreement with the experimental values estimated by ^{1}H-NMR (**Table 6.1**).

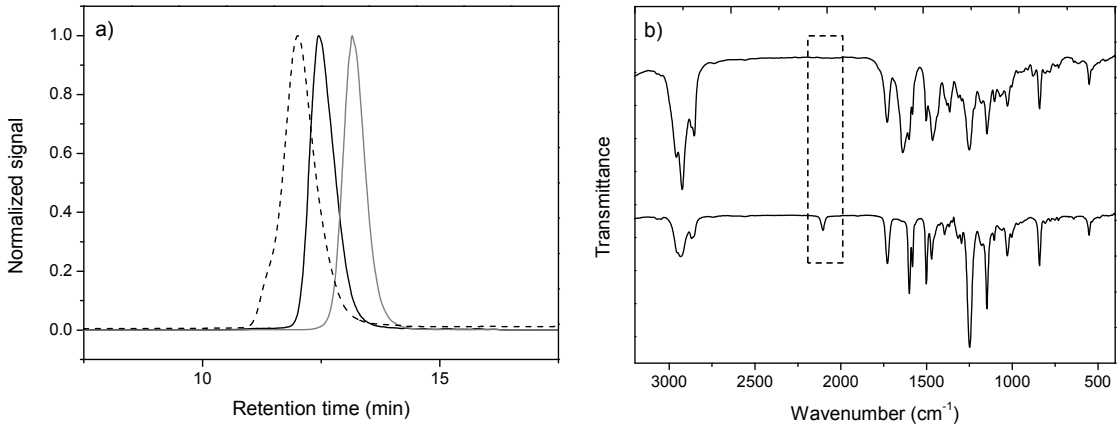

Figure 6.7 a) *SEC traces of* ***$(N_3)_3$-PAZO$_{17}$*** *(black line),* ***PDEAA$_{55}$*** *(grey line) and* ***PAZO$_{17}$-(PDEAA$_{55}$)$_3$*** *(dashed line). b) FTIR spectra of* ***$(N_3)_3$-PAZO$_{17}$*** *(bottom) and* ***PAZO-(PDEAA$_{55}$)$_3$*** *(top)*

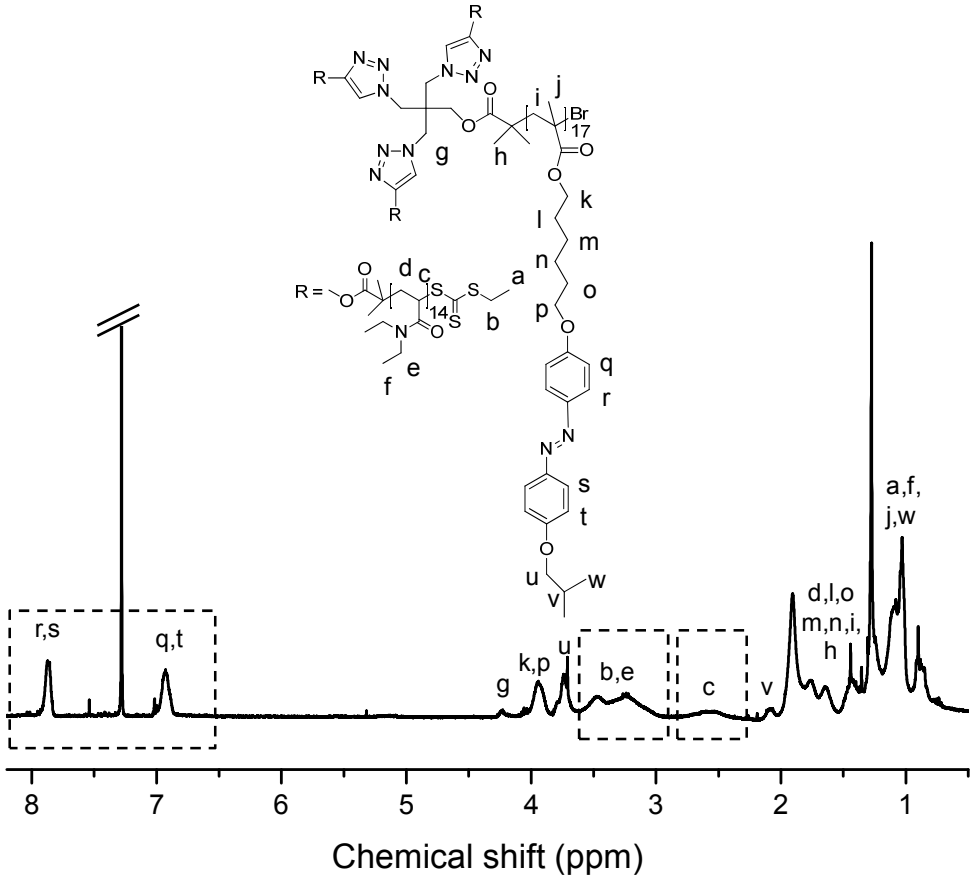

Figure 6.8 *^{1}H-NMR spectrum of* ***PAZO$_{17}$-(PDEAA$_{14}$)$_3$*** *showing the signals used to composition calculation in $CDCl_3$ (400MHz)*

Thermal properties of the synthesised polymers are collated in **Table 6.2**. The thermal stability of the preformed blocks and miktoarm polymers was studied by TGA using powdered samples. All the samples, including the miktoarm polymers, exhibited a good thermal stability up to around 300 ºC, far above the temperature transition to an isotropic liquid state. The thermal transitions were studied by DSC and POM. For **$(N_3)_3$-PAZO$_{17}$**, a melting process to the isotropic liquid was detected by POM and confirmed by DSC as an endothermic peak detected at 110 ºC on the heating curve. The corresponding crystallisation process was detected at 103ºC upon cooling. By contrast, the **PDEAA$_m$** polymers are amorphous materials with a T_g in the range between 45 and 64ºC, increasing the T_g value on increasing the molecular weight of these polymers as expected. The miktoarm polymers resulting from the coupling of **$(N_3)_3$-PAZO$_{17}$** and **PDEAA$_m$** exhibited DSC curves showing a solid-isotropic liquid transition at close to 100 ºC, corresponding melting processes of the azobenene containing arms. T_g values corresponding to the thermoresponsive blocks were not accurately calculated due to the overlap with cold crystallisation processes (**Figure 6.9**).

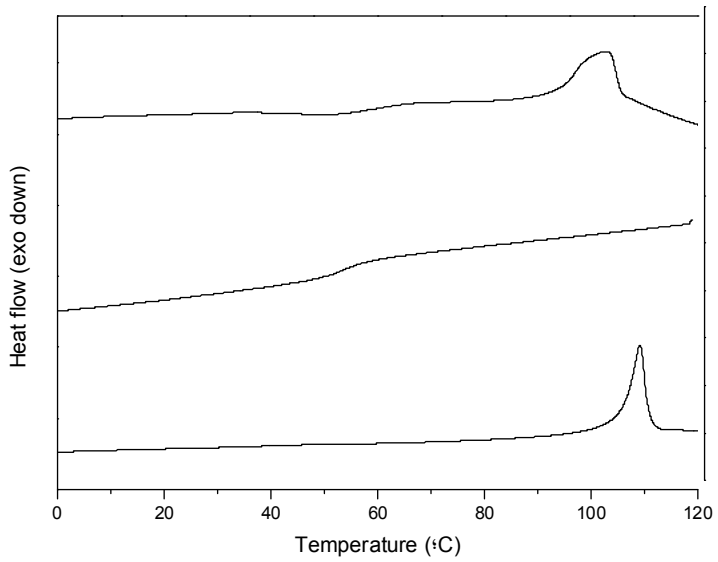

Figure 6.9 *DSC curves (10ºC/min) corresponding to the second heating of* ***$(N_3)_3$-PAZO$_{17}$, PDEAA$_{14}$*** *and* ***PAZO$_{17}$-(PDEAA$_{14}$)$_3$*** *(from bottom to top)*

Table 6.2. *Thermal properties of the miktoarm star polymers and the corresponding building blocks*

	TGA [a]	DSC [b]		
Polymer	T_d	T_g	T_m	ΔH_m
$(N_3)_3$-PAZO$_{17}$	337	-	110	10
PDEAA$_{14}$	366	45	-	-
PDEAA$_{22}$	375	53	-	-
PDEAA$_{55}$	389	64	-	-
PAZO$_{17}$-(PDEAA$_{14}$)$_3$	303	-[c]	99	10
PAZO$_{17}$-(PDEAA$_{22}$)$_3$	343	-[c]	103	9
PAZO$_{17}$-(PDEAA$_{55}$)$_3$	367	-[c]	90	11

[a] Thermogravimetric analysis: T_d (in ºC): Decomposition temperature associated with the mass loss calculated by TGA at the onset point in the weight loss curve. [b] Data of Differential Scanning Calorimetry (DSC) calculated from the second heating scan recorded at 10ºC/ min. T_g (in ºC): glass transition temperature; T_m (in ºC) and ΔH_m (in kJ per mole of azobenzene unit): crystallisation temperature and associated enthalpy. [c] T_g was not clearly detected.

6.3.2 Self-Assembly of the Miktoarm Polymers in Water

Polymeric self-assemblies of **PAZO$_{17}$-(PDEAA$_{14}$)$_3$**, **PAZO$_{17}$-(PDEAA$_{22}$)$_3$** and **PAZO$_{17}$-(PDEAA$_{55}$)$_3$** were prepared by dissolving the miktoarm polymers in THF and adding water gradually while measuring the turbidity at room temperature (**Figure 6.10a**). Once the turbidity reached an almost constant value, the resulting dispersion was dialyzed against water to remove the organic solvent. After dialysis, a stable micellar solution was obtained for **PAZO$_{17}$-(PDEAA$_{55}$)$_3$**, while precipitation was observed for **PAZO$_{17}$-(PDEAA$_{14}$)$_3$** and **PAZO$_{17}$-(PDEAA$_{22}$)$_3$** indicating that relatively short **PDEAA** arms are not able to stabilise self-assemblies in water. As a consequence, the study of micellar solutions was only focussed on **PAZO$_{17}$-(PDEAA$_{55}$)$_3$**.

The critical micellar concentration (CMC) in water of **PAZO$_{17}$-(PDEAA$_{55}$)$_3$** was determined using Nile Red.[21-23] The CMC was calculated to be close to 45 µg/mL (**Figure 6.10b**).

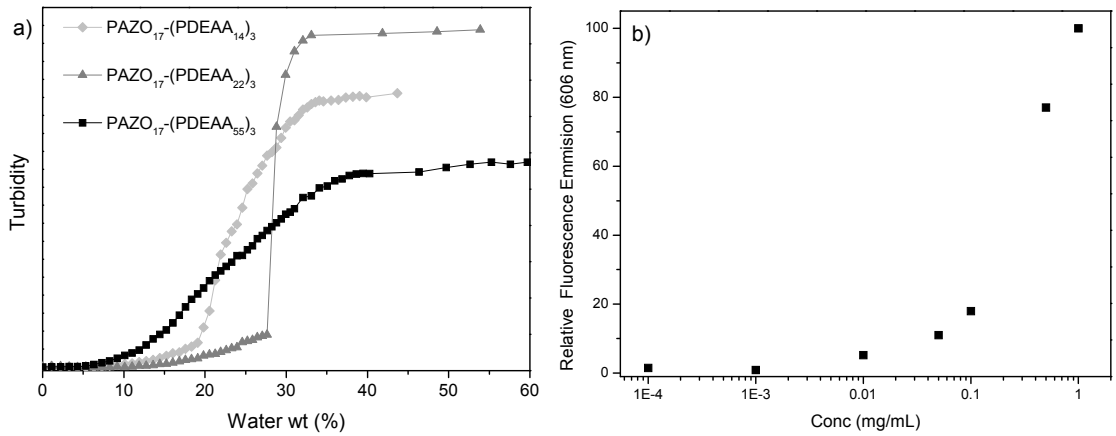

Figure 6.10 *a) Turbidity evolution of the miktoarm polymer THF solutions as a function the amount of added water. b) Flurorescence intensity of Nile Red at 606 nm (λ_{exc} = 550 nm) versus miktoarm polymer* ***PAZO$_{17}$-(PDEAA$_{55}$)$_3$*** *concentration (mg/mL)*

The morphology of the **PAZO$_{17}$-(PDEAA$_{55}$)$_3$** self-assemblies was investigated by transmission electron microscopy (TEM) on dried samples stained with uranyl acetate. TEM images (**Figure 6.11a**) evidence the presence of spheric micellar self-assemblies with a diameter of approx. 30 nm. The size of the polymeric micelles was additionally evaluated by DLS measurements providing the hydrodynamic diameter (D_h). Two size distributions were found (**Figure 6.12**); one centred at 31 nm corresponding to single micelles composed of an azopolymer core and a PDEAA shell and a second distribution, less intense, centred at 275 nm, which can be attributed to aggregation of the single micelles forming a more complex aggregate. The aggregation of the micelles was also confirmed by TEM due to the occasional presence of complex micellar aggregates in some region of the grid as can be observed in **Figure 6.11b**, although it should be remarked that these aggregates were observed in lesser number than the singles micelles, with **Figure 6.11a** being more representative of the morphologic TEM study. A similar behaviour has been also reported by Wang *et al*. for other thermoresponsive micelles.[24]

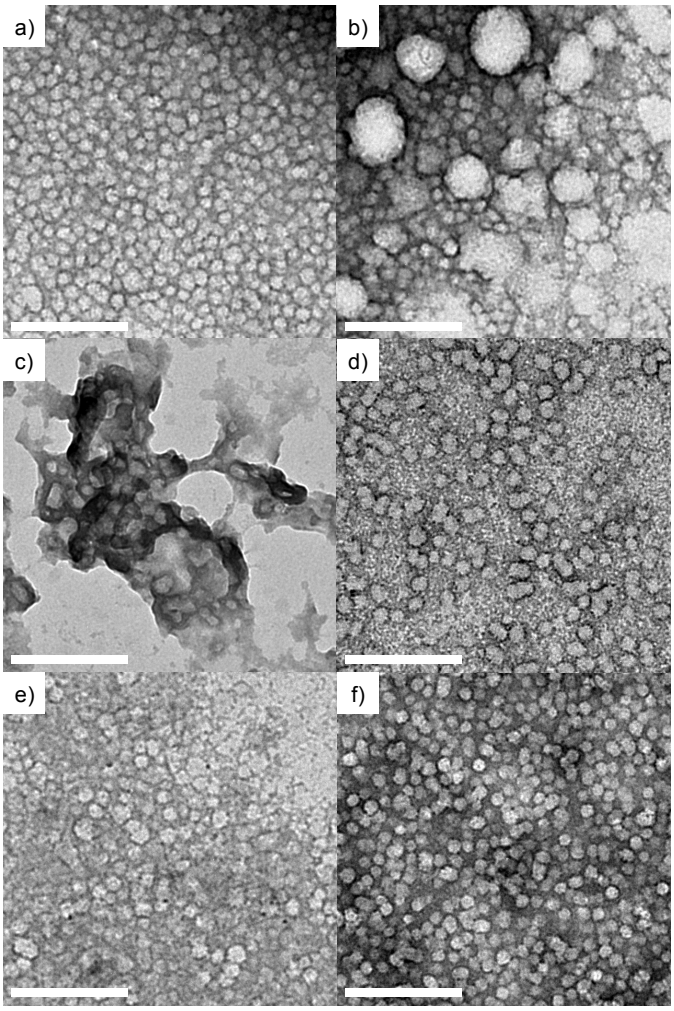

Figure 6.11 *TEM images of a water suspension of* ***PAZO$_{17}$-(PDEAA$_{55}$)$_3$*** *at different initial conditions: a) and b) at 20 ºC and non irradiated, c) quenched at 40 ºC; d) 20 ºC (after heating at 40 ºC for 1 h and then slowly cooled to room temperature), e) irradiated at room temperature, f) 24 h after irradiation. The length of the scale bar corresponds to 200 nm*

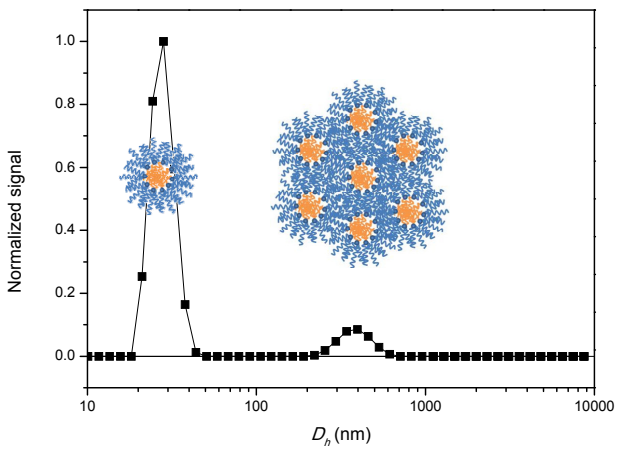

Figure 6.12 *Volume distribution of a water suspension micelles of* ***PAZO$_{17}$-(PDEAA$_{55}$)$_3$*** *and representative cartoon of single and aggregated micelles*

6.3.3 Thermo- and Photoresponsive Behaviour of the Self-Assemblies

The synthesised miktoarm polymers contain thermo and photoresponsive moieties and consequently they may have a dual response to external stimuli. The effect of the temperature on **$PAZO_{17}$-$(PDEAA_{55})_3$** micelles was initially assessed. First, the LCST of **$PDEAA_{55}$** was calculated by DSC (see Experimental Section for further details).[10] This critical temperature was found to be close to 27 ºC, indicating that **$PDEAA_{55}$** is a hydrophilic polymer at rrom temperature (approx. 20 ºC) and is becomes hydrophobic at temperatures above the LCST.

Once determined the LSCT of the thermoresponsive arms, an aqueous suspension of **$PAZO_{17}$-$(PDEAA_{55})_3$** (concentration of 1 mg/mL) was heated to 40 ºC (i.e. a temperature above the LSCT) for 30 min. Subsequently, a TEM analysis of the sample was performed. As the TEM experiment was carried out at room temperature, the suspension was placed in the grid and dehydrated immediately after being heated in order to maintain the morphology reached at 40 ºC. TEM image confirmed the collapse of the micelles (**Figure 6.11c**) due to the polarity change of the micelles' shell, which became hydrophobic. The collapse can also be followed macroscopically, since a precipitate appeared in the suspension. An additional experiment was carried by using the aqueous suspension that was heated at 40ºC for 1 h (above LSCT of the thermoresponsive arms) and then slowly cooled to room temperature in an attempt to reverse the thermal process suffered by the PDEAA arms. At room temperature, PDEAA became hydrophilic, turning the miktoarm polymer again into an amphiphilic polymer. In fact, partial reassembly of the micelles was observed by TEM. As can be seen in **Figure 6.11d**, spherical micelles similar to the initials ones were again observed, although featuring a higher diameter of approx. 50 nm. **Scheme 6.3a** despites the representation of the proposed thermoinduced morphological changes.

DLS measurements at different temperatures were additionally carried out (**Table 6.3** and **Figure 6.13a**). As noted above, micelles with a 31 nm hydrodynamic diameter (D_h) were found at 20 ºC. Upon heating to 40 ºC, the size of the aqueous dispersion was not able to be accurately measured due to

the limited stability of the suspension at that temperature. Nevertheless, once the suspension was cooled and equilibrated at 20 ºC, a distribution centred at 53 nm was found, in agreement with TEM observations.

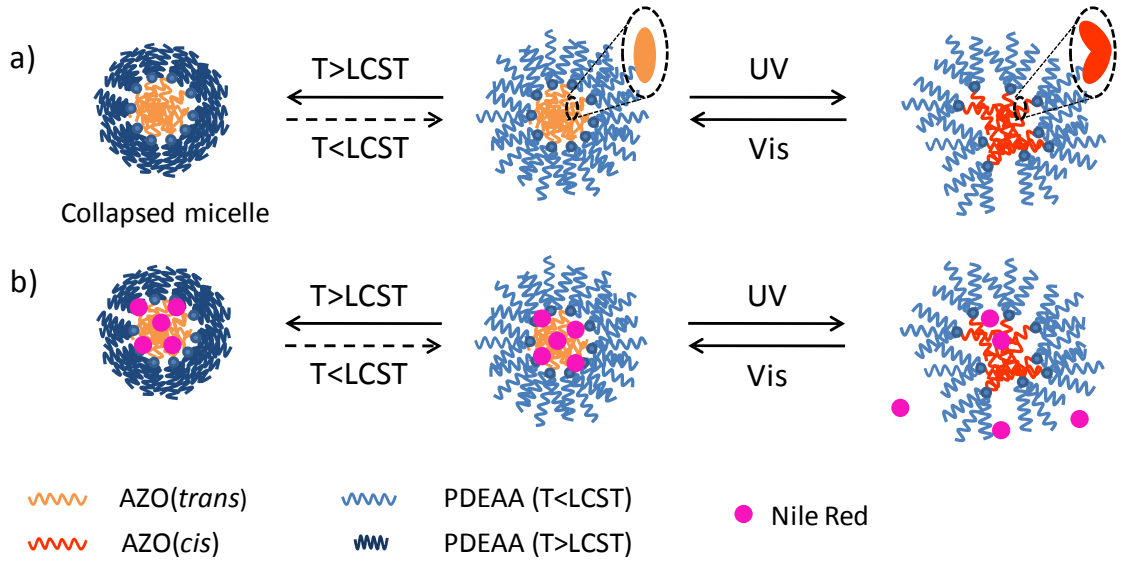

Scheme 6.3 *a) Schematic representation of the proposed thermo and photoinduced morphology changes in* ***PAZO$_{17}$-(PDEAA$_{55}$)$_3$*** *micelles. b) Schematic representation of the proposed thermo and photoinduced Nile Red release*

Table 6.3. *Mean hydrodynamic diameters (D_h) of* ***AZO-(PDEAA$_{55}$)$_3$*** *micelles determined by DLS.*

Sample	Conditions	D_h (nm)
Initial	20 ºC	31
Heated	40 ºC	-[a]
Heated at 40 ºC and cooled down to 20 ºC	20 ºC	53
Irradiated at 350-400 nm for 10 min	20 ºC	23
24 h after irradiation	20 ºC	32

[a] Data could not be calculated accurately

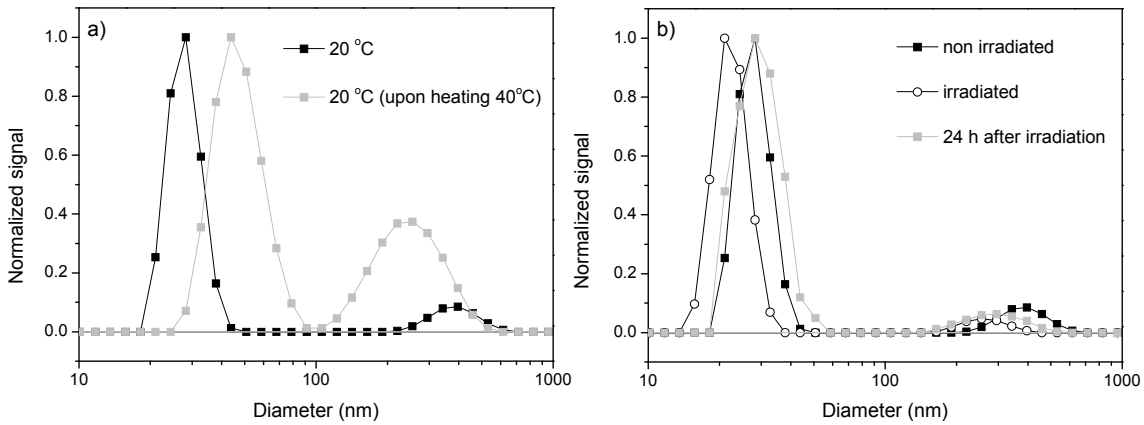

Figure 6.13 *Volume distribution of a water suspension micelles of* ***PAZO$_{17}$-(PDEAA$_{55}$)$_3$*** *at different conditions: a) at different temperatures (distribution at 40ºC was not measure accurately due to instability of the suspension) and b) upon irradiation at 20ºC*

In order to study the photoresponse of **PAZO$_{17}$-(PDEAA$_{55}$)$_3$** micelles, an aqueous suspension (concentration of 1mg/mL) was irradiated with a mercury UV lamp (9W) emitting between 350 and 400 nm and the evolution of the UV-Vis spectra was followed. Initially, the spectrum of the micellar suspension showed a broad π-π* transition with an absorption maximum close to 324 nm, indicating the dominating formation of H-aggregates of azobenzene units (**Figure 6.14a**). Furthermore, a shoulder at higher wavelengths, around 350 nm, was observed which corresponds to the absorption non aggregated chromophores, as was determined in these solution spectrum of **PAZO$_{17}$-(PDEAA$_{55}$)$_3$** shown in **Figure 6.14a** as reference. Upon irradiation, a remarkable decrease of the π-π* transition was observed accompanied by an increase of the absorbance at 450 nm, corresponding to the n-π* transition as can be observed in **Figure 6.14b**. This behaviour is attributed to the photoisomerisation of the *trans*-azobenzene to the *cis* isomer accompanied by changes of the molecular aggregation. After 2 min of irradiation, a photostationary state was reached and no further evolution in the UV-Vis spectra was detected. Thermal *cis*-to-*trans* back isomerisation took place after 24 h in the dark and UV-Vis spectra almost recovered the initial shape.

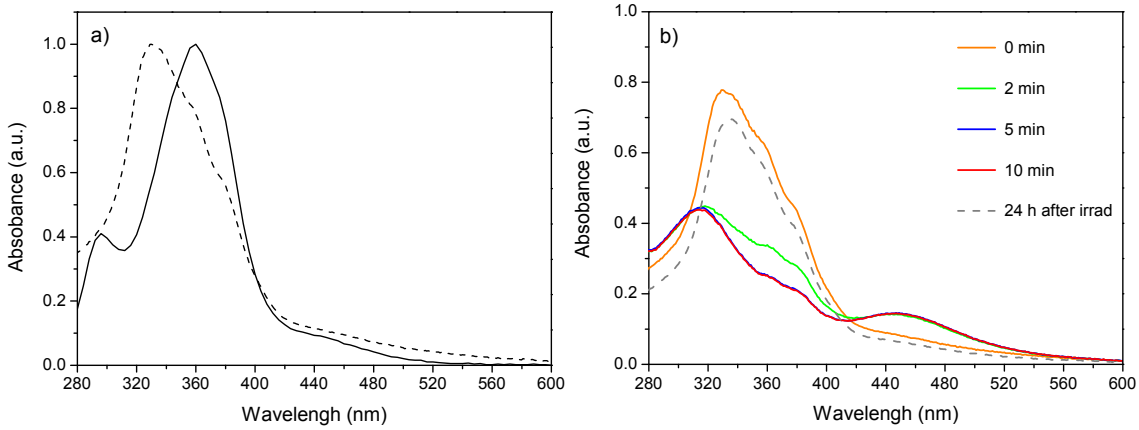

Figure 6.14 *a) UV-Vis spectra of* ***PAZO$_{17}$-(PDEAA$_{55}$)$_3$*** *in a 5x10^{-6} M solution in CHCl$_3$ (straight line) and a water suspension of* ***PAZO$_{17}$-(PDEAA$_{55}$)$_3$*** *micelles (dashed line). b) UV-Vis spectra of* ***PAZO$_{17}$-(PDEAA$_{55}$)$_3$*** *irradiated micelles (concentration of 1 mg/mL) at different times (350-400 nm, 9W) and 20ºC*

Having evaluated the evolution of UV-Vis spectra of the micellar suspension by irradiation, TEM observation of the polymeric micelles in combination with DLS measurements were also performed to gain further information about photoinduced morphological changes (**Table 6.3**). The TEM image recorded after irradiation shows the presence of micellar aggregates less defined than the initial ones accompanied by material without clear morphology (**Figure 6.9e**). A change of 8 nm in the D_h was detected by DLS measurements, evidencing a morphological change in the micelles (**Table 6.3** and **Figure 6.13b**). TEM image of an irradiated suspension after 24 h in the dark was additionally taken. Under these conditions, thermal *cis*-to-*trans* back isomerisation took place and reformation of the spherical initial shape of the micelles occurred as it is shown in **Figure 6.11f**. By DLS, the D_h evaluated before and 24 h in the dark after irradiation were almost identical, i.e. 31 and 32 nm, respectively (**Figure 6.13b**). These values were in agreement with TEM observations and demonstrated a reversible light induced morphological change of the polymeric micelles (**Scheme 6.3a**).

6.3.4 Encapsulation and Thermo and Photoinduced Release of Nile Red

The hydrophobic core of the spherical micelles can be loaded with hydrophobic molecules and delivered using temperature or light as external stimulus. With this aim, a suspension of the micelles loaded with Nile Red was prepared and the fluorescence of Nile Red encapsulated at the core was initially recorded (**Figure 6.15a**). Upon heating to 40 ºC (i.e. a temperature above the LSCT of the thermoresponsive arms), an increase of the fluorescence intensity occurred, which indicates that Nile Red is in a more hydrophobic environment.[25] As noted in the previous section, at 40 ºC, the PDEAA shell becomes more hydrophobic and the micelles collapse. A *priori* it would be reasonable to assume that disruption of the micelles might provoke Nile Red release. However, the increase of the fluorescence indicates that release of the Nile Red did not occur. We propose that the collapse of the micelles keeps the Nile Red inside, provoking a slight increase in the fluorescence due the increase of the hydrophobicity in their environment (**Scheme 6.3b**). After cooling, the original Nile Red fluorescence was almost reached, probably due to a partial reassembly of the micelles and recovery of the initial hydrophobic environment of the Nile Red.

In a further experiment, a suspension of the loaded micelles was irradiated with low intensity UV light, and the fluorescence of Nile Red was recorded after predetermined exposure times (**Figure 6.15b**). An abrupt decrease of the fluorescence intensity was observed after irradiation, indicating that the environment of the probe becomes more hydrophilic. Such a behaviour can be related to an increase in the polarity of the micelle core due to *trans*-to-*cis* isomerisation of azobenzene accompanied by a morphological change of the micelles and the subsequent release of Nile Red into water (**Scheme 6.3b**). After 24 h, the Nile Red fluorescence was not completely recovered, pointing to that part of the Nile Red was delivered into the aqueous medium under UV irradiation as consequence of the photoinduced disruption of micelles mediated by the *trans*-to-*cis* isomerisation of the azobenzene chromophores.

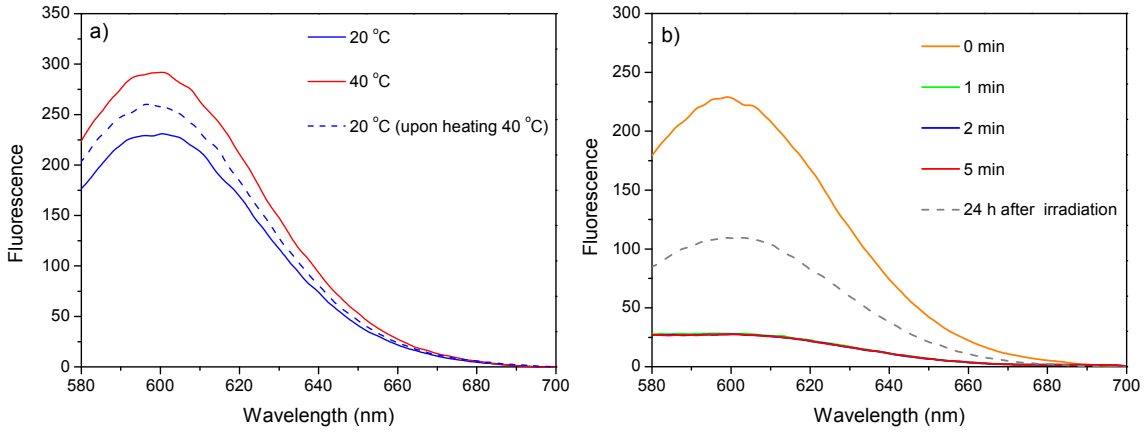

Figure 6.15 *Emission spectra of the Nile Red encapsulated micelles of* ***PAZO$_{17}$-(PDEAA$_{55}$)$_3$*** *(concentration of 1 mg/mL) recorded at a) different temperatures and b) different irradiation times at 20ºC*

6.4 Conclusions

Combination of ATRP, RAFT polymerization and CuAAC has been employed for the preparation of three miktoarm polymers composed of a photo responsive arm, **$PAZO_{17}$**, and three thermoresponsive **$PDEAA_m$** arms, containing different philic/phobic ratio ranging from 56/44 to 26/74. Only a stable micellar solution in water was obtained for **$PAZO_{17}$-$(PDEAA_{55})_3$**

A dual response of the **$PAZO_{17}$-$(PDEAA_{55})_3$** micelles was demonstrated. Collapse of the micelles takes place either upon heating and reversible morphological changes accompanied by partial distortion of the micelles occurred by UV irradiation.

The ability to act as controlled delivery systems was investigated *via* encapsulation of hydrophobic molecules such as Nile Red. Upon heating, it was found that the fluorescence probe is retained in the micellar core, while light induced micelles deformation provoked controlled Nile Red release.

6.5 Experimental section

Materials

Experimental details for the synthesis of 6-[4-(4'-isobutyloxyphenylazo) phenoxy]hexyl methacrylate **(mAZO)** and 2,2,2-tris(azidomethyl)ethanol solution are given in Chapter 5. The alkyne functionalised CTA, prop-2-yn-1-yl 2-(((ethylthio)carbonothioyl)thio)-2-methylpropanoate, was provided by B.Schmidth (Macroarc group, KIT).[20,26] 2,2'-Azobis(2-methylpropionitrile) (AIBN) was recrystallised twice from ethanol. *N,N*-diethylacrylamide was passed over a short column of basic alumina prior to use. All other reagents were purchased from Sigma-Aldrich and used as received without further purification.

6.5.1 Experimental Details for the Synthesis of the Azopolymer $(N_3)_3$-$PAZO_{17}$

Synthesis and Characterisation of the Trifunctional ATRP Initiator ($(N_3)_3$-Br)

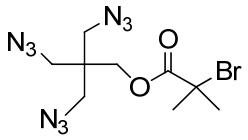

$(N_3)_3$-Br

2,2,2-tris(azidomethyl)ethanol, **$(N_3)_3$-OH**, solution (3.41 g, 4.50 mmol, 27 wt% in toluene) was placed in a round bottom flask and diluted with dry toluene (6 mL). The reaction flask was flushed with argon and cooled in an ice bath. Triethylamine (0.8 mL, 5.63 mmol) and α-bromoisobutyryl bromide (0.7 mL, 5.63 mmol) were added. The mixture was stirred at room temperature overnight under argon atmosphere. The white precipitate formed was filtered off, and the solution was washed twice with HCl 0.1 N, twice with NaOH 0.1 N, and then with water. Caution!! The organic solution was concentrated, but not higher than to 1 M in azide. The final concentration of the triazide was determined by ^{1}H-NMR (33 wt%). Yield 90%. ^{1}H-NMR (250 MHz, $CDCl_3$, toluene peaks omitted) δ (ppm): 4.06 (s, 2H), 3.37 (s, 6H), 1.93 (s, 6H).

ATRP Polymerization

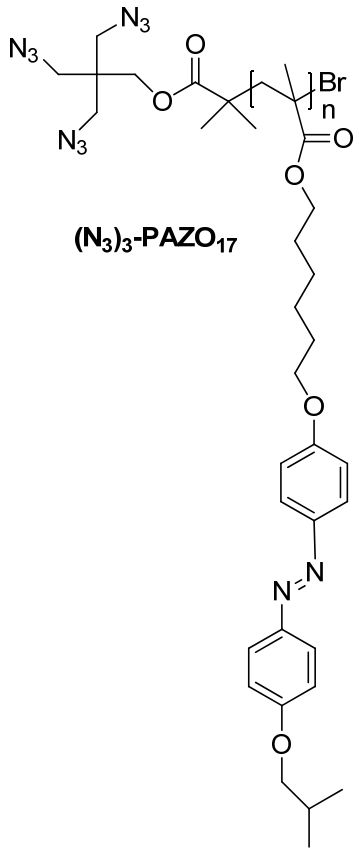

$(N_3)_3$-PAZO$_{17}$

Azobenzene-containing methacrylate (**mAZO**) (0.20 g, 0.46 mmol), initiator solution (21.6 mg of a 33 wt% solution in toluene, 20.2 µmol,) and CuBr (2.8 mg, 20.2 µmol) were added to a Schlenk tube. *N,N,N',N'',N''*-pentamethyldiethylenetriamine (PMDETA) (4.0 µL, 20.20 µmol) and deoxygenated toluene (1 mL) were added with an argon-purged syringe, and the flask was further degassed by three freeze-pump-thaw cycles and flushed with argon. The reaction mixture was stirred under an argon atmosphere at 80 ºC for 24 h. The mixture was diluted with THF and subsequently passed through a short column of neutral alumina. The solvent was partially evaporated and the resulting polymer solution was carefully precipitated into cold methanol. Yield 75%. IR (KBr), ν (cm^{-1}): 2103, 1727, 1600, 1581, 1500, 1248, 1147, 840. ^{1}H-NMR ($CDCl_3$, 400MHz) δ (ppm): 7.80-7.74 (m), 6.99-6.76 (m, Ar), 4.00-3.85 (m), 3.82-3.64 (m), 3.27 (s), 2.16-2.02 (m), 1.98-1.57 (m), 1.56-1.35 (m), 1.33-1.19 (m), 1.01-0.87 (m). Anal. Calc: C, 72.39%; H, 8.00 %; N, 9.54 % Found: C, 71.89 %; H, 7.96 %; N, 8.91%

6.5.2 Experimental Details for the Synthesis of the Thermoresponsive Polymers $PDEAA_m$

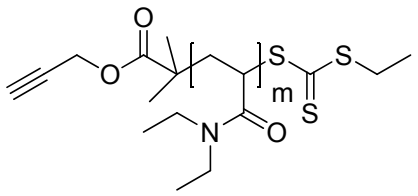

$PDEAA_m$

RAFT Polymerization

Procedure for $PDEAA_{14}$ is given as an example. Alkyne functionalised CTA (269.0 mg, 1.03 mmol), *N,N*-diethylacrylamide (10.00 g, 78.62 mmol), azobisisobutyronitrile (AIBN) (15.0 mg, 0.09 mmol), and DMF (45 mL) were added into a Schlenk-tube. The reaction mixture was degassed by three freeze-pump-thaw cycles and flushed with argon, placed in an oil bath at 60 °C and removed after 1 h. The tube was subsequently cooled with liquid nitrogen to stop the reaction. The residue was dialyzed against deionised water with a SpectraPor® membrane (MWCO = 1000 Da) for 3 days at room temperature. The solution was freeze-dried to yield the polymer as yellow solid. Yield 20-30%.

Characterisation Data for $PDEAA_{14}$: IR (KBr), ν (cm^{-1}): 1728, 1635, 1451, 1381. ^{1}H-NMR ($CDCl_3$, 400MHz) δ (ppm): 4.71 (m), 3.71-2.88 (m), 2.85-2.22 (m), 2.01-1.48 (m), 1.43-0.88 (m). Anal. Calc: C, 63.58 %; H, 9.79 %; N, 9.52 %; S, 4.67 % Found: C, 64.05 %; H, 10.21 %; N, 9.12 %; S, 4.55 %.

Characterisation Data for $PDEAA_{22}$: IR (KBr), ν (cm^{-1}): 1728, 1635, 1451, 1381. ^{1}H-NMR ($CDCl_3$, 400MHz) δ (ppm): 4.71 (m), 3.71-2.88 (m), 2.85-2.22 (m), 2.01-1.48 (m), 1.43-0.88 (m). Anal. Calc: C, 64.42 %; H, 9.96 %; N, 1.02%; S, 3.13 % Found: C, 65.07 %; H, 10.25 %; N, 0.82 %; 3.68 S, %

Characterisation Data for $PDEAA_{55}$: IR (KBr), ν (cm^{-1}): 1728, 1635, 1451, 1381. ^{1}H-NMR ($CDCl_3$, 400MHz) δ (ppm): 4.71 (m), 3.71-2.88 (m), 2.85-2.22 (m), 2.01-1.48 (m), 1.43-0.88 (m). Anal. Calc: C, 65.22 %; H, 10.21 %; N, 10.64 %; S, 1.33 % Found: C, 65.92 %; 10.68 H, %; N, 9.98%; S, 0.99%

6.5.3 Experimental Details for the Synthesis of the Miktoarm Polymers

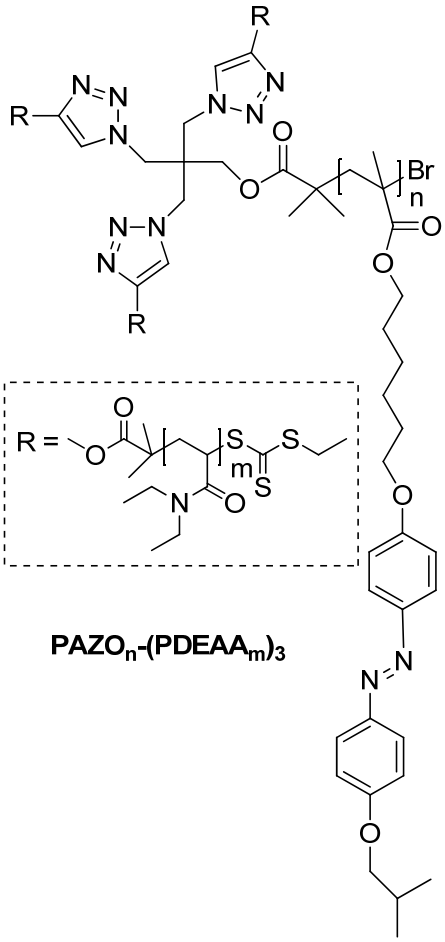

PAZO$_n$-(PDEAA$_m$)$_3$

General Procedure for Coupling Reactions

(N$_3$)$_3$-PAZO$_{17}$ (1eq), 1.2 fold excess of alkyne functionalised **PDEAA$_m$** (3.6 eq) and two-fold excess of CuBr were placed into a Schlenk tube. Two-fold excess of PMDETA and deoxygenated THF (around 1 mL per 100 mg of polymer) were added with an argon-purged syringe, and the flask was further degassed by three freeze-pump-thaw cycles and flushed with argon. The reaction mixture was stirred at 40ºC for 48 h. Subsequently, an azido functionalised resin was added under argon flow to remove the excess of PDEAA and the reaction mixture was stirred for further 24 h. The mixture was diluted with THF, the resin was filtered off and then passed through a short column of neutral alumina. The solvent was partially evaporated and the resulting polymer solution was carefully precipitated into cold ethanol. Yield 75-85%.

Characterisation Data for $PAZO_{17}$-$(PDEAA_{14})_3$: IR (KBr), ν (cm^{-1}): 1728, 1635, 1600, 1583, 1499, 1463, 1253, 841. ^{1}H-NMR ($CDCl_3$, 400MHz) *δ* (ppm): 7.92-7.73 (m), 6.92-6.74 (m), 4.30-4.24 (s), 4.01-3.82 (m), 3.80-3.62 (m), 3.60-2.92 (m), 2.75-2.29 (m), 2.14-2.02 (m), 2.01, 1.81-1.54 (m), 1.52-1.18 (m), 1.16-0.94 (m), 0.93-0.78 (m). Anal. Calc: C, 69.51 %; H, 8.87 %; N, 8.86 %; S, 2.14 % Found: C, 70.11 %; H, 9.25 %; N, 8.68 %; S, 2.42 %

Characterisation Data for $PAZO_{17}$-$(PDEAA_{22})_3$: IR (KBr), ν (cm^{-1}): 1728, 1635, 1601, 1582, 1501 (Ar), 1463, 1253, 841 (Ar). ^{1}H-NMR ($CDCl_3$, 400MHz) *δ* (ppm): 7.92-7.73 (m), 6.92-6.74 (m), 4.30-4.24 (s), 4.01-3.82 (m), 3.80-3.62 (m), 3.60-2.92 (m), 2.75-2.29 (m), 2.14-2.02 (m), 2.01, 1.81-1.54 (m), 1.52-1.18 (m), 1.16-0.94 (m), 0.93-0.78 (m). Anal. Calc: C, 69.90 %; H, 9.12 %; N, 9.26; % S, 2.14 % Found: C, 70.51 %; H, 9.42 %; N, 8.88 %; S, 1.92 %

Characterisation Data for $PAZO_{17}$-$(PDEAA_{45})_3$: IR (KBr), ν (cm^{-1}): 1729, 1635, 1600, 1582, 1500 (Ar), 1463, 1250, 839 (Ar). ^{1}H-NMR (400 MHz, $CDCl_3$) δ (ppm): 7.92-7.73 (m), 6.92-6.74 (m), 4.30-4.24 (s), 4.01-3.82 (m), 3.80-3.62 (m), 3.60-2.92 (m), 2.75-2.29 (m), 2.14-2.02 (m), 2.01, 1.81-1.54 (m), 1.52-1.18 (m), 1.16-0.94 (m), 0.93-0.78 (m). Anal. Calc: C, 67.70 %; H, 9.60 %; N, 10.02; % S, 0.01 % Found: C, 67.15 %; H, 10.22 %; N, 9.85 %; S, --%

6.5.4 General procedures

The preparation of the vesicles, determination of the critical aggregation concentration (CAC), the sample preparation for the different microscopies techniques as well as the irradiation experiments has been performed following the same procedures described in Chapter 4.

LSCT calculation

The LCST was calculated by DSC in a Q20 from TA Instruments using a 10 wt% solution of **$PDEAA_{55}$** in water sealed in an aluminium pan that calculated as the peak maximum in the first derivative of heat flow.

References

1 Savic, R.; Luo, L. B.; Eisenberg, A.; Maysinger, D. Micellar nanocontainers distribute to defined cytoplasmic organelles. *Science* **2003**, 300, 615-618.

2 Riess, G. Micellization of block copolymers. *Progress in Polymer Science* **2003**, 28, 1107-1170.

3 Gohy, J.-F. in *Block Copolymers II* Vol. 190 *Advances in Polymer Science* (ed Volker Abetz) Ch. 48, 65-136 (Springer Berlin Heidelberg, 2005).

4 Lavasanifar, A.; Samuel, J.; Kwon, G. S. Poly(ethylene oxide)-block-poly(l-amino acid) micelles for drug delivery. *Advanced Drug Delivery Reviews* **2002**, 54, 169-190.

5 Adams, M. L.; Lavasanifar, A.; Kwon, G. S. Amphiphilic block copolymers for drug delivery. *Journal of Pharmaceutical Sciences* **2003**, 92, 1343-1355.

6 Schacher, F. H.; Rupar, P. A.; Manners, I. Functional Block Copolymers: Nanostructured Materials with Emerging Applications. *Angewandte Chemie International Edition* **2012**, 51, 7898-7921.

7 Gil, E. S.; Hudson, S. M. Stimuli-reponsive polymers and their bioconjugates. *Progress in Polymer Science* **2004**, 29, 1173-1222.

8 Stuart, M. A.; Huck, W. T.; Genzer, J.; Müller, M.; Ober, C.; Stamm, M.; Sukhorukov G. B.; Szleifer, I.; Tsukruk, V. V.; Urban, M.; Winnik, F.; Zauscher, S.; Luzinov, I.; Minko, S. Emerging applications of stimuli-responsive polymer materials. *Nature Materials* **2010**, 9, 101-113.

9 Liu, F.; Urban, M. W. Recent advances and challenges in designing stimuli-responsive polymers. *Progress in Polymer Science* **2010**, 35, 3-23.

10 Idziak, I.; Avoce, D.; Lessard, D.; Gravel, D.; Zhu, X. X. Thermosensitivity of Aqueous Solutions of Poly(N,N-diethylacrylamide). *Macromolecules* **1999**, 32, 1260-1263.

11 Abulateefeh, S. R.; Spain, S. G.; Aylott, J. W.; Chan, W.C.; Garnett, M.C.; Alexander C. Thermoresponsive Polymer Colloids for Drug Delivery and Cancer Therapy. *Macromolecular Bioscience* **2011**, 11, 1722-1734.

12 Gaucher, G.; Dufresne, M. H.; Sant, V. P.; Kang, N.; Maysinger, D.; Leroux, J. C. Block copolymer micelles: preparation, characterization and application in drug delivery. *Journal of Controlled Release* **2005**, 109, 169-188.

13 Xu, J.; Liu, S. Polymeric nanocarriers possessing thermoresponsive coronas. *Soft Matter* **2008**, 4, 1745-1749.

14 Hu, Z.; Cai, T.; Chi, C. Thermoresponsive oligo(ethylene glycol)-methacrylate-based polymers and microgels. *Soft Matter* **2010**, 6, 2115-2123.

15 Pasparakis, G.; Vamvakaki, M. Multiresponsive polymers: nano-sized assemblies, stimuli-sensitive gels and smart surfaces. *Polymer Chemistry* **2011**, 2, 1234-1248.

16 Jochum, F. D.; Theato, P. Temperature- and light-responsive smart polymer materials. *Chemical Society Reviews* **2013.** DOI: 10.1039/C2CS35191A

17 Feng, Z.; Lin, L.; Yan, Z.; Yu, Y. L. Dual Responsive Block Copolymer Micelles Functionalized by NIPAM and Azobenzene. *Macromolecular Rapid Communications* **2010**, 31, 640-644.

18 Jochum, F. D.; Theato, P. Thermo- and light responsive micellation of azobenzene containing block copolymers. *Chemical Communications* **2010**, 46, 6717-6719.

19 Boissiere, O.; Han, D.; Tremblay, L.; Zhao, Y. Flower micelles of poly(N-isopropylacrylamide) with azobenzene moieties regularly inserted into the main chain. *Soft Matter* **2011**, 7, 9410-9415.

20 Schmidt, B. V. K. J.; Hetzer, M.; Ritter, H.; Barner-Kowollik, C. Miktoarm star polymers via cyclodextrin-driven supramolecular self-assembly. *Polymer Chemistry* **2012**, 3, 3064-3067.

21 Goodwin, A. P.; Mynar, J. L.; Ma, Y. Z.; Fleming, G. R.; Frechet, J. M. J. Synthetic micelle sensitive to IR light via a two-photon process. *Journal of the American Chemical Society* **2005**, 127, 9952-9953.

22 Mynar, J. L.; Goodwin, A. P.; Cohen, J. A.; Ma, Y.; Fleming J. R.; Fréchet J.M.J. Two-photon degradable supramolecular assemblies of linear-dendritic copolymers. *Chemical Communications* **2007**, 2081-2082.

23 Ferreira, S. A.; Coutinho, P. J. G.; Gama, F. M. Self-Assembled Nanogel Made of Mannan: Synthesis and Characterization. *Langmuir* **2010**, 26, 11413-11420.

24 Dong, J.; Wang, Y.; Zhang, J.; Zhan, X.; Zhu, S.; Yang, H.; Wang, G. Multiple stimuli-responsive polymeric micelles for controlled release. *Soft Matter* **2013**, 9, 370-373.

25 Jin, Q.; Liu, G.; Ji, J. Micelles and reverse micelles with a photo and thermo double-responsive block copolymer. *Journal of Polymer Science Part A: Polymer Chemistry* **2010**, 48, 2855-2861.

26 Díaz, D. D.; Punna, S.; Holzer, P.; McPherson, A. K.;Sharpless, K. B.;Fokin, V. V.; Finn, M. G. Click chemistry in materials synthesis. 1. Adhesive polymers from copper-catalyzed azide-alkyne cycloaddition. *Journal of Polymer Science Part A: Polymer Chemistry* **2004**, 42, 4392-4403.

CHAPTER 7

Light Responsive Surfaces

Published in *Adv. Funct. Mat.* **2013**.

DOI: 10.1002/adfm.201203602

7.1 Introduction and Aims

Engineering surface chemistry and topography affords technological advancements for a variety of applications ranging from biosensors to microelectronics.[1,2] Surface functionalisation is an essential process for the construction of patterned surfaces and microarrays, surface immobilisation of biological molecules or just to tune or confer new properties to substrates. It can be completed by physical deposition (physisorption), but covalent immobilisation (chemisorption) is preferable because of the added stability of the coating. Smart functional surfaces can be created by covalent inmmobilisation of stimuli responsive molecules to tailor-made properties and generate substrates with switchable properties such as pH or wetability.[3-5] In particular, the attachment of photoresponsive molecules onto surfaces is very attractive as the properties of the surfaces can be controlled by light as an external and non contact stimulus (see section 1.4). One critical aspect of the immobilisation is retaining the activity of the molecule once it is immobilised onto the surface.

To cover demands, the development of fabrication methods for soft material surfaces with precise control over functionality, architecture, reactivity and domain size is required. During the last years, development of the 'click chemistry' methods has had an enormous impact on surface functionalisation.[6,7] These reactions provide an efficient strategy because of the functional group versatility, high yields with no side products and simple reaction conditions. Nevertheless, in some applications an efficient reaction is not enough since patterning of the surface with spatial control of chemical functionality might also be required. The utilisation of light initiated 'click reactions' represents a powerful ligation protocol. These UV induced reactions include thiol-ene/thiol-yne coupling,[8] 1,3-dipolar cycloaddition reactions[9,10] and Diels–Alder reactions[11] among others (**Scheme 7.1**).

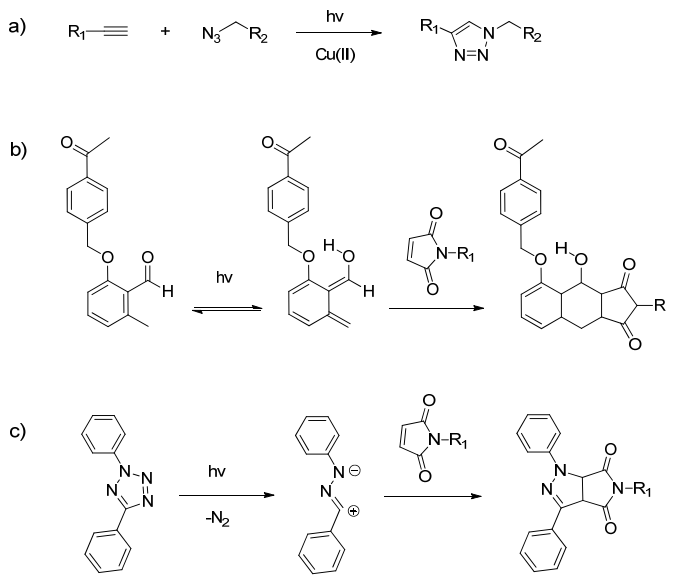

Scheme 7.1 *Examples of light induced reactions employed for the preparation of patterning surfaces: a) CuAAC,[9,12] b) photoenol chemistry,[13] c) NITEC reaction[14]*

Bowman and coworkers have recently developed a new photochemical protocol for the in situ generation of Cu(I) from a Cu(II) complex using light to catalyze a CuAAC reaction between azides and alkynes. Patterned material fabrication was achieved with this reaction by using standard photolithographic techniques (**Figure 7.1**).[9,12] Barner-Kowollik and coworkers have introduced a novel procedure for click conjugations based on a Diels–Alder reaction of hydroxy-o-quinodimethanes (photoenols) generated by photoisomerisation of o-methylphenyl ketones or aldehydes.[15,16] Photoenols are highly reactive dienes that can react with activated alkenes. This chemistry has been successfully applied to polymer conjugation as well as to surface patterning using different maleimide derivatives.[17] The nitrile imine-mediated 1,3-dipolar cycloaddition of a tetrazole and an alkene derivative (NITEC reaction) was firstly reported by Huisgen and Sustmann in 1967[18] and recently significantly expanded by Lin and coworkers.[19] The NITEC reaction proceeds *via* the generation of a nitrile imine dipole by irradiation with UV light of a tetrazole compound. The nitrile imine intermediate is able to react spontaneously with a large variety of alkenes forming a pyrazoline cycloadduct in near quantitative yields.[19-21] This strategy have also been successfully employed for room temperature grafting of

polymers onto variable surfaces such as silicon or cellulose by Barner-Kowollik and coworkers.[22]

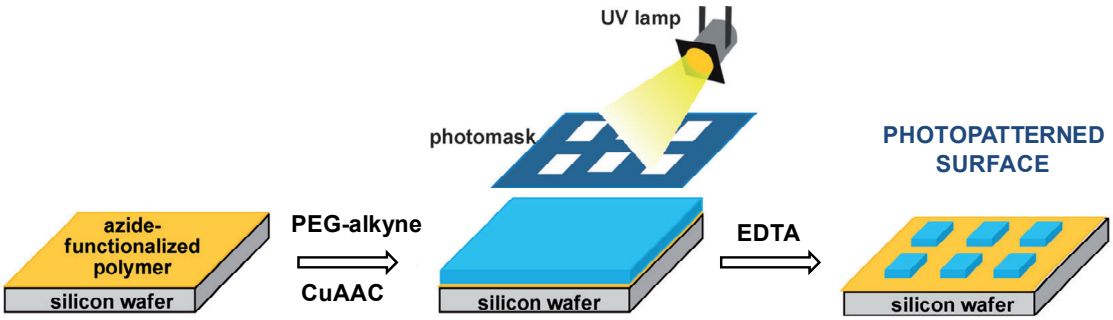

Figure 7.1 *Photopatterning of an azide functionalised polypropylene using a photomask (Image adapted from ref. 9)*

In the current chapter, the preparation and study of responsive surfaces using exclusively light as a stimulus for both the preparation of azobenzene modified surfaces and the subsequent control of the surface properties is approached by using chromophores analogues to those described in previous chapters. The preparation of these spatially controlled photoresponsive surfaces is addressed by use of the NITEC reaction using azobenzene dipolarophiles as it is collected in **Scheme 7.2**. In this strategy, the previously activated surfaces were modified with a silane derivative containing a tetrazole group. Then, a NITEC reaction between tetrazole and dipolarophiles was employed to obtain the photoresponsive surfaces. The dipolarophiles consist of a maleimide containing either a single azobenzene (**AZO1**) moiety or a first-generation dendron carrying two azobenzene units (**AZO2**). To the best of our knowledge, this reaction has not been used before in the presence of species exhibiting strong absorption in the UV−Vis region. Again, 4-isobutyloxyazobenzene unit was chosen due to the increment in polarity difference between the *trans* and the *cis* isomers.

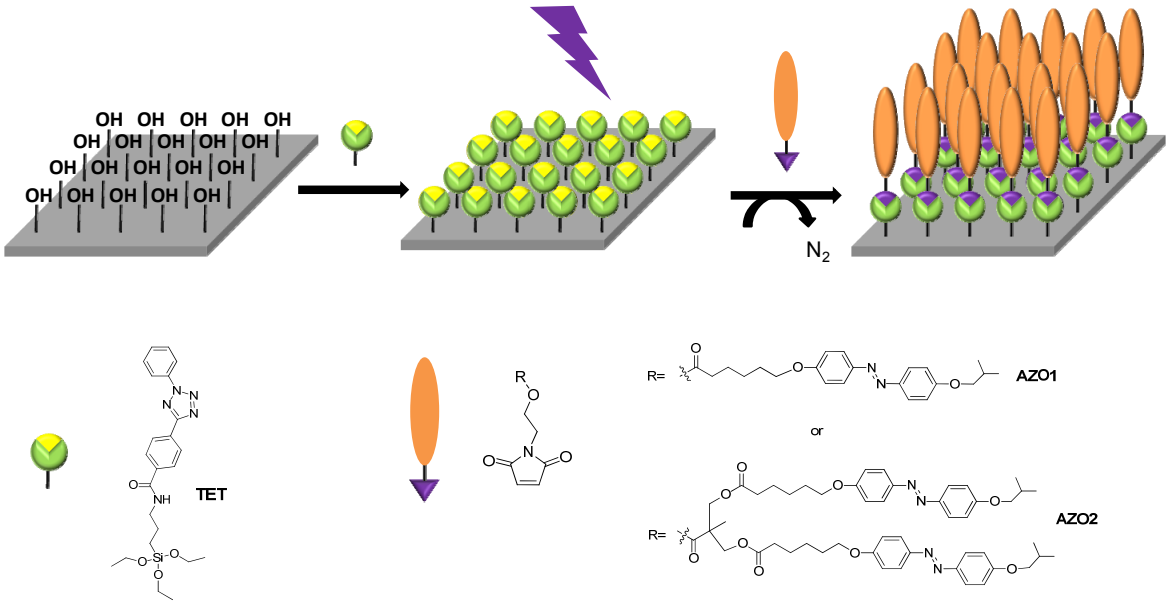

Scheme 7.2 *Azobenzene functionalisation of surfaces via the NITEC reaction*

7.2 Tasks and Methods

- Synthesis and characterisation of a tetrazole functionalised silane (**TET**) and two maleimide-containing azo derivatives containing either a single azobenzene moiety (**AZO1**) or a first-generation dendron carrying two azobenzene units derivates (**AZO2**).

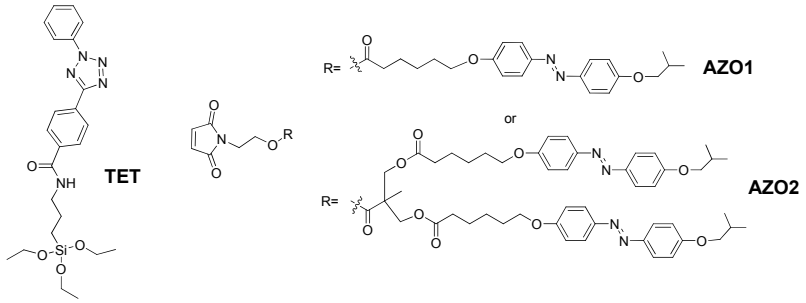

Figure 7.2 *Chemical structure of the aimed tetrazole functionalised silane (**TET**) and the two aimed maleimide-containing azobenzene derivates (**AZO1** and **AZO2**)*

- Study of the viabilility of the NITEC reaction in solution using maleimide containing azobenzene derivatives as dipolarophiles.

- Preparation and characterisation of azobenzene functionalised surfaces by employing NITEC reaction (**Scheme 7.2**)

- Preparation of azobenzene patterned surfaces

- Study of the photoresponsive behaviour of the functionalised surfaces

7.3. Results and Discussion

7.3.1 Synthesis and Characterisation

The tetrazole functionalised silane (**TET)** and the azo derivatives **AZO1** and **AZO2**, were first prepared. The 2,5-disubstituted tetrazole (**18**) was synthesised by reaction of the phenylsulfonylhydrazone, terephthalaldehyde and benzene-diazonium salt.[19] The subsequent reaction of tetrazole (**18**) with 3-aminopropyltriethoxysilane gave the target tetrazole functionalised silane (**TET**)[22] (**Scheme 7.3**). As the photolysis of diaryl tetrazoles easily takes place upon light exposure, the tetrazole derivates were storaged and manipulated in the dark. It should be noted that in spite of the mentioned precautions, the tetrazole derivatives were obtained in low yields.

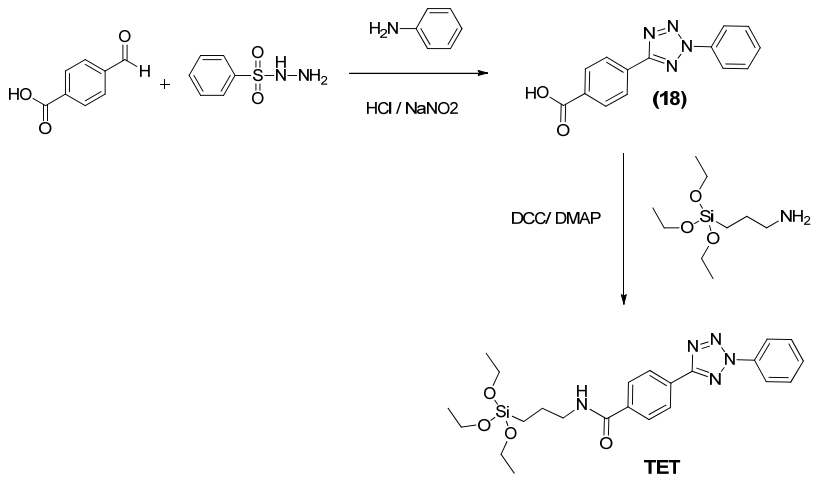

Scheme 7.3 *Synthesis of the tetrazole containing silane* ***TET***

The synthesis of the target maleimide containing azobenzene **AZO1** and **AZO2** is depicted in **Scheme 7.4**. **AZO1** was prepared in two steps starting from 6-[4-(4'-isobutyloxyphenylazo) phenyloxy]hexanoic acid, **isoAZOb**, whose synthesis was described in Chapter 3. Esterification of **isoAZOb** with the protected maleimide containing a hydroxyl group (**20**) using DCC/DPTS rendered the intermediate (**21**) that was readily deprotected by a heat induced retro-Diels-Alder reaction in quantitative yields.

The synthesis of the first-generation azodendron derived from bis-MPA with a maleimide group at the focal point, **AZO2**, was prepared in several steps. First, esterification of the acetal protected bis-MPA (**1**) with the hydroxyl protected maleimide (**20**) and subsequent hydrolysis of the acetal using an acidic resin render the hydroxyl terminated intermediate (**23**). The 4-isobutyloxyazobenzene unit was appended by an esterification reaction between the acid chloride of **isoAZOb** and (**23**) to give compound (**24**). Finally, compound **AZO2** was afforded by a heat induced retro-Diels-Alder reaction of (**24**) in quantitative yields.

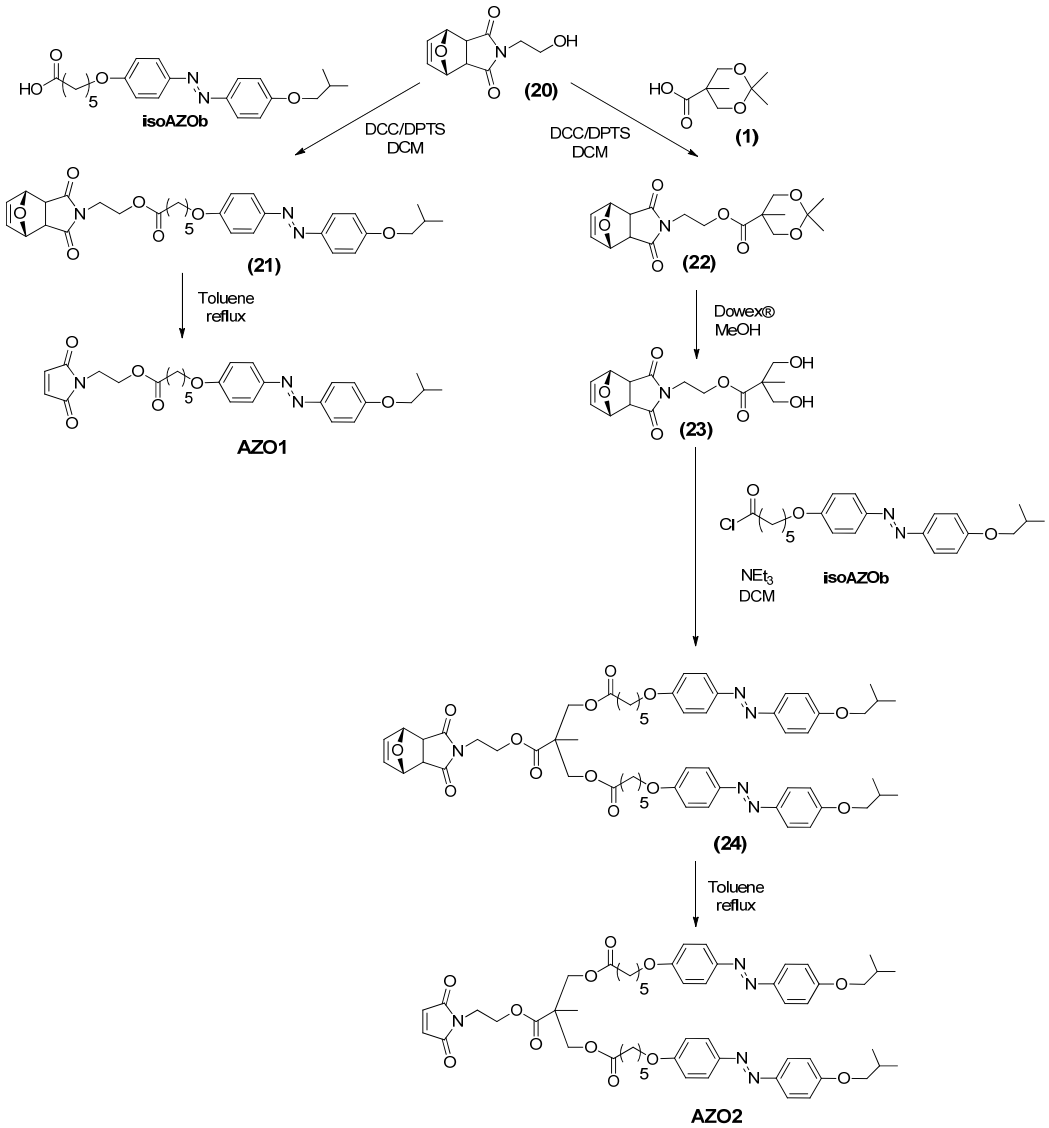

Scheme 7.4 *Synthesis of the azobenzene maleimides*

FTIR and ^{1}H-NMR spectroscopies as well as mass spectrometry (see Experimental Section) confirmed the expected structures of all intermediates and final products. **Figure 7.3** depicts ^{1}H-NMR spectrum of **AZO2** as an example. Besides the signals corresponding to the 4-isobutyloxyazobenzene moiety, a new signal at 6.70 ppm corresponding with the protons of the malimide group (see peak labelled as '*a*' in **Figure 7.3**) appeared proving the formartion of the target dipolarophile.

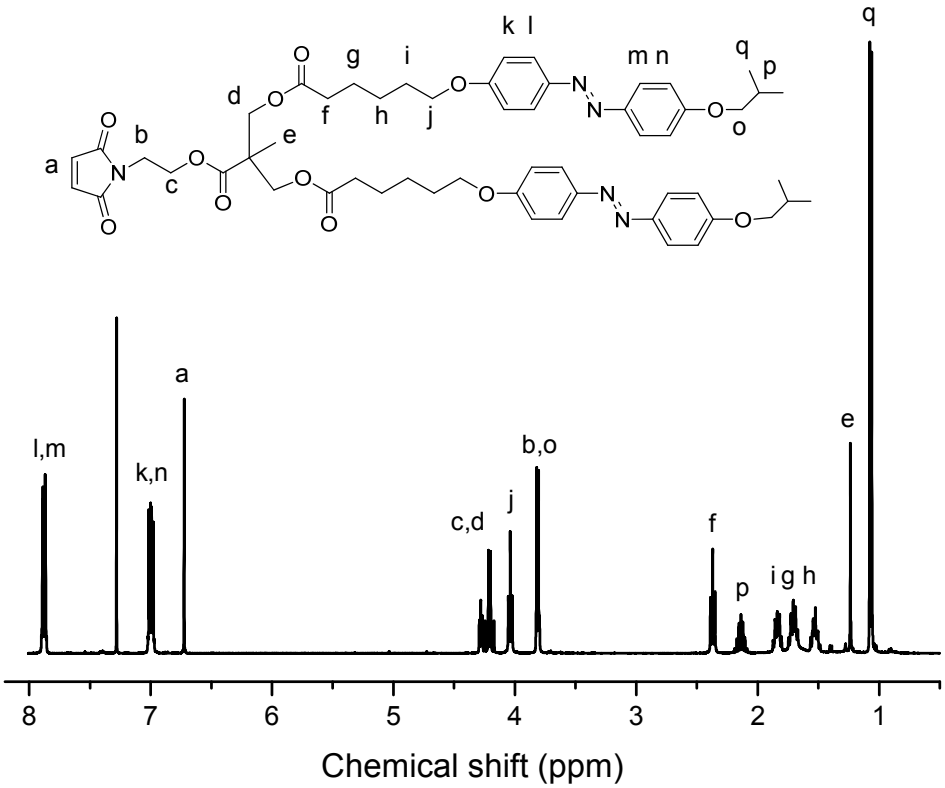

Figure 7.3 *^{1}H-NMR spectrum of the azobenzene maleimide* ***AZO2*** *in $CDCl_3$ (400 MHz)*

7.3.2 Premilinary Test of the NITEC Reaction with Azobenzene

As noted above, the NITEC approach is a very efficient light triggered ligation technique for both small molecules and macromolecular conjugation.[18-21,23-31] However, as mentioned the NITEC UV initiated reaction has not been employed before using chromophores with a strong absorption in the UV region such as azobenzenes. For this reason, a series of preliminary experiments in solution were approached using the tetrazole compound **TET** and the maleimide **AZO1** to assess and evaluate the reaction conditions as well as the conjugation efficiencies.

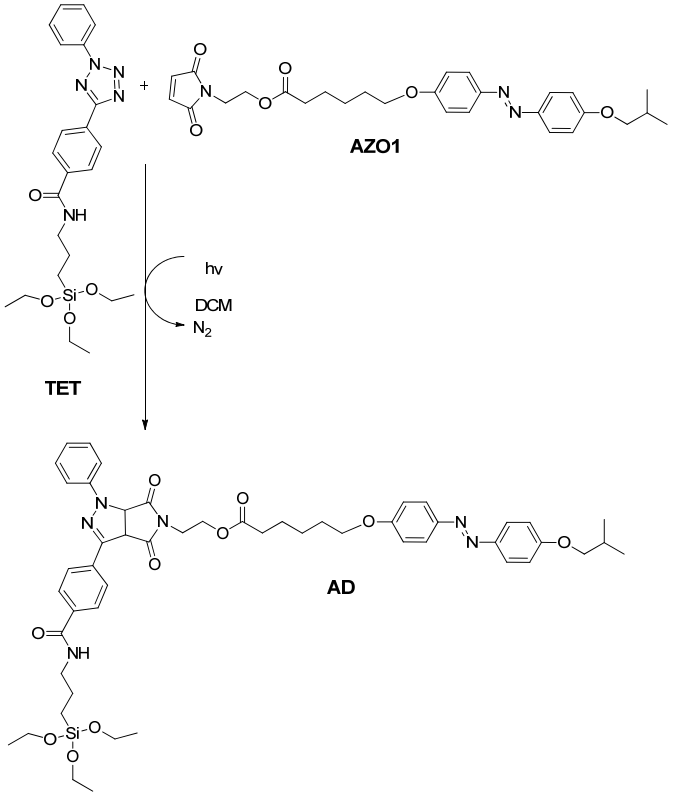

Scheme 7.5 *Synthetic scheme of the NITEC reaction in solution using the tetrazole* ***TET*** *and the maleimide* ***AZO1***

The reaction between the tetrazole functionalised silane **TET** and a 1.5-fold excess of maleimide-containing azobenzene **AZO1** was carried out in DCM (concentration of **AZO1** 7mM) at room temperature (**Scheme 7.5**). Electrospray ionisation coupled to mass spectrometry (ESI-MS) was employed to confirm the photoadduct formation.

Firstly, the selection of suitable photochemical conditions was addressed. In solution, the tetrazole **TET** shows an absorption band with the maximum at 280 nm while the *trans*-azobenzene **AZO1** presents two well described absorption bands, a strong one centred at 360 nm and a weak one at about 450 nm (**Figure 7.4**). Following a previously established procedure,[22] the reaction was performed at 254 nm, where both the tetrazole and the azobenzene chromophores present similar absorptions. Only low conversions were achieved by using a UV hand-held lamp but decomposition of the compounds occurred using a higher power light source (OSRAM Puritec HNS L 36 W). Therefore, in view of these results, a lamp with the maximum emission at 290-315 nm (Philips PL-S 9 W/12) was employed to avoid the azobenzene absorption band. This time, the formation of the desired adduct **AD** was confirmed by ESI-MS by the presence of the molecular ion peak at *m*/*z*= 949.4 $[M-H]^+$ and 971.7 $[M-Na]^+$.

Figure 7.5 depicts the evolution of the reaction. The initial ESI-MS spectrum, t=0, consist of the peaks corresponding to the initial products **TET** (*m*/*z*= 492.3 $[M-Na]^+$ and 961.3 $[2M-Na]^+$) and **AZO1** (*m*/*z*= 508.3 $[M-H]^+$ and 530.4 $[M-Na]^+$). After 20 min the formation of the coupling product **AD** was detected (*m*/*z*= 949.4 $[M-H]^+$, 971.7 $[M-Na]^+$) and after 40 min almost all tetrazole (*m*/*z*= 492.3 $[M-Na]^+$) was consumed. After 1 h, ESI-MS showed complete consumption of the tetrazole and charged ions corresponding to the photoproduct **AD** and to the azobenzene **AZO1** employed in excess (*m*/*z*= 508.3 $[M-H]^+$ and 530.4 $[M-Na]^+$) were detected. Thus, the lamp with the maximum emission at 290-315 nm is more suitable to carry out the NITEC reaction in presence of the azobenzene group.

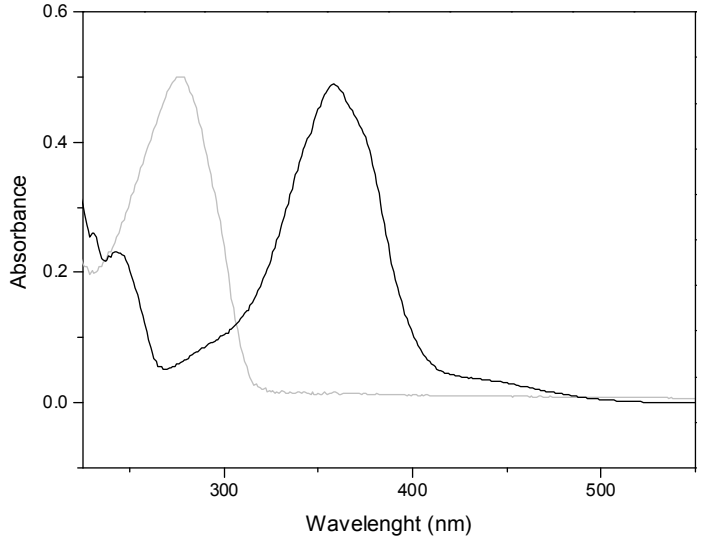

Figure 7.4 *UV spectra of the tetrazole functionalised silane* ***TET*** *(grey line) and maleimide-containing azobenzene* ***AZO1*** *(black line) solution in acetonitrile (10^{-4} M)*

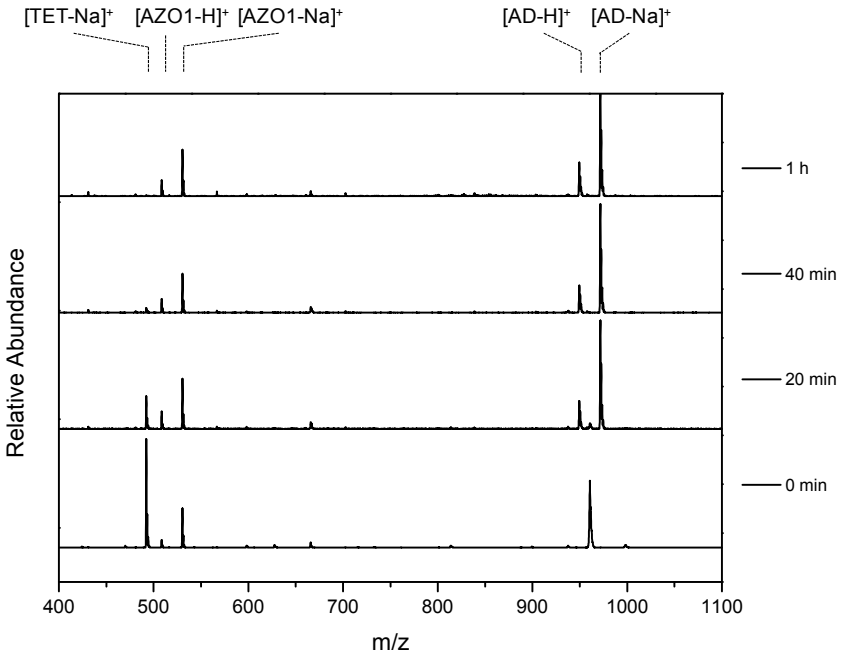

Figure 7.5 *ESI-MS spectra of the NITEC reaction depicted in Scheme 7.5 at different reaction times*

7.3.3 Azobenzene Surface Functionalisation

After evidencing the efficiency of the NITEC reaction in the presence of azobenzene and in solution, the following step was to carry out the same reaction with tetrazole functionalised silicon wafers (**Scheme 7.6**). The silicon after were cleaned and hydroxylated with Piranha solution and subsequently the covalent binding of the tetrazole containing silane was performed by heating an activated silicon wafer with **TET** in toluene at 50 ºC (see Experimental Section). The tetrazole functionalised silicon wafer (**Si-TET**) was thoroughly rinsed with fresh solvent and sonicated to ensure no physisorbed tetrazole was present onto the surface. XPS was employed to prove the functionalisation of the surface. In the XPS spectra (**Figure 7.6a**) it is possible to observe intense peaks around 285-290 eV corresponding to C 1s and around 400-402 eV attributed to N 1s. As it was reported, peaks at 286.6 eV and 288.5 eV can be assigned to carbon atoms single bonded with oxygen and nitrogen (C-O, C-N) and to carboxylic groups (-N-C=O, -O-C=O) respectively .[32,33] The N 1s spectrum presents a strong peak at 400.2 eV that can be assigned to the tetrazole species[34] and a weak one at 402.7 eV that probably correspond to positively charged nitrogen.[35]

Then, the NITEC reaction was employed to graph **AZO1** onto the surface by using the optimum conditions identified in the solution tests (290-315 nm). The **Si-TET** silicon wafer was placed in a quartz flask containing a maleimide **AZO1** solution in DCM (7 mM) and exposed to UV light (9W, 290-315 nm) The azobenzene functionalised wafers **Si-AZO1** were analysed by XPS and compared with the tetrazole functionalised one (**Si-TET**). As in the case of **Si-TET** (**Figure 7.6a**), XPS spectra of **Si-AZO1** shows peaks at 285.0 at 286.6 and 288.5 eV corresponding to C 1s and around 400.2 and 402.7 eV attributed to N 1s (**Figure 7.6b**). In order to establish comparison, the relative peak areas were calculated by using (C-O, C-N) signal at 286.6 eV as reference (**Figure 7.7**). As expected, in comparison with **Si-TET** the N / (C-O, C-N) ratio decreased from 1.12 to 0.50 on the functionalised surface **Si-AZO1** evidencing the presence of azobenzene on the surface (**Figure 7.6b**).

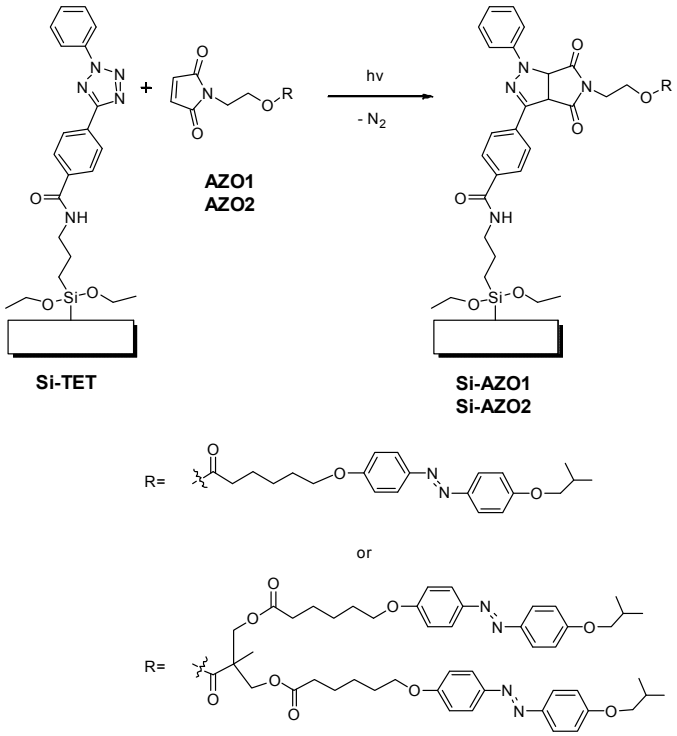

Scheme 7.6 *NITEC reaction between a tetrazole-functionalised surface and the azobenzene derivatives* ***AZO1*** *and* ***AZO2****. To simplify, only one Si-anchoring has been considered*

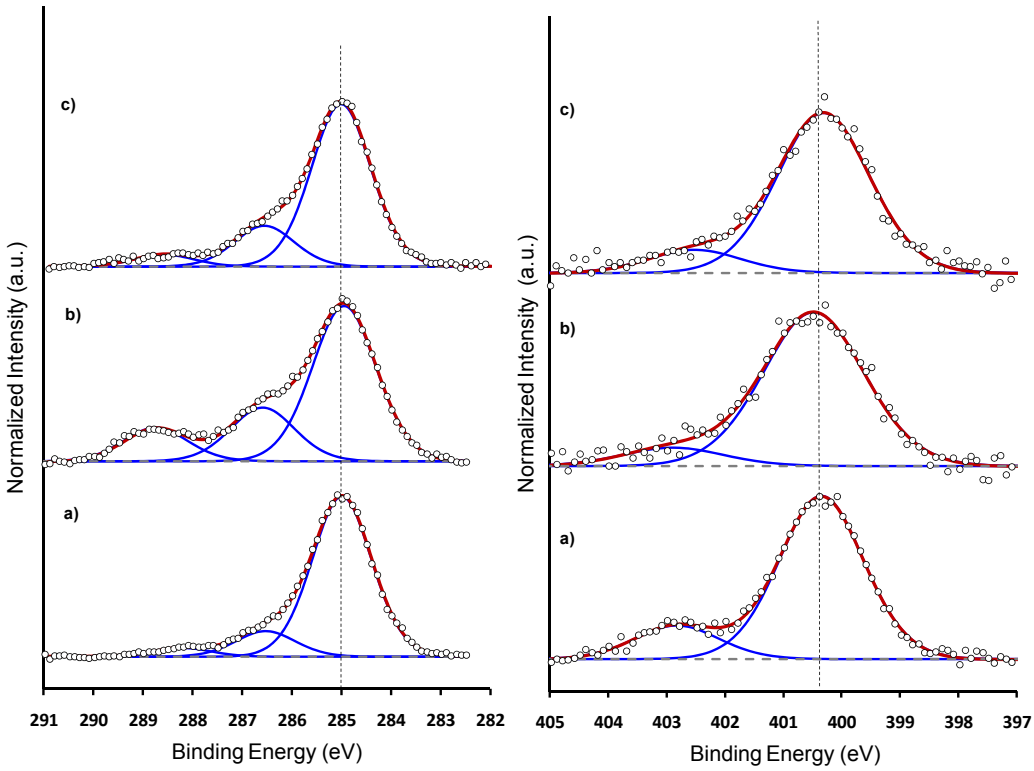

Figure 7.6 *Comparison of the C 1s (left) and N 1s (right) normalised regions of the XPS spectra of functionalised silicon wafers: a)* ***Si-TET****, b)* ***Si-AZO1*** *and c)* ***Si-AZO2***

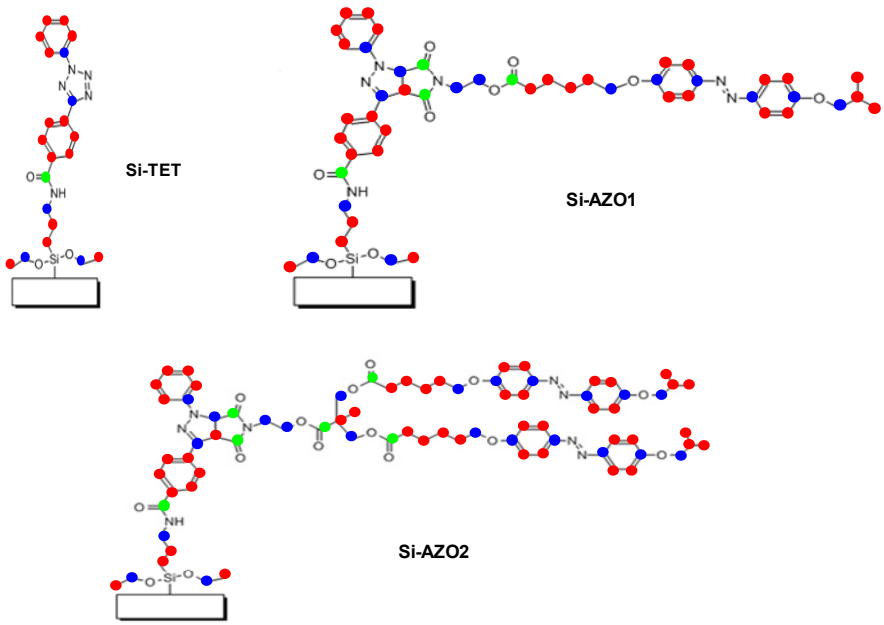

Surface	C-C, C-H	C-O, C-N	N-C=O, O-C=O	N	C-C, C-H)/ C-O, C-N	N-C=O, O-C=O/ C-O, C-N	N/ C-O, C-N
Si-TET	13	3	1	5	4.33	0.33	1.67
Si-AZO1	29	12	4	6	2.42	0.33	0.50
Si-AZO2	46	20	6	8	2.33	0.30	0.40

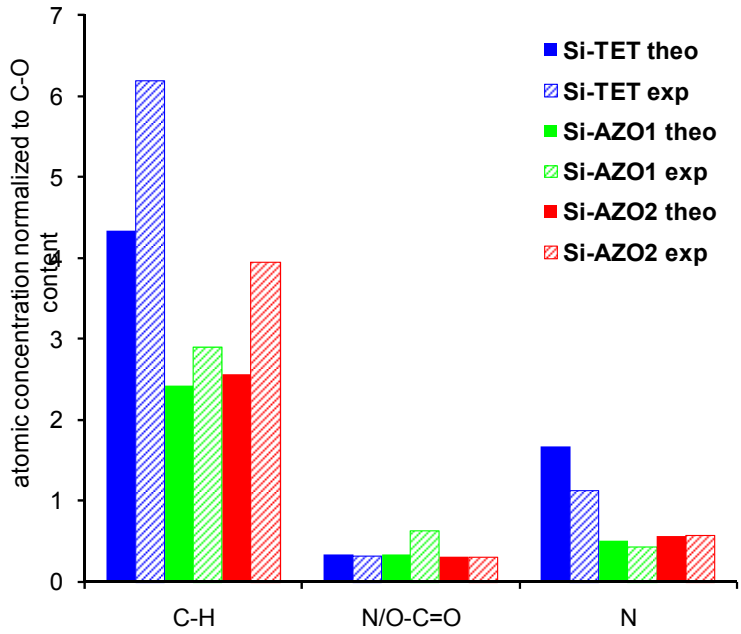

Figure 7.7 *Chemical structures and theoretical C 1s and N 1s XPS peak abundances (top) for the modified silicon wafers* ***Si-TET****,* ***AZO1*** *and* ***AZO2****. Bar chart comparing theoretical and experimental C 1s and N 1s XPS peak abundances for the silicon wafers* ***Si-TET****,* ***Si-AZO1*** *and* ***Si-AZO2*** *(bottom). For wafer* ***Si-AZO2*** *a theoretical reaction yield of 50% is assumed, the experimental data are based on 6 h reaction time. The high experimental intensity of all C-H components is due to adventitious carbon.*

The photoligation reaction was also carried out with the first-generation azodendron **AZO2**. The silicon wafer **Si-TET** was immersed into a solution of **AZO2** in DCM (3.5 mM) in a quartz flask and irradiated at 290-315 nm. The functionalised silicon wafer **Si-AZO2** was analysed by XPS (**Figure 7.6c**). The relative areas of the signals were again compared using C-O, C-N as reference and it was observed that the N/(C-O, C-N) ratio decreased from 1.12 in for **Si-TET** to 0.57 for **Si-AZO2** (**Figure 7.7**). Nevertheless, in this case the experimental result is not in agreement with the theoretical value (N/(C-O, C-N) ratio of 0.40) evidencing incomplete functionalisation of the surface.

In order to optimise the efficiency of the photoconjugation, the progress of the reaction with **AZO2** was followed by XPS from the changes in N/(C-O, C-N) ratio (**Figure 7.8)** The best result was achieved with 6 h of reaction for which a functionalisation close to 50% was reached according to the XPS data. The lower efficiency might be attributed to a higher steric hindrance in the case of the azodendron **AZO2** in comparison with the single molecule **AZO1**.

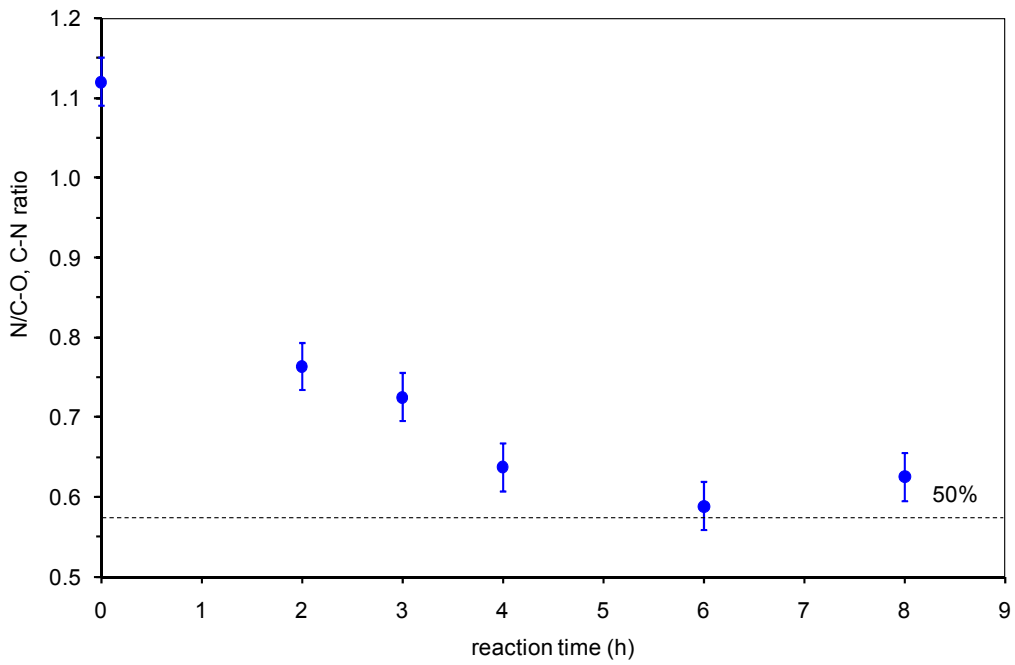

Figure 7.8 *Time dependent evolution of the XPS N / (C-O, C-N) ratio of* ***Si-AZO2****. Dashed line indicates the assumed max. 50% reaction yield, 0 h reaction time represents pure wafer* ***Si-TET****. Error bars represent standard deviations of the measurements.*

7.3.4 Azobenzene Surface Patterning

To prove the spatial control in azobenzene functionalisation, the concept was extended to the formation of a micropatterned substrate by using a photomask. Tetrazole functionalised surfaces, **Si-TET**, were covered with a shadow mask containing a micropattern, immersed in an azobenzene solution of **AZO1** or **AZO2** and UV illuminated in the same conditions as before (**Scheme 7.7**). After removing the mask and washing the surfaces, the patterns were revealed by time-of-flight secondary ion mass spectrometry (ToF-SIMS). This is a surface-sensitive analytical method providing chemical images generated by collecting mass spectra at a high lateral resolution (see Appendix).

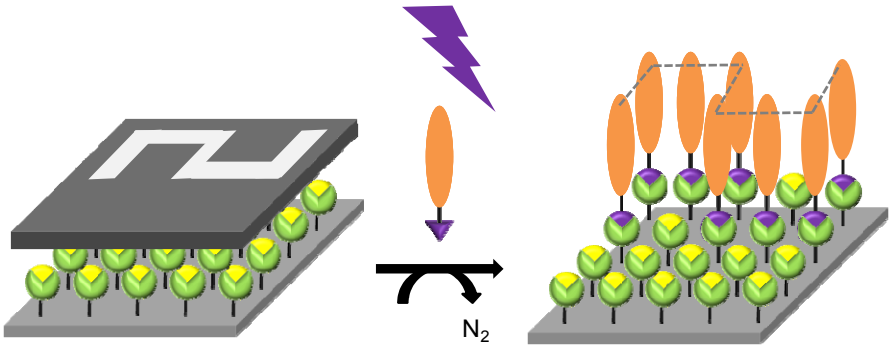

Scheme 7.7 *Azobenzene functionalisation of the surfaces with spatial control employing a micropatterned shadow mask.*

Figure 7.9a and **Figure 7.9b** depicts the ToF-SIMS images of the patterned surfaces. Two azobenzene fragments, $C_{16}H_{17}N_2O_2^-$ (*m*/*z*=269.2) and $C_{12}H_8N_2O_2^-$ at 212.1 *m*/*z,* were exclusively detected in the UV exposed areas, and not in the non irradiated regions. Further, the $[M\text{-}Na]^-$ ions (*m*/*z*=530.4 for **AZO1** and 1012.5 for **AZO2**) cannot be detected after the photografting step discarding physisorption of the precursor molecules **AZO1** and **AZO2** and consequently unambiguously evidencing a covalent attachment. **Figure 7.10** shows as an example the SIMS data in the region of the molecular ion of **AZO2**, where $[M\text{-}Na]^-$ was not detected in the case of the covalently functionalised surface.

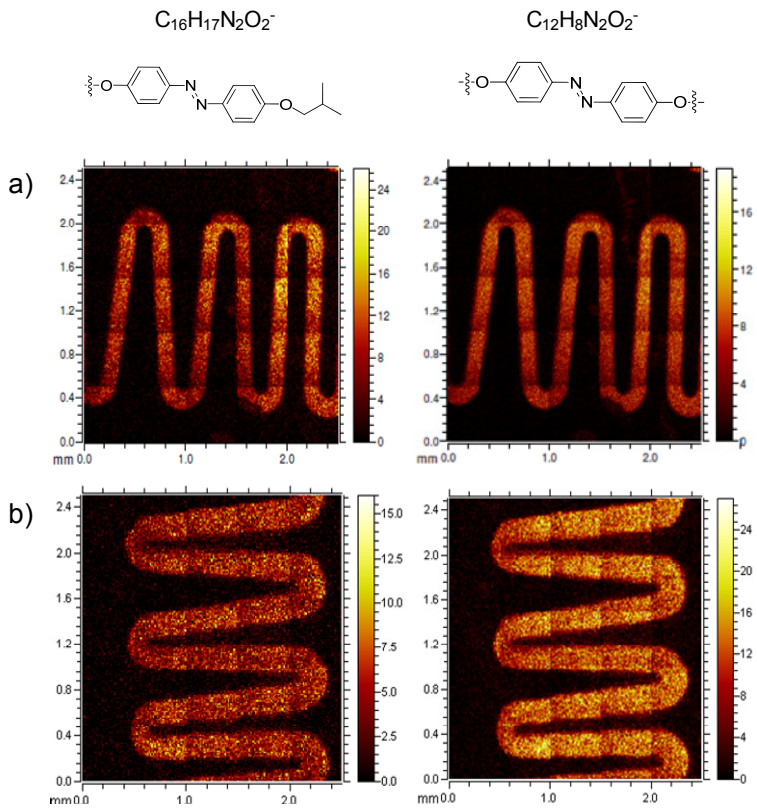

Figure 7.9 *ToF-SIMS images of a) the azobenzene* ***AZO1*** *and b) azobenzence* ***AZO2*** *immobilised in a zigzag pattern defined by the applied photomask. Negative polarity SIMS, 269.1 u and 212.1 u, assigned to* $C_{16}H_{17}N_2O_2^-$ *(left) and* $C_{12}H_8N_2O_2^-$ *(right)*

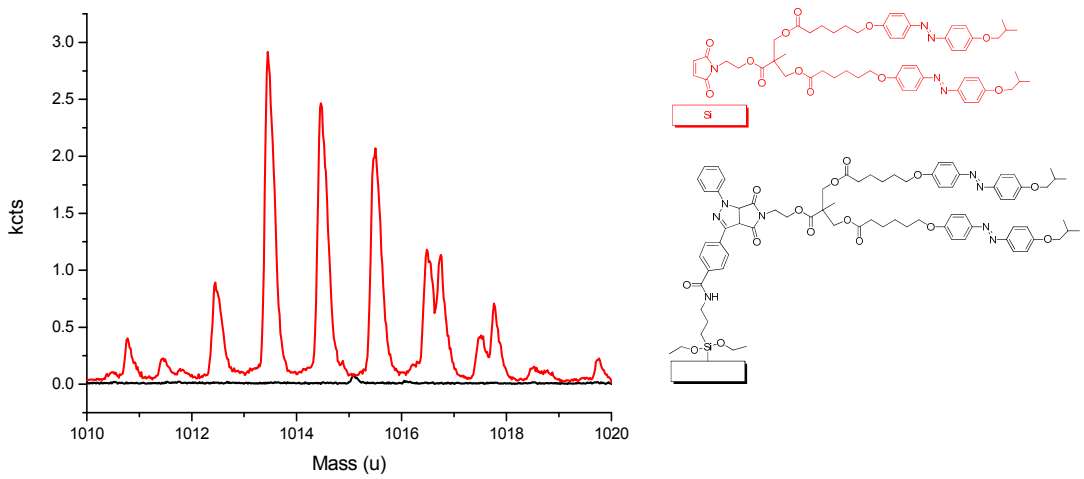

Figure 7.10 *SIMS spectrum of the azobenzene* ***AZO2*** *physically adsorbed by solvent-casting deposition (red) and grafted (black) onto silicon wafers*

7.3.5 Wettability Study

After evidencing the presence of azobenzene on the surface by XPS and ToF-SIMS, azobenzene *trans*-to-*cis* photoisomerisation was provoked by UV irradiation of the surface. For this photoisomerisation, a lamp with the maximum emission wavelength close to 355 nm was chosen (the strongest absorption band of *trans*-azobenzene is centered about 360 nm).

Functionalised surfaces **Si-AZO1** and **Si-AZO2** were illuminated through a mask covering half of the surface as a way to generate two regions having different polarities due to the azobenzene isomerisation in the selectively exposed areas (**Scheme 7.8**). This would allow fine tuning of the surface wettability. A simple and effective technique employed to macroscopically monitor the photoisomerisation is the contact angle (CA) measurement. Advancing and receding CAs were measured in non irradiated (*trans*-azobenzene rich areas) and irradiated (*cis*-azobenzene rich areas) regions of both surfaces (**Table 7.1**). On an ideal surface, the advancing and the receding angles will be identical.[36] It is well known that roughness or chemical heterogeneity can cause CA hysteresis, yet it has also been reported that even surfaces – which are initially smooth and homogeneous – can exhibit CA hysteresis because of a reorganisation of surface molecules.[37,38] In the present case, no significant modification in the advancing CA can be observed. However, a significant change of 15º in receding CA occurred on **Si-AZO1** surface evidencing that the photoisomerisation occurs and has influence on the wettability of the surface. In the case of **Si-AZO2** surface, smaller differences were detected between the non-irradiated and the irradiated zone were detected, probably due to a more heterogeneous and less azobenzene functionalised surface being produced. As expected, the contact angle in the *cis*-azobenzene region in both cases decreased as a consequence of the increase on the dipole moment. Reported differences in CA on *trans* and *cis* azobenzene functionalised smooth surfaces did not exceed 10º[39,40] whereas higher differences were achieved in the azobenzene functionalised surface **Si-AZO1**.

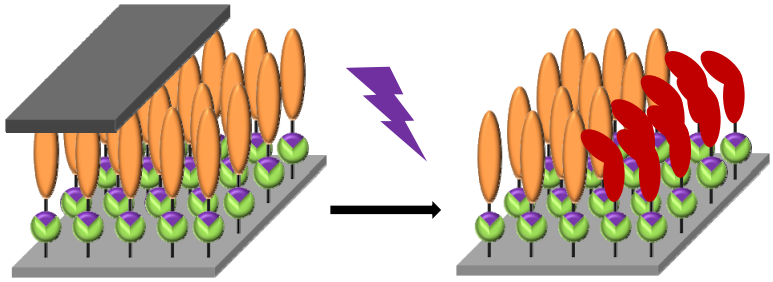

Scheme 7.8. *Spatially controlled photoisomerisation of an azobenzene functionalised surface by using a mask to cover half of the surface.*

Table 7.1 *Contact angle measurements of the azofunctionalised surfaces*

Surface	Advancing angle	Receding angle
AZO1 (non-irradiated)	87.0º ± 1.0	56.7º ± 3.5
AZO1 (irradiated)	86.7º ± 1.5	41.7º ± 1.5
AZO2 (non-irradiated)	83.0º ± 2.5	52.3º ± 2.5
AZO2 (irradiated)	83.5º ± 3.0	42.3º ± 4.5

Visual experiments by using a water droplet were performed to demonstrate the photoswitchable wettability of the functionalised surface. It was evidenced that when azobenzenes at the surface adopt the *trans* configuration a water droplet can slips the surface whereas the water droplet is sticky if azobenzenes are in the *cis* configuration. Such a different behaviour is more pronounced in the case of surface modified with azobenzene **Si-AZO1**. For a visual demonstration of the switching effect, please refer to the movies (http://onlinelibrary.wiley.com /doi/10.1002/adfm.201203602/suppinfo). In these experiments, a water droplet was placed in each region of the surface, irradiated as well as non-irradiated, and it was forced to move over the surface. Reversible *cis* to *trans* thermal isomerisation was checked by keeping the surface in the dark for 24 hours before evaluating the water droplet behavior again. After 24 h, the water droplet slipped over the entire surface proving that azobenzene adopted *trans*

configuration in both regions. Although the thermal isomerisation is slow (hours) it can be readily accelerated by heating or by exposure to visible light.

7.4 Conclusions

A novel and spatial resolved photocontrolled functionalisation of surface with azobenzene moieties by employing the NITEC (nitrile imine-mediated tetrazole ene cycloaddition) has been achieved. Photoligation reaction has been carried out in presence of a molecule featuring a single azobenzene unit and a maleimide group was performed as well as with a first-generation dendron containing two azobenzene groups.

XPS was employed to prove the functionalisation of the silicon wafers with both azobenzene derivates. In the case of **AZO2**, the experimental result is not in agreement with the theoretical value evidencing incomplete functionalisation of the surface.

On the other hand, ToF-SIMS images proved functionalised surfaces in a highly spatial controlled fashion in both cases.

Photocontrolled *trans*-to-*cis* azobenzene isomerisation of the surface provokes a change in the dipolar moment allowing the tuning of the surface wettability. Visual experiments by using a water droplet demonstrated the photoswitchable wettability. An optimum photoresponse has being achieved when the photoligation is performed with azobenzene **AZO1**.

Thus, it has been demonstrated that *trans*-to-*cis* azobenzene isomerisation of spatially resolved surfaces allows tuning the surface properties.

7.5 Experimental Section

Experimental details for the synthesis of isopropylidene-2,2-bis(methoxy) propionic acid **(1)** and 6-[4-(4'isobutyloxiphenylazo) phenyloxy]hexanoic acid (**isoAZOb**) are given in Chapter 2 and 3, respectively. All other reagents were purchased from Aldrich and used as received without further purification.

7.5.1 Experimental Details for the Synthesis of the Tetrazole Derivatives

Synthesis and Characterisation of 4-(2-phenyl-2H-tetrazol-5-yl)benzoic acid (18)

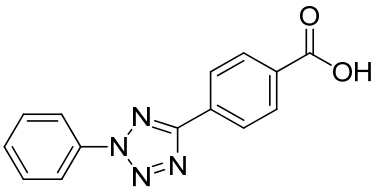

(18)

A solution of 4-formylbenzoic acid (2.10 g, 13.30 mmol) in ethanol (130 mL) and benzenesulfonohydrazide (2.29 g, 13.30 mmol) was prepared. The mixture was stirred for 30 min. After addition of water (250 mL), a white precipitate was formed and collected in a funnel. The white solid was dissolved in pyridine (50 mL). In parallel, a solution of $NaNO_2$ (0.92 g, 13.30 mmol) in water (10mL) was added dropwise to a cooled mixture of aniline (1.24 g, 13.30 mmol) dissolved in a mixture of water-ethanol (1:1) (20mL) and concentrated HCl (3.4 mL). This solution was slowly added to the pyridine solution cooled with an ice-salt bath. The reaction mixture was then extracted with ethyl acetate 3 times and HCl 3N added to the organic layer. A precipitated formed that was collected and dried. IR (KBr), ν (cm^{-1}): 3300, 1695, 1650, 1308, 1094, 1016, 802. ^{1}H-NMR (DMSO-d_6, 400MHz) δ (ppm): 12.29 (s, 1H), 8.34-8.26 (m, 2H), 8.19 (td, J = 5.5, 2.9 Hz, 4H), 7.78-7.27 (m, 3H); ^{13}C-NMR (DMSO-d_6, 100 MHz) δ (ppm): 166.7, 163.8, 136.1, 132.8, 130.4, 130.3, 130.2, 126.8, 120.0

Synthesis and Characterisation of the Tetrazole Functionalised Silane (TET)

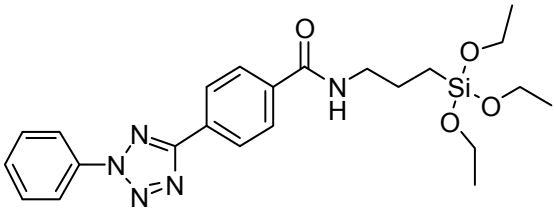

(TET)

A solution of carboxy functionalised tetrazole (**18**) (0.80 g, 3.00 mmol), (3-aminopropyl)triethoxysilane (0.65 g, 3.00 mmol), and 4-dimethylaminopyridine (0.05 mg, 0.45 mmol) in dry DCM (25 mL) was prepared. *N,N'*-dicyclohexylcarbodiimide (0.77 g, 3.60 mmol) in dry DCM (10 mL) was then added dropwise. The mixture was then stirred at room temperature for 18 h. The white precipitate formed was removed by filtration and the solvent was evaporated. The crude product was purified by column chromatography on silica gel and eluted with DCM:acetate 1:1 and then crystallised in hexane giving a pink powder. Yield 20 %. IR (KBr), ν (cm^{-1}): 3300, 3260, 1636, 1552, 1102, 1076, 860, 798. ^{1}H-NMR ($CDCl_3$, 400MHz) δ (ppm): 8.35-8.33 (m, 2H), 8.24-8.20 (m, 2H), 7.95-7.92 (m, 2H), 7.64-7.50 (m, 3H), 6.69 (t, *J* = 5.4 Hz, 1 H), 3.85 (q, *J* = 7.0 Hz, 6H), 3.53-3.50 (m, 2H), 1.83-1.76 (m, 2H), 1.24 (t, *J* = 7.0 Hz, 9H), 0.83 (t, *J* = 7.5 Hz, 2H).

7.5.2 Experimental Details for the Synthesis of the Azobenzene Derivatives

Synthesis and Characterisation of 4,10-dioxatricyclo[5.2.1.02,6]dec-8-ene-3,5-dione (19)

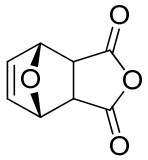

(19)

A suspension of maleic anhydride (30.02 g, 0.31 mmol) in toluene (150 mL) was heated to 80 ºC and then furan (33.4 mL, 0.46 mmol) was slowly added. The resulting turbid solution was stirred for 6 h, and then the mixture was cooled to room temperature and the stirring stopped. After 1 h, the resulting white crystals were collected by filtration and washed twice with petroleum ether (2x30mL). The solvent was evaporated and the product was obtained as small white needless. Yield: 90% IR (KBr), ν (cm^{-1}): 1857, 1780, 1309, 1282, 1211, 1145, 1083. ^{1}H-NMR ($CDCl_3$, 400MHz) δ (ppm): 6.57 (t, *J* =1.0 Hz, 2H), 5.45 (t, *J* = 1.0 Hz, 2H), 3.17 (s, 2H). ^{13}C-NMR ($CDCl_3$, 100 MHz) δ (ppm): 170.0, 137.1, 82.4, 48.9.

Synthesis and Characterisation of 4-(2-hydroxyethyl)-10-oxa-4-azatricyclo [5.2.1.02,6]dec-8-ene-3,5-dione (20)

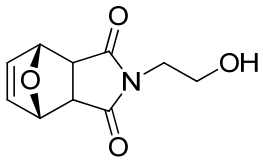

(20)

The anhydride **19** (2.00 g, 12.0 mmol) was suspended in methabol (50 mL) and the mixture cooled to 0 ºC. A solution of 2-aminoethanol (0.72 mL, 12.0 mmol) in MeOH (20 mL) was added dropwise and the resulting mixture was stirred for 5 min at 0 ºC, then 30 min at room temperature, and finally refluxed for 4 h. After cooling to room temperature, the solvent was removed under reduced pressure, and the white residue was dissolved in DCM (150 mL) and washed with water. The organic layer was dried and the solvent evaporated. The solid was purified by flash column chromatography on silica gel and eluted with ethyl

acetate. The product was obtained as a white solid. Yield: 50%. IR (KBr), ν (cm^{-1}): 3472, 1681, 1269, 1168, 1100, 1053. ^{1}H-NMR ($CDCl_3$, 400MHz) δ (ppm): 6.52 (t, *J*= 1.0 Hz, 2H), 5.28 t, *J* =1.0 Hz, 2H), 3.76-3.78 (m, 2H), 2.90 (s, 2H), 1.90 (s, 1H). ^{13}C-NMR ($CDCl_3$, 100 MHz) δ (ppm): 177.0, 136.6, 81.0, 60.2, 47.5, 41.8.

Synthesis and characterisation of (21)

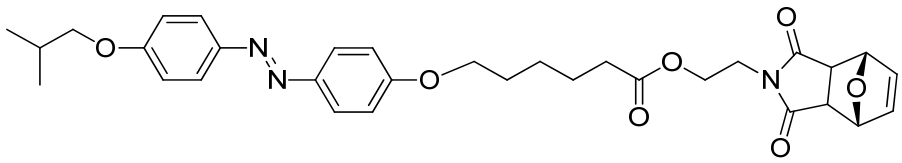

(21)

The protected maleimide (**20**) (0.41 g, 2.20 mmol), 6-[4-(4'-isobutyloxyphenylazo)phenyloxy] hexanoic acid (**isoAZOb**) (1.02 g, 2.60 mmol) and 4-(dimethylamino)pyridinium 4-toluenesulfonate (0.62 g, 2.20 mmol) were dissolved in DCM (15 mL). The reaction flask was flushed with argon, and *N,N'*-dicyclohexylcarbodiimide (0.63 g, 2.85 mmol) was added. The mixture was stirred at room temperature for 24 h under argon atmosphere. The white precipitate formed was filtered off, and the solvent was evaporated. The crude product was purified by flash column chromatography on silica gel and eluted with 1:9 ethyl acetate:DCM. The target product was obtained as a yellow powdery solid. Yield: 70 %. IR (KBr), ν (cm^{-1}): 1743, 1713 (C=O), 1601, 1580, 1499, 1396, 1247, 840. ^{1}H-NMR ($CDCl_3$, 400MHz) δ (ppm): 7.90-7.86 (m, 4H), 7.07-6.95 (m, 4H), 6.50 (t, *J* = 1.0 Hz, 2H), 5.27 (t, *J* = 1.0 Hz, 2H), 4.33-4.19 (t, *J* = 5.2 Hz, 2H), 4.05 (t, *J* = 6.4 Hz, 2H), 3.89 – 3.66 (m, 4H), 2.86 (s, 2H), 2.34 (t, *J* = 7.5 Hz, 2H), 2.19-2.09 (m, 1H), 1.88-1.81 (m, 2H), 1.74-1.67 (m, 2H), 1.64-1.45 (m, 2H), 1.07 (d, *J* = 6.7 Hz, 6H). ^{13}C-NMR ($CDCl_3$, 100 MHz) δ (ppm): 176.0, 173.3, 161.3, 161.2, 146.9, 146.8, 136.5, 124.3, 114.7, 114.6, 80.9, 74.7, 67.9, 60.5, 47.4, 37.9, 33.9, 29.7, 28.3, 25.6, 24.4, 19.3.

Synthesis and Characterisation of AZO1

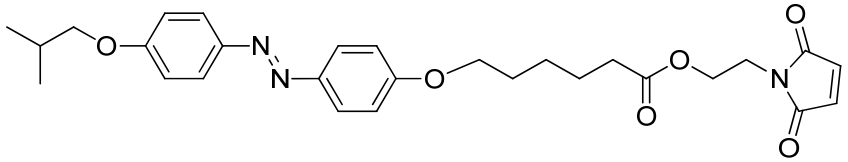

AZO1

The azobenzene (**21**) (0.20g, 0.35 mmol) was suspended in toluene (150 mL) and heated to reflux while the reaction was monitored by thin layer chromatography. After 4 h, the solvent was removed under reduced pressure to give **AZO1** as a yellow powder. Yield: 100%. IR (KBr), ν (cm^{-1}): 1735, 1707, 1601, 1580, 1499, 1402, 1242, 839. Yield: 98%. ^{1}H-NMR ($CDCl_3$, 400MHz) δ (ppm): 7.90-7.82 (m, 4H), 7.04-6.91 (m, 4H), 6.71 (s, 2H), 4.30-4.19 (t, *J* = 5.3 Hz, 2H), 4.03 (t, *J* = 6.4 Hz, 2H), 3.89-3.66 (m, 4H), 2.34 (t, *J* = 7.4 Hz, 2H), 2.19-2.09 (m, 1H), 1.90-1.81 (m, 2H), 1.74-1.67 (m, 2H), 1.64-1.45 (m, 2H), 1.07 (d, *J* = 6.7 Hz, 6H). ^{13}C-NMR ($CDCl_3$, 100 MHz) δ (ppm): 173.3, 170.4, 161.3, 147.0, 134.2, 124.3, 114.7, 114.6, 74.7, 67.9, 61.3, 36.9, 33.9, 28.8, 28.3, 25.6, 24.4, 19.2. MALDI-TOF MS (matrix: dithranol, m/z): 508.3 $[M-H]^+$, 530.4 $[M-Na]^+$. Anal. Calc. for $C_{28}H_{33}N_3O_6$: C, 66.26 %; H, 6.55 %; N, 8.28 %; Found: C, 66.21 %; H, 6.83 %; N, 8.22 %.

Synthesis and Characterisation of (22)

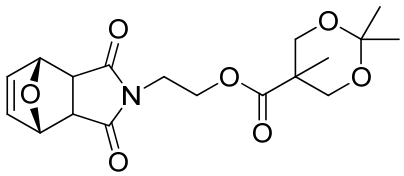

(22)

The protected maleimide (**20**) (1.20 g, 5.71 mmol), protected bis-MPA acid **(1)** (1.20 g, 6.90 mmol) and 4-(dimethylamino)pyridinium 4-toluenesulfonate (1.72 g, 5.7 mmol) were dissolved in DCM (50 mL). The reaction flask was flushed with argon, and *N,N'*-dicyclohexylcarbodiimide (2.23 g, 7.4 mmol) was added. The mixture was stirred at room temperature for 24 h under argon atmosphere. The white precipitate formed was filtered off, and the solvent was evaporated. The crude product was purified by flash column chromatography on silica gel and eluted with 7:3 ethyl acetate/DCM. The target product was obtained as a yellow powdery solid. Yield: 80 %. IR (KBr), ν (cm^{-1}): 1772, 1723, 1698, 1279,

1247. ^{1}H-NMR ($CDCl_3$, 400MHz) δ (ppm): 6.51 (t, *J* = 1.0 Hz, 2H), 5.26 (t, *J* = 1.0 Hz, 2H), 4.32-4.27 (m, 2H), 4.13 (d, *J* = 11.8 Hz, 2H), 3.83 - 3.73 (m, 2H), 3.58 (d, *J* = 11.8 Hz, 2H), 2.86 (s, 2H), 1.40 (s, 3H), 1.37 (s, 3H), 1.18 (s, 3H). ^{13}C-NMR ($CDCl_3$, 100 MHz) δ (ppm): 175.8, 173.8, 136.4, 97.9, 80.7, 65.7, 61.1, 47.4, 41.6, 37.7, 23.8, 23.2, 18.4.

Synthesis and Characterisation of (23)

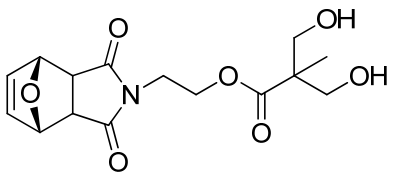

(23)

DOWEX-50-X2 resin (0.10 g) was added to a solution of compound (**22**) (0.50 g, 1.50 mmol) in methanol (15 mL). The mixture was stirred for 3 h at room temperature. Subsequently, the resin was filtered off and the solvent removed under vacuum to give (**23**) as a colourless viscous oil. Yield: 90%. IR (KBr), ν (cm^{-1}): 3500, 1772, 1721, 1699, 1279, 1246. ^{1}H-NMR ($CDCl_3$, 400MHz) δ (ppm): 6.45 (t, *J* = 1.0 Hz, 2H), 5.22 (t, *J* = 1.0 Hz, 2H), 4.32 – 4.19 (m, 2H), 3.75-3.69 (m, 4H), 3.64-3.60 (m, 2H), 2.83 (s, 2H), 2.81 (t, J=6.8 Hz ,1H), 0.97 (s, 3H). ^{13}C-NMR ($CDCl_3$, 100 MHz) δ (ppm): 175.8, 173.8, 136.4, 80.7, 65.7, 61.1, 47.4, 41.6, 37.7, 18.4.

Synthesis and Characterisation of (24)

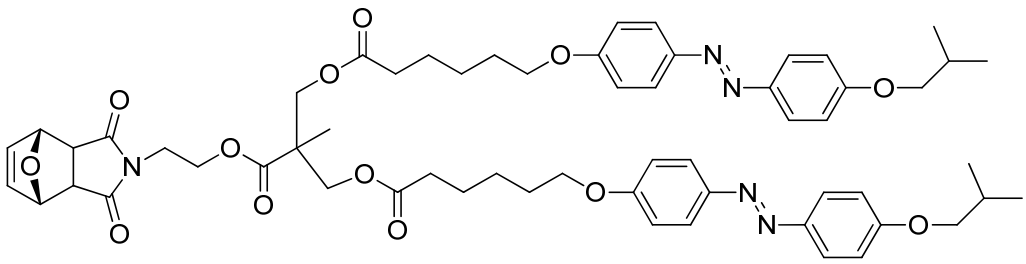

(24)

The acid chloride derivate of 6-[4-(4'-isobutyloxyphenylazo)phenyloxy] hexanoic acid (**isoAZOb**) was prepared by reaction of **isoAZOb** (0.93 g, 2.43 mmol) with oxalyl chloride (0.4 mL, 4.86 mmol) in DCM (20mL). After stirring at room temperature for 4h, the solvent was distilled. The acid chloride derivated was directly added to a solution of compound **23** (0.40 g, 1.12 mmol) and

triethylamine (0.23 g, 2.40 mmol) in DCM (20 mL). The mixture was stirred for 3 h at room temperature under argon atmosphere. After this time, the white precipitate formed was filtered off, and the solvent was removed under vacuum. The crude product was purified by flash column chromatography on silica gel using 7:3 ethyl acetate:DCM as eluent. Yield: 65%. IR (KBr), ν (cm^{-1}): 1739, 1703, 1601, 1581, 1498, 1243, 1149, 1024, 843. ^{1}H-NMR ($CDCl_3$, 400MHz) δ (ppm): 7.90-7.86 (m, 8H), 6.96-6.90 (m, 8H), 6.48 (t, *J* = 1.0 Hz, 2H), 5.29 (t, *J* = 1.0 Hz), 4.26-4.08 (m, 6H), 4.01 (t, *J* = 6.4 Hz, 4H), 3.82-3.73 (m, 6H), 2.86 (s, 2H), 2.35 (t, *J* = 7.4 Hz, 4H), 2.10-2.03 (m, 2H), 1.86-1.75 (m, 4H), 1.73-1.64 (m, 4H), 1.54-1.44 (m, 4H), 1.22 (s, 3H), 1.05 (d, *J* = 6.7 Hz, 12H). ^{13}C-NMR ($CDCl_3$, 100 MHz) δ (ppm): 175.9, 172.9, 172.3, 161.9, 160.9, 146.8, 146.8, 136.4, 124.1, 114.6, 114.5, 80.7, 74.6, 67.8 , 64.9, 61.4, 47.4, 46.2, 37.6, 33.8, 28.8, 28.2, 25.5, 24.5, 19.2, 17.5.

Synthesis and Characterisation of AZO2

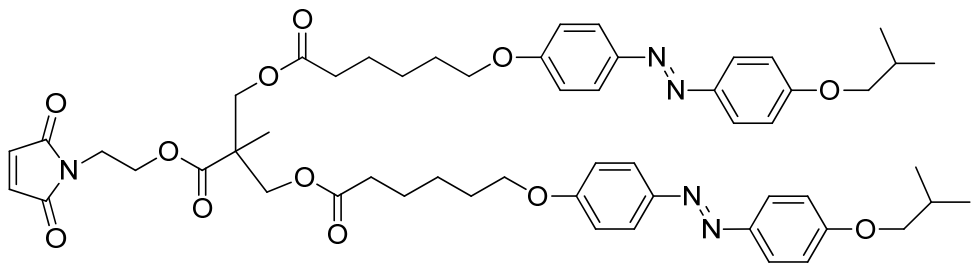

AZO2

The protected maleimide (**24**) was suspended in toluene (150 mL) and heated to reflux. The reaction was monitored by thin layer chromatography After 4 hours, the solvent was removed under reduced pressure to give **AZO2** as a yellow powder. Yield: 100%. IR (KBr), ν (cm^{-1}): 1731, 1713, 1601, 1582, 1498, 1243, 1149, 1034, 845. ^{1}H-NMR ($CDCl_3$, 400MHz) δ (ppm): 7.90-7.86 (m, 8H), 6.96-6.90 (m, 8H,), 6.70 (s, 2H), 4.27-4.12 (m, 6H), 4.01 (t, *J* = 6.4 Hz, 4H), 3.82-3.73 (m, 6H), 2.35 (t, *J* = 7.4 Hz, 4H), 2.10-2.03 (m, 2H), 1.86-1.75 (m, 4H), 1.73-1.64 (m, 4H), 1.54-1.44 (m, 4H), 1.22 (s, 3H), 1.05 (d, *J* = 6.7 Hz, 12H). ^{13}C-NMR ($CDCl_3$, 100 MHz) δ (ppm): 172.9, 172.3, 170.3, 161.9, 160.9, 146.8, 146.8, 134.2, 124.1, 114.6, 114.5, 74.6, 67.8, 64.9, 61.4, 46.2, 37.6, 33.8, 28.8, 28.2 (CH), 25.5, 24.5, 19.2, 17.5. MALDI-TOF MS (matrix: dithranol, m/z): 990.6 $[M-H]^+$, 1012.5 $[M-Na]^+$. Anal. Calc. for $C_{55}H_{67}N_5O_{12}$: C, 66.72 %; H, 6.82 %; N, 7.07 %. Found: C, 66.53 %; H, 7.01 %; N 7.05 %.

7.5.3 General Procedures

Solution Tests

Solution tests were performed in a quartz cuvette by employing a hand-held UV lamp and low pressure mercury lamp OSRAM Puritec HNS L 36 W (dominant wavelength 254 nm). The photoreaction was carried out in DCM (7mM **AZO1**) at room temperature.

Activation of Silicon Wafers

Prior to surface activation, the silicon wafers (p-type, boron doped (100) from Si-Mat Silicon Materials, Landsberg, Germany) were cleaned with chloroform, acetone and ethanol. The wafers were rinsed thoroughly with fresh solvent and sonicated 5 min several times with each solvent. After cleaning, the silicon wafers were activated by immersion in Piranha solution (H_2SO_4 95%/H_2O_2 35% 3:1 vol/vol) at 90 °C for 1h. After extensive rinsing with deionised water, they were dried under a stream of argon.

Functionalisation of Silicon Wafers with Tetrazole (**Si-TET**)

The activated silicon wafers were placed in a flask containing a solution of silane functionalised tetrazole (**TET**) in dry toluene (4.8 mg in 1 mL). The flask was heated to 50 °C overnight. Subsequently, the wafers were rinsed thoroughly with fresh toluene and chloroform and sonicated for 5 min. The wafers were finally dried in a stream of argon.

Functionalisation of Silicon Wafers with Azobenzene (Si-AZO1 and Si-AZO2)

The tetrazole functionalised silicon wafers were placed in a quartz flask containing an azobenzene solution in DCM (7mM for **AZO1** and 3.5 mM for **AZO2**). The flask was introduced into a photoreactor with two lamps and irradiated for a pre-set time interval. Subsequently the wafers were rinsed thoroughly with fresh chloroform and sonicated for 5 min. The wafers were finally dried in a stream of argon. The experiments were carried out with

compact low-pressure fluorescent lamps Philips PL-S 9W/12 emitting UV irradiation between 290 and 315 nm.

Photoisomerisation of Azobenzene Functionalised Silicon Wafers

The azobenzene functionalised silicon wafers were introduced in a photoreactor fixed with two lamps and irradiated for 30 min. After this time, the wafers were kept in the dark. The experiments were performed using compact low-pressure fluorescent lamps Philips CLEO PL-L 36W emitting between 310 and 400 nm (λ_{max}=355 nm).

References

1 Shipway, A. N.; Katz, E.; Willner, I. Nanoparticle arrays on surfaces for electronic, optical, and sensor applications. *Chemphyschem* **200**, 1, 18-52.

2 Falconnet, D.; Csucs, G.; Grandin, H. M.; Textor, M. Surface engineering approaches to micropattern surfaces for cell-based assays. *Biomaterials* **2006**, 27, 3044-3063.

3 Russell, T. P. Surface-responsive materials. *Science* **2002**, 297, 964-967.

4 Sun, T. L.; Feng, L.; Gao, X. F.; Jiang, L. Bioinspired surfaces with special wettability. *Accounts of Chemical Research* **2005**, 38, 644-652.

5 Mendes, P. M. Stimuli-responsive surfaces for bio-applications. *Chemical Society Reviews* **2008**, 37, 2512-2529.

6 Binder, W. H.; Sachsenhofer, R. 'Click' chemistry in polymer and materials science. *Macromolecular Rapid Communications* **2007**, 28, 15-54.

7 Binder, W. H.; Sachsenhofer, R. 'Click' chemistry in polymer and material science: An update. *Macromolecular Rapid Communications* **2008**, 29, 952-981.

8 Hoyle, C. E.; Lowe, A. B.; Bowman, C. N. Thiol-click chemistry: a multifaceted toolbox for small molecule and polymer synthesis. *Chemical Society Reviews* **2010**, 39, 1355-1387.

9 Adzima, B. J.; Tao, Y.; Kloxin, C. J.; Forest, C. A.; Anseth, K.S.; Bowman, C. N. Spatial and temporal control of the alkyne-azide cycloaddition by photoinitiated Cu(II) reduction. *Nature Chemistry* **2011**, 3, 256-259.

10 Poloukhtine, A. A.; Mbua, N. E.; Wolfert, M. A.; Boons, G.-J.; Popik, V. V. Selective Labeling of Living Cells by a Photo-Triggered Click Reaction. *Journal of the American Chemical Society* **2009**, 131, 15769-15776.

11 Arumugam, S.; Popik, V. V. Light-Induced Hetero-Diels−Alder Cycloaddition: A Facile and Selective Photoclick Reaction. *Journal of the American Chemical Society* **2011**, 133, 5573-5579.

12 Chen, R. T.; Marchesan, S.; Evans, R. A.; Styan, K. E.; Such, G. K.; Postma, A.; McLean, K.M.; Muir, B.W.; Caruso, F. Photoinitiated Alkyne–Azide Click and

Radical Cross-Linking Reactions for the Patterning of PEG Hydrogels. *Biomacromolecules* **2012**, 13, 889-895.

13 Pauloehrl, T.; Delaittre, G.; Winkler, W.; Welle, A.; Bruns, M.; Börner, H. G.; Greiner, A. M.; Bastmeyer, M.; Barner-Kowollik, C. Adding Spatial Control to Click Chemistry: Phototriggered Diels-Alder Surface (Bio)functionalization at Ambient Temperature. *Angewandte Chemie-International Edition* **2012**, 51, 1071-1074.

14 Dietrich, M.; Delaittre, G.; Blinco, J. P-; Inglis, A.J.; Bruns, M.; Barner-Kowollik, C. Photoclickable Surfaces for Profluorescent Covalent Polymer Coatings. *Advanced Functional Materials* **2012**, 22, 304-312.

15 Gruendling, T. Oehlenschlaeger, K. K.; Frick, E.; Glassner, M.; Schmid, C. Barner-Kowollik, C. Rapid UV Light-Triggered Macromolecular Click Conjugations via the Use of o-Quinodimethanes. *Macromolecular Rapid Communications* **2011**, 32, 807-812.

16 Glassner, M., Oehlenschlaeger, K. K., Gruendling, T. & Barner-Kowollik, C. Ambient Temperature Synthesis of Triblock Copolymers via Orthogonal Photochemically and Thermally Induced Modular Conjugation. *Macromolecules* **2011**, 44, 4681-4689.

17 Pauloehrl, T.; Delaittre, G.; Bruns, M.; Meissler, M.; Börner, H. G.; Greiner, A. M.; Bastmeyer, M.; Barner-Kowollik, C. (Bio)Molecular Surface Patterning by Phototriggered Oxime Ligation. *Angewandte Chemie International Edition* **2012**, 51, 9181 (2012).

18 Clovis, J. S.; Eckell, A.; Huisgen, R.; Sustmann, R. 1.3-Dipolare Cycloadditionen, XXV. Der Nachweis des freien Diphenylnitrilimins als Zwischenstufe bei Cycloadditionen. *Chemische Berichte* **1967**, 100, 60-70.

19 Song, W.; Wang, Y.; Qu, J.; Madden, M. M.; Lin, Q. A Photoinducible 1,3-Dipolar Cycloaddition Reaction for Rapid, Selective Modification of Tetrazole-Containing Proteins. *Angewandte Chemie International Edition* **2008**, 47, 2832-2835.

20 Wang, Y. Z.; Hu, W. J.; Song, W. J.; Lint, R. K. V.; Lin, Q. Discovery of long-wavelength photoactivatable diaryltetrazoles for bioorthogonal 1,3-dipolar cycloaddition reactions. *Organic Letters.* **2008**, 10, 3725-3728.

21 Wang, Y. Z.; Vera, C. I. R.; Lin, Q. Convenient synthesis of highly functionalized pyrazolines via mild, photoactivated 1,3-dipolar cycloaddition. *Organic Letters* **2007**, 9, 4155-4158.

22 Dietrich, M.; Delaittre, G.; Blinco, J. P-; Inglis, A.J.; Bruns, M.; Barner-Kowollik, C. Photoclickable Surfaces for Profluorescent Covalent Polymer Coatings. *Advanced Functional Materials* **2012**, 22, 304-312.

23 Meier, H.; Heimgartner, H. Intramolekulare 1,3-dipolare Cycloadditionen von Diarylnitriliminen aus 2,5-Diaryltetrazolen. *Helv. Chim. Acta* **1985**, 68, 1283-1300.

24 Lohse, V.; Leihkauf, P.; Csongar, C.; Tomaschewski, G. Photochemie diarylsubstituierter 2H-Tetrazole. VI. Quantenausbeuten der Photolyse diarylsubstituierter 2H-Tetrazole. *J. Prakt. Chem.* **1988**, 330, 406-414.

25 Darkow, R.; Yoshikawa, M.; Kitao, T.; Tomaschewski, G.; Schellenberg, J. Photomodification of a poly(acrylonitrile-co-butadiene-co-styrene) containing diaryltetrazolyl groups. *Journal of Polymer Science Part A: Polymer Chemistry* **1994**, 22, 1657-1664.

26 Bertrand, G.; Wentrup, C. Nitrile Imines: From Matrix Characterization to Stable Compounds. *Angewandte Chemie-International Edition* **1994**, 33, 527-545.

27 Moderhack, D. Ring Transformations in Tetrazole Chemistry. *Journal für Praktische Chemie/Chemiker-Zeitung* **1998**, 340, 687-709.

28 Wang, J.; Zhang, W.; Song, W.; Wang, Y.; Yu, Z.; Li, J.; Wu, M.; Wang, L.; Zang, J.; Lin, Q. A Biosynthetic Route to Photoclick Chemistry on Proteins. *Journal of the American Chemical Society* **132**, 14812-14818, doi:10.1021/ja104350y (2010).

29 Song, W.; Wang, Y.; Qu, J.; Lin, Q. Selective Functionalization of a Genetically Encoded Alkene-Containing Protein via “Photoclick Chemistry” in Bacterial Cells. *Journal of the American Chemical Society* **2008**, 130, 9654-9655.

30 Wang, Y.; Song, W.; Hu, W. J.; Lin, Q. Fast Alkene Functionalization In Vivo by Photoclick Chemistry: HOMO Lifting of Nitrile Imine Dipoles. *Angewandte Chemie, International Edition* **2009**, 48, 5330-5333.

31 Madden, M. M.; Rivera Vera, C. I.; Song, W.; Lin, Q. Facile synthesis of stapled, structurally reinforced peptide helices via a photoinduced intramolecular 1,3-dipolar cycloaddition reaction. *Chemical Communications* **2009**, 5588-5590.

32 De Marco, C.; Eaton, S.M; Suriano, R.; Turri, S.; Levi, M.; Ramponi, R.; Cerullo, G.; Osellame, R. Surface Properties of Femtosecond Laser Ablated PMMA. *ACS Applied Materials & Interfaces* **2010**, 2, 2377-2384.

33 Lock, E. H.; Petrovykh, D. Y., Mack, P.; Carney, T.; White, R. G.; Walton, S. G.; Fernsler, R. F. Surface Composition, Chemistry, and Structure of Polystyrene Modified by Electron-Beam-Generated Plasma. *Langmuir* **2010**, 26, 8857-8868.

34 Szocs, E.; Bakó, I.; Kosztolányi, T.; Bertóti, I.; Kálmán, *Electrochimica Acta* **2004**, 49, 1371-1378.

35 Rouxhet, P. G.; Misselyn-Bauduin, A. M.; Ahimou, F.; Genet, M. J.; Adriaensen, Y.; Desille, T.; Bodson, P.; Deroanne, C. XPS analysis of food products: toward chemical functions and molecular compounds. *Surface and Interface Analysis* **2008**, 40, 718-724.

36 Strobel, M.; Lyons, C. S. An Essay on Contact Angle Measurements. *Plasma Processes Polym.* **2011**, 8, 8-13.

37 Ichimura, K.; Oh, S. K.; Nakagawa, M. Light-driven motion of liquids on a photoresponsive surface. *Science* **2000**, 288, 1624-1626.

38 Chen, Y. L.; Helm, C. A.; Israelachvili, J. N. Molecular mechanisms associated with adhesion and contact angle hysteresis of monolayer surfaces. *The Journal of Physical Chemistry B.* **1991**, 95, 10736-10747.

39 Siewierski, L. M.; Brittain, W. J.; Petrash, S.; Foster, M. D. Photoresponsive Monolayers Containing In-Chain Azobenzene. *Langmuir* **1996**, 12, 5838-5844.

40 Delorme, N.; Bardeau, J. F.; Bulou, A.; Poncin-Epaillard, F. Azobenzene-containing monolayer with photoswitchable wettability. *Langmuir* **2005**, 21, 12278-12282.

Conclusiones

Capítulo 2

Se han sintetizado y caracterizado nuevos copolímeros bloque dendrítico-lineales formados por un bloque dendrítico funcionalizado con unidades 4-cianoazobenceno en la periferia y un bloque lineal variable en cuanto a composición –poli(metacrilato de metilo), poli(metacrilato de etilo) o poliestireno– y su masa molecular –10000 y 20000 g/mol aprox– mediante combinación de polimerización radicalaria por transferencia de átomo (ATRP) y la cicloadición 1,3 dipolar entre azidas y alquinos catalizada por Cu(I).

Se han estudiado las propiedades térmicas tanto de los bloques como de los copolímeros mediante microscopía óptica de luz polarizada (MOP), termogravimetría (TGA) y calorimetría diferencia de barrido (DSC). El dendrón funcionalizado con azobenceno y todos los copolímeros bloque preparados presentan comportamiento cristal líquido. El estudio de DSC ha puesto de manifiesto la tendencia a la microsegregación de estos copolímeros, que se corroboró por microscopía electrónica, observándose una morfología de tipo lamelar en todos los casos.

Capítulo 3

Se han preparado nuevos copolímeros bloque dendrítico-lineales –**PEG-b-d16isoAZO** y **PEG-b-d16isoAZOb**– a partir de un dendrón funcionalizado en la periferia con dieciséis unidades 4-isobultiloxiazobenceno y un bloque lineal de poli(etilenglicol) de 2000 g/mol. Con el copolímero **PEG-b-d16isoAZOb** se obtuvieron vesículas estables en agua capaces de responder a la irradiación con luz UV de baja intensidad. Esta respuesta es notablemente superior a la que presentan los copolímeros bloque dendritico-lineales derivados de cianoazobenceno.

Se ha demostrado que la deformación de las vesículas debida a la fotoisomerización del azobenceno, provoca un aumento en la permeabilidad de la membrana y con ello es posible la liberación fotoestimulada de sustancias previamente encapsuladas.

Capítulo 4

Se han sintetizado y caracterizado nuevos copolímeros bloque dendrítico-lineales –**d(isoAZOb/C18)-75/25**, **d(isoAZOb/C18)-50/50** y **d(isoAZOb/C18)-25/75**– formados por bloques dendríticos funcionalizados en la periferia con unidades 4-isobultiloxiazobenceno y cadenas hidrocarbonadas distribuidas aleatoriamente en diferente proporción (condendrones) y un bloque lineal de polietilenglicol de 2000 g/mol. Todos los copolímeros fueron capaces de autoensamblarse en agua formando vesículas estables.

Las vesículas formadas por el copolímero **PEG-*b*-d(isoAZO/C18)-75/25** presentan un comportamiento similar a las del homodendrón análogo totalmente funcionalizado con azobenceno.

Las vesículas con el contenido en azobenzeno más bajo, **PEG-*b*-d(isoAZOb/C18)-25/75**, no presentan fotorrespuesta. Este hecho puede ser debido a que el cambio de polaridad y morfología durante la fotoisomerización del azobenceno no es suficiente para provocar una deformación en la memebrana de las vesículas.

Sin embargo, la estabilidad de las vesículas formadas por el copolímero **PEG-*b*-d(isoAZOb/C18)-50/50** se ve alterada de forma drástica al ser irradiadas con luz UV, provocando una liberación rápida y eficiente de las sustancias encapsuladas.

Así, los resultados indican que ajustando la proporción AZO/C18 en estas estructuras dendríticas se puede modular la fotorrespuesta de los ensamblados formados en agua.

Capítulo 5

Se preparado un nuevo copolímero con una arquitectura macromolecular tipo “miktoarm” de composición AB_3 formado por una rama de un azopolímero de cadena lateral y tres ramas idénticas de poli(etilenglicol) combinando la

polimerización radicalaria por transferencia de átomo (ATRP) y la cicloadición 1,3 dipolar entre azidas y alquinos catalizada por Cu(I).

Este copolímero es capaz de autoensamblarse en agua formando vesículas que mostraron fotorrespuesta al irradiar con luz UV.

Capítulo 6

Se han sintetizado y caracterizado una serie de copolímeros “miktoarm” de tipo AB_3 –**$PAZO_{17}$-$(PDEAA_{14})_3$**, **$PAZO_{17}$-$(PDEAA_{22})_3$** y **$PAZO_{17}$-$(PDEAA_{55})_3$**– que contienen una rama de un azopolímero de cadena lateral y tres ramas idénticas de poli(*N*-etilacrilamida un polímero termosensible, combinando técnicas de polimerización radicalaria por transferencia de átomo (ATRP) y transferencia por adición-fragmentación reversible (RAFT), y la cicloadición 1,3 dipolar entre azidas y alquinos catalizada por Cu(I).

Tras estudiar el ensamblaje en agua de todos los polímeros preparados, se obtuvieron dispersiones micelares estables para el copolímero **$PAZO_{17}$-$(PDEAA_{55})_3$** de las que se estudió su respuesta tanto a la luz como a la temperatura como estímulos externos. La respuesta dual de las micelas fue evaluada mediante TEM y DLS observando cambios en la morfología de las micelas, llegando al colapso al calentar por encima de la temperatura de transición critica. La luz induce deformación micelar y permite controlar la liberación de sustancias hidrófobas encapsuladas en su interior.

Capítulo 7

Se han preparado superficies fotosensibles funcionalizadas con dos moléculas que contienen bien una o dos unidades de 4-isobultiloxiazobenceno (**AZO1** y **AZO2**) utilizando luz, mediente una reacción de cicloadición fotoinducida (NITEC). El uso de luz abre la posibilidad de utilizar técnicas fotolitográficas para la estructuración de la superficie.

La caracterización de las superficies se llevó a cabo mediante XPS. Se observó una completa funcionalización de la superficie en el caso **AZO1,** mientras que en el caso de la superficie funcionalizada con **AZO2** se ha observado una funcionalización incompleta. Mediante la técnica ToF-SIMS ha demostrado la posibilidad de obtener superficies funcionalizadas y estructuradas con un gran control espacial.

Por último, medidas de ángulos de contacto en la superficie irradiada y sin irradiar demuestran la posibilidad de utilizar estos materiales para modular la afinidad de la superficie por el agua con luz (control hidrofobia-hidrofilia de la superficie con luz)

Como conclusión general de esta tesis doctoral se establece que el diseño adecuado de estructuras fotocrómicas complejas permite obtener materiales con una respuesta controlada con luz útil para campos tan diversos como la liberación controlada o las superficies fotoactivas.

APPENDIX

Characterisation Techniques

Fourier Transform Infrared Spectroscopy (FT-IR)

FT-IR spectra were obtained on a Nicolet Avatar 360-FT-IR spectrometer (Chapter 2) and Bruker FT-IR spectrometer using KBr pellets.

Nuclear Magnetic Resonance Spectroscopy (NMR)

^{1}H-NMR and ^{13}C-NMR spectra were measured on a Bruker AV-400 spectrometer at 400 MHz and on a Bruker AM250 spectrometer at 250 MHz (Chapter 5 and 6)

Mass spectrometry (MS)

MALDI-TOF MS was performed on an Autoflex mass spectrometer (Bruker Daltonics). Number-average molecular weight (M_n) and polydispersity of the BCs were calculated from the mass spectra using PolyTools 1.0 (Bruker).

ESI-MS spectra (Chapter 7) were recorded on an Autoflex mass spectrometer (Bruker Daltonics) and a LXQ mass spectrometer (ThermoFisher Scientific) equipped with an atmospheric pressure ionization source operating in the nebuliser-assisted electrospray mode. The instrument was calibrated in the *m*/*z* range 195-1822 using a standard comprising caffeine, Met-Arg-Phe-Ala acetate (MRFA), and a mixture of fluorinated phosphazenes (Ultramark 1621, all from Aldrich).

Elemental Analysis (EA)

EA was performed using a Perkin–Elmer 2400 microanalyzer.

Size Exclusion Chromatography (SEC)

SEC was carried out on a Waters e2695 Alliance liquid chromatography system (Chapter 2, 3 and 4) equipped with a Waters 2424 evaporation light scattering

detector and a Waters 2998 PDA detector using two Ultrastyragel® columns, HR4 and HR2 from Waters, of 500 and 10^4Å pore size and on a Polymer Laboratories PL-GPC 50 Plus Integrated System (Chapter 5 and 6), comprising an autosampler, a PLgel 5 mm bead-size guard column (50 7.5 mm) followed by three PLgel 5 mm MixedC columns (300 7.5 mm) and a differential refractive index detector. Measurements were performed in THF with a flow of 1 mL/min using narrow molecular weight PS and PMMA standards.

Preparative SEC (Chapter 2) was carried out on a Waters 600 pump and a Waters 2998 PDA detector using two Ultrastyragel™ columns, 19×300 mm, of 500 and 10^4Å pore size. Separations were carried in THF using a rate of 6 mL/min.

UV-Vis Spectroscopy

UV-Vis spectra were recoreded on an ATI-Unicam UV4-200 spectrophotometer.

Fluorescence Spectroscopy

Fluorescence measurements were recorded using a Perkin Elmer LS 50B fluorescence spectrophotometer.

Thermogravimetry (TGA)

TGA were performed using a Q5000IR from TA Instruments under nitrogen atmosphere using 2-5 mg of the sample.

Differential Scanning Calorimetry (DSC)

Thermal transitions were determined by DSC using a DSC Q-2000 from TA Instruments with powdered samples (2-5 mg) sealed in aluminium pans. Glass transition temperatures were determined at the midpoint of the baseline jump

and the isotropic temperatures were determined at the maximum of the corresponding peaks.

Polarised optical microscopy (POM)

Mesomorphic behaviour was evaluated by POM using an Olympus BH-2 polarizing microscope fitted with a Linkam THMS600 hot stage.

Transmission Electronic Microscopy (TEM)

Morphologic study of the polymers was studied by TEM in a JEOL-2000 FXIII and (Chapter 2, 3, 5 and 6) in a Tecnai T20 electron microscope (Chapter 4) electron microscope operating at 200kV.

Cryogenic Transmission Electronic Microscopy (Cryo-TEM)

Cryo-TEM observations were carried out in a JEM-2011 electronic microscope on samples rapidly frozen in liquid ethane.

Dynamic light scattering (DLS)

DLS measurements were carried out in a Malvern Instrument Nano ZS using a He-Ne laser with a 633 nm wavelength, a detector angle of 173º at 25ºC using a He-Ne laser with a 633. The self-assembiles concentration was 0.05 mg/mL (Chapter 3, 4 and 5) and 0.10 mg/mL (Chapter 6) and size measurements were performed at least three times on each sample to ensure consistency.

Confocal Microscopy

Fluorescence vesicles were observed with a Olympus FV10i confocal scanning microscope. Images were collected using a 60x oil immersion lens (lens

specification, Plan S-APO 60xO, NA 1.35), a line average of 8 and a format of 1024x1024 pixels. The confocal pinhole was 1 Airy unit.

Contact Angle Measurements

Advancing and receeding contact angle measurements were performed with an OCA5 instrument (Dataphysics, Filderstadt, Germany). HPLC grade water was used and all measurements were performed on several spots of the substrate and averaged (n>3).

Surface Analysis

Effective and powerful methods for surface analysis are necessary for basic research on solid surfaces as well as for technical applications. These methods must be capable of giving detailed information, particularly about the chemical composition of the surface. In this section, fundamentals of two powerful techniques for surface analysis, i.e X-ray Phototelectron Spectroscopy (XPS) and time-of-flight Secondary Ions Mass Spectrometry (ToF-SIMS), will be briefly described.

X-Ray Phototelectron Spectroscopy (XPS)

XPS[1], also known as Electron Spectroscopy for Chemical Analysis (ESCA) is a widely used technique to investigate the elemental composition, chemical state and electronic state of a surface element. This technique is based on the photoelectric effect outlined by Einstein in 1905. In the photoelectric effect, electrons are emitted from solids, liquids or gases when they are exposed to sufficiently energetic electromagnetic radiation (**Figure AP.1a**). The kinetic energy, E_k, of these photoelectrons is determined by the energy of the X-ray radiation, h, and the electron binding energy, E_b, as given by:

$$E_k = h - E_b$$

The experimentally measured energies of the photoelectrons are given by:

$$E_k = h - E_b - E_w$$

where E_w is the work function of the spectrometer.

Since the energy of the emitted photoelectrons is exactly the energy of the incident photon minus the material's work function or binding energy, the work function of a sample can be determined by bombarding it with a monochromatic X-ray source or UV source, and measuring the kinetic energy distribution of the electrons emitted. The peak areas obtained can be used (with appropriate sensitivity factors) to determine the composition of the materials surface. The shape of each peak and the binding energy can be slightly altered by the

chemical state of the emitting atom. Therefore, XPS can also provide chemical bonding information. XPS is not sensitive to hydrogen or helium, but can detect all other elements.

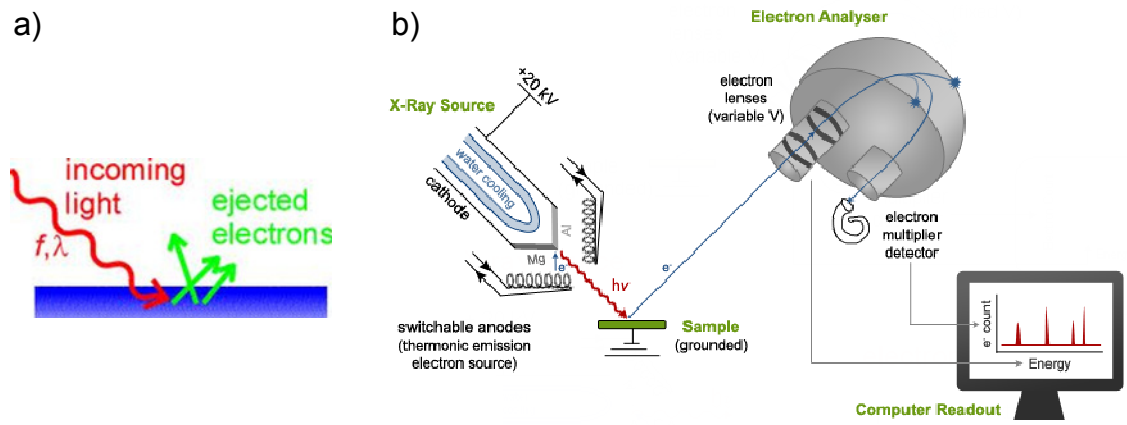

Figure AP.1 *a) Scheme of the photoelectric effect. b) Diagram of an X-ray photoelectron spectrometer.*

XPS instruments consist of an X-ray source, an energy analyzer for the photoelectrons, and an electron detector (**Figure AP.1b**) For the analysis and detection of photoelectrons, the sample must be placed in a high-vacuum chamber. Since the photoelectron energy depends on X-ray energy, the excitation source must be monochromatic, Al K_α (1486.6eV) or Mg K_α (1253.6eV) are often the photon energies chosen. The energy of the photoelectrons is analyzed by an electrostatic analyzer, and the photoelectrons are detected by an electron multiplier tube or a multichannel.

XPS measurements were performed using a K-Alpha XPS spectrometer (ThermoFisher Scientific, East Grinstead, UK). All samples were analyzed using a microfocused, monochromated Al K_α X-ray source (400 µm spot size). The kinetic energy of the electrons was measured by a 180° hemispherical energy analyzer operated in the constant analyzer energy mode (CAE) at 50 eV pass energy for elemental spectra. Data acquisition and processing using the Thermo Avantage software is described elsewhere.[2] The spectra were fitted with one or more Voigt profiles (binding energy uncertainty: ± 0.2 eV). The analyzer transmission function, Scofield sensitivity factors,[3] and effective

attenuation lengths (EALs) for photoelectrons were applied for quantification. EALs were calculated using the standard TPP-2M formalism.[4] All spectra were referenced to the C1s peak of hydrocarbon at 285.0 eV binding energy controlled by means of the well known photoelectron peaks of metallic Cu, Ag, and Au, respectively.

Time-of-Flight Secondary Ions Mass Spectrometry (ToF-SIMS)

ToF-SIMS is a very effective and universally applicable method for the chemical analysis of surfaces.[5-7]

When a surface is bombarded by energetic ions, they penetrated into the solid surface and transfer their kinetic energy to the atoms of the solid in a succession of individual collisions. The majority of species emitted are neutral but it is secondary ions which are detected and analysed by a mass spectrometer (**Figure AP.2**).

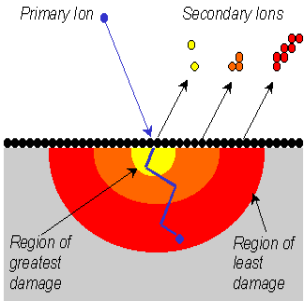

Figure AP.2 *Scheme of the SIMS process*

The ToF ion mass spectrometer consists of three main components: the ion gun, the accelerating and flight path system and the detector (**Figure AP.3**). The primary ion source (tipically Cs or Ga) produces mass separated pulses. The emited secondary ions travel through the time-of-flight analyzer at different velocities, depending on their mass to charge ratio ($k=½mv^2$). For each primary ion pulse, a full mass spectrum is obtained by measuring the arrival times of the secondary ions at the detector and performing a simple time to mass conversion.

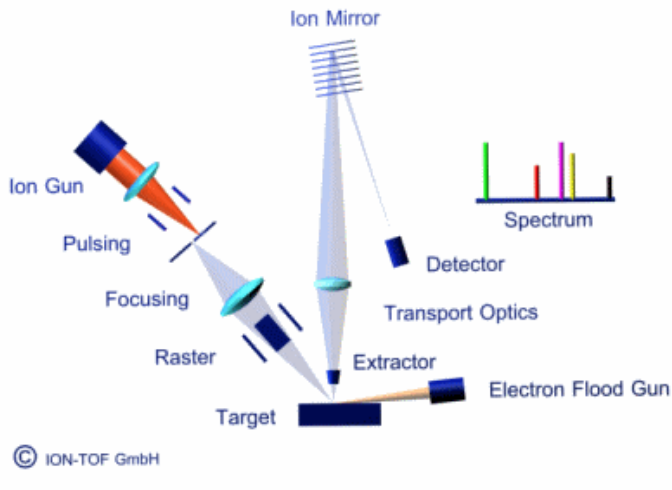

Figure AP.2 *Diagram of the time-of-flight ion mass spectrometer*

By reducing the diameter of the primary ion beam and scanning it over the surface it is possible to measure the lateral distribution of the secondary ion emission and therefore that of the surface constituents responsible for the emission. The primary ions beam is positioned in particular positions of the sample and the spectrum is recorded and stored with its corresponding coordinates. From these data, it is possible to construct an image (chemical map) for each secondary ion species or group of species showing the distribution of the surface.

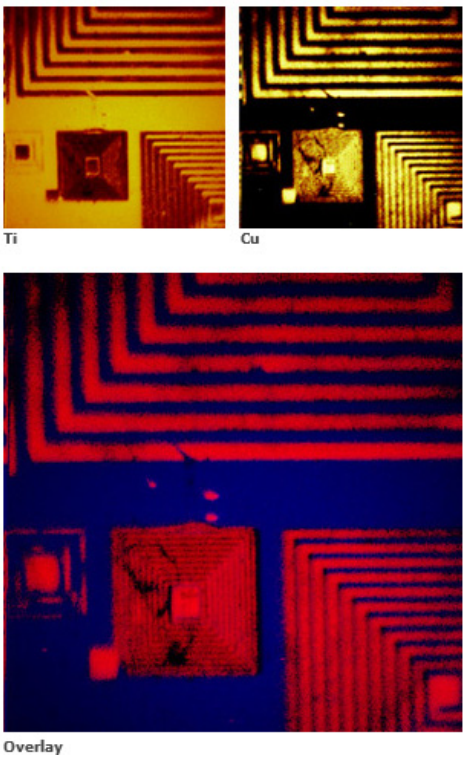

Figure AP.3 *ToF-SIMS images of a metal structure showing the Ti and Cu distribution (top) and an overlay (bottom)*

ToF-SIMS[5,7] (Time-of-Flight Secondary Ion Mass Spectrometry) was performed on a TOF.SIMS5 instrument (ION-TOF GmbH, Münster, Germany), equipped with a Bi cluster liquid metal primary ion source and a non-linear time of flight analyzer. UHV base pressure was < $5x10^{-9}$ mbar. The Bi source was operated in the bunched mode providing 1.1 ns Bi^{1+} ion pulses at 25 keV energy and a lateral resolution of approx. 4 µm. The short pulse length allowed for high mass resolution to analyze the complex mass spectra of the immobilised organic layers. Images larger than the maximum deflection range of the primary ion gun of 500×500 μm^2 were obtained using the manipulator stage scan mode. Spectra were calibrated on the C^-, C_2^-, C_3^-, or on the C^+, CH^+, CH_2^+, and CH_3^+ peaks. Primary ion doses were kept below 10^{11} ions/cm^2 (static SIMS limit). Advancing and receding contact angle measurements were performed with an OCA5 instrument (dataphysics, Filderstadt, Germany). HPLC grade water was used and all measurements were performed on several spots of the substrate and averaged (n>3).

References

1 Elipe, A. R. G.; Munuera, G.; Contreras, G. M.; Universidad de Sevilla. Secretariado de, P. *Fundamentos y aplicaciones de la espectroscopia de fotoelectrones: (XPS/ESCA)*. (Universidad de Sevilla, Secretariado de Publicaciones, 1986).

2 Parry1, K. L.; Shard, A.G.; Short, R.D.; White, R.G.; Whittle, J.D.; Wright, A. ARXPS characterisation of plasma polymerised surface chemical gradients. *Surf. Interface Anal.* **2006**, 28 ,1497-1504.

3 Scofield, J. H. Hartree-Slater subshell photoionization cross-sections at 1254 and 1487 eV. *J. Electron Spectrosc. Relat. Phenom.* **1976**, 8, 129-137.

4 Tanuma, S.; Powell, C. J.; Penn, D. R. Calculations of electron inelastic mean free paths. V. Data for 14 organic compounds over the 50–2000 eV range. *Surf. Interface Anal.* **1994**, 21, 165-176.

5 Leggett, G. J. & Vickerman, J. C. *Static secondary ion mass spectrometry (SSIMS) - an emerging surface mass spectrometry*. *Annu. Rep. Prog. Chem., Sect. C* **1993**, 88, 77-133.

6 Benninghoven, A. Chemical Analysis of Inorganic and Organic Surfaces and Thin Films by Static Time-of-Flight Secondary Ion Mass Spectrometry (TOF-SIMS). *Angewandte Chemie International Edition in English* **1994**, 33, 1023-1043.

7 Arlinghaus, H. F. *Possibilities and limitations of high-resolution mass spectrometry in life sciences*. *Appl. Surf. Sci.* **2008**, 1058-1063.